Development of Therapeutics for the Treatment of Leishmaniasis and Chagas Disease

PERERA, WADUWARAGE,DONA,HIRUNIKA

Development of Therapeutics for the Treatment of Leishmaniasis and Chagas Disease

A Thesis Presented for the Degree of Doctor of Philosophy

The Department of Chemistry

Durham University, Ustinov College

W.D. Hirunika Nawanjani Perera

Supervised by Prof. Steven Cobb, Prof. Paul Denny, and Prof. Ariel Silber

2023

Statement of Copyright

Author's Declaration

I declare that this thesis is a presentation of original work, and it is the work of the author unless otherwise stated. This work was conducted in the Department of Chemistry and Biosciences at Durham University and collaborative work was mentioned where applicable. The work has not been submitted for a degree in this or other university.

Abstract

Neglected tropical diseases (NTDs) are an increasing global health challenge exacerbated by a shortfall in funding and new developments in the field. The social and economic repercussions of these diseases can be as overwhelming as their health effects. Current frontline treatments for leishmaniasis and chagas disease suffer from range of issues such as, high cost, prolonged treatments, severe side effects and drug resistance. Hence, there is a need for new drugs. A library of molecules with highly diverse chemical space was screened against *Leishmania mexicana* parasites. Four of the derivatives from Class One and Two, **40**, **46**, **60** and **64** showed EC_{50} values of less than 10 µM against *L. mexicana* intracellular amastigotes (3.12, 7.37, 4.86 and 3.27 µM respectively) and 9,10-phenanthrenedione (Class One) and 1,10-phenanthroline (Class Two) were identified as novel chemical scaffolds which could be developed as anti-leishmanial therapeutic agents. The repurposing ability of three FDA approved drugs; pyrithione (**104**), ciclopirox (**105**) and piroctone olamine (**106**) as a treatment for cutaneous leishmaniasis was investigated. Having EC_{50} values lower than 2 µM against *L. mexicana* intracellular amastigotes and selectivity index (SI) values greater than 10 proved that all three drugs have the potential to be repurposed. The promising anti-leishmanial activities reported for the four novel derivatives (**116-119**) synthesized from pyrithione (**104**) showed that the activity is not due to the metal chelation and modification of the N-oxide functionality of pyrithione (**104**) did not significantly change its biological activity. Furthermore, it was evident from in-gel fluorescence assays that pyrithione (**104**) and the novel derivatives (**116-119**) inhibit DUB16 enzyme, an enzyme essential for the viability of procyclic promastigotes, in *L. mexicana* promastigotes. However, DUB16 overexpression did not provide any resistance towards antileishmanial activity, meaning that these inhibitors may have other targets beyond this enzyme. Two fluorinated compound libraries in were screened against *L. mexicana* and *Trypanosoma cruzi* parasites. From these libraries 4-(benzenesulfonyl)-

2,3,5,6-tetrafluoropyridine (**198**) was the only molecule found to be active against both the parasite species [EC_{50} (*L. mexicana* promastigotes); 1.33 µM, EC_{50} (*L. mexicana* axenic amastigotes); 0.433 µM, IC_{50} (*T. cruzi* epimastigotes); 1.55 µM, EC_{50} (*T. cruzi* infected stage); 0.05 µM]. Subsequently, the effect of **198** on programmed cell death in *T. cruzi* epimastigotes was investigated and results indicated that **198** triggers plasma membrane permeabilization and alters the *T. cruzi* epimastigotes mitochondrial function by collapsing mitochondrial potential, decreasing the intracellular Ca^{2+} concentration and disrupting the intracellular ATP levels. Additionally, it was discovered that **198** also arrest the G_0 phase of cell cycle at higher concentrations. This suggests that **198** could be an interesting lead compound in Chagas disease drug discovery and development. A second-generation library derived from **198** was synthesised and their anti-parasitic activities were evaluated against *L. mexicana* axenic amastigotes. Finally, a label free MS-based proteomics analysis was performed to identify the target proteins of **230** in *L. mexicana* promastigotes and 19 proteins were identified as potential target proteins of **230**.

Acknowledgements

First and foremost, I would like to thank my principal supervisor, Professor Steven Cobb for accepting me for this GCRF-CDT project and for providing invaluable advice, guidance, and support throughout my PhD. I am truly grateful for the opportunities that have been offered to me during this period, including the scope to learn various techniques, exercise my intellectual creativity and attend Chemistry courses to expand my knowledge. I would also like to thank my co-supervisor, Professor Paul Denny, who has immensely contributed to the progression of my project, for providing advice and his expertise in the parasite biology. I am particularly grateful to Dr Will Brittain for his massive help with all my chemistry queries. Additionally, I extend thanks to Associate Professor Kalesh Karunakaran for his tremendous support and guidance throughout the proteomics analysis.

I would like to extend my deepest gratitude to Professor Douglas Halliday (Director of the Durham university Global Challenge Centre for Doctoral Training), Abir Van-Hunen (GCRF-CDT Coordinator) for all the training sessions, workshops and trips they have organized for our GCRF-CDT cohort over the last couple of years. Thanks to all the members of the GCRF cohort for their support and friendship.

I would like to thank a number of people for their collaboration work as part of this research project. A special thanks to Professor Ariel Silber and Dr Richard Girard for screening the fluorinated compound libraries we sent for their anti - *T. cruzi* activity and continuing programmed cell death studies at University of Sao Paulo, Brazil. I am also grateful to Professor Jeremy C. Mottram and his PhD student Mr Sergios Antoniou at University of York for their contribution in screening *L. mexicana* DUBs inhibitors. Thanks to Dr Anke Deckers (Professor Stefan Brase- Group) at Karlsruhe Institute of Technology (KIT), Germany for supplying a library of diverse molecules to determine their anti-leishmania activity and carrying out cytotoxicity assay in their institute.

In addition, I would like to thank Dr Juan Aguilar of the NMR service, Dr Dave Parker and Mr Peter Stoles of the mass spectrometry service and Dr Dmitry Yufit of the X-ray crystallography service within the Department of Chemistry at Durham University. I would also like to thank Professor Robert Pal, who oversees the Clean Room facility, for his assistance and Associate Professor Steve Chivasa in the Department of Biosciences for giving me the training for the Typhoon scanner.

A massive thanks to all the members (both past and present) of the Cobb group (Carissa Lloyd, Yazmin Santos, Diana Kalos, Izzy Zawadzki, Katie Dowell, Eleanor Taylor-Newman, Liam Beardmore, and Lewis Picken) and Paul Denny's group (Yasmin Kumordzi, Dr Edubiel Alpizar-Sosa, Dr Gabriela Burle, Dr Zisis Koutsogiannis, Laura Filipe) for their support and friendship throughout my PhD.

Last but not least, I would like to thank my parents, my brother and sister for their love and immeasurable support over the last couple of years. I am also grateful to Dr Kanthi Senanayaka for her immense support over my time at Durham University. Without your help this journey would not have been possible.

Memorandum

The work within this thesis has been presented by the author at the following meetings:

Poster presentation at the NTD network- Early career researcher Conference, 10th March 2022, Durham University

Poster presentation at the 20th RSC fluorine postgraduate meeting, 31st March 2022, Durham University

Abbreviations

ABPP	Affinity based protein profiling
ADME	Absorption, distribution, metabolism, and excretion
AIDS	Acquired immune deficiency syndrome
Amp B	Amphotericin B
BSA	Bovine serum albumin
BTAH	Benzoyltrifluoroacetone
BZN	Benznidazole
$CaCl_2$	Calcium chloride
CC_{50}	50% cytotoxicity concentration
CD	Chagas disease
CDC	Centers for Disease Control
$CDCl_3$	Deuterated chloroform
CDF	(1E,6E)-4-[(3,4-difluorophenyl)-methylidene]-1,7 bis (4-hydroxy-3-methoxyphenyl) hepta-1,6-diene-3,5 dione
CI	Confidence interval
CL	Cutaneous leishmaniasis
CO_2	Carbon dioxide
CPX	Ciclopirox olamine
Cys	cysteine
DAT	Direct agglutination tests
DCL	Diffuse cutaneous leishmaniasis
DCM	Dichloromethane
DIA	Data independent acquisition
DMF	Dimethyl formaldehyde
DMEM	Dulbecco's Modified Eagle's $Medium_{10}$
DMSO	Dimethyl Sulfoxide

DNA	Deoxyribonucleic acid
DNDi	Drugs for neglected diseases
DTT	Dithiothreitol
DUBs	Deubiquitinating enzymes
EC_{50}	Half maximum effective concentration
ECG	Electrocardiogram
EDTA	Ethylenediaminetetraacetic acid
ELISA	Enzyme-linked immunosorbent assay
ESI	Electrospray ionization
EtOAc	Ethyl Acetate
FA	Formic acid
FADH	Flavine adenine dinucleotide
FMNH	Flavine mononucleotide
FBS	Foetal bovine serum
FCS	Foetal calf serum
FCCP	carbonyl cyanide-4-(trifluoromethoxy) phenylhydrazone
FDA	Food and Drug Administration
FML	Fucose-mannose ligand
FRET	Fluorescence resonance energy transfer
FITC	Fluorescein isothiocyanate
GO	Gene ontology
GIPLs	Glycosylinositolphospholipids
GPI	Glycosylphosphatidylinositol
GSK	GlaxoSmithKline
GSH	Glutathione
GSSG	Glutathione-oxidised form
hrs	Hours

HAT	Human African trypanosomiasis
HDACs	Histone deacetylase
HBD	Hydrogen bond donor
HBA	Hydrogen bond acceptor
HCl	Hydrochloric
HIFCS	Heat-inactivated foetal calf serum
HIV	Human immunodeficiency virus
HPLC	High-performance liquid chromatography
HRMS	High-resolution mass spectrometry
HTRF	Homogeneous time resolved fluorescence
HTS	High-Throughput Screening
Hcy	homocysteine
IC_{50}	Half maximal inhibitory concentration
IPCs	inositolphosphorylceramides
iPS	Induced pluripotent system
IFAT	Indirect fluorescent antibody test
KCl	Potassium Chloride
K_2CO_3	Potassium Carbonate
LD_{50}	Leishmanicidal effect
LFQ	Label free quantification
LIT	Liver Infusion Tryptose
Log P	Dissociation constant
LPG	Lipophosphoglycan
MBHA3	3-Hydroxy-2-methylene-3-(4 nitrophenylpropanenitrile)
MCL	Mucocutaneous leishmaniasis
MDA	Mass drug administration
MeCN	Acetonitrile

MHz	Megahertz (unit of frequency)
MMOA	Molecular mechanisms of action
MST	Montenegro skin test
MTP	Microtiter plate
MW	Molecular weight
$NaHCO_3$	Sodium Bicarbonate
NaCl	Sodium Chloride
NaH_2PO_4	Monosodium Phosphate
NaOH	Sodium hydroxide
NADPH	Nicotinamide adenine dinucleotide phosphate
NCE	New chemical entities
NFX	Nifurtimox
NFT	Nifuratel
NMT	N-myristoyl-transferase
NMR	Nuclear magnetic resonance
NT	Not tested
NTDs	Neglected Tropical Diseases
OD	Optical density
PCR	Polymerase Chain Reaction
PBS	Phosphate buffered saline
PCD	Programmed cell death
PDD	Phenotypic drug discovery
PFP	Pentafluoropyridine
phen	1,10-phenanthroline
PI	Phosphatidylinositol
PI	Propidium iodide
PKDL	Post-kala-azar dermal leishmaniasis

PKTs	Protein tyrosine kinase
pNPP	p-nitrophenyl phosphate
PMSF	phenylmethylsulfonyl fluoride
PO	Piroctone olamine
PPGs	Proteophosphoglycan
PTPs	Protein tyrosine phosphatases
PTMs	Post translational modifications
hPTP1B	humanPTP1B
PV	Parasite vacuole
QSAR	Quantitative structure activity relationship
r^2	Correlation
RAS	Rapid analogue synthesis techniques
RDT	Rapid diagnostic tests
Rh123	Rhodamine 123
RNAi	RNA interference
rpm	revolutions per minute
RPMI	Roswell Park Memorial Institute
ROS	Reactive oxygen species
SDS	Sodium dodecyl sulfate
SAR	Structure-activity relationship
SI	Selectivity index
SPR	Structure-property relationship
SL	Sphingolipids
TBTA	tris[{1-benzyl-4triazoyl}methyl]amine (TBTA)
TCR	T-cell receptor
TCEP	tris[2-carboxyethyl] phosphine
TDD	Target-based drug discovery

TFA	Trifluoroacetic acid
TFP	tetrafluoropyridine
TPP	Target protein profile
TLC	Thin layer Chromatography
t-RNA/r-RNA	Transfer/ribosomal ribonucleic acid
TSB	Tris-buffered saline
Ub-PRG	Ubiquitin propargylamine
UPS	Ubiquitin-proteosome system
UPLC	Ultra Performance Liquid Chromatography
VL	Visceral leishmaniasis
WHO	World Health Organization
WR	Working reagents
ZPT	Zinc Pyrithione

Contents

1 Introduction

1.1 Neglected Tropical Diseases

Neglected tropical diseases (NTDs) are a diverse group of conditions which affect more than 1.7 billion of the world's population with millions of others at risk of infection. The official list of NTDs compiled by the World Health Organization (WHO) currently consist of 20 conditions that are prevalent in tropical and subtropical regions.[1] These diseases predominantly affect the poorest one-sixth of the world's population who live without adequate sanitation, appropriate housing, nutrition, and healthcare services.[1] Apart from having significant mortality rates, many NTDs can cause disability that persist for a lifetime, including blindness, fatigue, and disfigurement. The social and economic repercussions of these diseases can be as devastating as their health effects.[2] Historically NTDs have not received as much attention as other diseases, such as the 'Big three' global infectious diseases, HIV/AIDS, tuberculosis and malaria.[3] Until very recently, NTDs have been largely ignored by many researchers, funders, and most noticeably pharmaceutical companies.

The WHO road map for NTDs (2021 – 2030) sets global targets and milestones for prevention, control, and eradication as well as cross-cutting targets aligned with the sustainable development goals.[4] Controlling vectors, that transmit these diseases and improving basic water quality, sanitation and hygiene and scaling up mass drug administration have proved to be highly effective strategies against these NTDs.[5] Furthermore, there are Global NTD programmes, such as the Global programme to eliminate lymphatic filariasis, Global health initiative run by WHO and Centers for Disease Control and Prevention (CDC) with different collaborations focusing on identifying regions and countries where NTDs are widespread and working on controlling and eliminating them.[6] CDC works within countries and through regional collaborations to help improve existing NTD interventions, such as mass drug administration (MDA) campaigns.[7]

1.2 Leishmaniasis

1.2.1 Life cycle of leishmaniasis

Leishmaniasis is a vector-borne parasitic disease caused by obligate protozoan parasites from the genus *Leishmania* (Trypanosomatida: Trypanosomatidae).[8] Leishmaniasis is one of the NTDs endemic in large areas of the tropics, subtropics, and the Mediterranean basin around the world. It presents a significant global health issue, where there are 12 million cases of infections and a total of 350 million people at risk of getting the infection.[9] Over 90 species of female *Phlebotomus* sand flies in the old world and *Lutzomyia* in the new world are known to transmit leishmaniasis.[7] Approximately 53 species of *Leishmania* species have been identified including all five subgenera and complexes: *Leishmania*, *Viannia*, *Sauroleishmania*, *L. enrietti* complex, and *Paraleishmania*; of these, 31 species have been found in mammals and 20 species are pathogenic for human beings.[9]

In many geographical areas where leishmaniasis is common, there can be one or more reservoir hosts to maintain the transmission cycle of the parasites.

(1) Zoonotic, which includes animal reservoir hosts (rodents, dogs, marsupials, and hyraxes) along with sand flies in the transmission cycle. Generally, *L. infantum, L. major* and *L. mexicana* species are the sources of this transmission.[10]

(2) Anthroponotic, in which infected people are the sole source of infection for the vector, sources: *L. tropica* and *L. donavani*.[11]

Leishmania parasites were first detected by Cunningham in 1885 and described subsequently by Leishman in 1900 and Donavan in 1903.[12] The digenetic life cycle of *Leishmania* consists of motile, flagellated, extracellular promastigotes (infective stage) and non-motile intracellular amastigotes with a short, immotile flagellum (tissue form).[13] In the sand fly, the flagellum in promastigotes is required for the movement through the midgut, whereas the amastigotes flagellum likely provides sensory functions.[14]

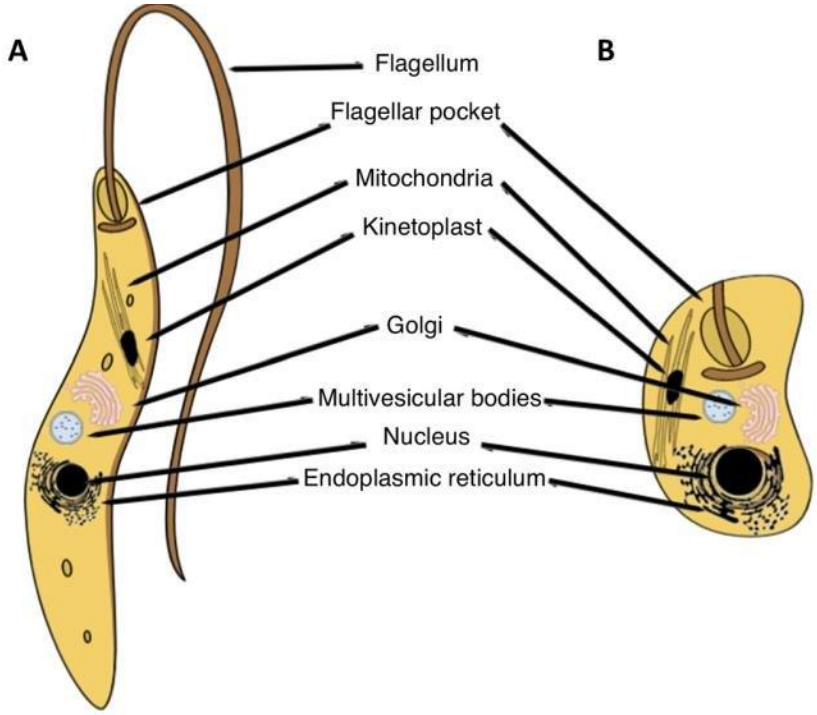

Figure 1.1 Schematic images of promastigote (**A**) and amastigote (**B**) with flagellum and flagellar pockets labelled with key structures in the cells.[15]

The life cycle proceeds as follows: the promastigote form of the parasite is injected into a human host through their proboscis when a sandfly attempts to obtain a blood meal. By analogy with African trypanosomes, the developmental stage of the parasite has been named 'metacyclic' and the dividing, immature form that presents in the fly has been named 'procyclic'. These promastigotes will be phagocytosed by neutrophils and the neutrophils are consumed by macrophages. With this transformation, the promastigotes face two major environmental changes, a temperature shift to 35 - 37 °C and a pH shift to pH 5. Promastigotes sense this new environment and transform into amastigotes inside the macrophages and multiply intracellularly by binary fission. These infected cells get ruptured and release amastigotes which infect other cells in various tissues causing either asymptomatic or symptomatic forms of the disease based on underlying host and parasite species factors.[12,16]

These parasitic amastigotes are localized in three ways.

1. Lodged in reticuloendothelial cells of various organs
2. Localised to skin in cutaneous forms
3. Localised to skin and metastases to mucosae in the mucocutaneous form

Sandflies ingest the macrophages infected with amastigotes while taking a blood meal from an infected person. Then parasitized cells are digested, and the amastigotes are released into the midgut and the conditions in the midgut of sandfly stimulate their transformation into promastigotes. The parasites reproduce by binary fission within the midgut and migrate to proboscis (**Figure 1.2**).[7]

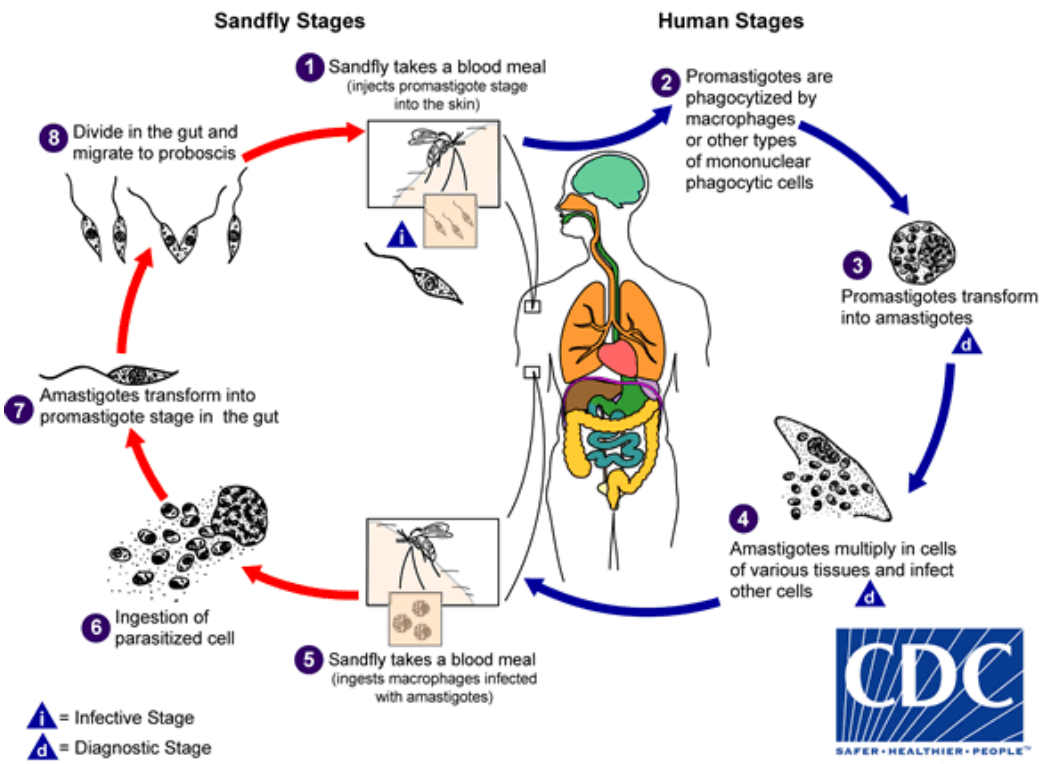

Figure 1.2 Life cycle of *Leishmania.*[17]

However, in addition to the vector mediated transmission, leishmaniasis can be spread via contaminated needles or blood transfusions. Congenital and sexual transmission have

been previously reported. A case study by Souza, has shown that visceral leishmaniasis caused by *L. infantum* can be transmitted from male to female through sexual contact.[18]

1.2.2 Clinical manifestations of leishmaniasis

Leishmaniasis has been classified into three main clinical forms, namely: Visceral leishmaniasis (VL), Cutaneous leishmaniasis (CL), and Mucocutaneous leishmaniasis (MCL), which differ in immunopathologies and the degree of morbidity and mortality. Changes in natural and human-made environments make leishmaniasis an emerging public health concern. This includes deforestation, rapid urbanization, increase in international travel, lack of vaccination, endemic AIDS, adaptation of the *Leishmania* parasite to additional vectors and development of resistance to chemotherapy. Moreover, *Leishmania* has emerged as an opportunistic pathogen in children and as well as HIV-infected adults.[19]

Cutaneous leishmaniasis (CL), endemic to 42 countries, is the most common form of the disease and it is caused by more than 15 species of parasites including *L. tropica, L. major* and species of *L. mexicana* complex. It usually develops sores on the exposed parts of the body, such as ears, nose, upper lips, arms and legs within a few weeks or months of the sand fly bites (**Figure 1.3** (**a**)). The sores can change in size and appearance over time, and they may start as papules or nodules and end up as ulcers. This ulcer may spontaneously heal or in other cases may disseminate to remote skin sites giving rise to diffuse cutaneous leishmaniasis (DCL). This is due to a deficient cellular-mediated immune response. Sometimes these lesions can be up to 200 in number and eventually cause serious disability. When the ulcers heal, they invariably leave permanent scars, which often cause serious social prejudice.[20,17]

Visceral leishmaniasis (VL), also known as Kala-azar can be fatal if left untreated. Unlike in CL, VL typically develops after months or years of the sand fly bite and usually affects internal organs such as spleen, liver and bone marrow causing symptoms of irregular bouts of fever, weight loss, swollen spleen and liver, leukopenia, thrombocytopenia, and

anaemia (**Figure 1.3**(**b**)). Pre-school children and immunocompromised and undernourished individuals are at-risk populations.[20] Post-kala-azar dermal leishmaniasis (PKDL) is a complication of VL and is characterized by a hypopigmented macular, maculopapular and nodular rash usually in patients who have recovered from VL (**Figure 1.3** (**c**)). This is believed to be caused by an immune response to residual parasites from previous infections. It usually appears 6 months to 1 or more years after the cure of the initial disease, but it can occur earlier or concurrently with VL. In some geographical areas like Africa, PKDL heals spontaneously but rarely in patients in India. *L. donavani* complex is mainly responsible for VL.[3,2]

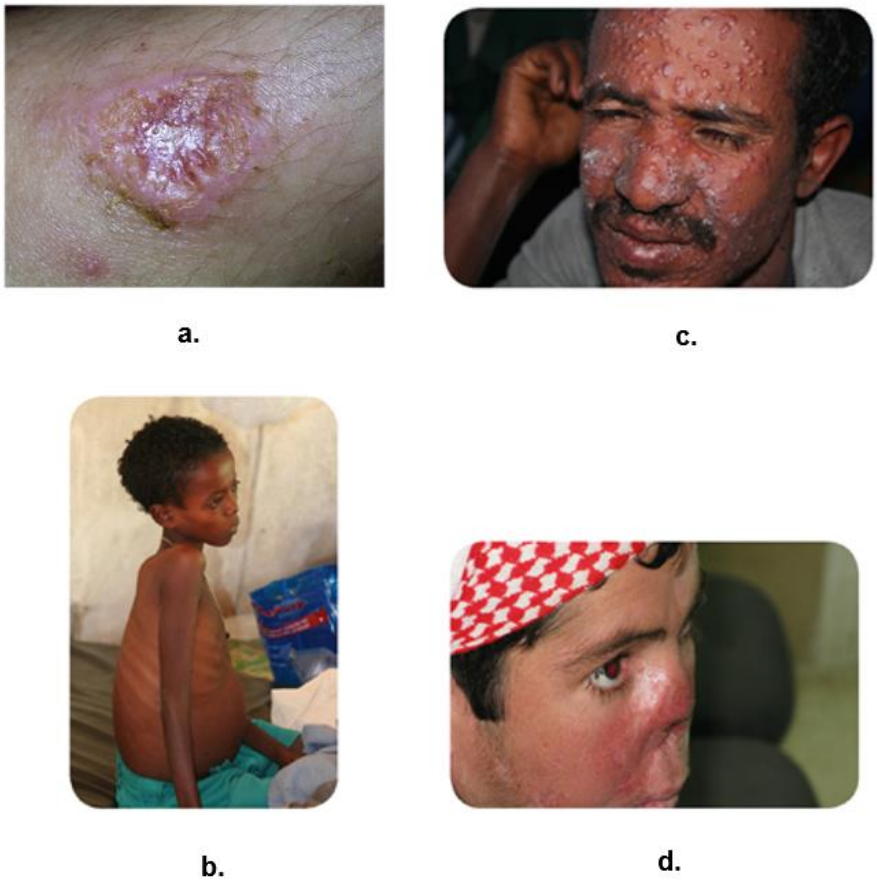

Figure 1.3 Clinical manifestations of leishmaniasis (a) Cutaneous leishmaniasis (CL), (b) Visceral leishmaniasis (VL), (c) Post-kala-azar dermal leishmaniasis (PKDL), (d) Mucocutaneous leishmaniasis (MCL).

Mucocutaneous leishmaniasis (MCL) is the least common form of the disease and it can occur as a consequence of initial CL infection. In South America and in endemic areas, it has been noted that in 1-10% of patients with CL form evolves into MCL after 5 years of having healed. Parasites can spread from the skin and cause sores in the mucous membranes of the nose, mouth, and throat (**Figure 1.3** (**d**)). Lesions can lead to partial or complete destruction of the mucous membranes of the nose, mouth and throat cavities and surrounding tissues. This disabling form can also raise social stigma.[2,20]

1.2.3 Epidemiology of leishmaniasis parasites

The epidemiology of leishmaniasis is diverse. According to the WHO records in 2020, 79 countries are endemic for VL, and 90 countries are endemic for CL (**Figure 1.4** and **1.5**). The ecological distribution ranges from rainforests to deserts. In 2020, 90% of global VL cases were reported from ten countries: Brazil, China, Ethiopia, Eritrea, India, Kenya, Somalia, South Sudan, Sudan and Yemen and the majority of CL cases (over 85%) occurred in ten countries: Afghanistan, Algeria, Brazil, Colombia, Libya, Pakistan, Iraq, Peru, Tunisia, and Syria. In the western part of the world (New world), leishmaniasis is mainly found in Central and South American countries except for Chile and Uruguay. However, only a handful of cases of CL have been reported from the North American Peninsula. In the Eastern part of the world (Old world), the disease is found in some parts of Asia including the Middle East and Indian subcontinent, Africa and Southern parts of the Europe while no cases of leishmaniasis have been reported in the Pacific islands or Australia.[7,21] It has been estimated that 15 million people around the world currently suffer from the disease with 50,000 to 90,000 VL and 0.6 to 1.0 million CL new cases emerging worldwide annually. As for MCL, over 90% of reported cases were found in Bolivia, Brazil, Ethiopia and Peru.[22]

Status of endemicity of cutaneous leishmaniasis worldwide, 2020

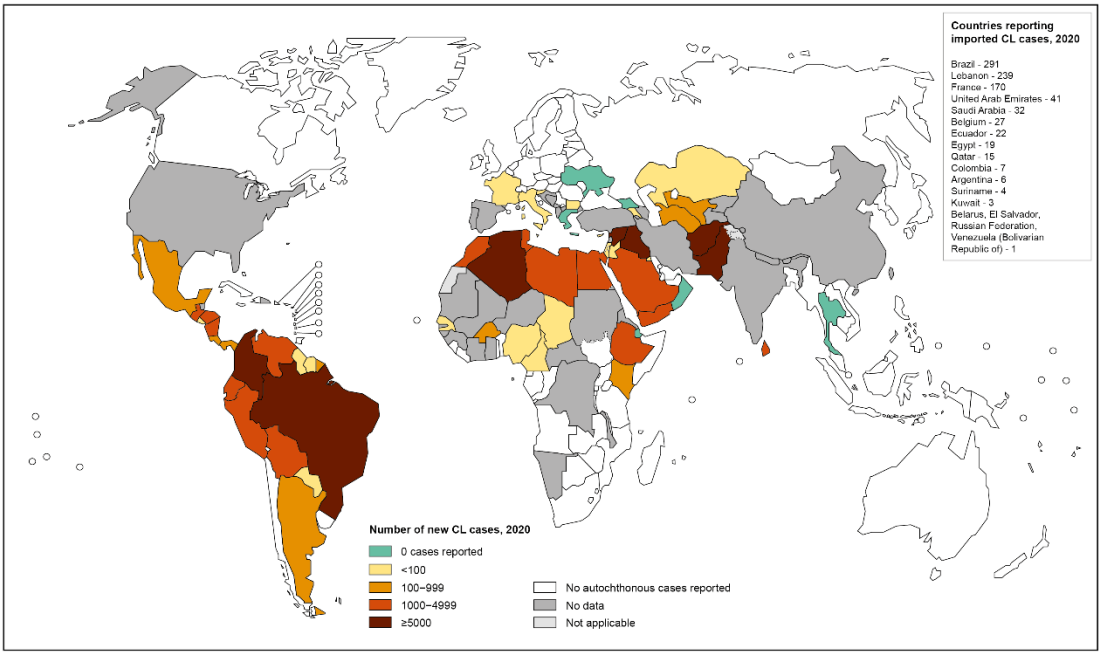

The boundaries and names shown and the designations used on this map do not imply the expression of any opinion whatsoever on the part of the World Health Organization concerning the legal status of any country, territory, city or area or of its authorities, or concerning the delimitation of its frontiers or boundaries. Dotted lines on maps represent approximate border lines for which there may not yet be full agreement. © WHO 2021. All rights reserved

Data Source: World Health Organization
Map Production: Control of Neglected Tropical Diseases (NTD)
World Health Organization

World Health Organization

Figure 1.4 Status of endemicity of cutaneous leishmaniasis (CL) worldwide, 2020.[23]

Status of endemicity of visceral leishmaniasis worldwide, 2020

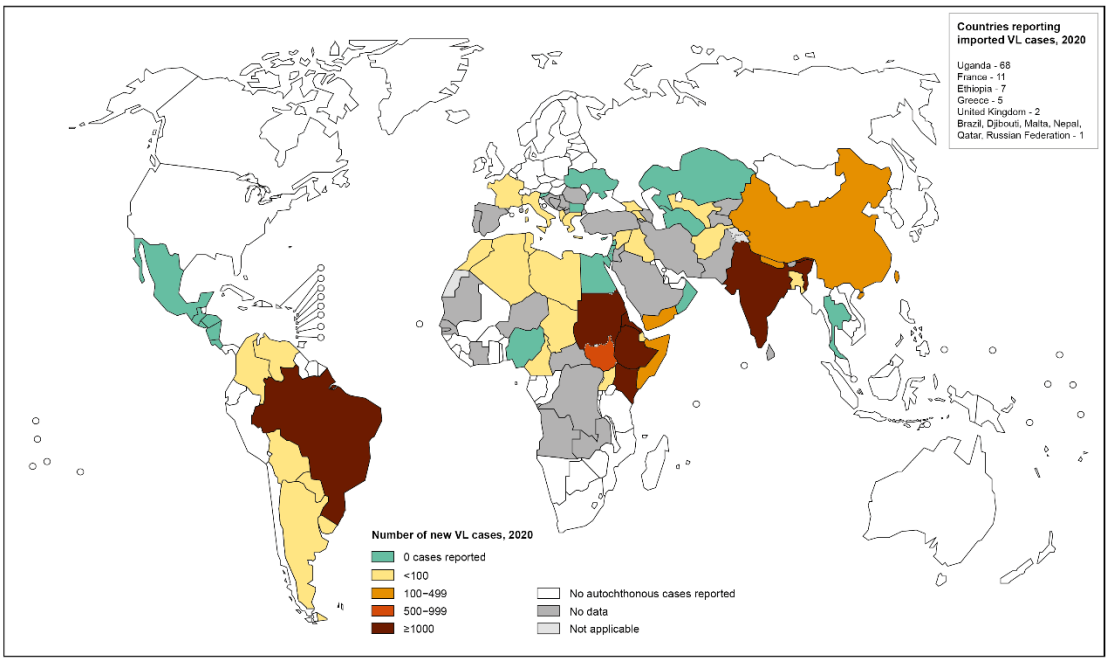

The boundaries and names shown and the designations used on this map do not imply the expression of any opinion whatsoever on the part of the World Health Organization concerning the legal status of any country, territory, city or area or of its authorities, or concerning the delimitation of its frontiers or boundaries. Dotted lines on maps represent approximate border lines for which there may not yet be full agreement. © WHO 2021. All rights reserved

Data Source: World Health Organization
Map Production: Control of Neglected Tropical Diseases (NTD)
World Health Organization

World Health Organization

Figure 1.5 Status of visceral leishmaniasis (VL) worldwide, 2020.[23]

In 2019, 5719 deaths were reported from VL and 5-10% of people treated for VL develop PKDL in South Asia, where as in East Africa it was 50-60%.[24] Currently, geographical distribution of leishmaniasis has extended, and the risk has increased due to the incidence of HIV/*Leishmania* co-infection. People with co-infection have the chance of developing the full-blown clinical disease and high relapse and mortality rates.

As of 2021, 45 countries have been reported to have patients with *Leishmania*-HIV co-infection.[25] However, these numbers only reflect the reported cases and there are likely to be many unreported cases due to lack of surveillance systems and frequency of disease in remote areas.[24]

1.3 Clinical pathology of leishmaniasis

Due to the wide spectrum of clinical manifestations present for leishmaniasis (ulcerative skin lesions developing at the site of the sand fly bite, multiple non-ulcerative nodules, destructive mucosal inflammation and disseminated, potentially fatal, visceral infection) diagnosis of leishmaniasis can be challenging. VL is diagnosed by combining clinical signs with parasitological or antibody-based diagnostics. The principal signs are prolonged fever, weight loss, spleen enlargement and anaemia. Serological testing involves the detection of antibodies using rK39 rapid diagnostic tests (RDT) or Direct agglutination test (DAT) to confirm infection. CL and MCL are diagnosed by clinical manifestation with parasitological tests to confirm the infection. Serological tests have limited success in this matter.[24]

1.4 Prevention and Control measures for leishmaniasis

Leishmaniasis has been listed as one of the nine major neglected tropical parasitic diseases and it is considered as one of the most difficult to control diseases due to its zoonotic nature and genetic and species diversities of parasite and vectors. Since vaccines against leishmaniasis are still under development,[26] early diagnosis and effective case management, vector control, constructive disease surveillance, control of reservoir

hosts and social mobilization are the key strategies for leishmaniasis prevention and treatment.[27]

Sandflies are more active during night-time, especially from the dusk till dawn. Personal protective measures include minimizing nocturnal outdoor activities, wearing protective clothing and applying insect repellent to exposed skin.[3,2] Vector control by insecticide spraying on the walls of houses, silos, animal shelters and other domestic buildings is efficient but it is difficult to sustain due to high cost and logistic constraints. Sustainability is crucial as interruption or cessation of spraying processes lead to re-emergence of leishmaniasis. Insecticide impregnated bed nets is an alternative to residual- insecticide house spraying.[28] Their efficacy has been proved in anthroponotic foci of CL in Afghanistan and Syria and VL in Nepal and Sudan by reducing the number of incidences. Pyrethroid treated dog collars are under evaluation and they already showed evidence of reducing the incidence of canine VL and consequently human VL.[7,29,30]

Most research on vaccines is strategic, not applied. The only proven vaccine agent in human beings is live *L. major* (leishmanisation), now discontinued due to unacceptable lesions presenting in some patients.[27] Therapeutic vaccine trials continue to use dead cultured parasites with the combination of anti-leishmanial drugs (efficacy 0-75%).[31] One second generation recombinant vaccine contains a trifusion recombinant protein and some of its epitopes are shared by L. *donovani* and L. *infantum*.[32] Recently, some investigators demonstrated the protective efficacy of DNA vaccines, which includes the T cell-based immunity against VL.[33] The vaccine antigens are selected as conserved regions in diverse *Leishmania* species and provide a variable strategy for DNA vaccine development. However, despite having many genes identified as vaccine candidates, the disappointing potency of the DNA vaccines highlights the challenges encountered in pre-clinical and clinical realities.[34] Leishmune® is the first licensed vaccine against canine leishmaniasis and it contains the fucose-mannose ligand (FML) antigen of *L. donovani*

and has a reported efficacy of 76-80%.[35] LiESAp-MDP vaccine was reported to have an efficacy of 92% when tested on naturally exposed dogs in the south of France.[31]

1.4.1 Current drug treatments for leishmaniasis

Control of leishmaniasis predominantly relies on chemotherapy. However, available drugs are limited in number, and each has various associated issues. For several decades pentavalent antimonials, such as sodium stibogluconate (**1**) and meglumine antimoniate (**2**) have been the mainstay of anti-leishmanial therapy (**Figure 1.6**). But there are numerous shortcomings to these antimonials. These treatments require daily injections for three weeks and often the patient needs to be hospitalised in order to monitor toxic effects. This implies high cost of the treatment and inaccessibility for most patients resulting in incomplete therapeutic actions, either by lack of follow-up medication or by patient discouragement.[36] In addition, more than 60% of VL cases have seen the emergence of drug resistance in North Bihar, India since 1980s.[37] Taking higher dosages over a long period of time is the crucial reason for the development of drug resistance. Treatments with combination of existing drugs below their individual dose limit has become a short-term strategy to combat emerging drug resistance, reduce adverse side effects and shorten the therapy duration. The first attempt to this approach occurred in the early 1990s, with a combination of sodium stibogluconate (**1**) and paromomycin (**3**) (**Figure 1.7**) tested in Kenya, Sudan and Bihar state in India.[38] Daily administration of a combination of 12 mg/kg of paromomycin (**3**) and 20 mg/kg of sodium stibogluconate (**1**) for 20 days yielded an 88% cure rate in India. In Sudan 97% of cure rate was found after administrating 15 mg/kg of paromomycin (**3**) and 20 mg/kg of sodium stibogluconate(**1**) for 17 days.[39,40]

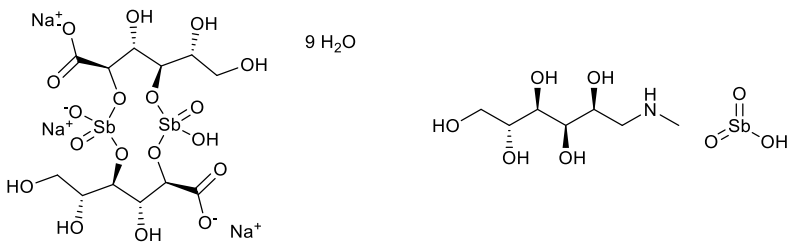

1 2

Figure 1.6 Structures of first line treatments Sodium stibogluconate (**1**), meglumine antimoniate (**2**).

Paromomycin (**3**) (**Figure 1.7**) is an aminoglycoside broad spectrum antibiotic which inhibits proteosynthesis by binding to 16S rRNA. It was first isolated from *Streptomyces krestomuceticus* in the 1950s and shown to be efficacious in the treatment of CL and VL in Kenya in 1966 and 1990 respectively.[38] The most common adverse event with paromomycin is the injection site pain and the main advantage is its affordability. Due to its limited use, resistance is not yet reported.[41]

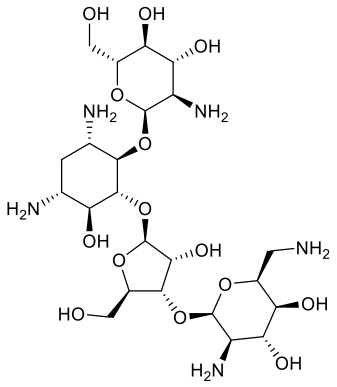

3

Figure 1.7 Chemical structure of Paromomycin (**3**).

The isethionate or methanesulphonate salts of pentamidine (**4**) (**Figure 1.8**) have been used as second line drugs in the treatment of VL. Recent studies have shown that pentamidine accumulates in the mitochondria and enhances the efficacy of mitochondrial respiratory chain complex II inhibitors. In *in vitro* pentamidine-resistant mutants, the drug does not accumulate in the mitochondria and the cytosolic fraction of the drug is extruded

outside the cell (**Figure 1.9**).[36] However, the efficacy of these are shown to be rapidly declining in India, suggesting that parasites are becoming resistant.[42] Furthermore, there is a considerable amount of toxicity associated with pentamidine which always restricts its use as a second line of treatment.[43]

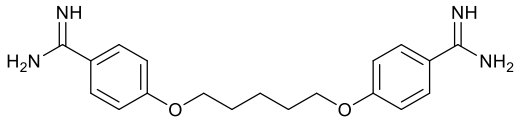

4

Figure 1.8 Chemical structure of Pentamidine (**4**).

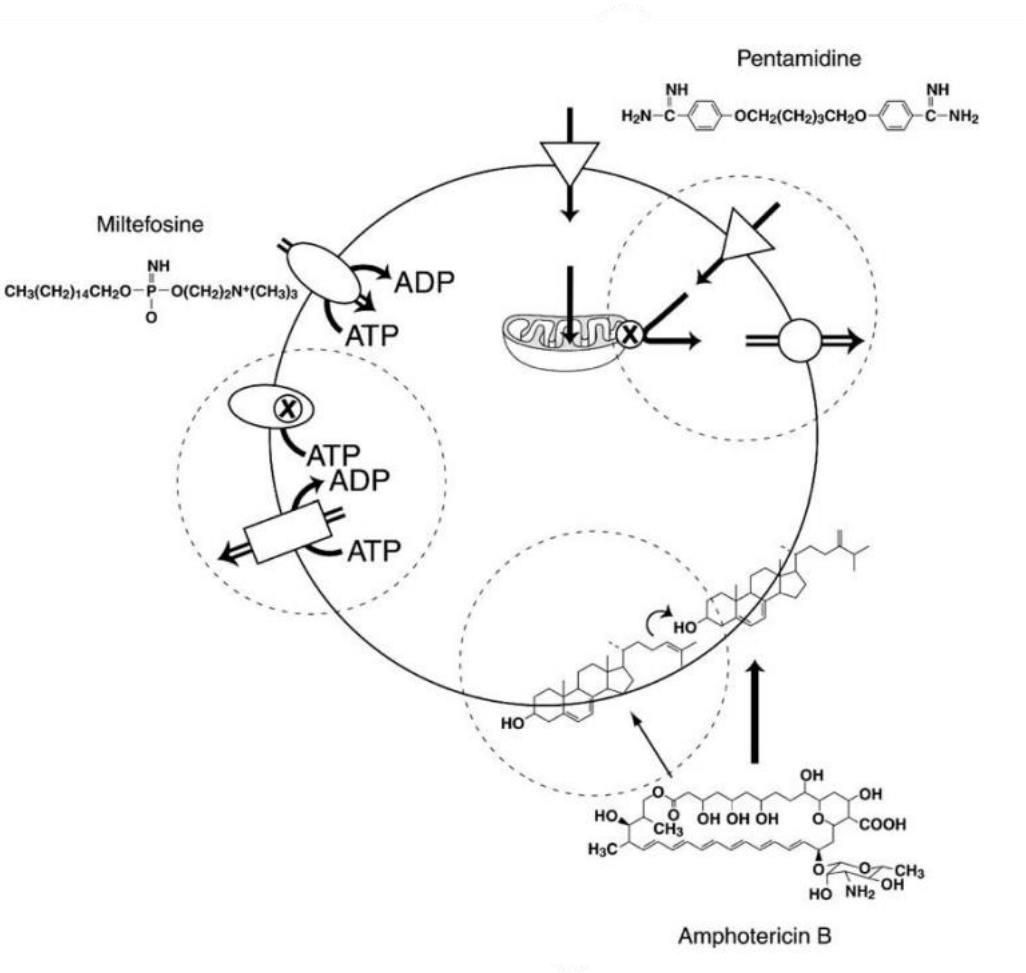

Figure 1.9 Modes of action and resistance of selected antileishmanial drugs.[36]

Amphotericin B (Amp B) (**5**) (**Figure 1.10**) is a polyene antibiotic isolated from *Streptomyces nodosus* in 1955 and it is commonly used in the treatment of systemic fungal infections.[44] Amp B (**5**) interacts with fungal membrane sterols and ergosterol. Its activity against *Leishmania* was first reported in 1960 and the first successful treatment of patients with VL was reported in 1963 in Brazil.[38] *Leishmania* have ergostane based sterols as their major membrane sterol as same as fungi and this explains the success of Amp B (**5**) against *Leishmania* parasites (**Figure 1.9**). The drug increases membrane permeability by binding to ergosterol present in *Leishmania* plasma membrane.[36,41] Amp B (**5**) is used in complex with deoxycholate or various lipids and all formulations are administered by intravenous infusion. The deoxycholate form of the drug has many adverse effects including infusion reactions, nephrotoxicity, hypokalaemia, and myocarditis and needs close monitoring and hospitalization for 4-5 weeks. Although Amp B (**5**) is toxic and has severe side effects, it is clearly the drug choice where there is high level of pentavalent antimonial resistance seen. Lipid formulations of Amp B (**5**) retain their antifungal activity while decreasing toxicity. A similar situation is seen in *Leishmania* treatments, where various lipid formulations of Amp B (**5**) at lower doses were found to be highly active and associated with low toxicity. But the high cost of the treatment again affects patients in low-income settings. Resistance to Amp B (**5**) does not appear to be emerging rapidly, although relapses are sometimes found after treatments, especially in HIV-positive patients.[38,36]

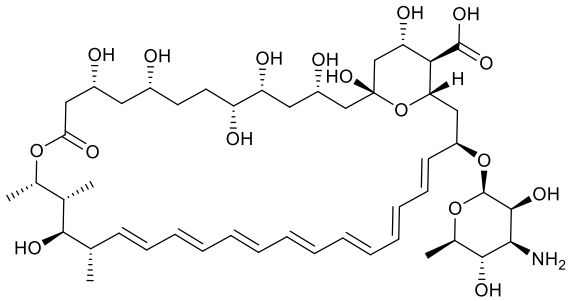

5

Figure 1.10 Chemical structure of Amphotericin B (**5**).

Miltefosine (**6**) (**Figure 1.11**) is an alkyl phospholipid, originally developed as an anticancer agent.[38] Antileishmanial activity of miltefosine (**6**) was first discovered in 1990s in several laboratories and afterwards it was approved as an oral treatment for VL in India for the first time in 2002.[45] This was considered as a breakthrough in anti-leishmanial chemotherapy. Very little is known about the mode of action of miltefosine, but it is believed to be associated with changes in alkyl-lipid metabolism, and phospholipid biosynthesis. Specifically, intracellular accumulation of the drug, and subsequent regulation of two transporters, belonging to the amino-phospholipid translocase family (Amino-phospholipid P-type ATPase) are believed to be linked to its activity. This theory is supported by the fact that point mutations in these aforementioned transporters can lead to a decrease in accumulation of miltefosine by extruding it to the outside of the cell and to parasite resistance (**Figure 1.9**).[36] In the promastigote stage of *L. donovani* parasites a cell death process similar to apoptosis was observed[46] and it was evident that there is a drastic reduction (>95%) in the accumulation of miltefosine (**6**) in the *L. donovani* resistant line.[47] The most common adverse side effects for miltefosine (**6**) include gastrointestinal effects, occasional hepato- and nephrotoxicity and teratogenicity. Miltefosine (**6**) has a long half-life, approximately 152 hours, which could encourage the resistance. However, clinical resistance in the field is not yet reported.[43,41]

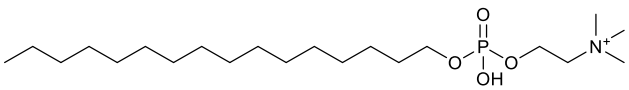

6

Figure 1.11 Chemical structure of Miltefosine (**6**).

1.5 Life cycle of Chagas disease

Chagas disease (CD), also known as American trypanosomiasis is a potentially life-threatening neglected tropical disease caused by a protozoan parasite *Trypanosoma cruzi* (Order Kinetoplastida, Family Trypanosomatidae). The disease is named after the

Brazilian physician Carlos Chagas, who discovered the disease in 1909.[48] CD is a zoonotic disease which is endemic in Latin America with an estimated 7-8 million people infected across 21 countries; only 30% of those infected have been diagnosed, and a total of 70 million people at risk of contracting the disease. According to the Drugs for Neglected Diseases initiative (DNDi), CD result 12,000 deaths and 30,000 new cases per year, making it one of the leading causes of cardiovascular morbidity in the endemic regions.[49,50] Infected hematophagous triatomine bugs (Family Reduviidae), also known as kissing bugs transmit *T. cruzi* parasites by biting people and defecating or urinating closer to the bite site. Common triatomine insect species which cause trypanosomiasis belong to the genera of *Triatoma*, *Rhodinus*, and *Panstrongylus*. *T. cruzi* can also be transmitted by non-vectorial mechanisms, for example, by blood transfusion, organ transplantation, congenital transmission and orally by ingestion of parasite contaminated food and drinks.[51]

The life cycle of *Trypanosoma cruzi* involves two intermediate hosts: invertebrate vector (triatomine insects) and the vertebrate host (human) (**Figure 1.12**). The infection of human begins with the non-dividing metacyclic trypomastigotes present in the excreta of the blood-feeding insect vector, which penetrate through the bite wound or through intact mucosal membranes. Inside the host, metacyclic trypomastigotes bind to receptors on a wide range of phagocytic and non-phagocytic cells and enter to form a parasitophorous vacuole (PV). Upon entry, they differentiate into small round shaped intracellular amastigotes and escape the PV into the cytoplasm, where the transformation is completed. The amastigotes multiply by binary fission until the cells fill with these replicative forms. At this stage, the amastigotes differentiate into non-replicative trypomastigotes. These elongated cells with a flagellum show continuous and intense movement which induce lysis of the host cell membrane. Once released, they can invade a variety of adjacent tissues and transform into intracellular amastigotes in new infection sites or enter the blood and lymph and disseminate. Clinical manifestations can develop at this stage. The bloodstream trypomastigotes do not replicate and can be taken up by

triatomine vectors. Most of the ingested cells are broken down in the vector's midgut while the surviving cells transform into the epimastigote form a few days later. Epimastigotes then move to the intestine where they proliferate and attach to the perimicrovillar membrane. This parasite attachment in the insect hindgut is essential for the process metacyclogenesis, which involves the transformation of the non-infective epimastigotes into highly infective metacyclic trypomastigotes.[48,52,53]

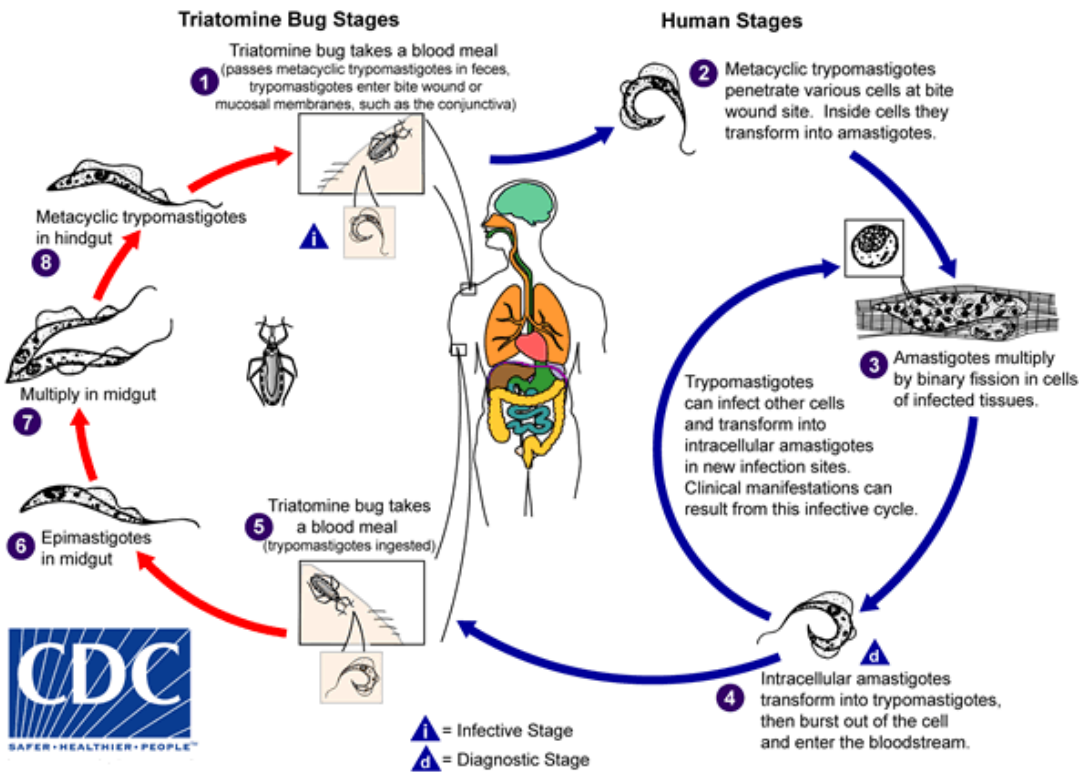

Figure 1.12 Life cycle of *Trypanosoma cruzi.*[48]

1.6 Distribution of Chagas disease

CD was once entirely confined to continental rural areas of the region of the Americas except the Caribbean islands. The classical endemic area of CD ranges from southern part of USA to the north part of Argentina and Chilli, comprising 21 countries (**Figure 1.13**). It is also found in non-endemic areas such as North America, Europe (Austria, Belgium, France, Germany, Italy, Netherlands, Sweden, Portugal, Spain Switzerland, and United

Kingdom), Japan and Australia due to increased population mobility over previous decades.[50]

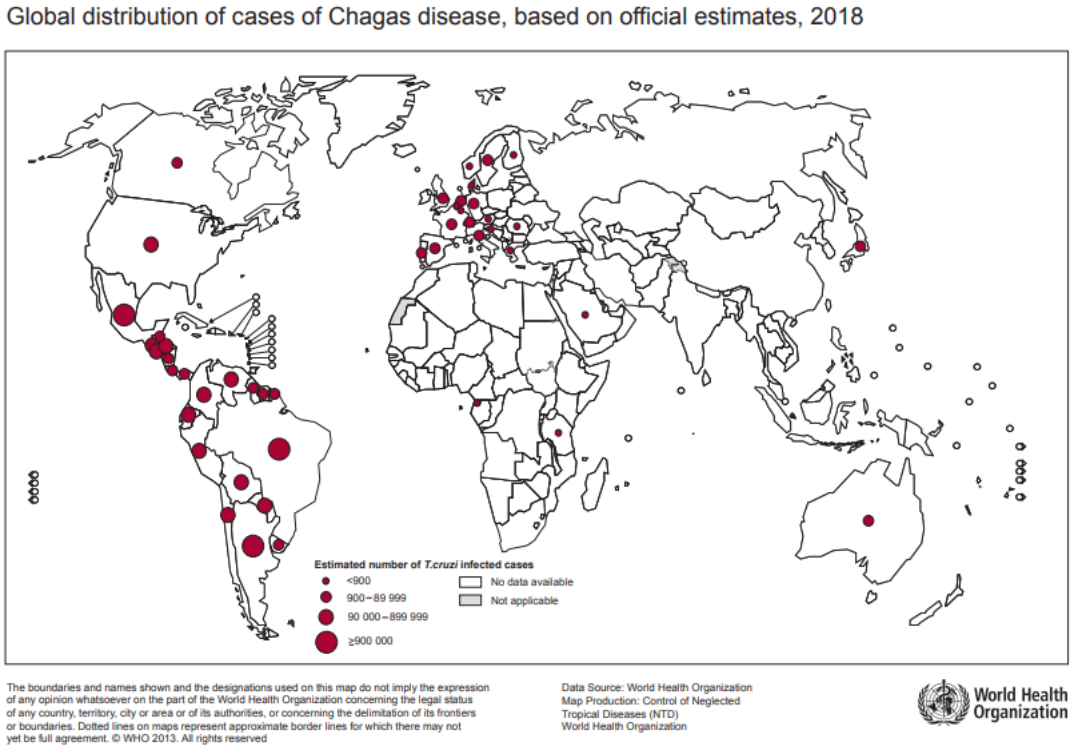

Figure 1.13 Prevalence map of Chagas disease, 2018.[54]

1.7 Clinical manifestations of Chagas disease

CD has two clinical phases: an acute and a chronic phase. If untreated, infection can be lifelong. The pathology of CD is modulated by three factors: (1) complex genetic interactions between the host and the parasite, (2) environmental and social factors, and (3) mixed infections, reactivations, and re-infections. The acute phase of the disease occurs immediately after infection and can last up to weeks or months. It is characterised by high parasitaemia (a high number of parasites circulate in the blood), often accompanied by systemic symptoms, such as fever, headache, swelling around the site of inoculation, and diarrhoea, among others, and rarely lymphadenopathy, hepatomegaly, splenomegaly, myocarditis, and meningoencephalitis. While most infected people continue with an asymptomatic phase, around 30% of infected people progress to the

chronic phase in which people develop severe and, in some cases, life-threatening medical issues over the course of their lives. At this stage the parasites mainly reside in the heart and digestive muscles, a few or no parasites are found in the blood. Complications may include heart rhythm abnormalities that can cause sudden death, a dilated heart that doesn't pump blood very well, and a dilated oesophagus or colon, that cause difficulties with eating or passing stools. CD can reactivate parasites in people who have suppressed immune systems due to Acquired immune deficiency syndrome (AIDS) or chemotherapy, causing severe medical complications.[48,53]

1.8 Diagnosis of Chagas disease

In the acute stage, it is possible to determine the presence of the parasites circulating in the blood by parasitological tests, that can be a direct blood examination under a microscope, or by multiplication as haemoculture, xenodiagnoses, and polymerase chain reaction (PCR). In the chronic phase, at least two serological tests must be performed to detect anti-*T. cruzi* IgG antibodies, such as indirect immunofluorescence (IIF), hemagglutination, and enzyme-linked immunosorbent assay (ELISA). In addition to parasitological and serological tests, routine laboratory tests, electrocardiogram (ECG), X-rays, and hepatogram are requested both in acute and chronic stage diagnosis.[55,56]

1.9 Prevention and control measures

It is known that 140 species of *Triatominae* are capable of transmitting *T. cruzi* and are broadly distributed in the Americas.[56] So far, a vaccine for CD is not available. Hence, primary prevention has been based on vector control by continuous application of insecticides in infested homes. Despite advances in domestic vector control since 1991, It is impossible to eradicate the infection due to the large reservoir of *T. cruzi* parasites in wild animals of the Americas.[50] Mandatory blood screening is necessary to prevent infection through transfusion and organ transplantation and to increase the detection of affected population around the world. Additionally, house improvements, house cleanliness and good hygiene practice while handling food will also help to reduce the

burden of disease.[57] However, the main challenges in non-endemic countries are funding for healthcare education programs, screening programs for donors and pregnant women, access to healthcare for infected individuals, socioeconomic factors as well as cultural and language barriers faced by immigrants.[56]

1.10 Current treatments for Chagas disease

Currently, there are only two nitro-heterocyclic drugs, benznidazole (BZN) (**7**) (**Figure 1.14**) and nifurtimox (NFX) (**8**) (**Figure 1.14**), available for the treatment of CD and both of them were developed more than 50 years ago.[50] The recommended dose of BZN is 10 mg/kg in children or adults with acute infection, or 2.5 mg/kg twice daily for 60 days for adults with chronic disease. Maximum daily dose recommended is 300 mg.[58]

7 **8**

Figure 1.14 Structures of nitroaromatic drugs used to treat *T. cruzi* infections, benznidazole (**7**) and nifurtimox (**8**).

BZN (**7**) and NFX (**8**) act as prodrugs and are activated inside the parasite cell by mitochondrial-localised flavin-dependant enzyme, type 1 nitroreductase TcNTR-1. Substrate specificity and the lack of TcNTR-1 in the mammalian host accounts for the selectivity of the drugs. Reduction of the nitro group by the nitroreductase generate a series of reactive metabolites that have trypanocidal activity, most notably glyoxal in the case of BZN (**7**) (**Figure 1.15**), and an unsaturated open-chain nitrile with NFX (**8**) (**Figure 1.16**).[59] Drug-induced mutagenesis has been identified as a possible mode of action for benznidazole which cause disruption of DNA-repair mechanisms and chromosome instability.[59] Benznidazole and nifurtimox are highly effective if given shortly after infection (at the beginning of the acute phase), during the early chronic phase, and for cases of congenital transmission and reactivation. However, the longer the patient has been

infected, the efficacy of the drugs diminishes, and adverse reactions are more persistent at older age (occurring in up to 40% of treated adult patients).[57] Moreover, these drugs require long treatment periods (60-90 days), have severe side effects, have not been proven effective in people with severe chronic symptoms, and are contraindicated to use during pregnancy, kidney, or liver failure.[57,49] NFX (**8**) is also prohibited for people with a history of neurological or psychiatric disorders. Side effects, such as cutaneous, gastrointestinal, and neurological complications are reported in up to 90% of patients. As a result, a high drop-out rate of patients can be seen.[59] Limited access to currently available treatments, has also been an issue. Hence, the actual number of patients treated remains very low.

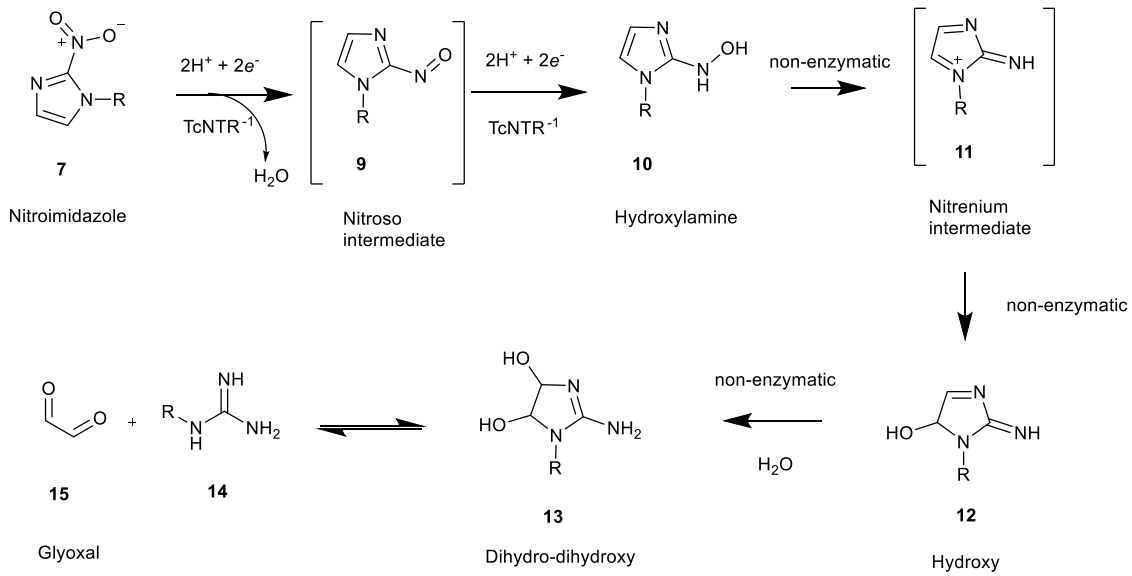

Figure 1.15 Reductive metabolism of benznidazole (**7**), initiated by TcNTR-1(R= N-benzylacetamide).[60]

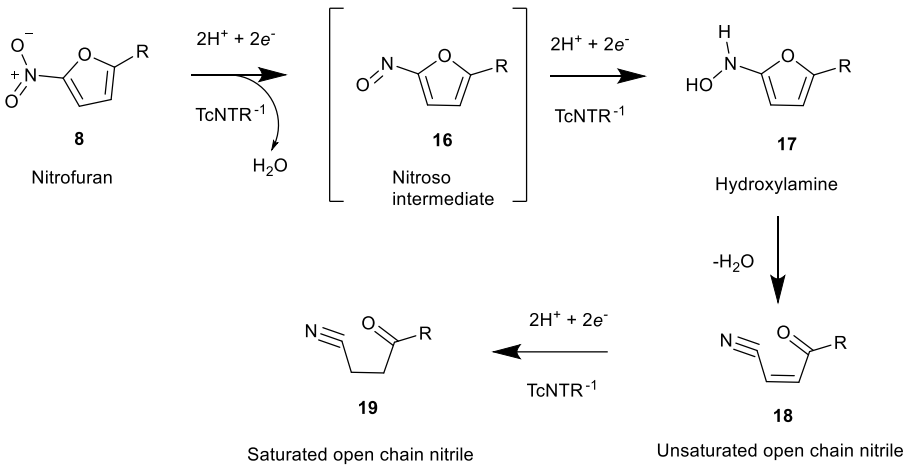

Figure 1.16 Nifurtimox (**8**) reduction process by TcNTR-1(R= 3-methyl-4-(methyleneamino)thiomorpholine 1,1-dioxide).[61]

The resistance of parasite strains against BZN (**7**) and NFX (**8**) cause complications in pharmaceutical management of CD and treatment failure. An analysis of the sensitivity of benznidazole against Colombian *T. cruzi* strains by Jaramillo et al., revealed that 36% of the strains were sensitive, 48% were moderately sensitive and 16% were resistant to the drug.[62] Additionally, in a recent study, a dormant form of the parasite was identified, which allows the infection to persist after the treatment with BZN (**7**) for up to 30 days. And this could be the reason why treatment so often fails to cure CD.[62] New drugs with improved safety and efficacy would alter risk-benefit balance and increase the number of patients who receive treatment.[51]

1.11 Drug discovery, Development and Challenges of neglected tropical diseases.

Drugs, vaccines, diagnostics, and vector controlling play an important role in prevention and treatment of NTDs. In contrast to other non-neglected diseases, a very small number of new therapeutics are invented for NTDs. In the period of 1975 and 1999, 1393 new drugs were approved but only 13 (0.93%) of them were for NTDs and between the year 2000 to 2011, only 5 (0.59%) out of 850 registered drugs were indicated for NTDs. All of

which were new indications or formulations of existing drugs; none were new chemical entities (NCEs).[63] As already discussed, access to medicines for the treatment of leishmaniasis and CD is problematic in the poverty-stricken countries with highest burden of cases. In addition, all of the current medications have limitations in efficacy and safety, and many are not well adapted to the needs of patients. Therefore, many patients are still in need of more effective, safer, and more convenient treatments. Despite this, there has been limited funding available to support the research and development of new therapeutics for NTDs. Given the fact that an average income of a patient in an endemic area is less than $2 per day, these are not economically attractive diseases for new drug development for pharmaceutical companies. Institutions and research groups on the other hand have worked on some strategies that can help to address the issue, which include the modification of conventional drug dosages, drug repurposing and combined therapy. Some have studied the parasites to identify essential genes that can be used as therapeutic targets to design new drugs.[64]

Rationally, both target-based and phenotype-based screening assays are often employed in drug discovery for NTDs. Target-based screening approach has been impeded by the lack of genetic tools for validating drug targets in the parasites. However, phenotypic screening reflects all the targets and biological pathways as the whole organism is being treated with the candidate drug molecules. Phenotypic screening approaches have been developed in both academic and industrial settings and have been proven most successful in identifying molecular targets.[65] Therefore, conducting a phenotypic assay in advance during a primary screening cascade is considered as a viable alternative to discover ‘hits’ as chemical probes for target identification in the end. Altogether, a balance between target-based approaches with careful target selection and phenotypic-based methods might be the best strategy in this regards.[63] Next, ‘hit expansion’ is performed to verify if a hit is genuine and whether there is scope for continue working with the chemotype. In the ‘hit to lead’ phase, the compound is refined through a cyclic process of ‘design-make-test’

until it has significant activity in animal models of infection. Subsequently, the biological activity, pharmacokinetics and safety profiles are optimized during 'lead optimization'. 'Candidate selection' is an important phase in a drug discovery pathway, as this involves selecting a single compound for progression and carry out regulatory toxicology and scale-up processes to enable human studies (clinical trials; phase I, phase II, phase III) (**Figure 1.17**).[66]

The drug discovery pathway is extensively guided by 'target protein profiles' (TPPs). These describe the desired features and efficacy of a final drug molecule, such as duration of treatment, whether it is an oral or parenteral treatment, cost of treatment, pharmacokinetic properties and acceptable safety margins.[67] TPPs have been defined for leishmaniasis, human african trypanosomiasis (HAT), CD, malaria, cryptosporidiosis and dengue fever, but are absent for many other diseases.

Despite substantial research into the biology of these parasites, discovery of candidate molecules is hampered by lack of well-validated druggable targets. Apart from that, there are more challenges to the drug discovery process, such as, poor representation of the human disease by the existing animal models of NTDs, development of drug resistance and dormant infections (**Figure 1.17**).[66]

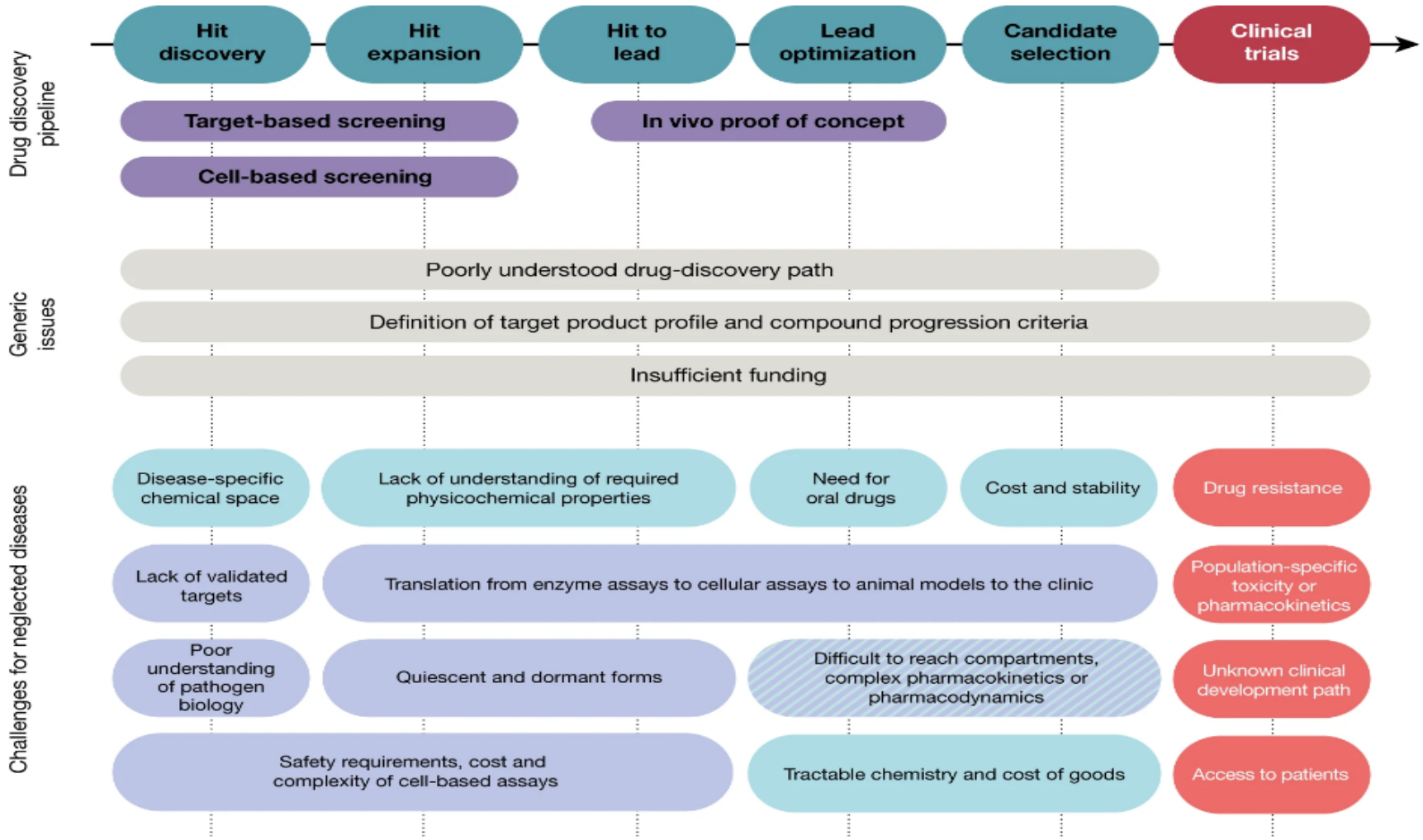

Figure 1.17 The drug-discovery process and the challenges associated at particular stages of the drug-discovery process for neglected diseases.[66]

Investigation into potential new drugs and targets for the treatment of leishmaniasis has been an active area of research in recent years. A broad range of compounds and chemical classes have been identified as potential 'hits' and 'leads', and some of them have now proceeded to clinical trials.[68] Among the most promising candidates are compounds impairing thiol dependent redox metabolism (e.g., Trypanothione), aminopyrazoles, nitroimidazole, benzoxaborole, proteosome inhibitors, nucleoside analogues, and repurposed compounds.[68,69,70]

The search for new drugs against CD using different strategies of drug design and discovery have also proven to be effective. This includes molecular simplification, privileged structures use, prodrugs, quantitative-structure activity relationship (QSAR), and molecular docking.

Molecular simplification strategy is widely applied in natural compounds and a study of indole-pyrimidine derivatives found 7-chloro-N-[3-(morpholin-4-yl)propyl]quinolin-4-amine (**20**) (**Figure 1.18**) that had great potential as candidates in lead optimization for CD.[71] **20** was the most active compound against cruzain enzyme (IC_{50} = 15 µM), the major cysteine protease of *T. cruzi*, and it was also active against *T. cruzi* (IC_{50} = 67.7 µM).

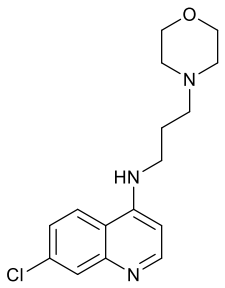

20

Figure 1.18 Structure of 7-chloro-N-[3-(morpholin-4-yl)propyl]quinolin-4-amine (**20**).[72]

Use of oral E1224 (**21**) (**Figure 1.19**) (fosravuconazole L-lysine ethanol) (a water soluble ravuconazole (**22**) prodrug-the first NCE developed for CD in decades) in combination with

benznidazole for the treatment of adults with chronic indeterminate CD has displayed improved efficacy.[73]

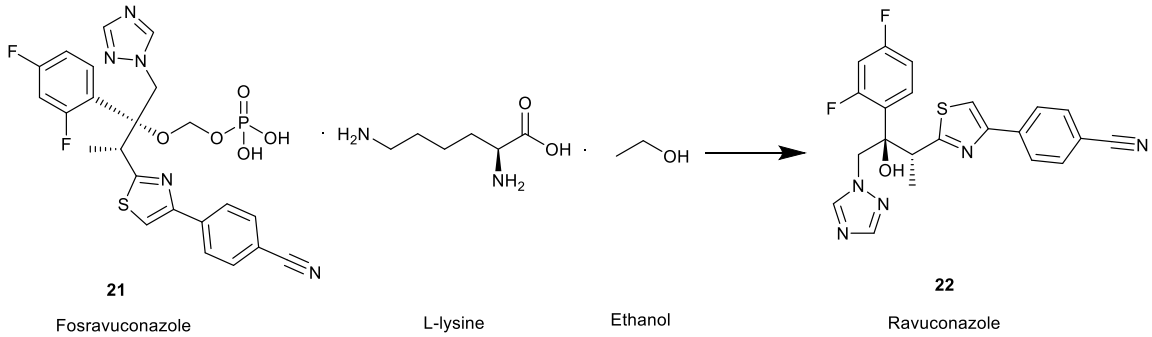

Figure 1.19 Structures of E1224 (fosravuconazole L-lysine ethanolate) (**21**). E1224 is a water soluble prodrug that is rapidly converted to ravuconazole (**22**) by alkaline phosphatases in the body.[74]

The strategy of using privileged structures to find suitable starting points in developing new therapeutics for NTDs, including CD is widely applied in the drug discovery field. Some of these promising, frequently explored scaffolds are thiosemicarbazone (**23**) and thiazolidinone (**24**) (**Figure 1.20**).[71]

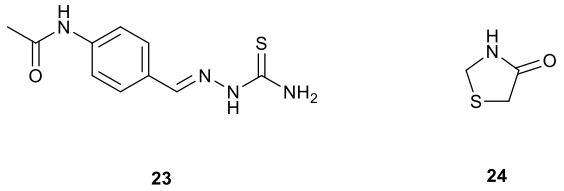

Figure 1.20 Structures of thiosemicarbazone (**23**) and thiazolidinone (**24**).

Introduction of a new drug from the beginning to public release is an expensive, high risk and a slow process. The complete process of drug development is estimated to take 10 to 17 years (**Figure 1.21**) and cost around 1.8 billion dollars.[75] Besides, the typical success rate is less than 10% and failures in late stages of clinical trials are also significant and common.[76] Some studies have focused on repurposing drugs for other diseases and adapting them to treat CD. Most of these drugs have been used in combination with benznidazole to reduce side effects, treatment time, and increase its efficacy.[59] Modifying

dose regimens and treatment times of benznidazole to increase the efficacy in different stages of the disease and to reduce side effects have also been another focus of studies. DND*i* has developed a paediatric formulation of benznidazole for infants and children up to 2 years of age in association with countries like Brazil, the USA, Argentina.[77] Therefore, drug repurposing and re-dosing for current drugs are the fastest approach to improve CD treatment. This can reduce the time and cost required to develop new therapeutics.[64,71]

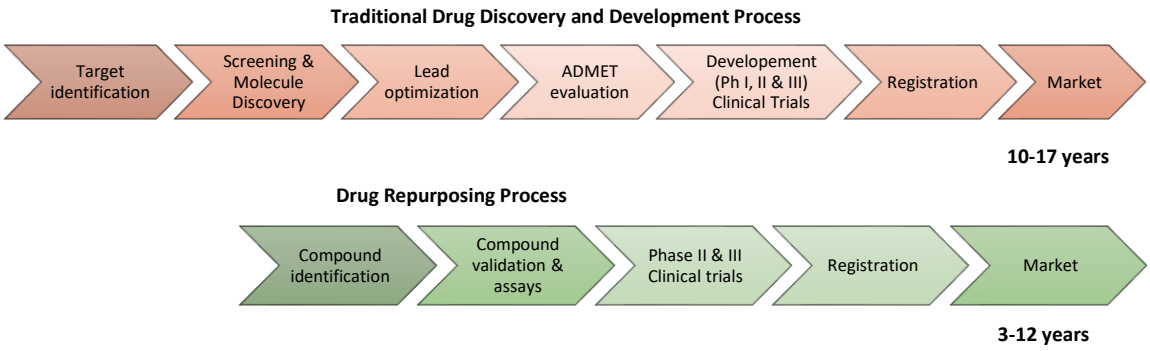

Figure 1.21 An overview of traditional drug discovery and development and drug repurposing processes.

1.12 Drug repurposing/repositioning

Drug repurposing, also known as drug repositioning, is a process of identifying new uses for approved drugs that are outside the scope of the original medical indication. This offers a shorter and faster path to reach patients since this can bypass several development phases necessary to develop a drug (**Figure 1.21**).[76] All the information about their pharmacokinetic and safety profiles are already available and it is less likely to fail at least from a safety point of view in subsequent efficacy trials. Another advantage is less investment in terms of time and money are needed since the drug has already passed preclinical phase trials.[78] It has been estimated that the cost of bringing a repurposed drug to market to be $300 million on average, and $2-3 billion for a new chemical entity.[79] Moreover, repurposed drugs may reveal new targets and pathways that can be further exploited. Therefore, the process of finding new uses for drugs outside their original indications is becoming successful. Most of the existing drugs for leishmaniasis were

repurposed from other therapeutic indications. Amphotericin B (**3**) is an antifungal agent, Paromomycin (**4**) is an antibiotic used to treat intestinal infections and Miltefosine (**5**) was originally developed as an anticancer agent.[78]

Repurposing strategies can be grouped into four major categories based on the type of chemical matter that is being repurposed, the kind of information that is typically available at the starting point and the type of optimization that is required.

1st Category; Drug repurposing

In this approach, Food and Drug Administration (FDA)- approved chemical entities for a particular treatment are used for another treatment without any further structural modifications or the optimization of the compound. Although changes in dose limits and dosing regimens may be required. As a result of all the available information profiles, both the time and cost of drug development are drastically diminished using this approach.[2]

2nd Category; Target repurposing

True target repurposing begins with a defined parasitic target with a direct, established homolog in another species (human or otherwise). The chemical entity that targets the host protein is often an approved drug or clinical candidate, which is then used as a starting point to develop compounds that inhibit the parasitic target. This requires medicinal chemistry optimization after the initial lead compound is identified, with the goals of improving selectivity for the parasite homolog as well as achieving disease modifying efficacy for the given NTD. One of the major advantages in target repurposing is that the parasitic target of the campaign is known, enabling structure-based drug design either through homology modelling or X-ray crystallography of the parasitic target, and simplifying potential mode of action studies.[2]

3rd Category; Target Class repurposing

Target Class repurposing is different from target repurposing. In this strategy, the specific parasitic target may not be known, and therefore most target class repurposing programs rely on phenotypic assays in the beginning. In the case of NTDs, the most obvious phenotype is parasite cell death or proliferation inhibition. A significant disadvantage in this as compared to target repurposing is that the specific parasitic target is not directly proven, which can obstruct optimization approaches. On the other hand, the broad range of potential targets engaged in this approach may provide more opportunity to discover a novel mechanism of action, to find a target unique to the parasite.[2]

4th Category; Lead repurposing

In contrast to the three other approaches already discussed, a lead repurposing strategy seeks to repurpose an early-stage chemical entity. Research programmes in this area typically begin with a high- throughput screen (HTS) of a class of targeted lead molecules, such as kinase or protease targeting inhibitors. However, lead repurposing has advantages over traditional (random) HTS. There is an abundance of information about the lead chemical entity that is not typically available in unbiased screens. Furthermore, lead repurposing starts with libraries of compounds specifically designed for drug-likeness and target family activity, providing better starting points as compared to unbiased library collections or natural products. Similar to target class repurposing, phenotypic assays are typically used in this category. Despite the challenges, lead repurposing campaigns have yielded some high-quality compounds and progressable chemotypes.[2]

The potential of tamoxifen (**25**) (**Figure 1.22**) as an alternative option for the treatment of leishmaniasis has been investigated in recent years.[80] Tamoxifen is a registered early-stage breast cancer drug used in the treatment of estrogen receptor positive tumours. The anti-leishmanial activity of tamoxifen was first reported in 2007 and various *in vivo* and *in vitro* studies have revealed that it is active against several species of *Leishmania*.[81] It was

tested against the promastigote form of five species of *Leishmania* (including *L. amazonensis*), and against the intracellular amastigote of *L. amazonensis*, and was shown to have promising effects on all species with micromolar IC_{50} values (IC_{50} values against *L. amazonensis* promastigotes and amastigotes; 16.40 ± 0.2 and 11.10 ± 0.2 mM, respectively). *In vivo* studies were carried out in mouse models (BALB/c) of leishmaniasis and in a 15-day treatment of *L. amazonensis* infected mice, tamoxifen reduced the parasite burden by 99% compared to untreated mice.[80] The mechanism of action in *Leishmania* was also investigated and was shown to be independent of host estrogen receptor modulation.[2,81] It is a multi-target drug interfering in distinct cell pathways, such as sphingolipid (SL) metabolism.[82] In *Leishmania*, SLs are an essential component in the cell membrane and are important mediators of cell signalling.[83,84] After treatment of *L. amazonensis* promastigotes with tamoxifen, a major disruption in the metabolism of inositolphosphorylceramides (IPCs) and phosphatidylinositols (PIs) were observed. An *in vitro* enzymatic assay showed that tamoxifen was able to inhibit the *Leishmania* IPC synthase with an IC_{50} value of 8.48 µM, suggesting that IPC synthase is most likely one of the targets in the parasites.[85] IPC is the most abundant SL in *Leishmania*, unlike mammalian cells, which synthesize sphingomyelin, and this can help achieving selective toxicity. It has been proven that tamoxifen also causes mitochondrial damage, with loss of plasma membrane potential with no disruption of its integrity.[86]

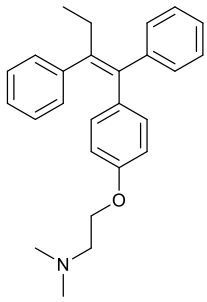

25

Figure 1.22 Chemical structure of Tamoxifen (**25**).

Additionally, a dose-dependent *T. cruzi* epimastigote growth inhibition assay resulted in 90% lysis of blood trypomastigotes after the treatment with 10 µM tamoxifen, while 86% inhibition of intracellular amastigote was obtained at 50 µM concentration. Analysing lipid extracts from treated and non-treated *T. cruzi* epimastigotes by High-performance liquid chromatography-Electrospray ionization mass spectrometry (HPLC-ESI-MS) revealed a dramatic increase in the level of ceramide and a restrained increase of sphingosine triggering apoptosis-like cell death.[87] Ceramide is metabolized to IPC (the most abundant SL in *T. cruzi*) in *T. cruzi* and other kinetoplasitid protists whereas in mammals it is mainly incorporated into sphingomyelin. In *T. cruzi*, in contrast to *Leishmania* spp., IPC functions as lipid anchor constituent of glycoproteins and free glycosylinositolphospholipids (GILPs).[88] The act of tamoxifen on the *T. cruzi* SL pathway indicate that this pathway may become a potential therapeutic target for CD.[87]

Studies on nitroheterocycles drugs, such as nimesulide (**26**) (**Figure 1.23 (A)**) and fexinidazole (**27**) (**Figure 1.23 (B)**) against *T. cruzi* have shown the potential application of these drugs in the treatment of CD. Nimesulide is a well-known non-steroidal anti-inflammatory drug that showed inhibitory effects on both the replication of amastigotes and the release of trypomastigote form of the parasite. Moreover, the effects of nimesulide and its corresponding amine (obtained by chemo selective reduction of nitro group of nimesulide) on mitochondria induce *T. cruzi* epimastigote cell death by necrosis and apoptosis.[89] Fexinidazole was registered to treat sleeping sickness in 2018 and has shown high efficacy in curing acute and chronic infections in mice models infected with different *T. cruzi* strains, including benznidazole-resistant strain.[64] Fexinidazole metabolites, fexinidazole sulfoxide and fexinidazole sulfone, effectively treated *T. cruzi* in a mouse model of acute infection, with better cure rates compared to fexinidazole itself or benznidazole.[90] DND*i*'s recent work on phase II clinical studies showed that all the patients treated with fexinidazole had early and complete T*. cruzi* clearance, which was sustained for 12 months. Some adult patients with chronic CD reported clearance within 8 days

suggesting that shorter treatment regimens and lower doses may improve safety outcomes. However, further evaluation of fexinidazole (**27**) is necessary to establish the minimum effective dose and risk-benefit relationship.[91]

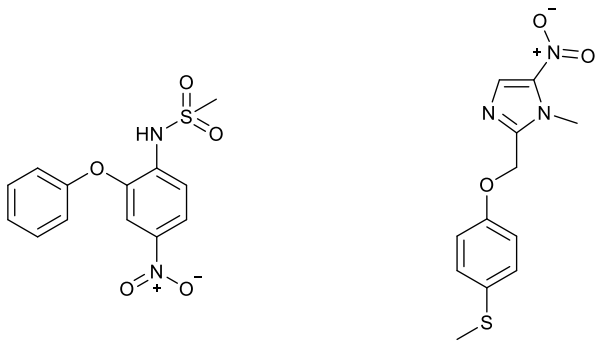

Figure 1.23 Chemical structures of Nimesulide (**26**) and Fexinidazole (**27**).

1.13 Barriers to drug repurposing

As highlighted, there have already been some notable successes for drug repurposing strategies. Nevertheless, drug repurposing does not always succeed, and many drug candidates identified via these approaches fail in phase III clinical trials. The repurposed drug may fail to confer a benefit-risk profile in clinical trials that would support approval of the new indication. Some failures in late-stage development are obviously to be expected, as with the development of completely new drugs, although these failures should be less likely to be due to toxicity because the safety profiles of the candidates were previously characterized. Even if the safety profiles are already well understood, there are other considerations that may limit the advantage of the existing knowledge of the drug. As an example, selecting the appropriate dose is critical. Thus, further studies may have to be carried out to establish a dose-response relationship. However, there are also other reasons for failure in the repurposing field related to barriers that are specific to drug repurposing, including patent considerations, regulatory considerations and organizational hurdles.[92]

1.14 Aims of the project.

Given the aforementioned reasons concerning the treatments available for leishmaniasis and CD, the main aim of this research project was to identify and/or develop novel drug candidates for the treatment of leishmaniasis and chagas disease. In particular, we focused on screening and synthesising novel molecules against parasite species and the target identification of active compounds.

A library of small, novel molecules encompassing a highly diverse chemical space synthesised by the group of Professor Stefan Bräse at the Karlsruhe Institute of Technology-KIT, Germany has been provided for evaluation. These compounds will be screened for anti-leishmanial properties with the aim of identifying novel chemical entities with activity. The long term aim here will be to identify novel drug targets (specifically entities that occupy a novel chemical space) within the target parasite species.

It has been shown that some FDA approved anti-fungal drug molecules can be repurposed to inhibit the growth of *Leishmania* species. The Cobb group has identified the anti-leishmanial activity of Pyrithione against axenic amastigotes and intracellular amastigotes of *L. mexicana* (Liam Nattrass- MChem Thesis) and the DND*i* has published data for the activity of Ciclopirox Olamine against axenic amastigotes and intracellular amastigotes of *L. donavani.*[93] With regards to continuing this work, the aim in this project it to prepare a modified compound library of Pyrithione derivatives and then to subsequently determine their anti-leishmanial activity (against *L. mexicana*), cytotoxicity, and target identification.

Two libraries of novel fluorinated aromatic compounds previously synthesised by Dr Will D.G. Brittain (Cobb group) and Prof. Graham Sandford's research group (GS group) at Durham University, UK have been selected for evaluation. The anti-leishmanial activity against *L. mexicana* will be carried out in Durham University and the biological testing associated with *T. cruzi* epimastigotes will be carried out at University of Sao Paulo, Brazil in collaboration with Professor Ariel Silber. Our aim is to discover new molecules which

are active against both parasite species and to evaluate their effect on programmed cell death in *T. cruzi* epimastigotes and *L. mexicana*.

With the aim of developing more active compounds and analysing structure activity relationship, we will synthesise a second-generation library from the active compounds (active against *L. mexicana* and *T. cruzi* parasite species) in the aforementioned fluorinated libraries. The second-generation library will be screened to determine its anti-leishmanial properties and mass spectrometry-based proteomics tools will be used for the identification studies.

1.15 References

1. National Institute of Allergy and Infectious Diseases-Neglected Tropical Diseases. https://www.niaid.nih.gov/research/neglected-tropical-diseases#:~:text=Neglected tropical diseases (NTDs)%2C,much attention as other diseases (2016).

2. Klug, D. M., Gelb, M. H. & Pollastri, M. P. Repurposing strategies for tropical disease drug discovery. *Bioorganic Med. Chem. Lett.* **26**, 2569–2576 (2016).

3. WHO | What is leishmaniasis? https://www.who.int/news-room/fact-sheets/detail/leishmaniasis (2023).

4. Ending the neglect to attain the Sustainable Development Goals: A road map for neglected tropical diseases 2021–2030. https://www.who.int/publications/i/item/9789240010352 (2021).

5. CDC - Leishmaniasis-Prevention & Control. https://www.cdc.gov/parasites/leishmaniasis/prevent.html (2020).

6. CDC - Neglected Tropical Diseases - Global NTD Programs. https://www.cdc.gov/globalhealth/ntd/global_program.html#ghi (2020).

7. CDC - Leishmaniasis. https://www.cdc.gov/parasites/leishmaniasis/ (2023).

8. Maroli, M., Feliciangeli, M. D., Bichaud, L., Charrel, R. N. & Gradoni, L. Phlebotomine sandflies and the spreading of leishmaniases and other diseases of public health concern. *Med. Vet. Entomol.* **27**, 123–147 (2013).

9. Akhoundi, M. *et al.* A Historical Overview of the Classification, Evolution, and Dispersion of Leishmania Parasites and Sandflies. *PLoS Negl. Trop. Dis.* **10**, e0004349 (2016).

10. Karunaweera, N. D. & Ferreira, M. U. Leishmaniasis: Current challenges and prospects for elimination with special focus on the South Asian region. *Parasitology* **145**, 425–429 (2018).

11. Bhattarai, N. R. *et al.* Domestic animals and epidemiology of visceral leishmaniasis, Nepal. *Emerg. Infect. Dis.* **16**, 231–237 (2010).

12. Handman, E. Cell biology of Leishmania. *Adv. Parasitol.* **44**, 1–39 (1999).

13. Sunter, J. & Gull, K. Shape, form, function and Leishmania pathogenicity: From textbook descriptions to biological understanding. *Open Biol.* **7**, 170165 (2017).

14. Wheeler, R. J., Gluenz, E. & Gull, K. Basal body multipotency and axonemal remodelling are two pathways to a 9+0 flagellum. *Nat. Commun.* **6**, 1–12 (2015).

15. Abbasi, M. *et al. Carbonic Anhydrase in Acid Acclimatization of Leishmania*. *International Congress of Cell Biology* (2018). doi:10.13140/RG.2.2.15117.26085.

16. Mann, S. *et al.* A Review of Leishmaniasis: Current Knowledge and Future Directions. *Curr. Trop. Med. Reports* **8**, 121–132 (2021).

17. CDC - Leishmaniasis - Biology. https://www.cdc.gov/parasites/leishmaniasis/biology.html (2020).

18. Souza, T. D., Turchetti, A. P., Fujiwara, R. T., Paixão, T. A. & Santos, R. L. Visceral leishmaniasis in zoo and wildlife. *Vet. Parasitol.* **200**, 233–241 (2014).

19. Alvar, J. *et al.* Leishmaniasis worldwide and global estimates of its incidence. *PLoS One* **7**, e35671 (2012).

20. Arenas, R., Torres-Guerrero, E., Quintanilla-Cedillo, M. R. & Ruiz-Esmenjaud, J. Leishmaniasis: A review. *F1000Research* **6**, 1–15 (2017).

21. Piscopo, T. V & Azzopardi, C. M. Leishmaniasis (Reprinted from vol 82, pg 649-657, 2006). *Postgrad. Med. J.* **83**, 649–657 (2007).

22. Ostad, M. *et al.* Control of cutaneous leishmaniasis using geographic information systems from 2010 to 2014 in Khuzestan Province, Iran. *PLoS One* **11**, 1–7 (2016).

23. WHO-THE GLOBAL HEALTH OBSERVATORY-Map data. https://www.who.int/data/gho/map-gallery-search-results?&maptopics=910b5dfc-ce2e-4440-8b43-8d83f4a85485 (2023).

24. About Leishmaniasis – DNDi. https://www.dndi.org/diseases-projects/leishmaniasis/ (2020).

25. WHO-factsheets. https://www.who.int/news-room/fact-sheets/detail/leishmaniasis (2023).

26. Kedzierski, L., Zhu, Y. & Handman, E. Leishmania vaccines: Progress and problems. *Parasitology* **133**, S87–S112 (2006).

27. Murray, H. W., Berman, J. D., Davies, C. R. & Saravia, N. G. Advances in leishmaniasis. *Lancet* **366**, 1561–1577 (2005).

28. Alexander, B. & Maroli, M. Control of phlebotomine sandflies. *Med. Vet. Entomol.* **17**, 1–18 (2003).

29. Carvalho, G. M. L., Filho, J. D. A., Falcão, A. L., Rocha Lima, A. C. V. M. & Gontijo, C. M. F. Naturally infected Lutzomyia sand flies in a Leishmania-endemic area of Brazil. *Vector-Borne Zoonotic Dis.* **8**, 407–414 (2008).

30. Reinhold-Castro, K. R. *et al.* Impact of control measures and dynamics of sand flies in southern Brazil. *J. Vector Ecol.* **38**, 63–68 (2013).

31. Ready, P. D. Leishmaniasis emergence in Europe. *Euro Surveill.* **15**, 29–39 (2010).

32. Reed, S. G. & Campos-Neto, A. Vaccines for parasitic and bacterial diseases. *Curr. Opin. Immunol.* **15**, 456–460 (2003).

33. Samant, M. *et al.* Immunization with the DNA-Encoding N-Terminal Domain of Proteophosphoglycan of Leishmania donovani Generates Th1-Type Immunoprotective Response against Experimental Visceral Leishmaniasis . *J. Immunol.* **183**, 470–479 (2009).

34. Kumar, A. & Samant, M. DNA vaccine against visceral leishmaniasis: A promising approach for prevention and control. *Parasite Immunol.* **38**, 273–281 (2016).

35. Nogueira, F. S. *et al.* Leishmune® vaccine blocks the transmission of canine visceral leishmaniasis: Absence of Leishmania parasites in blood, skin and lymph nodes of vaccinated exposed dogs. *Vaccine* **23**, 4805–4810 (2005).

36. Ouellette, M., Drummelsmith, J. & Papadopoulou, B. Leishmaniasis: Drugs in the clinic, resistance and new developments. *Drug Resist. Updat.* **7**, 257–266 (2004).

37. Sundar, S. *et al.* Amphotericin B Treatment for Indian Visceral Leishmaniasis: Conventional versus Lipid Formulations. *Clin. Infect. Dis.* **38**, 377–383 (2004).

38. Nagle, A. S. *et al.* Recent developments in drug discovery for leishmaniasis and

human african trypanosomiasis. *Chem. Rev.* **114**, 11305–11347 (2014).

39. MO, H. *et al.* Who is a typical patient with visceral leishmaniasis? Characterizing the demographic and nutritional profile of patients in Brazil, East Africa, and South Asia. *Trans. R. Soc. Trop. Med. Hyg.* **86**, 615–616 (1992).

40. Musa, A. *et al.* Sodium stibogluconate (ssg) & paromomycin combination compared to ssg for visceral leishmaniasis in east africa: A randomised controlled trial. *PLoS Negl. Trop. Dis.* **6**, e1674 (2012).

41. Singh, N., Kumar, M. & Singh, R. K. Leishmaniasis: Current status of available drugs and new potential drug targets. *Asian Pac. J. Trop. Med.* **5**, 485–497 (2012).

42. Sundar, S. Drug resistance in Indian visceral leishmaniasis.[Erratum appears in Trop Med Int Health 2002 Mar;7(3):293]. *Trop. Med. Int. Heal.* **6**, 849–854 (2001).

43. Andrade-Neto, V. V. *et al.* Leishmaniasis treatment: Update of possibilities for drug repurposing. *Front. Biosci. - Landmark* **23**, 967–996 (2018).

44. Kamiński, D. M. Recent progress in the study of the interactions of amphotericin B with cholesterol and ergosterol in lipid environments. *Eur. Biophys. J.* **43**, 453–467 (2014).

45. Sundar, S. *et al.* Efficacy of miltefosine in the treatment of visceral leishmaniasis in India after a decade of use. *Clin. Infect. Dis.* **55**, 543–550 (2012).

46. Paris, C., Loiseau, P. M., Bories, C. & Bréard, J. Miltefosine Induces Apoptosis-Like Death in Leishmania donovani Promastigotes. *Antimicrob. Agents Chemother.* **48**, 852–859 (2004).

47. Pérez-Victoria, F. J., Castanys, S. & Gamarro, F. Leishmania donovani resistance to miltefosine involves a defective inward translocation of the drug. *Antimicrob. Agents Chemother.* **47**, 2397–2403 (2003).

48. Chagas disease-CDC. https://www.cdc.gov/parasites/chagas/ (2022).

49. About Chagas disease-DNDi. https://dndi.org/diseases/chagas/facts/ (2020).

50. Mansoldo, F. R. P. *et al.* Chagas Disease: Perspectives on the Past and Present and Challenges in Drug Discovery. *Molecules* **25**, 1–14 (2020).

51. Chatelain, E. Chagas disease drug discovery: Toward a new era. *J. Biomol. Screen.* **20**, 22–35 (2015).

52. Onyekwelu, K. C. Life Cycle of Trypanosoma cruzi in the Invertebrate and the Vertebrate Hosts. in *Biology of Trypanosoma cruzi* (ed. Souza, W. De) 1–19 (IntechOpen, 2019). doi:DOI: 10.5772/intechopen.84639.

53. Martín-Escolano, J. *et al.* An Updated View of the Trypanosoma cruzi Life Cycle: Intervention Points for an Effective Treatment. *ACS Infect. Dis.* **8**, 1107–1115 (2022).

54. Global distribution of Chagas disease, based on official estimates, 2018. https://www.who.int/docs/default-source/ntds/chagas-disease/chagas-2018-cases.pdf (2018).

55. Soiza, R. L., Donaldson, A. I. C. & Myint, P. K. Vaccine against arteriosclerosis: an update. *Ther. Adv. Vaccines* **9**, 259–261 (2018).

56. Lidani, K. C. F. *et al.* Chagas disease: From discovery to a worldwide health

problem. *J. Phys. Oceanogr.* **49**, 1–13 (2019).

57. WHO. Chagas disease. https://www.who.int/news-room/fact-sheets/detail/chagas-disease-(american-trypanosomiasis) (2023).

58. Ribeiro, A. L., Nunes, M. P., Teixeira, M. M. & Rocha, M. O. C. Diagnosis and management of Chagas disease and cardiomyopathy. *Nat. Rev. Cardiol.* **9**, 576–589 (2012).

59. Francisco, A. F. *et al.* Challenges in Chagas Disease Drug Development. *Molecules* **25**, 1–14 (2020).

60. Hall, B. S. & Wilkinson, S. R. Activation of benznidazole by trypanosomal type I nitroreductases results in glyoxal formation. *Antimicrob. Agents Chemother.* **56**, 115–123 (2012).

61. Hall, B. S., Bot, C. & Wilkinson, S. R. Nifurtimox activation by trypanosomal type I nitroreductases generates cytotoxic nitrile metabolites. *J. Biol. Chem.* **286**, 13088–13095 (2011).

62. Sánchez-Valdéz, F. J., Padilla, A., Wang, W., Orr, D. & Tarleton, R. L. Spontaneous dormancy protects trypanosoma cruzi during extended drug exposure. *Elife* **7**, 1–20 (2018).

63. Weng, H. B., Chen, H. X. & Wang, M. W. Innovation in neglected tropical disease drug discovery and development. *Infect. Dis. Poverty* **7**, 1–9 (2018).

64. García-Huertas, P. & Cardona-Castro, N. Advances in the treatment of Chagas disease: Promising new drugs, plants and targets. *Biomed. Pharmacother.* **142**, 112020 (2021).

65. Kotz, J. Phenotypic screening, take two. *Sci. Exch.* **5**, 380–380 (2012).

66. De Rycker, M., Baragaña, B., Duce, S. L. & Gilbert, I. H. Challenges and recent progress in drug discovery for tropical diseases. *Nature* **559**, 498–506 (2018).

67. G. Wyatt, P., H. Gilbert, I., D. Read, K. & H. Fairlamb, A. Target Validation: Linking Target and Chemical Properties to Desired Product Profile. *Curr. Top. Med. Chem.* **11**, 1275–1283 (2011).

68. Olías-molero, A. I., de la Fuente, C., Cuquerella, M., Torrado, J. J. & Alunda, J. M. Antileishmanial drug discovery and development: Time to reset the model? *Microorganisms* **9**, 1–18 (2021).

69. Brindha, J., Balamurali, M. M. & Chanda, K. An Overview on the Therapeutics of Neglected Infectious Diseases—Leishmaniasis and Chagas Diseases. *Front. Chem.* **9**, 1–19 (2021).

70. Van Bocxlaer, K. *et al.* Novel benzoxaborole, nitroimidazole and aminopyrazoles with activity against experimental cutaneous leishmaniasis. *Int. J. Parasitol. Drugs Drug Resist.* **11**, 129–138 (2019).

71. Cristovão-Silva, A. C., Brelaz-De-Castro, M. C. A., Lima Leite, A. C., Alves Pereira, V. R. & Hernandes, M. Z. Chagas Disease Treatment and Rational Drug Discovery: A Challenge That Remains. *Front. Pharmacol.* **10**, 1–6 (2019).

72. Braga, S. F. P. *et al.* Synthesis and biological evaluation of potential inhibitors of the cysteine proteases cruzain and rhodesain designed by molecular simplification. *Bioorganic Med. Chem.* **25**, 1889–1900 (2017).

73. Torrico, F. *et al.* Treatment of adult chronic indeterminate Chagas disease : proof-

of-concept randomized placebo-controlled study of benznidazole and three E1224 dosing regimens. *Lancet. Infect. Dis.* **18**, 419–430 (2022).

74. Hata, K. Development of E1224 by leveraging a strategic partnership for the medicines creation against neglected tropical diseases. *Parasitol. Int.* **81**, 102278 (2021).

75. Paul, S. M. *et al.* How to improve RD productivity: The pharmaceutical industry's grand challenge. *Nat. Rev. Drug Discov.* **9**, 203–214 (2010).

76. Charlton, R. L., Rossi-Bergmann, B., Denny, P. W. & Steel, P. G. Repurposing as a strategy for the discovery of new anti-leishmanials: The-state-of-the-art. *Parasitology* **145**, 219–236 (2018).

77. DNDi. R&D portfolio. https://dndi.org/research-development/portfolio/ (2022).

78. Braga, S. S. Multi-target drugs active against leishmaniasis: A paradigm of drug repurposing. *Eur. J. Med. Chem.* **183**, 111660 (2019).

79. Pushpakom, S. *et al.* Drug repurposing: Progress, challenges and recommendations. *Nat. Rev. Drug Discov.* **18**, 41–58 (2018).

80. Miguel, D. C., Yokoyama-Yasunaka, J. K. U. & Uliana, S. R. B. Tamoxifen is effective in the treatment of Leishmania amazonensis infections in mice. *PLoS Negl. Trop. Dis.* **2**, e249 (2008).

81. Miguel, D. C., Yokoyama-Yasunaka, J. K. U., Andreoli, W. K., Mortara, R. A. & Uliana, S. R. B. Tamoxifen is effective against Leishmania and induces a rapid alkalinization of parasitophorous vacuoles harbouring Leishmania (Leishmania) amazonensis amastigotes. *J. Antimicrob. Chemother.* **60**, 526–534 (2007).

82. Morada, S. A. F. & Cabot, M. C. Tamoxifen regulation of sphingolipid metabolism—therapeutic implications. *Biochim Biophys Acta. 2015 Sept.* **1851**, 1134–1145 (2015).

83. Zewdie, K. A., Hailu, H. G., Ayza, M. A. & Tesfaye, B. A. Antileishmanial Activity of Tamoxifen by Targeting Sphingolipid Metabolism: A Review. *Clin. Pharmacol. Adv. Appl.* **14**, 11–17 (2022).

84. Denny, P. W., Goulding, D., Ferguson, M. A. & Smith, D. F. Sphingolipid-free Leishmania are defective in membrane trafficking, differentiation and infectivity. *Mol. Microbiol.* **52**, 313–327 (2004).

85. Trinconi, C. T. *et al.* Tamoxifen inhibits the biosynthesis of inositolphosphorylceramide in Leishmania. *Int. J. Parasitol. Drugs Drug Resist.* **8**, 475–487 (2018).

86. Reimão, J. Q. & Uliana, S. R. B. Tamoxifen alters cell membrane properties in Leishmania amazonensis promastigotes. *Parasitol. Open* **4**, 4–9 (2018).

87. Landoni, M. *et al.* Tamoxifen acts on Trypanosoma cruzi sphingolipid pathway triggering an apoptotic death process. *Biochem. Biophys. Res. Commun.* **516**, 934–940 (2019).

88. De Lederkremer, R. M., Agusti, R. & Docampo, R. Inositolphosphoceramide metabolism in Trypanosoma cruzi as compared with other trypanosomatids. *J. Eukaryot. Microbiol.* **58**, 79–87 (2011).

89. Trindade, J. D. A. S., Freire-De-Lima, C. G., Côrte-Real, S., Decote-Ricardo, D. & Freire de Lima, M. E. Drug repurposing for Chagas disease: In vitro assessment of nimesulide against Trypanosoma cruzi and insights on its mechanisms of

action. *PLoS One* **16**, 1–15 (2021).

90. Bahia, M. T. *et al.* Antitrypanosomal activity of fexinidazole metabolites, potential new drug candidates for Chagas disease. *Antimicrob. Agents Chemother.* **58**, 4362–4370 (2014).

91. Torrico, F. *et al.* A Phase 2, Randomized, Multicenter, Placebo-Controlled, Proof-of-Concept Trial of Oral Fexinidazole in Adults With Chronic Indeterminate Chagas Disease. *Clin. Infect. Dis.* **76**, e1186–e1194 (2023).

92. Breckenridge, A. & Jacob, R. Overcoming the legal and regulatory barriers to drug repurposing. *Nat. Rev. Drug Discov.* **18**, 1–2 (2018).

93. Kaiser, M. *et al.* Antiprotozoal activity profiling of approved drugs: A starting point toward drug repositioning. *PLoS One* **10**, 1–16 (2015).

2 Phenotypic screening of a novel library of compounds.

2.1 High-Throughput Screening (HTS) screening in drug discovery

High-Throughput Screening (HTS) is a well-established technique in drug discovery that has gained widespread popularity over the last couple of decades and has become a standard method for lead discovery in the pharmaceutical industry. Increasingly, it is also being used for basic and applied research in academia. In simple terms, HTS is a process of screening and assaying a large number of chemical libraries against selected and specific biological targets.[1] HTS assay principles and methods are used for screening of combinatorial chemistry, genomics, protein, and peptide libraries that are often composed of hundreds of thousands of potential drug candidates. HTS techniques help to accelerate the drug discovery process by screening large compound libraries at a rate that may exceed a few thousand compounds per day or per week. Speed is of vital importance, because parallel and combinatorial chemical synthesis methods, availability of various compound collections from commercial sources, have significantly increased the size of novel compound collections. A successful HTS consists of several steps such as target identification, reagent preparation, compound management, assay development and high-throughput library screening. Primary screening of compound libraries is less quantitative than biological assays. Often, compounds are tested with a molar concentration ranging as low as 1-10 micromolar for combinatorial chemistry synthesis. If a positive result or a “HIT” is discovered in such a test, a more accurate and precise secondary screening is conducted and calculations of EC_{50}/IC_{50} values are performed. Secondary screening is performed by means of adopted biological and biochemical assays.[2,3] Assays are typically one of two types either heterogeneous or homogeneous. Heterogeneous assays consist of five steps such as filtration, centrifugation, fluid addition, incubation and reading while homogeneous assay consists of the latter three steps. HTS are frequently performed using

miniaturized cell-based assays enabling chemical libraries to be screened for molecules that present different biological activities.[2,3,4] Identified ‘‘HIT’’ molecules are used as starting points for medicinal chemistry optimization during drug discovery and development.

Nowadays, high-density arrays of micro reaction wells are gaining popularity in pharmaceutical analysis and drug discovery.[5] During the Initial stage of HTS in 1990s, 96-well microtiter plates (MTPs) were used in compound screening, now this format is being replaced by higher density alternatives - 384 well (typical working volume of about 50µL per well) and 1586-well (typical working volume of about 5µL per well) MTPs. Further studies towards miniaturization are still ongoing and several examples of 3456-well MTPs (typical working volume of about 1-2 µL per well) have been reported.[6] However, the use of ultra-low volume reactions seem to affect the surface to volume ratio resulting in occasional consequences on reagent absorption and stability.[1,6] Overall, HTS is playing an important role in early stage of drug development, providing qualitative and quantitative characterization of compound libraries and analytical support for preclinical and clinical absorption, distribution, metabolism, and excretion (ADME) studies. Given this latter point, HTS can also facilitate the early elimination of unsuitable compounds from a given compound library.[5]

Natural products have long been a rich source of lead molecules within drug discovery. They often possess exquisite potency, and frequently have mechanistic specificity and biological compatibility and as they often have high molecular weights, numerous hetero atoms and complex structures enabling them to display advanced binding characteristics.[4] However, often natural products have to be removed from a HTS, because of their required purity, availability and behaviour in the automated liquid handling systems (consistency and viscosity of the extracts) mean they do not fulfil the requirements for them to be considered developable ‘HIT’s. Furthermore, few natural products are entering

clinical trials as research in this area has been scaled back or even discontinued in many pharma companies because of the high cost associated with it.[7]

2.2 Phenotypic drug discovery

In the past when molecular target information was limited or unknown, phenotypic screening was the foundation in drug discovery. Then, in the past three decades, target-based screening, in which the starting point is a defined molecular target, has been the dominant approach to drug discovery in the pharmaceutical industry. However, phenotypic screening is now re-established in the industry and academia as an approach to discover novel drug targets, pathways and ‘‘HIT and lead’’ molecules.[8] This includes testing a molecule in cells, isolated tissues or organs, or animals to see whether it exerts the desired effects and the actual mechanism, its target, is often determined later. Analysis of the discovery strategies and the molecular mechanisms of action (MMOAs) for new molecular entities that were approved by The United States Food and Drug Administration (FDA) between 1999 and 2008 by Swinney and Anthony revealed that 75 of 269 agents approved were first-in-class drugs with new MMOAs.[9] Of these, 28 (56%) were discovered through phenotypic screening and 17 (34%) were discovered through target-based methods (5 out of 75 (10%) were discovered based on natural substrate or natural substance). This showed that the contribution of phenotypic screening to the discovery of first-in-class small molecule drugs exceeded that of target-based approach and phenotypic drug discovery (PDD), and has been recently recognised by various scientists as a potential solution to the discerned poor productivity of target-based drug discovery (TDD).[9] Moreover, recent advances in various technologies for cell-based phenotypic screening such as induced pluripotent stem (iPS), CRISPR-Cas, organoids and imaging assays have enabled the development of novel cell-based models that can realistically recapitulate human disease biology.[10]

The concept of HTS techniques to identify novel chemical scaffolds with biological activity by screening vast number of chemical libraries has been applied in this project. The scale

of the screening process is considerably smaller compared to “true” drug discovery platforms, but we tried to keep the libraries evaluated as diverse as possible, with regards to chemical space. In this chapter (and in later ones, Chapters 3. 4 and 5) we have implemented a phenotypic screening method to evaluate the biological activity of novel chemical libraries with the purpose of discovering privileged scaffolds for the early stage of drug discovery process.

2.3 Application of PDD in drug discovery for leishmaniasis

As discussed in the Chapter 1, many of the drugs in use for all forms of leishmaniasis have major drawbacks, including severe side effects for the patients and emerging drug resistance. Therefore, new drugs or formulations are urgently needed. For the purpose of anti-leishmanial drug discovery, many different phenotypic assays, using either promastigotes, axenic amastigotes or intracellular amastigotes, have been developed to screen random/novel compound collections to identify leads that are active against *Leishmania* spp.[11] This screening strategy has been largely a practical endeavour in pharmaceutical industry for many years. Phenotypic screening assays use free-living parasites to assess the effect of compounds on cell viability. The main advantage of this assay format is that it allows a fast and easy screening of large compound collections required for the successful identification of developable HITs.[3] A weak HIT, (pyrazolopyrimidine-3) (**28**) from a phenotypic screening against *L. donovani* axenic amastigotes, albeit with no activity against intracellular parasites, was subjected to lead optimization, identifying GSK3186899/DDD853651(**30**), a preclinical candidate for the treatment of visceral leishmaniasis (VL) (**Figure 2.1**). Subsequently, Cdc2-related kinase 12 (CRK12) was identified as the principal target of GSK3186899/DDD853651(**30**), although this was unknown during the lead optimization.[12,13]

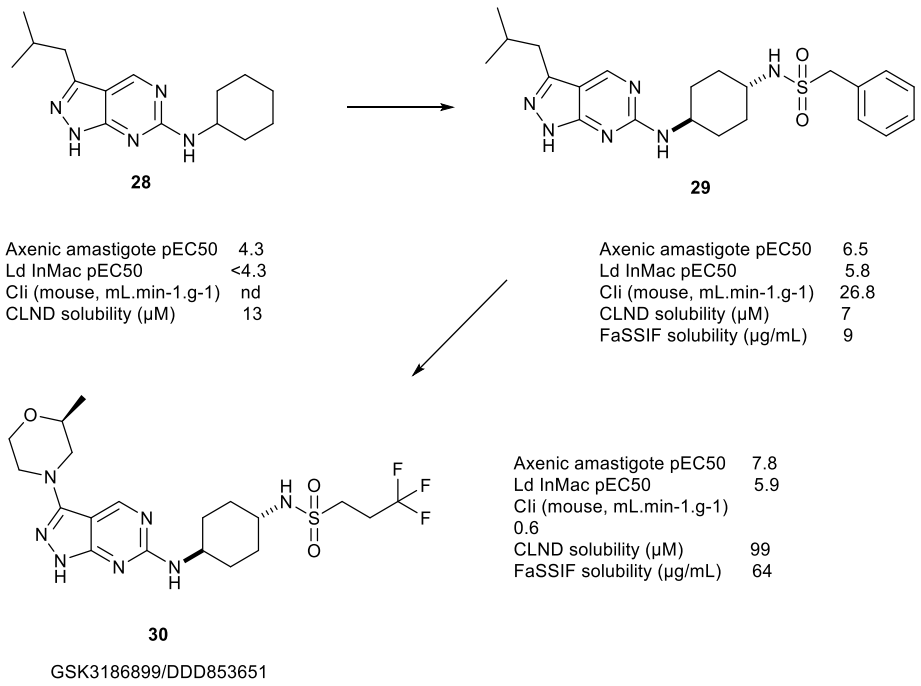

Figure 2.1 Lead optimization of pyrazolopyrimidine (**28**) to develop GSK3186899/ DDD853651 (**30**).

Jair L. Siqueira-Neto et.al., adapted an *in vitro* fluorometric assay (Alamar Blue®) to an HTS format to screen a library containing 26,500 structurally diverse chemical compounds at 10 µM against *L. major* promastigotes and a cut-off of 70% growth inhibition and identified 567 active compounds (**Figure 2.2**).[14]

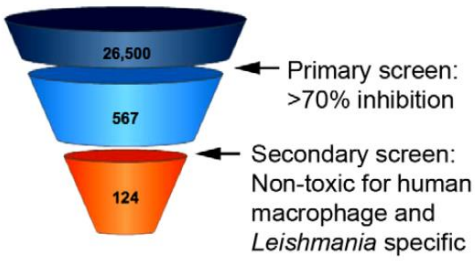

Figure 2.2 Antileishmanial HTS with 26,500 compounds. A funnel representing selection of antileishmanial activity from 26,500 compounds to 124 HIT compounds after primary screening and secondary screening.[14]

To exclude potentially toxic compounds from the active compounds list, a secondary screening using non-differentiated human macrophage cell line THP-1 was performed. To

confirm the activity of the resultant 124 compounds from the secondary screening, activity against the intracellular parasites (THP-1 macrophages infected with *L. major* amastigotes) was tested and this has led to the final selection of the two most active compounds, CH872 (**31**) and CA272 (**32**) (**Figure 2.3**) with EC_{50} <10 µM, for further characterization.[14]

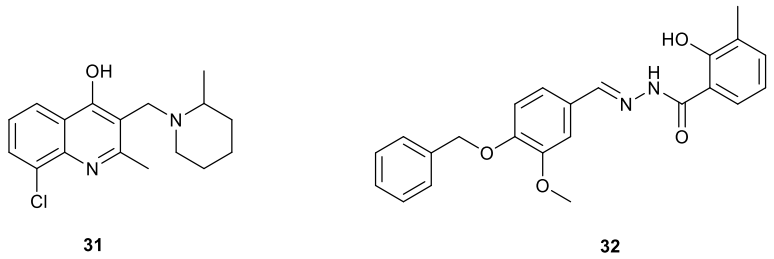

Figure 2.3 Chemical structures of CH872 (**31**) and CA272 (**32**).[14]

Ortiz and co-workers conducted a screening of 60,000 small molecules for growth inhibition against the promastigote form of the parasites of *L. mexicana* and identified 2,703 compounds that inhibit the growth by over 65% at a single point concentration of 10 µM.[15] The selected compounds were then subjected to intra-macrophage amastigote assays and cytotoxicity assays with normal human fibroblasts cells (BJ cells), which revealed nine unique chemical scaffolds with high potency. Two of the compounds (**33** and **34**) proved to be orally effective in a murine model of cutaneous leishmaniasis (CL) infected with *L. mexicana* (**Figure 2.4**). However, they were not as effective as the current treatment Miltefosine (**6**).[15] Observations from HTS assays of two step phenotypic screening strategy suggest that medicinal chemistry optimisation of these novel scaffolds to generate a substantial number of structural analogues for further structure-activity relationship (SAR) and structure-property relationship (SPR) analysis could lead to promising candidates for anti-parasitic treatments.

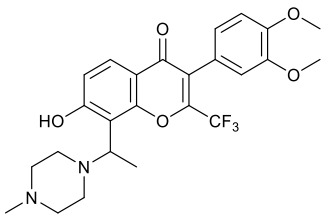

33

L. mexicana =0.08 ± 0.01 μM
L. donovani = 0.6 ± 0.5 μM

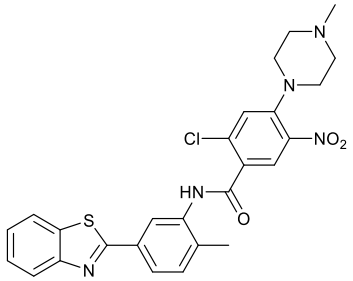

34

L. mexicana =0.022 ± 0.003 μM
L. donovani = 0.029 ± 0.027 μM

Figure 2.4 Structures and EC_{50} values (against intracellular amastigotes) of orally effective compounds against a murine model of cutaneous leishmaniasis.
33; 3-(3,4-dimethoxyphenyl)-7-hydroxy-8-(1-(4-methylpiperazin-1-yl)ethyl)-2-(trifluoromethyl)-4H-chromen-4-one.
34; N-(5-(benzo[d]thiazol-2-yl)-2-methylphenyl)-2-chloro-4-(4-methylpiperazin-1-yl)-5-nitrobenzamide.

Additionally, in a similar application of whole-cell phenotypic assay, a 1.8 million GlaxoSmithKline (GSK) compound collection was screened against *L. donovani*, *T. cruzi* and *T. brucei* between October 2012 and May 2014, identifying non-cytotoxic, anti-parasitic compounds; 351, 500 and 700 respectively.[16] A secondary screen using *L. donovani* LdBob-infected THP-1 cells has identified 192 with anti-leishmanial activity that are now known as 'Leish-Box'. In 2019, S. Lamotte et al., applied an improved, *ex vivo* assay to evaluate anti-leishmanial activity of 188 compounds from the 'Leish-Box', using bone marrow-derived macrophages infected with lesion derived amastigotes of viscerotropic *L. donovani* Ld1S or dermotropic *L. amazonensis* LV79 strains.[17] 20 HITs were identified with the most potent activity against the intracellular stage of both species being recorded at 10 μM, thus offering promising candidates for further lead development. Five compounds which showed EC_{50} values ranging between 0.48 - 6.88 μM against *L. donovani* are shown in **Table 2.1**.[17] It is worth noting that not all the 'Leish-Box' HITs identified in the previous study are active in the *ex vivo* assay. The use of avirulent parasites that fail in establishing an effective intracellular infection and the use of immortalized host cells with intrinsic anti-apoptotic properties ultimately can result false

positive HITs that fail in subsequent pre-clinical trials. Physiologically more relevant *ex vivo* assays implemented in here can likely overcome this problem.[17]

Entry No.	Compounds	Selectivity	Structure
1	TCMDC-143163 EC_{50} (*L. donovani* Am): 0.79µM EC_{50} (BMDM); >10µM	>10	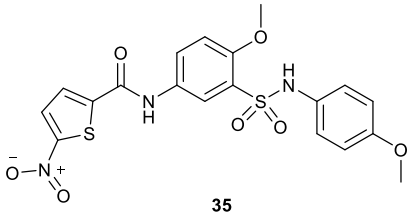 **35**
2	TCMDC-143169 EC_{50} (*L. donovani* Am): 6.88 µM EC_{50} (BMDM); >10µM	>1.5	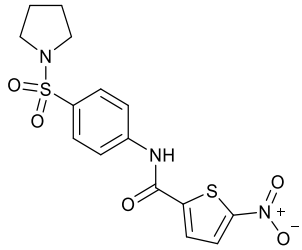 **36**
3	TCMDC-143295 EC_{50} (*L. donovani* Am): 0.48 µM EC_{50} (BMDM); >10µM	>10	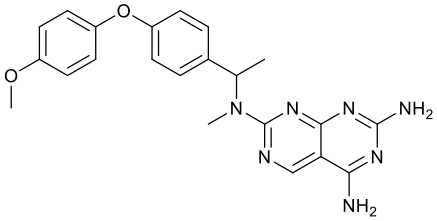 **37**
4	TCMDC-143563 EC_{50} (*L. donovani* Am): 0.59 µM EC_{50} (BMDM); >6.25 µM	>10	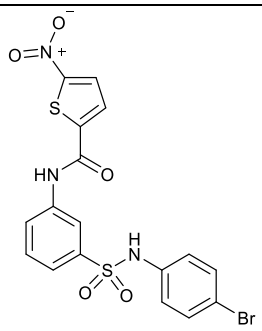 **38**
5	TCMDC-143577 EC_{50} (*L. donovani* Am): 1.25 µM EC_{50} (BMDM); >5.09 µM	4.7	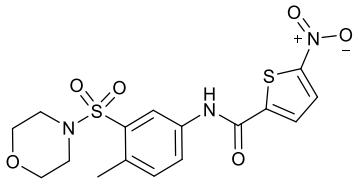 **39**

Table 2.1 'Five' HIT compounds active on both *L. donovani* and *L. amazonensis* intramacrophage amastigotes. Chemical structures, EC_{50}s for anti-parasitic activity against *L. donovani* and toxicity against macrophages, selectivity index. BMDM-bone marrow-derived macrophages.

2.4 Assay development and validation

The phenotypic drug discovery approach has been implemented throughout this project to identify active compounds from the diverse chemical libraries screened. All the test compounds were screened against *L. mexicana* promastigotes and axenic amastigotes using an Alamar Blue® fluorescence assay. To validate parasite cell concentrations and incubation time periods used in the inhibition assay protocols, two separate experiments were designed. Detailed protocols can be found in **Chapter 7** (**Section 7.4.6**). Briefly, two 96 well microtiter plates were set up for each *L. mexicana* parasite stage, four in total, with cell concentration ranging from 1.562×10^4 to 2×10^6 cells/mL in triplicates. Two different incubation arrangements were evaluated along with Alamar Blue® addition (10% v/v).

1. 20 hr + 4 hr incubation after addition of Alamar Blue® (total 24 hrs)
2. 44 hr + 4 hr incubation after addition of Alamar Blue® (total 48 hrs)

Plates with *L. mexicana* promastigotes were incubated at 26 ºC and for axenic amastigotes, incubation temperature was 33 ºC. The fluorescence measurements (at 590 nm) were taken after the incubation intervals previously mentioned and Microsoft Excel was used to analyse the readings, calculate correlation (R^2) values and plot the graphs (**Figure 2.5**).

Graphs **A** and **B** (**Figure 2.5**) indicate the two different incubation periods (24 hrs and 48 hrs) of *L. mexicana* promastigotes at different cell concentrations.

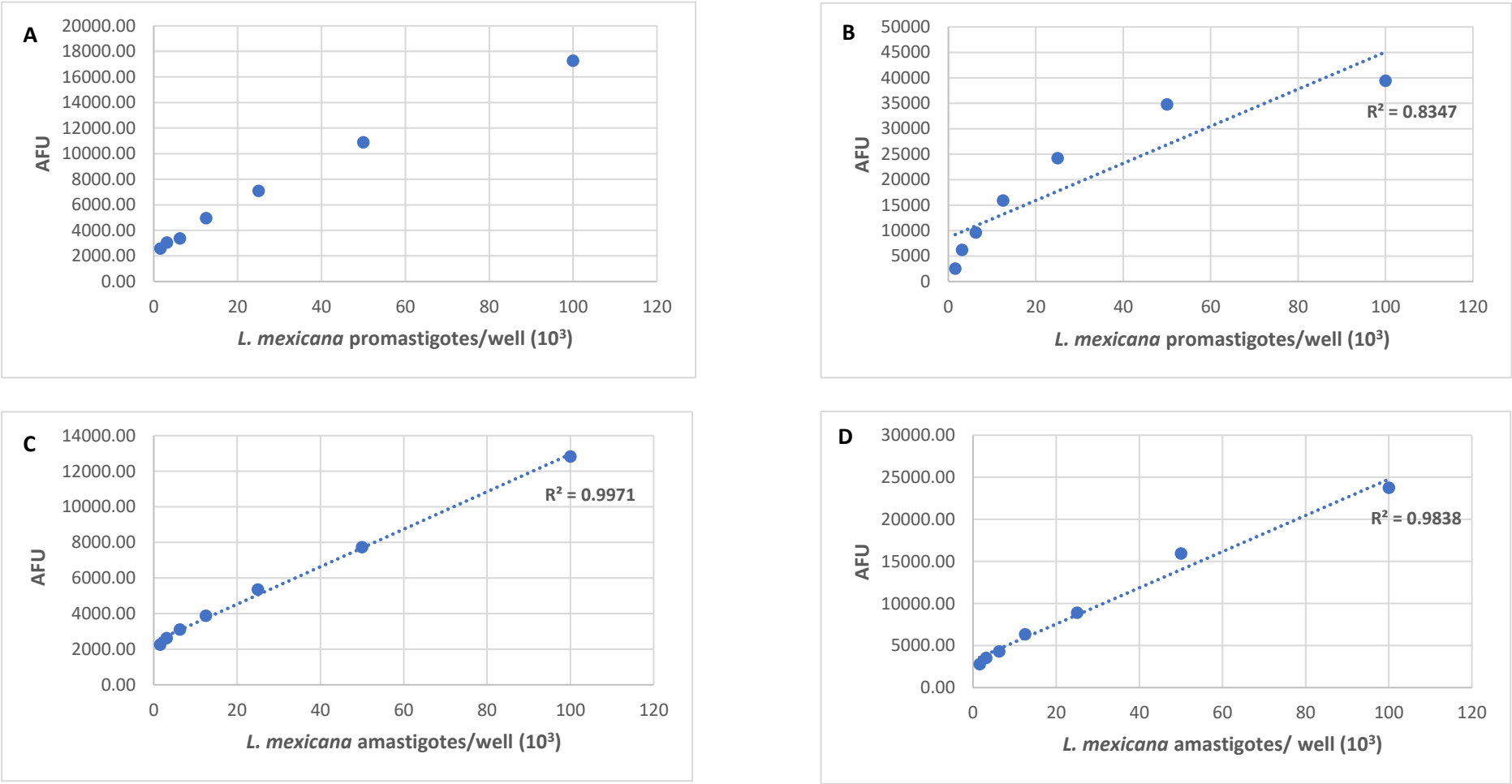

Figure 2.5 Alamar Blue® fluorescence assay validation for *L. mexicana.* Assay conditions; (A) *L. mexicana* promastigotes, 24 hr incubation, 26 ºC; (B) *L. mexicana* promastigotes, 48 hr incubation, 26 ºC; (C) *L. mexicana* amastigotes, 24 hr incubation, 33 ºC; (D) *L. mexicana* amastigotes, 48 hr incubation, 32 ºC.

As shown in the graph **A** (**Figure 2.5**), 1×10^6 cells/mL (1×10^5 cells/well) cell concentration is in the linear range with a 0.992 correlation, proving the incubation time frame (24 hr) and the cell concentration in the protocol will generate accurate results. Regarding the second incubation period tested for promastigotes, graph **B** shows that 1×10^6 cells/mL (1×10^5 cells/well) and 5×10^5 cells/mL (50×10^3 cells/well) cell concentrations deviate from the linearity. This indicates that a lower cell concentration or a shorter incubation period must be adopted in order to achieve better accuracy. Graph **C** and **D** (**Figure 2.5**) represent *L. mexicana* axenic amastigotes validation and have shown positive linear correlations in both graphs (0.997 and 0.983 respectively). Therefore, 1×10^6 cells/mL (1×10^5 cells/well) cell concentration and 48 hr incubation conditions were validated as in the standard protocol.

Alamar Blue® has been widely used over the past 50 years for research on cell viability and cytotoxicity. Alamar Blue® assays monitor the reducing activity of living cells to quantitatively determine cell viability via a fluorescent or colorimetric detection technique. Resazurin is the main active ingredient in Alamar Blue®, which is water soluble (stable in culture medium), non-toxic, cell permeable, and weakly fluorescent blue dye. This enters the living cells and irreversibly reduced to a pink coloured, highly fluorescent (λ_{em} 590 nm), resorufin by accepting electrons from nicotinamide adenine dinucleotide phosphate (NADPH), flavine adenine dinucleotide (FADH), flavin mononucleotide (FMNH) as well as from the cytochromes (**Figure 2.6**). Resazurin was first used in 1992 to assess bacterial or yeast contamination in milk by Pesch and Simmert.[18,19]

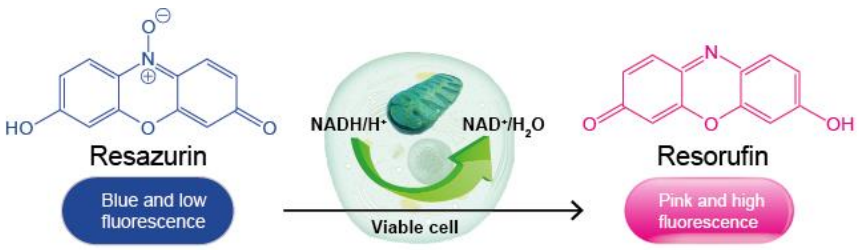

Figure 2.6 Reduction of Alamar Blue® in metabolically active cells; resazurin to resorufin[20]

2.5 Evaluation of the anti-leishmanial activity of a small, diverse chemical library against *Leishmania mexicana*

The concept of 'chemical space' is broadly used in drug discovery due to its numerous potential applications. For instance; in library design, compound or dataset classification, compound selection, exploration of SAR and SPR in general.[21] Chemical space is often defined as the 3D space that encompasses all the possible organic molecules.[22] Given the vastness of the chemical space now explored, the challenge for chemical biologists and drug discoverers is to identify those regions that are likely to contain the biological activity, that is, biologically relevant chemical space.[23] The chemical space of drug-like molecules, following Lipinski's rule of five, has been estimated to be in excess of 10^{60} molecules.[24] The diverse, novel compound library screened in this chapter was synthesised and provided by Professor Stefan Braise's research group at Karlsruhe Institute of Technology - Germany. The compound library consists of 53 compounds in total that could be sub-divided in to five distinct classes (Class One to Five) depending on their core structures and their anti-leishmanial activity was analysed using the SAR method.

2.5.1 Class One - Library screening

The first Class of compounds that were evaluated are built on a core of 9,10-phenanthrenedione scaffold (**Figure 2.7**).

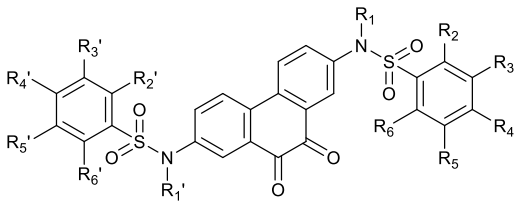

Figure 2.7 Structure of Class One compounds.

Initial testing of compounds involved a phenotypic screening against *L. mexicana* promastigotes and axenic amastigotes in an Alamar Blue® assay. All compounds in the

library were initially first screened at a fixed concentration of 50 µM, to avoid the off-target activity of the compound. With the intension of saving both time and resources, compounds which killed more than 50% of the cell population were selected to calculate EC_{50} and compounds with poor activity were eliminated without progressing them to EC_{50} determination. The preliminary screening protocol used is detailed in Chapter 7 (**Section 7.4.7**). Briefly, as per the assay validation discussed above, 200 µL of $1x10^6$ cells/mL *L. mexicana* promastigotes and axenic amastigotes were treated with the test compounds in triplicate for 20 hrs and 44 hrs respectively at a 50 µM concentration. Amphotericin B (**5**) and Dimethyl Sulfoxide (DMSO); which used to prepare 10 mM stock solutions of all the compounds were added to the plate as positive and negative controls. In addition, incorporating wells containing just media allowed the correction of background fluorescence. Next 20 µL of Alamar Blue® (10% v/v) was added to each well followed by another 4 hr incubation at 26 ºC and 33 ºC temperatures respectively. Cell viability was then calculated by measuring the intensity of fluorescence emitted from resorufin dye (at 590 nm) at the end of 4 hr incubation and analysing absorbance values using Microsoft excel.

The detailed experimental protocol for the inhibition (dose-response) assay and EC_{50} calculations can be found in Chapter 7 (**Section 7.4.8**). However, the only difference from the primary assay is instead of a fixed 50 µM concentration, a three-fold serial dilution of the test compound was carried out from 50 µM to 23 nM and incubated with the parasites. Finally, the intensity of fluorescence emitted from resorufin dye (at 590 nm) was measured and GraphPad Prism software was used to evaluate the data, calculate EC_{50} values and 95% Confidence interval (CI) level for each compound. The 95% CI is a range of values which in which we can be 95% certain that the true mean of the population lies. The best candidates with promising activities were subjected to cytotoxicity assays followed by infected macrophage assays.

Cytotoxicity assays were carried out at the Karlsruhe Institute of Technology (Germany) using HeLa cells – MTT assay (**Table 2.2**). Cytotoxicity assays assess the safety profile of the drug candidate during the non-clinical and clinical research phase of drug discovery and development. The method proves beneficial in identifying off target effects of drug candidates on the human body. HeLa cells were seeded in a 96 well microtiter plate at 1×10^4 cells/mL and incubated for 24 hrs before they were treated with various concentrations of the compounds, followed by a washing step to remove the medium. Triton X-100 (1%) was added as a positive control. The cells were incubated for further 72 hrs and thereafter, 15 µL of MTT reagent were added to the wells. The cells were lysed using the stop solution after 3 hr incubation with MTT to release the formazan. The cell viability was determined by measuring the absorbance of the resulting formazan at 595 nm using a multi-well plate reader. MTT assay is a colorimetric assay that measures cell viability in terms of reductive activity of an enzymatic conversion of the tetrazolium component (MTT) into water insoluble formazan crystals by NADH-dependent oxidoreductase enzymes (**Figure 2.8**). MTT is taken up through endocytosis and is reduced by mitochondrial enzymes as well as endosomal/lysosomal compartments, and then transported to cell surfaces to form MTT formazan crystals. In the MTT assay, MTT reagent was incubated with cells for approximately 3 hrs, followed by addition of stop/solubilization solution (DMSO or acidified ethanol solution, or a solution of the sodium dodecyl sulphate in diluted hydrochloric acid) to lyse the cells and solubilize the purple coloured crystals. The absorbance can be measured between 500 - 600 nm wavelength. The amount of colour produced is directly proportional to the number of viable cells.[25,26] A more detailed protocol for the cytotoxicity assay is given in Chapter 7 (**Section 7.4.9**).

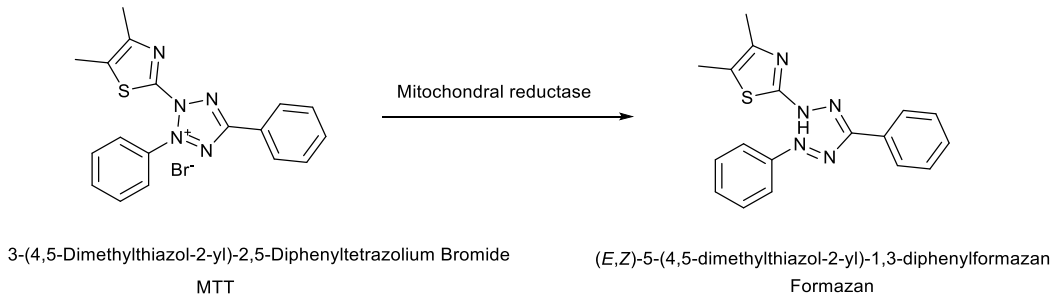

Figure 2.8 Enzymatic reaction of MTT converting to formazan.

Intramacrophage assays can be used to determine the ability of compounds to inhibit the growth of parasites proliferating inside macrophages. Murine macrophages (RAW 264.7) were selected for the intramacrophage assay since *Leishmania* amastigotes naturally proliferate inside macrophages during their life cycle. RAW 264.7 cells were seeded at 2.5×10^5 cells/mL and incubated 24 hrs before they were infected with 2.5×10^5 *L. mexicana* amastigotes. After another 24 hrs of incubation infected cells were treated with compounds in 2-fold dilutions from 100 µM to 0.781 µM. Then the cells were treated with 0.05% SDS followed by series of washing steps precisely described in **Chapter 7**. After 44 hrs incubation, the cell viability reagent Alamar Blue® was added to each well and further incubated for 4 hrs at 26 °C before fluorescence were measured.

Most of the compounds that were screened against *L. mexicana* axenic stages were found to have EC_{50} values lower than 10 µM (**Table 2.2**) and all the compounds subjected to intramacrophage assay showed decreased activities compared to that reported against the axenic amastigotes. From Class One, compound **40** (**Table 2.2, Entry 1**) is the most effective with an activity of 0.213 µM against *L. mexicana* axenic amastigotes and it was also able to retain its activity against infected macrophages with an EC_{50} of 3.12 µM activity. Compounds **43, 44, 46** and **47** (**Table 2.2, Entry 4, 5, 7 and 8**) are also worth highlighting because they also have EC_{50} values of less than 1 µM against the axenic amastigotes.

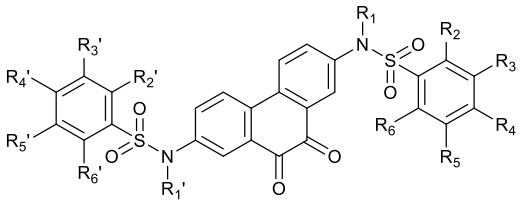

Entry no	Compound no.	X number	$R^1/R^{1'}$	$R^2/R^{2'}$	$R^3/R^{3'}$	$R^4/R^{4'}$	$R^5/R^{5'}$	$R^6/R^{6'}$	EC_{50} (*L. mexicana* axenic amastigotes) [µM]	EC_{50} (*L. mexicana* promastigotes) [µM]	CC_{50} (HeLa cells) [µM]	*L. mexicana* Intramacrophage amastigotes	
												EC_{50} [µM]	95% CI
1	**40**	X5747	H	H	H	H	*OCH_3*	H	0.213	9.02	6.00	3.12	2.15-4.64
2	**41**	X4119	H	OCH_3	H	H	*OCH_3*	H	9.01	n.a.	6.00	-	-
3	**42**	X4118	H	H	H	OCH_3	*OCH_3*	H	n.a.	n.a.	7.00	-	-
4	**43**	X4101	H	*CH_3*	H	CH_3	H	CH_3	0.227	0.746	20.0	35.1	19.3-63.7
5	**44**	X4111	H	*CH_3*	H	CH_3	H	H	0.354	4.14	1.00	>50.0	(Very wide)
6	**45**	X4117	H	*OCH_3*	H	OCH_3	H	H	n.a.	n.a.	>50.0	-	-
7	**46**	X5746	CH_3	H	H	*OCH_3*	H	H	0.369	9.02	16.0	7.37	5.12-10.6
8	**47**	X499	H	H	H	*OCF_3*	H	H	0.518	n.a.	5.00	>100	(Very wide)
9	**48**	X4109	H	H	H	*CH_3*	H	H	1.01	0.561	1.00	1.12	0.782-1.62
10	**49**	X4133	H	H	H	*F*	H	H	1.29	18.1	5.00	14.2	8.11-25.1
11	**50**	X5743	H	H	H	*OCH_3*	H	H	1.61	n.a.	1.00	28.3	20.3-39.5
12	**51**	X5211	H	H	H	*OCH_3*	H	H	21.2	n.a.	1.00	-	-
13	**52**	X4150	H	H	H	*$COCH_3$*	H	H	n.a.	n.a.	>50.0	-	-
14	**53**	X4103	H	H	H	*$NHCOCH_3$*	H	H	n.a.	n.a.	>50.0	-	-
15	**54**	X5752	H	H	H	*OH*	H	H	n.a.	n.a.	7.00	-	-
16	**55**	X4149	H	-N-S-N-		H	H	H	1.81	n.a.	6.00	-	-

Table 2.2 Structure and results of **Class One** compounds, including EC_{50} values against *Leishmania mexicana* axenic amastigotes, promastigotes, HeLa cells and intracellular macrophages/ infected Raw 264.7 cells. (n.a.- compounds which showed more than 50% cell viability at 50 µM concentrations, X number- in-house compound label given by KIT) Associated 95% Confidence Intervals for intramacrophage amastigotes are given in the last column.

Compounds **40** (**Table 2.2, Entry 1**) and **50** (**Table 2.2, Entry 11**) both have one methoxy group present on the aromatic rings. In **40** the methoxy group is (R^3 and $R^{3'}$) in *meta* position and in **50** it is in the *para* position. This difference looks to be important as it cause a ~10-fold difference in EC_{50} values seen against axenic amastigotes and intracellular amastigotes (1.61 µM and 28.3 µM respectively). Compounds **41**, **42** and **45** (**Table 2.2, Entry 2, 3, and 6**) all have two methoxy groups on the aromatic rings but only **41** (**Table 2.2, Entry 2**) is active: 9.01 µM against axenic amastigotes. Therefore, by looking at the chemical structures and activities of these compounds it can be suggested that both the number of methoxy groups and their position on the aromatic ring can affect the biological activity seen for the Class One compounds against the parasites.

Compounds **43** (**Table 2.2, Entry 4**) and **44** (**Table 2.2, Entry 5**) have methyl groups on their aromatic rings in the *ortho* and *para* positions. Here, the compound with three methyl groups, **43** has a slightly better EC_{50} value; 0.227 µM compared to **44;** 0.354 µM. But both seem to have no activity against intracellular stages (with >30 µM EC_{50} values). Moreover, higher cytotoxicity has been observed against HeLa cells compared to the infected stage. Based on the core structure and the hypothesized mechanisms, the type of subunits (electron donating and electron withdrawing groups) on the aromatic rings could also affect the biological activity. As an example, compound **49** (**Table 2.2, Entry 10**) has a fluorine attached to its para position showing 1.29 µM and compound **54** (**Table 2.2, Entry 15**) has a hydroxyl group in the same position with no activity.

Additionally, it is clearly noticeable that even though some promising activities were discovered against *L. mexicana* axenic amastigotes, most of these compounds have higher toxicity values against HeLa cells which makes them challenging to take further in drug discovery process without necessary structural optimizations. Compounds **40** (**Table 2.2 Entry 1**) and **46** (**Table 2.2, Entry 7**) found to have CC_{50} values of 6.00 µM, 16.0 µM respectively against HeLa cells.

Selectivity index (SI) is defined as the ratio of cytotoxicity (HeLa) to the EC_{50} of *Leishmania* spp. amastigotes [$CC_{50(HeLa)}/EC_{50(L.\ mexicana\ \text{intracellular amastigotes})}$]. Lenta et al. stated that SI values higher than 10 suggest a better safety of a product for use in mammalian hosts and is generally considered that biological efficacy is not due to *in vitro* cytotoxicity.[27] Considering the EC_{50} values of **40** and **46** against intracellular amastigotes (EC_{50} = 3.12 µM, 7.37 µM) and their SI values (SI; 1.92 and 2.17) the possibility of pursuing further studies on these compounds are very low. However, the cytotoxicity assay in this chapter needs to be performed again using Raw 264.7 cells, in order to obtain consistent SI values with the intracellular EC_{50} values reported.

2.5.2 Class One – Potential mode of action and further development

Several 9,10-phenanthrenediones and their derivatives have been previously identified as reversible inhibitors of CD45-mediated *p*-nitrophenyl phosphate (pNPP) hydrolysis and four of them were listed in **Table 2.3**.[28] Inhibition of CD-45 could be therapeutically useful in the treatment of diabetes and obesity. *In vitro* inhibitory activity of these compounds against the cytosolic portion of CD45 was evaluated initially using *p*NPP as the substrate and observing *p*-nitrophenol release.[29]

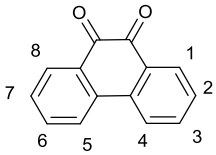

Entry no	Compound no	Substitution	Position of attachment	pNPP IC_{50} µM	Prolif. IC_{50} µM	CC_{50} µM
1	**56**	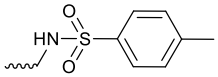	2	1.0 ± 0.0	6.4 ± 2.1	>30
2	**57**	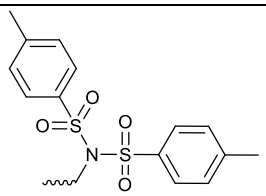	2	12.9 ± 1.2	0.8 ± 0.7	5.3 ± 1.6
3	**58**	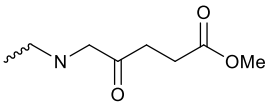	2,7	0.5 ± 0.2	1.1 ± 0.4	7.0 ± 1.0
4	**59**	-	-	0.7 ± 0.1	0.3 ± 0.2	1.3 ± 0.5

Table 2.3 *In vitro* activity of selected phenanthrenediones against CD45. Inhibition concentrations of pNPP hydrolysis, T cell proliferation and cytotoxicity were recorded.

CD45 belongs to the family of transmembrane protein tyrosine phosphatases (PTPs) that are expressed exclusively by hematopoietic cells. It plays a crucial role in T-cell receptor (TCR) mediated signalling by regulating the phosphorylation and the activity of src-family protein tyrosine kinase (PTKs) and their substrates.[28] Approximately, 100 PTPs are known so far and more than 500 gene products of human genome containing at least one phosphatase domain has been identified (these could map to 101 genes).[30] Protein tyrosine phosphorylation and dephosphorylation regulate multiple crucial processes in higher eukaryotic cells, including cellular phenotypic functions, differentiation, proliferation, and cell growth.[31] Protein phosphorylation patterns in *Leishmania* parasites and related trypanosomatids has shown to vary during differentiation associated with different life cycle stages, suggesting the role of protein kinases and phosphatases. Characterization of *Leishmania* PTP1 genes with the human PTP1B (hPTP1B) gene revealed that *Leishmania* PTP1 share close to 40% sequence identity with human PTP1B, including a number of important conserved amino acid residues within the hPTP1B signature catalytic

domain. To see if *Leishmania* PTP1 in amastigotes has therapeutic potential and represents a realistic drug target, *in silico* homology modelling was performed to compare the three-dimensional structures of the *L. infatum* PTP with the hPTP1B (**Figure 2.9**). The results obtained displayed that the active sites of the two proteins are similar, however, there are significant differences in residues further away from active site. For example, *L. infatum* enzyme has a proline residue at position 67 and the human enzyme has an arginine. Furthermore, residue 205 in the *L. infatum* sequence is a glutamine, whereas in all human tyrosine phosphates there is a phenylalanine residue at that position. These variations affect hydrophobicity of the substrate-binding pocket and may provide scope for designing an inhibitor that is more specific to *L. infatum* enzyme than to the human homologs.[32]

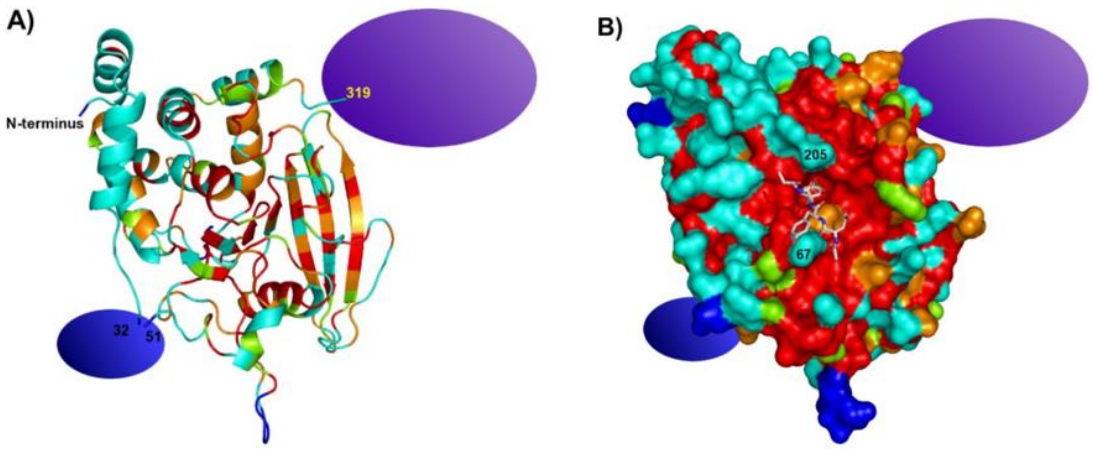

Figure 2.9 3-D homology model for the structure of *L. infatum* PTP1. **A)** the homology model is shown as a cartoon representation, highlighting -helices, -standards, and loops. Red represents identical residues, orange represents conserved substitutions, green represents semi-conversed substitutions, turquoise represents positional conservations and blue represents no conservation. Residues 32-52 and 319-493 could not be modelled, therefore schematically represented by ovals. The residues 32-51 that are present in the *Leishmania* sequence but not the human sequence is coloured blue, and the oval that represents the residues 319-493 that are present in both enzyme sequences but were not present in the structure of the human enzyme is colour mauve. **B)** Molecular surface representation of A with the same colour scheme used in A. The active site is shown occupied by the monophosphorylates peptide substrate from the human PTP1B peptide complex, which is represented by a stick model coloured by atom type as follows: white, carbon; blue, nitrogen; red, oxygen; yellow, phosphorous. Proline 67 and glutamine 205 residues which may affect substrate preference are also indicated.[32]

The proposed mechanism of action for the inhibition of CD45 by 9,10-phenanthrenediones is that the active site cysteine of the CD45 enzyme attacks a carbonyl of the dione, rendering the enzyme catalytically inactive (**Figure 2.10**). It is hypothesised that when the hemi thioketal is flanked by a vicinal carbonyl group, as it is in the proposed covalent inhibitor-enzyme abduct, a thiophosphate ester transition state is mimicked. [28] It is possible that the anti-parasitic compounds identified in the Class One library are exerting their mode of action via this type of mechanism.

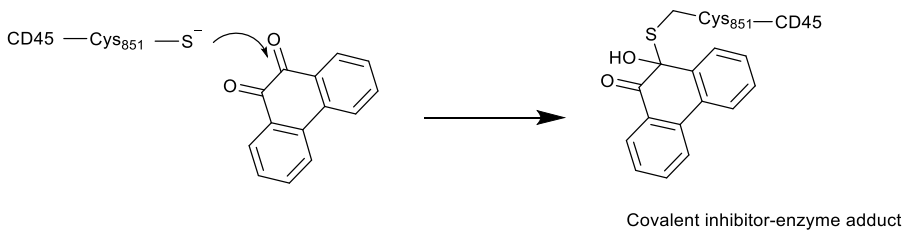

Figure 2.10 Hypothesized inhibitory mechanism of Dione based molecules against CD45.

There are pharmacokinetic principles accepted by researchers as one of the main evaluation parameters for the drug-likeness of any virtually screened molecules. This concept is used to ensure the efficacy of compounds in the drug discovery process. The standard used in this project is known as the 'Lipinski's Rule of 5' and it was developed in 1997. Considering orally active drugs, Lipinski's rule state that a drug-like compound must have molecular weight (MW) ≤ 500 Da, logarithm of the n-octanol/water partition coefficient (log P) ≤ 5, number of hydrogen bond donors (HBD) ≤ 5 and hydrogen bond acceptors (HBA) ≤ 10.[33,34] However, there are FDA approved drugs which violate one or two rules in the Lipinski's rule of 5 parameters.[35] Nearly after 20 years after creating Rule of 5, Lipinski has published another article discussing the applicability of his rule stating that the parameters initially proposed can still be used as a filter in candidate selection and small changes in one or another property may allow the discovery of novel drug-like compounds.[36]

Although most of these compounds in Class One have promising EC_{50} values, it should be noted that none are compliant with Lipinski's rule of five (**Table 2.4**). Though each compound in Class One has a molar mass greater than 500 g/mol, some of them still have log *P* values within the accepted range of Lipinski's rule of five. Log *P* is the measure of the lipophilicity of a drug, and it indicates its ability to cross a cellular membrane. Although the log *P* alone does not provide information regarding absorption, it characterizes the lipophilic-hydrophilic balance of a drug and supports the screening for their biological properties.[37] An up to date molecular mass cut off based on the properties of orally available small molecules approved in the past decade found to be more than 600Da.[38] Hence, for some test molecules, there is still a possibility of developing as drug molecules.

Entry no	Compound number	Lipinski's rule of five	Molar Mass g/mol	log *P*	H bond donor count	H bond acceptor count
1	**40**	×	578.61	3.57	2	8
2	**41**	×	638.66	3.26	2	10
3	**42**	×	638.66	3.26	2	10
4	**43**	×	602.72	6.97	2	6
5	**44**	×	574.67	5.94	2	6
6	**45**	×	638.66	3.26	2	10
7	**46**	×	606.66	4.02	0	8
8	**47**	×	686.55	6.75	2	8
9	**48**	×	546.61	4.92	2	6
10	**49**	×	554.54	4.17	2	6
11	**50**	×	578.61	3.57	2	8
12	**51**	×	578.61	3.57	2	8
13	**52**	×	602.63	3.00	2	8
14	**53**	×	632.66	2.63	4	8
15	**54**	×	550.56	3.28	4	8
16	**55**	×	634.67	4.18	2	10

Table 2.4 Physical properties of the **Class One** compounds (i.e., a molecule with a molecular mass less than 500 Da, no more than 5 hydrogen bond donors, no more than 10 hydrogen bond acceptors, and partition coefficient log *P* not greater than 5). Physical properties were calculated using ChemAxon online service https://chemicalize.com/welcome.

2.5.3 Class Two – Library screening

Phenanthrolines, are polycyclic aromatic hydrocarbons present in sterols, sex hormones, cardiac glycosides, bile acids, and morphine alkaloids. There are a wide range of biological and physiological activities shown by phenanthroline derivatives, such as antibacterial, antifungal and antitumor activities, thus the synthesis of new compounds containing a phenanthroline core is currently an interesting area for drug development.[39] Due to its ability to coordinate many metal ions, 1,10-phenanthroline (phen) (**Figure 2.11**) and its derivatives are frequently used as ligands for catalysis and as heterocyclic ligands for a large number of metal complexes.[40]

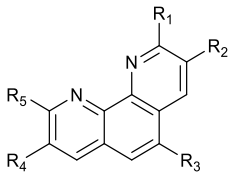

Figure 2.11 Core structure of the Class Two compound library - 1,10-phenanthroline.

All the Class Two compounds followed the same screening procedure as previously described for the Class One compounds. Effective concentrations calculated for the 1, 10-phenanthrolines (**Figure 2.11**) are reported in **Table 2.5**. From the screening results it was shown that compounds **64** (**Table 2.5, Entry 5**) and **60** (**Table 2.5, Entry 1**) are the most active; 0.174 µM and 0.561 µM against *L. mexicana* axenic amastigotes. It is also interesting to note that five out of eight of the compounds assayed were active against the axenic amastigotes with EC_{50} values of less than 10µM.

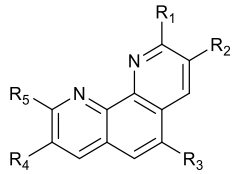

Entry no.	Compound No.	X number	R^1	R^2	R^3	R^4	R^5	EC_{50} (*L. mexicana* axenic amastigotes) [µM]	EC_{50} (*L. mexicana* promastigotes) [µM]	CC_{50} (HeLa cells) [µM]	*L. mexicana* Intramacrophage amastigotes	
											EC_{50} [µM]	95% CI
1	**60**	X6150	CH_2CH_2CCH	H	H	H	CH_3	0.561	0.726	12.0	4.86	2.98-7.91
2	**61**	X3009	H	H	*tert-butyl (2-amino-2-oxoethyl) carbamate*	H	H	4.17	20.2	25.0	-	-
3	**62**	X8019	H	Br	H	Br	H	n.a.	n.a.	-	-	-
4	**63**	X7628	H	H	*Br*	H	H	6.53	1.45	10.0	-	-
5	**64**	X9266	H	H	NH_2	H	H	0.174	10.2	10.0	3.27	1.55-6.87
6	**65**	X9580	*CHO*	H	H	H	*CHO*	n.a.	n.a.	34.0	-	-
7	**66**	X8581	CH_2OH	H	H	H	CH_2OH	n.a.	n.a.	>50.0	-	-
8	**67**	X11228	H	H	NO_2	H	H	1.83	2.10	17.0	-	-

Table 2.5 Structure and results of **Class Two** compounds, including EC_{50} values against *Leishmania mexicana* axenic amastigotes, promastigotes, HeLa cells and intracellular macrophages/ infected Raw 264.7 cells. (n.a.- compounds which showed more than 50% cell viability at 50 µM concentrations, X number- in-house compound label given by KIT) Associated 95% Confidence Intervals for intramacrophage amastigotes are given in the last column.

Furthermore, **64** (**Table 2.5, Entry 5**) and **60** (**Table 2.5, Entry 1**) managed to maintain their activity against infected macrophages reporting > 5μM activities. By assessing the SI values of **64** and **60** (2.46 and 3.05 respectively), they need further structural optimizations to reduce cytotoxicity. However, as mentioned above, cytotoxicity assays need to be carried out against Raw 264.7 cells to more accurately determine and comment on the SI of these two compounds. Physiochemical properties of the compounds from Class Two are given in **Table 2.6**. All of the compounds fulfil the criteria of Lipinski's rule of five proving the drug likeness properties necessary for orally available small molecules.

Entry no.	Compound number	Lipinski's rule of five	Molar Mass g/mol	log *P*	H bond donor count	H bond acceptor count
1	**60**	✓	246.31	4.18	0	2
2	**61**	✓	352.39	2.09	2	4
3	**62**	✓	338.00	3.82	0	2
4	**63**	✓	259.10	3.05	0	2
5	**64**	✓	195.22	1.46	1	3
6	**65**	✓	236.23	3.06	0	4
7	**66**	✓	240.26	0.91	2	4
8	**67**	✓	225.20	2.22	0	4

Table 2.6 Physical properties of the **Class Two** compounds fall within Lipinski's rule of five (i.e., a molecule with a molecular mass less than 500 Da, no more than 5 hydrogen bond donors, no more than 10 hydrogen bond acceptors, and partition coefficient log *P* not greater than 5). Physical properties were calculated using ChemAxon online service https://chemicalize.com/welcome.

2.5.4 Class Two – Potential mode of action and future development

1,10-phenanthrolines play an important role in medicinal applications by functioning as chemical/artificial nucleases and therapeutic agents due to their ability to bind or interact with the DNA molecules. For instance, Copper (II) ph-phen complex (**68**) (**Figure 2.12**) has displayed broad-spectrum activity against cancer cell lines; human derived breast, prostate, colon and ovarian and the ability to cleave DNA through the generation of free radicals.[41] Furthermore, pronounced antibacterial activity of mixed ligand Cu(II) complexes

of Benzoyltrifluoroacetone (BTAH) with 1,10-phenanthroline (e.g. [*Cu(BTA)(Phen)Cl*] (**69**), **Figure 2.12**) against *Staphylococcus aureus*, *Bacillus subtilis* and *Pseudomonas aeruginosa* has been reported by Omoregie et al. in 2021.[42]

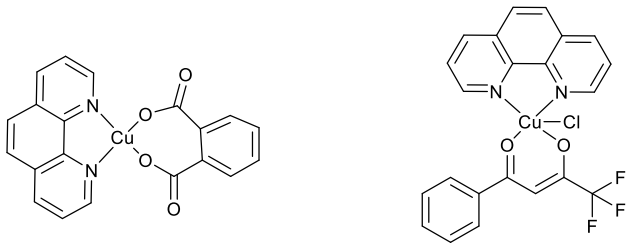

68 **69**

Figure 2.12 Structures of [Cu(ph)(phen)].2H_2O (**68**) and [Cu(BTA)(Phen)Cl] (**69**).

There were two distinct mechanisms published in 2012 to explain DNA-cleavage of these metal complexes.[41] First one is oxidative scission of deoxyribose residues through redox chemistry (**Figure 2.13**) and the second way is by hydrolysing the phosphodiester sugar backbone.[16]

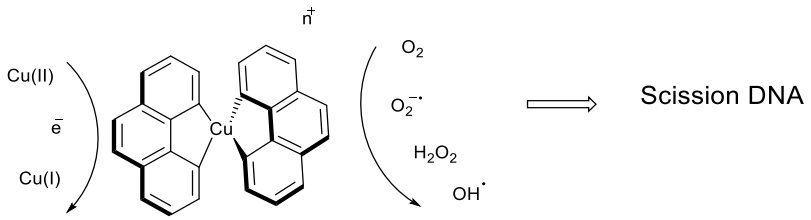

Figure 2.13 Generation of reactive oxygen species and DNA scission by complex $[Cu(phen)_2]^{2+}$.

Given this it is also possible that the mode of action for the Class Two compounds relate to their metal chelation properties. *Leishmania* parasites are capable of altering phagocyte biology through virulence factors such as lipophosphoglycan (LPG) and zinc metalloprotease GP63, both of which are prominent at the promastigote stage.[43] GP63 is down regulated in amastigotes but this might be compensated by the absence of LPG on the amastigote surface, where GP63 is no longer buried in LPG and can therefore play an

important role in the ability of amastigotes to modulate the host response despite of its lower numbers compared to promastigotes.[43,44] However, the role of GP63 in amastigotes is still subject to discussion. Nevertheless, evidence supports the role of GP63 in enabling the survival of parasites inside the macrophage.[45] GP63 cleaves proteins involved in the regulation of phagocyte functions; altered cell signalling, lipid metabolism, subversion of transcription and translation. Duque et al. used 1,10-phenanthroline-mediated chelation of Zn^{2+} ions to effectively inhibit degradation of Syt XI; a recycling endosome-and lysosome associated protein, by GP63 in *Leishmania* promastigotes. Zn^{2+} ions are critical for GP63 function.[46]

Previously, it was reported that 1,10-phenanthroline reduced the *in vitro* proliferation of *L. braziliensis* promastigotes in a dose- and time- dependant manner, as well as the association index to murine macrophages.[47]

2.5.5 Class Three - Library screening

There was no previously published biological data for any of the Class Three, Four or Five. compounds. Our screening found that most of the compounds in the Class Three series were, in general, inactive against *L. mexicana* parasites (**Table 2.7**). Compounds **77**, **78** and **79** (**Table 2.7, Entry 8, 9, and 10**) were the only compounds with activity in this Class. **77** (**Table 2.7, Entry 8**) is effective against only *L. mexicana* promastigotes; with an EC_{50} = 3.38 µM while **78** and **79** is effectual against both promastigote and axenic amastigote stages.

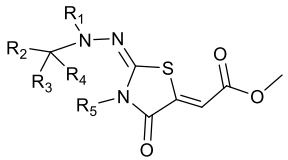

Entry no.	Compound No.	X number	R^1	R^2	R^3	R^4	R^5	EC_{50} (*L. mexicana* axenic amastigotes) [µM]	EC_{50} (*L. mexicana* promastigotes) [µM]	CC_{50} (HeLa cells) [µM]
1	**70**	X5526	N=C		CH_3	C_6H_5	C_6H_5	n.a.	n.a.	25.0
2	**71**	X5527	N=C		CH_3	C_6H_5	$CH_2C_6H_5$	n.a.	n.a.	>50.0
3	**72**	X5528	N=C		CH_3	C_6H_5	CH_2CHCH_2	n.a.	n.a.	35.0
4	**73**	X5529	N=C		CH_3	C_5H_5N	H	n.a.	n.a.	32.0
5	**74**	X5524	*H*	1-methyl-4sulfonylbenzene			H	n.a.	n.a.	>50.0
6	**75**	X5525	*H*	C_6H_5			H	n.a.	n.a.	>50.0
7	**76**	X5519	N=C		*Methyl-2-[(5Z)-3ethyl-4-oxo-1,3-thiazolidin-5-ylidene] acetate*		C_6H_5	n.a.	n.a.	-
8	**77**	X5520	H	CO C_6H_5			CO C_6H_5	n.a.	3.38	-
9	**78**	X5521	H	CO C_6H_5			C_6H_5	2.06	15.5	>50.0
10	**79**	X5522	H	CO C_6H_5			$COCHCHCH_3$	2.38	9.64	-
11	**80**	X5508	N=C		*H*	C_6H_4OH	1,4-dimethyl1-2-iminobutanedioate	n.a.	n.a.	-
12	**81**	X5509	N=C		*H*	Naphthalene	1,4-dimethyl1-2-iminobutanedioate	n.a.	n.a.	39.0
13	**82**	X5511	N=C		$COOCH_3$	CH_2COCH_3	NH_2	n.a.	n.a.	>50.0

Table 2.7 Structure and results of **Class Three** compounds, including EC_{50} values against *Leishmania mexicana* axenic amastigotes, promastigotes, HeLa cells. (n.a.- compounds which showed more than 50% cell viability at 50 µM concentrations, X number- in-house compound label given by KIT).

Compound **78** (**Table 2.7, Entry 9**) was found to have an EC_{50} of 2.06 µM against axenic amastigotes and EC_{50} of 15.5 µM against promastigotes. For **79**, (**Table 2.7, Entry 10**) they were EC_{50}= 2.38 µM and 9.64 µM consecutively. Considering the structures of these, all three has a benzoyl group attached to the nitrogen atom in the place of R^2, R^3, and R^4. But compound **77** (**Table 2.7, Entry 8**) has another benzoyl group attached to nitrogen in R^5 branch, assuming steric hindrance of this molecule could be a reason for incompetency against axenic amastigote stage. In contrast to the CC_{50} values observed in Class One and Two, Class Three has lower toxicity against HeLa cells. Though none of the compounds from the Class Three library were taken forward and screened in infected macrophage assays, a case could be made for testing compound **78** (**Table 2.7, Entry 9**) as it has a > 50.0 µM CC_{50} value. As there is no biological data previously reported for this compound Class, it is difficult to propose a mechanism without doing further analysis.

Physiochemical properties for Class Three compounds were generated using ChemAxon software and are given in **Table 2.8**. Compounds **77**, **78** and **79** have log *P* values within the accepted range (3.17, 3.21 and 2.46 respectively) (**Table 2.8**) which comply with the properties of orally available drug molecules.

Entry no.	Compound number	Lipinski's rule of five	Molar Mass g/mol	log *P*	H bond donor count	H bond acceptor count
1	**70**	✓	379.43	3.53	0	4
2	**71**	✓	393.46	3.60	0	4
3	**72**	✓	343.40	2.60	0	4
4	**73**	✓	304.32	0.43	1	5
5	**74**	✓	355.38	1.59	2	5
6	**75**	✓	277.30	2.16	2	4
7	**76**	✓	446.45	2.05	1	6
8	**77**	✓	409.42	3.17	1	5
9	**78**	✓	381.41	3.21	1	4
10	**79**	✓	373.38	2.46	1	5
11	**80**	✓	462.43	2.44	1	8
12	**81**	✓	496.49	3.73	0	7
13	**82**	✓	358.33	0.308	1	7

Table 2.8 Physical properties of the **Class Three** compounds fall within Lipinski's rule of five (i.e., a molecule with a molecular mass less than 500 Da, no more than 5 hydrogen bond donors, no more than 10 hydrogen bond acceptors, and partition coefficient log *P* not greater than 5). Physical properties were calculated using ChemAxon online service https://chemicalize.com/welcome.

2.5.6 Class Four – Library screening

Out of the 13 compounds in the Class Four series, only two (**85** and **87**) showed potent activity against the parasites (**Table 2.9**). **87** (**Table 2.9, Entry 5**) was only active against *L. mexicana* promastigotes; EC_{50} = 9.11 µM with > 50.0 µM CC_{50} value. **85** (**Table 2.9, Entry 3**) was active against both stages and more effective against axenic amastigotes; EC_{50} = 3.42 µM compared to 34.3 µM.

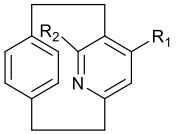

Entry no.	Compound no.	X number	R^1	R^2	EC_{50} (*L. mexicana* axenic amastigotes) [µM]	EC_{50} (*L. mexicana* promastigotes) [µM]	CC_{50} (HeLa cells) [µM]
1	**83**	X2103	*Tetrazole*	H	n.a.	n.a.	>50.0
2	**84**	X2119	H	4,(4,5-dihydro-1,2,3-triazol-1-yl)aniline	n.a.	n.a.	47.0
3	**85**	X2123	15-(1-phenyl-4,5-dihydro-1H-1,2,3-triazol-4-yl)-5-azatricyclo[8.2.2.2⁴,⁷]hexadeca-1(12),4,6,10,13,15-hexaene	H	3.42	34.3	-
4	**86**	X2124	4-{tricyclo[8.2.2.2⁴,⁷]hexadeca-1(12),4(16),5,7(15),10,13-hexaen-5-yl}-4,5-dihydro-1H-1,2,3-triazole	H	n.a.	n.a.	-
5	**87**	X2130	1,phenyl-4,5 dihydro-1,2,3triazole	H	n.a.	9.11	>50.0
6	**88**	X2132	Pyrimidin-2amine	H	n.a.	n.a.	>50.0
7	**89**	X2142	*Pyrazole*	H	n.a.	n.a.	>50.0
8	**90**	X2137	1H,1,2,3,4tetrazole	H	n.a.	n.a.	36.0
9	**91**	X2133	*1,phenyl-1H-pyrazole*	H	n.a.	n.a.	36.0
10	**92**	X2134	1,tert-butylpyrazole	H	n.a	n.a.	>50.0
11	**93**	X2145	3-dimethylaminoacrolein	H	n.a.	n.a.	40.0
12	**94**	X2150	CN	H	n.a.	n.a.	>50.0
13	**95**	X2143	H	H	n.a.	n.a.	>50.0

Table 2.9 Structure and results of **Class Four** compounds including EC_{50} values against *Leishmania mexicana* axenic amastigotes, promastigotes, HeLa cells. (n.a.-compounds which showed more than 50% cell viability at 50 µM concentrations, X number- in-house compound label given by KIT).

Although there were two compounds (**85** and **87**) with EC_{50} values lower than 10 µM, their physical properties make them less attractive for further development compared with some of the compounds from other Classes (**Table 2.10**). For example, **85**, **86**, **87**, **89** and **90** (**Table 2.10, Entry 3, 4, 5, 7 and 8**) violate Lipinski's rule of five, with all having log *P* values greater than 5 (**Table 2.10**). Lipophilicity is critical in drug discovery projects because of its importance in influencing target affinity, solubility, *in vivo* distribution, intestinal absorption, permeability, plasma protein binding, metabolism, and toxicity.[48]

Entry no.	Compound number	Lipinski's rule of five	Molar Mass g/mol	log *P*	H bond donor count	H bond acceptor count
1	**83**	✓	277.33	3.39	1	4
2	**84**	✓	367.45	5.02	1	4
3	**85**	×	626.76	8.96	0	6
4	**86**	×	482.63	8.56	0	3
5	**87**	×	352.44	5.85	0	3
6	**88**	✓	302.38	4.07	1	4
7	**89**	×	351.45	5.76	0	2
8	**90**	×	331.46	5.16	0	2
9	**91**	✓	277.33	3.39	1	4
10	**92**	✓	275.33	4.45	1	2
11	**93**	✓	306.40	4.01	0	3
12	**94**	✓	234.30	3.97	0	2
13	**95**	✓	209.29	3.79	0	1

Table 2.10 Physical properties of the **Class Four** compounds (i.e., a molecule with a molecular mass less than 500 Da, no more than 5 hydrogen bond donors, no more than 10 hydrogen bond acceptors, and partition coefficient log *P* not greater than 5). Physical properties were calculated using ChemAxon online service https://chemicalize.com/welcome.

2.5.7 Class Five - Library screening

The Class Five (**Table 2.11**) compounds have a benzene ring at the core of their structure. There are only three compounds in this series and none of these were found to be active against *L. mexicana* or toxic against HeLa cells (**Table 2.11**). The physical properties for the Class Five series are listed in **Table 2.12**.

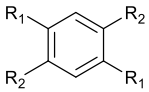

Entry no.	Compound No.	X number	R^1	R^2	EC_{50} (*L. mexicana* axenic amastigotes) [µM]	EC_{50} (*L. mexicana* promastigotes) [µM]	CC_{50} (HeLa cells) [µM]
1	**95**	X1627	*Br*	COC_6H5	n.a.	n.a	>50.0
2	**96**	X1834	C_5H_5N	$COCH_3$	n.a.	n.a.	-
3	**97**	X8022	Br	$COCH_3$	n.a.	n.a.	>50.0

Table 2.11 Structure and results of **Class Five** compounds including EC_{50} values against *Leishmania mexicana* axenic amastigotes, promastigotes, HeLa cells. (n.a.- compounds which showed more than 50% cell viability at 50 µM concentrations, X number- in-house compound label given by KIT).

Entry no.	Compound number	Lipinski's rule of five	Molar Mass g/mol	log P	H bond donor count	H bond acceptor count
1	**95**	×	444.12	6.429	0	2
2	**96**	✓	316.36	1.948	0	4
3	**97**	✓	319.98	2.626	0	2

Table 2.12 Physical properties of the **Class Five** compounds fall within Lipinski's rule of five (i.e., a molecule with a molecular mass less than 500 Da, no more than 5 hydrogen bond donors, no more than 10 hydrogen bond acceptors, and partition coefficient log *P* not greater than 5). Physical properties were calculated using ChemAxon online service https://chemicalize.com/welcome.

2.6 Chapter Summary

Overall, the Karlsruhe Institute of Technology (KIT) compound library screened in this Chapter comprises a highly diverse, novel set of chemical structures and for easy of analysis they were categorised into five distinct Classes depending on their core structures. Prior to carrying out the biological screening, we first standardised the assay parameters for *L. mexicana* axenic amastigotes and promastigotes to set a cell concentration and time of incubation. From the library of molecules screened, the Class One and Class Two series of compounds had the most active compounds. However, compound **40** (**Table 2.2, Entry 1**) and **46** (**Table 2.2, Entry 7**) from Class One and **60** (**Table 2.5, Entry 1**) and **64** (**Table 2.5, Entry 5**) from Class Two are the only compounds which can be considered as candidates worth taking forward along with further structural optimizations. Some of the compound Classes in this library have also been previously reported to have activity against targets that may also be present or of relevance in *Leishmania*. For instance, several 9,10-phenanthrenedione derivatives have been identified as reversible inhibitors of CD45 mediated p-nitrophenyl phosphate hydrolysis in humans; CD45 is a member of the transmembrane protein tyrosine phosphatases (PTPs). Since there are PTPs in *Leishmania* parasites, this could potentially be the target of the Class One compounds (**Section 2.4.2**).

Furthermore, cytotoxicity assays were carried out at KIT and the results show that most of the compounds in the library (all Classes) have higher toxicity towards the mammalian cell line (HeLa cells). Finally, intramacrophage assays were performed for the most active compounds in Class One and Two. Results showed decreased activities compared to the activity against axenic stages. Having higher cytotoxicity values and lower anti leishmanial activities against the intracellular stage make them more challenging to take forward in the drug discovery process. Nevertheless, 9,10-phenanthrenedione (Class One) and 1,10-phenanthroline (Class Two) were identified as novel chemical scaffolds which could be developed as anti-leishmanial therapeutic agents.

2.7 Reference

1. Mayr, L. M. & Bojanic, D. Novel trends in high-throughput screening. *Curr. Opin. Pharmacol.* **9**, 580–588 (2009).

2. Martis, E. A., Radhakrishnan, R. & Badve, R. R. High-throughput screening: The hits and leads of drug discovery-An overview. *J. Appl. Pharm. Sci.* **1**, 2–10 (2011).

3. Szymański, P., Markowicz, M. & Mikiciuk-Olasik, E. Adaptation of high-throughput screening in drug discovery-toxicological screening tests. *Int. J. Mol. Sci.* **13**, 427–452 (2012).

4. Koehn, F. E. High impact technologies for natural products screening. *Prog. Drug Res.* **65**, 176–210 (2008).

5. Zhang, J. H., Chung, T. D. Y. & Oldenburg, K. R. Confirmation of primary active substances from high throughput screening of chemical and biological populations: A statistical approach and practical considerations. *J. Comb. Chem.* **2**, 258–265 (2000).

6. Mayr, L. M. & Fuerst, P. The future of high-throughput screening. *J. Biomol. Screen.* **13**, 443–448 (2008).

7. Devlin, J. *High Throughput Screening-The discovery of Bioactive compounds*. (Marcel Dekker, INC, 1997). doi:https://doi.org/10.1201/9781482269802.

8. Alleyn T. Plowright, L. D. Phenotypic screening. *Annu. Rep. Med. Chem.* **50**, 263–299 (2017).

9. David C.Swinney, J. A. How were new medicines discovered? *Nat. Rev. Drug Discov.* **10**, 507–519 (2011).

10. Moffat, J. G., Vincent, F., Lee, J. A., Eder, J. & Prunotto, M. Opportunities and challenges in phenotypic drug discovery: An industry perspective. *Nat. Rev. Drug Discov.* **16**, 531–543 (2017).

11. Fumarola, L., Spinelli, R. & Brandonisio, O. In vitro assays for evaluation of drug activity against Leishmania spp. *Res. Microbiol.* **155**, 224–230 (2004).

12. Aulner, N., Danckaert, A., Ihm, J. E., Shum, D. & Shorte, S. L. Next-Generation Phenotypic Screening in Early Drug Discovery for Infectious Diseases. *Trends Parasitol.* **35**, 559–570 (2019).

13. Thomas, M. G. *et al.* Identification of GSK3186899/DDD853651 as a Preclinical Development Candidate for the Treatment of Visceral Leishmaniasis. *J. Med. Chem.* **62**, 1180–1202 (2019).

14. Siqueira-Neto, J. L. *et al.* Antileishmanial high-throughput drug screening reveals drug candidates with new scaffolds. *PLoS Negl. Trop. Dis.* **4**, 1–8 (2010).

15. Ortiz, D. *et al.* Discovery of novel, orally bioavailable, antileishmanial compounds using phenotypic screening. *PLoS Negl. Trop. Dis.* **11**, 1–22 (2017).

16. Peña, I. *et al.* New compound sets identified from high throughput phenotypic screening against three kinetoplastid parasites: An open resource. *Sci. Rep.* **5**, 8771 (2015).

17. Lamotte, S., Aulner, N., Späth, G. F. & Prina, E. Discovery of novel hit compounds with broad activity against visceral and cutaneous Leishmania species by comparative phenotypic screening. *Sci. Rep.* **9**, 1–11 (2019).

18. Rampersad, S. N. Multiple applications of alamar blue as an indicator of metabolic function and cellular health in cell viability bioassays. *Sensors (Switzerland)* **12**, 12347–12360 (2012).

19. Al-Nasiry, S., Hanssens, M., Luyten, C. & Pijnenborg, R. The use of Alamar Blue assay for quantitative analysis of viability, migration and invasion of choriocarcinoma cells. *Hum. Reprod.* **22**, 1304–1309 (2007).

20. Cell-Quant™ AlamarBlue Cell Viability Reagent. https://www.abpbio.com/product/cell-quant-alamarblue-cell-viability-reagent/ (2023).

21. Naveja, J. J. & Medina-Franco, J. L. Finding Constellations in Chemical Space Through Core Analysis. *Front. Chem.* **7**, 1–10 (2019).

22. Le Guilloux, V. *et al.* Visual characterization and diversity quantification of chemical libraries: 1. Creation of delimited reference chemical subspaces. *J. Chem. Inf. Model.* **51**, 1762–1774 (2011).

23. Lipinski, C. & Hopkins, A. Navigating chemical space for biology and medicine. *Nature* **432**, 855–861 (2004).

24. Reymond, J. L. & Awale, M. Exploring chemical space for drug discovery using the chemical universe database. *ACS Chem. Neurosci.* **3**, 649–657 (2012).

25. Mahajan, S. D. *et al.* Nanoparticle-mediated targeted delivery of antiretrovirals to the brain. in *Methods in Enzymology* vol. 509 41–60 (Elsevier Inc., 2012).

26. Kuete, V., Karaosmanoğlu, O. & Sivas, H. Anticancer Activities of African Medicinal Spices and Vegetables. in *Medicinal Spices and Vegetables from Africa* 271–297 (Academic Press, 2017). doi:10.1016/B978-0-12-809286-6.00010-8.

27. Ndjakou Lenta, B. *et al.* In vitro antiprotozoal activities and cytotoxicity of some selected Cameroonian medicinal plants. *J. Ethnopharmacol.* **111**, 8–12 (2007).

28. Urbanek, R. A. *et al.* Potent reversible inhibitors of the protein tyrosine phosphatase CD45. *J. Med. Chem.* **44**, 1777–1793 (2001).

29. Zhang, Z. Y. & VanEtten, R. L. Pre-steady-state and steady-state kinetic analysis of the low molecular weight phosphotyrosyl protein phosphatase from bovine heart. *J. Biol. Chem.* **266**, 1516–1525 (1991).

30. Bhattacharyya, T. & Sowdhamini, R. Genome-Wide Search for Tyrosine Phosphatases in the Human Genome Through Computational Approaches Leads to the Discovery of Few New Domain Architectures. *Evol. Bioinforma.* **15**, 1–10 (2019).

31. Tonks, N. K. PTP1B: From the sidelines to the front lines! *FEBS Lett.* **546**, 140–148 (2003).

32. Nascimento, M. *et al.* Identification and characterization of a protein-tyrosine phosphatase in Leishmania: Involvement in virulence. *J. Biol. Chem.* **281**, 36257–36268 (2006).

33. Lipinski, C. A., Ombardo, F., Dominy, B. W. & Feeney, P. J. Experimental and computational approaches to estimate solubility and permeability in drug discovery and development settings. *Adv. Drug Deliv. Rev.* **23**, 3–25 (1997).

34. Protti, Í. F. *et al.* Do Drug-likeness Rules Apply to Oral Prodrugs? *ChemMedChem* **16**, 1446–1456 (2021).

35. Pathania, S. & Singh, P. K. Analyzing FDA-approved drugs for compliance of pharmacokinetic principles: should there be a critical screening parameter in drug designing protocols? *Expert Opin. Drug Metab. Toxicol.* **17**, 351–354 (2021).

36. Lipinski, C. A. Rule of five in 2015 and beyond: Target and ligand structural limitations, ligand chemistry structure and drug discovery project decisions. *Adv. Drug Deliv. Rev.* **101**, 34–41 (2016).

37. Lau, E. Preformulation studies. in *Handbook of Modern Pharmaceutical Analysis* vol. 3 173–233 (Academic Press, 2001).

38. Mullard, A. Re-assessing the rule of 5, two decades on. *Nature Reviews Drug Discovery* vol. 17 777 (2018).

39. Bonacorso, H. G., Andrighetto, R., Frizzo, C. P., Zanatta, N. & Martins, M. A. P. Recent advances in the chemistry of 1,10-phenanthrolines and their metal complex derivatives: Synthesis and promising applications in medicine, technology, and catalysis. *Targets Heterocycl. Syst.* **19**, 1–27 (2015).

40. Accorsi, G., Listorti, A., Yoosaf, K. & Armaroli, N. 1,10-Phenanthrolines: Versatile building blocks for luminescent molecules, materials and metal complexes. *Chem. Soc. Rev.* **38**, 1690–1700 (2009).

41. Kellett, A. *et al.* Radical-induced DNA damage by cytotoxic square-planar copper(II) complexes incorporating o-phthalate and 1,10-phenanthroline or 2,2′-dipyridyl. *Free Radic. Biol. Med.* **53**, 564–576 (2012).

42. Omoregie, H. O., Eseola, A. O. & Akong, R. A. Mixed ligand complexes of copper(II) with benzoyltrifluoroacetone, 1,10-phenanthroline and 2,2′-bipyridine: Structure, spectroscopic and antimicrobial properties. *J. Mol. Struct.* **1250**, 131826 (2022).

43. Olivier, M., Atayde, V. D., Isnard, A., Hassani, K. & Shio, M. T. Leishmania virulence factors: Focus on the metalloprotease GP63. *Microbes Infect.* **14**, 1377–1389 (2012).

44. Isnard, A., Shio, M. T. & Olivier, M. Impact of Leishmania metalloprotease GP63 on macrophage signaling. *Front. Cell. Infect. Microbiol.* **2**, 72 (2012).

45. Chaudhuri, G., Chaudhuri, M., Pan, A. & Chang, K. P. Surface acid proteinase (gp63) of Leishmania mexicana. *J. Biol. Chem.* **264**, 7483–7489 (1989).

46. Arango Duque, G., Fukuda, M., Turco, S. J., Stäger, S. & Descoteaux, A. Leishmania Promastigotes Induce Cytokine Secretion in Macrophages through the Degradation of Synaptotagmin XI . *J. Immunol.* **193**, 2363–2372 (2014).

47. Lima, A. K. C., Elias, C. G. R., Souza, J. E. O., Santos, A. L. S. & Dutra, P. M. L. Dissimilar peptidase production by avirulent and virulent promastigotes of Leishmania braziliensis: Inference on the parasite proliferation and interaction with macrophages. *Parasitology* **136**, 1179–1191 (2009).

48. Leeson, P. D. & Empfield, J. R. Reducing the Risk of Drug Attrition Associated with Physicochemical Properties. in *Annual Reports in Medicinal Chemistry* vol. 45 393–407 (Elsevier Inc., 2010).

3 Assessing anti-leishmanial activity of Pyrithione-based compounds.

3.1 Introduction

As bringing a new drug to market is a time consuming and an expensive process, drug repurposing has been considered as a fast-track approach in drug discovery and developement.[1] By adopting this approach any new therapeutic uses identified can be immediately evaluated in phase II clinical trials, which usually lasts two years and can bypass almost 40% of the overall cost of bringing a drug to market.[2] 'Drug repurposing' has proven successful in bringing new therapeutics to the neglected tropical diseases (NTDs) in the developing world.[2] For example, current anti-leishmanial drugs, amphotericin B (**5**) and miltefosine (**6**) were originally developed as an anti-fungal and anti-cancer agents respectively (Chapter 1). Clofazimine (**99**) (**Figure 3.1**) is a lipophilic riminophenazine drug used in the treatment of leprosy and it has exhibited antiproliferative activity against *Leishmania donovani* infected macrophages (IC_{50} = 0.95 µM) along with an acceptable level of selectivity (SI ~10).[1] Interestingly, clofazimine (**99**) was more active against the intracellular stage than *L. donovani* axenic, amastigotes. Presumably due to the known feature of riminophenazines accumulation in macrophages.[3] The anti-leishmanial properties of clofazimine (**99**) have previously been reported in *in vivo* mouse models infected with *L. donovani* (VL), *L. amazonensis* (CL) and *L. major* (CL) (**Figure 3.1**).[4]

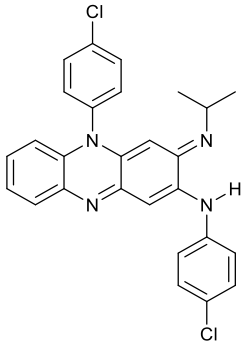

99

Strain	*In vitro* activity of Clofazimine against infected mouse peritoneal macrophage cells. ED_{50} (mg/l)	*In vivo* activity of Clofazimine *via* the oral route. ED_{50} (mg/kg)
L. amazonensis	2.3	280
L. donovani	1.4	650
L. major	0.5	96

Figure 3.1. Structure of clofazimine (**99**) and antileishmanial activity against different leishmanial strains.[4]

Over 100 registered drugs were selected in this drug repositioning study based on the potential to be repurposed and their respective target protein profiles.[1] A similar study of drug repurposing with a total of 1769 compounds has demonstrated that nifuratel (NFT) (**100**) (**Figure 3.2**); a drug used in gynaecology, has significantly reduced the parasite load *in vivo* in mouse models infected with *L. donovani* (VL) and *L. major* (CL), thus indicating that NFT could be a promising anti-leishmanial agent for VL (oral administration) and CL (intralesional administration).[5]

Other clinical studies have demonstrated the possible anti-leishmanial activity of ketoconazole (**101**) (**Figure 3.2**) and rifampicin (**102**) with omeprazole (**103**) (**Figure 3.3**). Ketoconazole (**101**), an imidazole derived antifungal agent has been shown to have beneficial effects against CL when administered orally at a dose of 200 - 400 mg/day.[6] In Saudi Arabia, oral ketoconazole treatment was found to be an effective treatment for CL caused by *L. major*. However, prolonged treatments from 8 -16 weeks were necessary to

achieve desired results. Although the treatment was well tolerated, side effects, particularly gastrointestinal and hepatotoxicity were observed.[7]

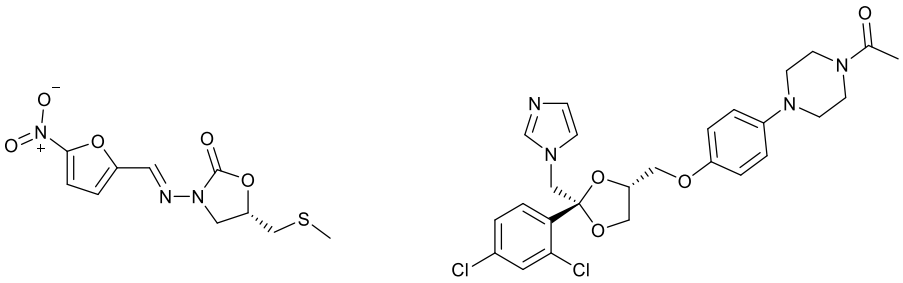

100 101

Figure 3.2 Chemical structures of nifuratel (**100**) and ketoconazole (**101**).

Rifampicin (**102**) (**Figure 3.3**) is an antibiotic used in the treatment of several types of bacterial infections including tuberculosis.[8] The effect of rifampicin (**102**) as an oral treatment for oriental sore or localised CL had shown some promising results. Omeprazole (**103**) (**Figure 3.3**) is used to treat gastroesophageal reflux and peptic ulcer conditions.[9] A short-term preliminary study conducted by Kochar et.al., has shown that a mixture of rifampicin (**102**) with omeprazole (**103**) was effective, cheap, well tolerated alternative oral treatment for anthroponotic CL caused by *L. tropica* and provided the basis for further studies with larger group of patients.[10]

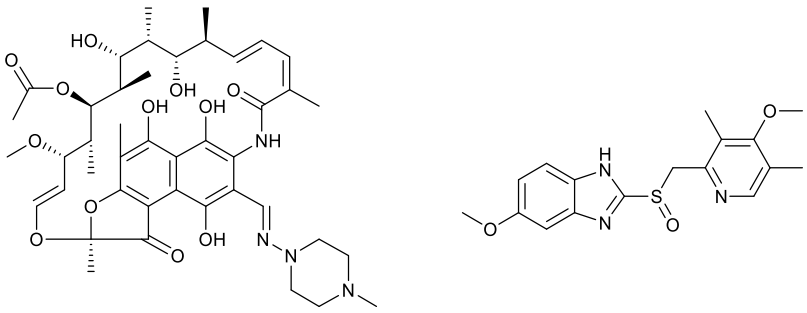

102 103

Figure 3.3 Chemical structures of rifampicin (**102**) and omeprazole (**103**).

Focused or knowledge based screening involves selecting a smaller subset of molecules, from a large chemical library, that are likely to have a specific target protein based on the literature of the target proteins and the chemical classes.[11] Based on previous literature,[12,13,1] pyrithione (**104**) (also known as 1-hydroxy-1,2-dihydropyridine-2-thione and 2-mercaptopyridine-*N*-oxide), ciclopirox (**105**) and piroctone olamine (**106**) drugs were selected in this chapter to be repurposed against *L. mexicana* (a causative agent of CL) (**Figure 3.4**). Zinc Pyrithione (ZPT) (**107**), a derivative of pyrithione (**104**), is an antidandruff agent that has been recently repurposed to treat human cancer. It has shown to target proteasome-associated deubiquitinating enzymes (DUBs) and inhibit their activities. ZPT also exhibits cytotoxic effects against various cancer cell lines *in vitro*, selectively kills bone marrow cells from leukaemia patients *ex vivo*, and inhibits the growth of lung adenocarcinoma cancer cell xenografts in nude mice.[12] DUBs play a crucial role in differentiation and intracellular survival of *Leishmania* and amastigotes are exquisitely sensitive to disruption of ubiquitination homeostasis.[13] Hence, pyrithione (**104**) was selected for this project as a potential DUBs inhibitor. Ciclopirox olamine (**105**) has shown activity against *L. donovani* with moderate selectivity[1] and piroctone olamine (**106**) was included because of the structural similarities shared with **104** and **105**.

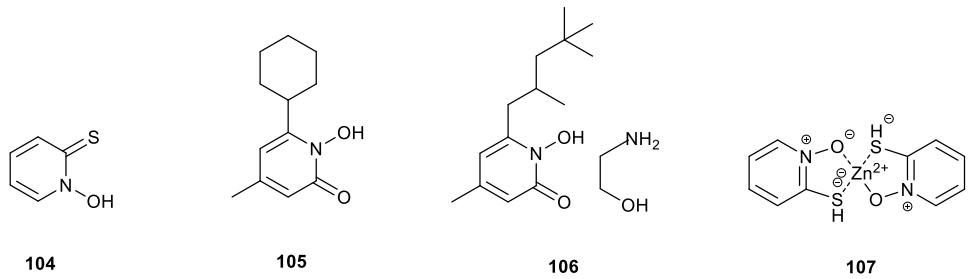

Figure 3.4 Chemical structures of FDA approved compounds: pyrithione (**104**), ciclopirox (**105**), piroctone olamine (**106**) and zinc pyrithione (**107**).

3.2 Deubiquitinating enzymes

Ubiquitin is a 76 amino acid protein present in all eukaryotic organisms, including trypanosomatids. It was first discovered in 1975 by Gideon Goldstein and initial the studies carried out in 1980s identified and partially characterised ubiquitin genes belonging to members of *Trypanosoma* and *Leishmania* genera.[14] Ubiquitination is a post translational modification in which ubiquitin is covalently attached to a target protein which influences the regulation of vital cellular mechanisms, including protein degradation through the ubiquitin-proteosome system (UPS), autophagy, DNA repair and protein trafficking.[15,16] Ubiquitination is catalysed by consecutive reactions of three enzymes, E1 activates ubiquitin in an ATP dependent manner, forming a thiol ester bond between the C-terminus of ubiquitin and the active cysteine of E1. The activated ubiquitin is subsequently transferred to the active site cysteine of ubiquitin conjugating enzyme, E2. Finally, ubiquitin ligase, E3, catalyses the transfer of ubiquitin from the E2 to a lysine residue in the substrate/target protein (**Figure 3.5**). Thereafter, ubiquitin molecules can be conjugated with each other to form chains via the N-terminus of the amino group or lysine on ubiquitin (poly-ubiquitination).[17,18]

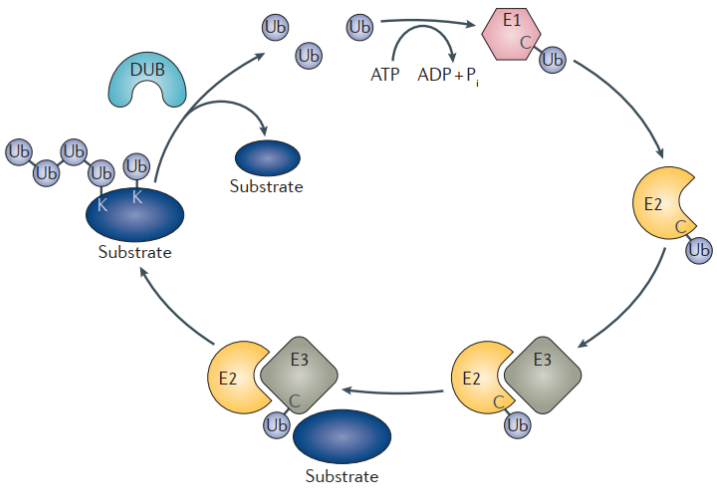

Figure 3.5; The ubiquitination cascade.[17] Schematic diagram of key events in ubiquitylation and deubiquitylation. Ubiquitin is activated by E1, and thioester conjugated first to E1, then to E2. The E2-Ub conjugate interacts with E3 ligase to transfer ubiquitin from E2 to a substrate.

DUBs, proteases that reverse modified proteins by removing ubiquitin or ubiquitin-like proteins from target proteins, have recently been considered as crucial regulators of both the ubiquitination-mediated protein degradation pathway and the regeneration of free ubiquitin from unanchored polyubiquitin.[15] Over 100 putative DUBs are encoded by the human genome and they are categorized into seven families based on sequence and domain conservation,[17]

- Ubiquitin specific proteases (USPs, Family C19)
- C-terminal hydrolyses (UCHs, Family C12)
- Ovarian tumour proteases (OTUs, Family C65)
- JAB1/MPN/MOV34 metalloenzymes (JAMM/MPN+, Family M67)
- Josephins, Family C86, MINDY
- Family C115, ZUFSP (Zinc finger with UFM1-specific peptidase domain protein)
- Family C78

DUBs play an important role in the regulation of numerous processes, such as tumour progression, immune regulation, and neurodegeneration.[19] Like the E1, E2 and E3 enzymes in UPS, DUBs have attracted interest as potential drug targets due to their involvement in various human diseases, including cancer. The deubiquitinase activity of USP7 stabilizes MDM2, a RING-finger ubiquitin E3 ligase, which in turn degrades p53. Inhibition of USP7 can therefore lead to p53 stabilization and tumour suppression.[20] The first USP inhibitor identified was HBX41,108 (**108**) (**Figure 3.6**), and this was developed by Hybergenics Pharma. It is an uncompetitive inhibitor and a cyano-indinopyrazine derivative, that was shown to stabilize p53 and induce p53 mediated apoptosis-like cell death in cancer cell lines.[21] P5091 (**109**), a trisubstituted thiophene with dichlrophenylthio, nitro and acetyl substitutions, is another USP7 inhibitor developed by Progenra. It is well known to induce apoptosis in multiple myeloma cells.[22]

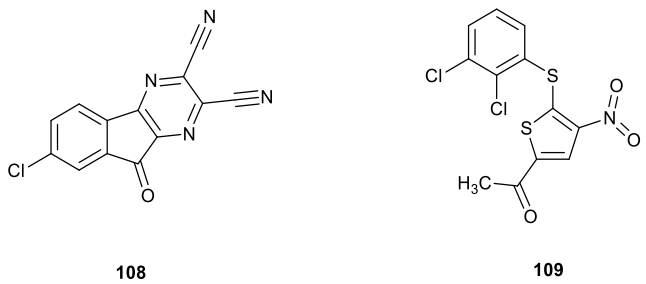

Figure 3.6 Chemical structures of HBX 41, 108 (**108**) and P5091 (**109**).

Considering the fact that the establishment of *Leishmania* in its host depends on host immune response modulation, it seems logical to investigate the relevance of deubiquitination in *Leishmania* infection.[19] 20 DUBs belonging to the C12, C19 and C65 families were identified in the *L*. *mexicana* genome. Analysis of DUBs in *L. mexicana* promastigote lysates using the Cy5UbPRG probe; a fluorescent activity-based probe, previously designed for its ability to react with active DUBs, identified 6 active DUBs (DUB2, DUB15, DUB16, DUB17, DUB18 and DUB19) by mass spectrometry, illustrating the presence of an active deubiquitinating system. Damianou *et al*. demonstrated the crucial role of DUBs in differentiation and intracellular survival of *Leishmania*.[13] DUBs 4, 7 and 13 play an essential role in the transformation of metacyclic promastigotes to amastigotes. Being unable to generate null mutant lines for DUBs 1, 2, 12 and 16 indicated that those are essential for the viability of procyclic promastigotes. Furthermore, DUBs 3, 5, 6, 8, 10, 11 and 14 are required for normal amastigote proliferation in mice.[13] Additionally, DUB2 plays an essential role in establishing the infection and is involved in endosomal trafficking (in *L. major*).[13,23] An example in *L. infantum* involves OtuLi, a DUB with the ability to stimulate lipid droplet biogenesis and the release of IL 6 and TNF-α from peritoneal macrophages.[19] Although the potential of OtuLi to be secreted into host cells has yet to be confirmed, this suggested a role for OtuLi DUB in the proinflammatory response of macrophages during *L. infantum* infection.[19] Given that *Leishmania* parasites are sensitive to disruption of ubiquitination homeostasis at different life cycles stages,

these recent studies have shown the potential of proteosome inhibition as a treatment for leishmaniasis.

Selective inhibition of the trypanosomatid proteosome appears possible, as exemplified by the ability of GNF6702 (**110**) (**Figure 3.7**), a non-competitive inhibitor shown to reduce the liver parasite burden by 90% in all five mice infected with *L. donovani,* and which was also shown to clear *T. cruzi* from all but one out of eight mice.[24] A greater than three log reduction in *L. donovani* parasites load was reported after 8-day treatment with 10mg/kg of GNF6702 (**110**) twice-daily. Simultaneously, a treatment with the same dose of GNF6702 (**110**) caused a five-fold decrease in footpad parasite burden, after a footpad infection of BALB/c mice with dermatotropic *L. major*.[24] Another parasite-selective proteosome inhibitor, GSK3494245 (**111**) (**Figure 3.7**), has also been shown to reduce parasite burden in a mouse model of VL.[25] When dosed orally at 25mg/kg, GSK3494245 (**111**) induced a >95% reduction of *L. donovani* parasite load after 10 days, similar to the efficacy of miltefosine.[25] Moreover, these studies proved that GNF6702 (**110**) and GSK3494245 (**111**) block the chymotrypsin-like activity catalysed by the β5 subunit without competing with substrate binding, and had no measurable activity on human proteosome (>100 folds less active against human proteosome). This shows that they have the potential to lead to new anti-leishmanial therapies.[24,25]

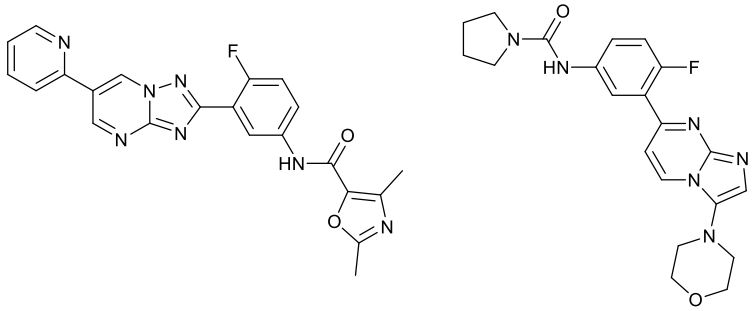

110 **111**

Figure 3.7. Chemical structures of *L. donovani* proteome inhibitors GNF6702 (**110**), GSK3494245 (**111**).

Progression of GNF6702 (**110**) into clinical trials were hampered by solubility limited oral absorption. LXE408 (**112**) (**Figure 3.8**) was identified by medicinal chemistry optimization of GNF6702 (**110**) as improving solubility and oral bioavailability.[26] Dosing LXE408 (**112**) at 1mg/kg twice daily has shown 95% reduction of *L. donovani* parasite burden in the liver in a murine model of VL, with an efficacy equivalent to a 12 mg/kg once a day regimen of miltefosine. Additionally, the *in vivo* efficacy of LXE408 (**112**) in a murine model of CL was evaluated. Oral administration of **112** for 10 days at 20 mg/kg twice a day produced a therapeutic effect comparable to that of liposomal Amp B.[26]

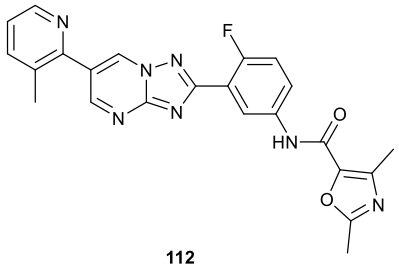

Figure 3.8 Chemical structure of LXE408 (**112**).

Originally, pyrithione (pyridine-2-thiole-N-oxide) (**104**) (**Figure 3.4**) and its derivatives were studied in the 1950s for their fungistatic and bacteriostatic properties. Pyrithione (**104**) is an analogue of naturally occurring antimicrobial metabolite aspergillic acid, synthesized by *Aspergillus flavus*.[27] Today, pyrithione (**104**) is known for its extensive uses as a topical antibiotic for the treatment of mild forms of dermatitis (e.g. seborrhoea, dandruff).[28] Zinc pyrithione (ZPT) (**107**) is a derivative of pyrithione (**104**) (**Figure 3.4**). Although the use of ZPT (**107**) as an anti-dandruff is widespread, its anti-fungal mechanism of action is still not well understood. There are a few theories as to how ZPT (**107**) may function. These include depolarization of membranes and preventing membrane transport, it may also induce iron starvation response in cells and inhibition of fungal growth by copper-mediated loss of function of iron-sulphur proteins. However, these studies do not completely describe the mechanism of action of ZPT (**107**).[29] Apart from that, pyrithione (**104**) was

evaluated for its antiviral activity, and it was proven to effectively inhibit human rhinovirus, coxsackievirus and mengovirus multiplication by interfering with the processing of viral polyprotein, abolishing the cleavage of cellular eukaryotic translation initiation factor eIF4GI by the rhinoviral 2A protease and facilitating the rapid import of extracellular zinc ions into the cells. Pyrithione (**104**) is believed to act as a zinc ionophore and this is widely accepted as the likely mode of action that underpins its antiviral and anticancer activity.[30]

In the drive for pharmaceutical control of tropical parasitic diseases, metal complexes perhaps appear to be one of the more promising approaches. For example, pyrithione (**104**) was reported to be active *in vitro* against *T. cruzi* by blocking the growth of parasites in culture and in infected mammalian myoblasts, with SI of 4.5.[31] Although it may have other intracellular targets, it inhibits the parasite specific enzyme NADH-fumarate reductase. This enzyme is responsible for the conversion of fumarate to succinate, the main respiratory substrates required for the energy production in parasites. The lack of NADH-fumarate reductase in mammalian cells makes this enzyme an interesting target for drugs for CD.[32] Coordination complexes of pyrithione with Pd (II) (**113**) and Pt (II) (**114**) metals (**Figure 3.9**) have demonstrated their effect on tumour cells and their ability to bind DNA as the main mechanism of action.[31] *In vitro* biological activity of the Pd (II) complex (**113**) (IC_{50}; 67 nM) against *T. cruzi* showed approximately threefold increase in anti-parasitic activity compared to pyrithione (**104**) (IC_{50}; 0.190 µM) and the Pt (II) complex (**114**) (IC_{50}; 0.200 µM). Pyrithione (SI = 4.5) and the Pt (II) complex (SI = >10) reported similar IC_{50}s but, importantly, the complex demonstrated an increased selectivity index (SI). Unlike in cancer cells, these two metal complexes (**113** and **114**) neither have any interaction with DNA nor inhibit trypanothione reductase, but they have proven to target NADH-fumarate reductase, similarly to the parental compound, pyrithione (**104**).[31]

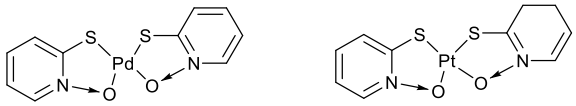

113 **114**

Figure 3.9 Chemical structures of Pd (II) (**113**) and Pt (II) (**114**) complexes with pyrithione (**104**).

In a similar study, a novel gold (I) triphenylphosphine complex with pyridine-2-thiol N-oxide (**115**) (**Figure 3.10**) showed potent *in vitro* antiproliferative activity against *L. mexicana*, *L. (V.) braziliensis* promastigotes and *T. cruzi* epimastigoes and low cytotoxicity for mammalian macrophages.[33]

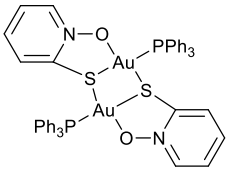

115

Figure 3.10 Proposed structure for Au(I) complex (**115**).[33]

Ciclopirox Olamine (CPX) (**105**) (**Figure 3.4**) is a polyvalent metal chelator, currently used for the treatment of mild to moderate cutaneous fungal infections.[34] Nowadays CPX (**105**) is being subjected to drug repurposing studies in various medical fields. CPX (**105**) has been evaluated as an anti-ischaemic stroke agent, an antibiotic against drug resistant *Acinetobacter baumannii*, *E. coli*, and *Klebsiella pneumoniae* and as a novel therapeutic agent for the treatment of haematologic malignancy.[35,36,37] A drug repositioning study towards NTDs has shown the effectiveness of CPX (**105**) against *L. donovani* (IC_{50} (axenic)= 1.640 µM, IC_{50} (intracellular) = 9.090 µM, SI:12) with moderate selectivity.[1]

Piroctone olamine (PO) (**106**) (**Figure 3.4**) is an ethanolamine salt of the hydroxamic acid derivative piroctone and was first synthesised in 1979 by Schwarzkopf-Henkel (Germany).[38] It is a component of anti-dandruff shampoo and hair rinses for scaly and

irritated skin. PO (**106**) has the ability to reduce microbial colonization of *Malassezia spp*. and other yeasts, which cause scaling and irritation of the scalp. Its mechanism of action is not completely understood but it is known that PO (**106**) penetrates the cell membrane and form complexes with Fe^{2+} and Fe^{3+}, inhibiting energy metabolism in mitochondria of the pathogenic fungi.[39] Additionally, antifungal activity of PO (**106**) has been evaluated against *Candida albicans* in the treatment of intra-abdominal candidiasis in an experimental model using Swiss mice.[40] It was recently confirmed that CPX (**105**) inhibits Wnt/beta catenin signalling in myeloma.[41] Since PO (**106**) has very similar chemical features to CPX (**105**), antitumor effect of PO (**106**) was investigated *in vitro* and *in vivo* in a murine myeloma model. The results revealed a significant selective induction of apoptosis by PO (**106**) in various human and murine myeloma and lymphoma cell lines and suggested a significant *in vivo* effect against myeloma.[38] The potential of using PO (**106**) as a repurposed drug against NTDs is hardly evaluated. PO (**106**) has been identified as one of the 121 active molecules active against *Schistosoma mansoni* parasites: the causative agent of schistosomiasis. However, PO (**106**) was only active against the schistosomula (the larval stage) in the *in vitro* screening.[42] In another study, anti-leishmanial activity of PO (**106**) coated Fe_3O_4 magnetic nanoparticles against CL was determined. Results indicated the high potency of PO (**106**) coated Fe_3O_4 nanoparticles (IC_{50}, 31.3 µg/mL) to inhibit the growth of amastigotes form *L. major* as well as improving the recovery of infected mice without significant cytotoxicity.[43]

3.3 Chemical synthesis of novel pyrithione derivatives

The discovery of a marketable bioactive molecule relies upon the ability to modify known active molecules to yield a candidate with an improved activity profile. In this chapter, one of the main aims of synthesising novel compounds from commercially available drugs is to improve their activity. With the motive of improving the activity of pyrithione (PO, **104**) and further investigating the proposed mechanism of metal binding via the *N*-oxide and

thioketone group of the compounds (**116**-**119**), a small library of analogues was synthesised (**Figure 3.11**).

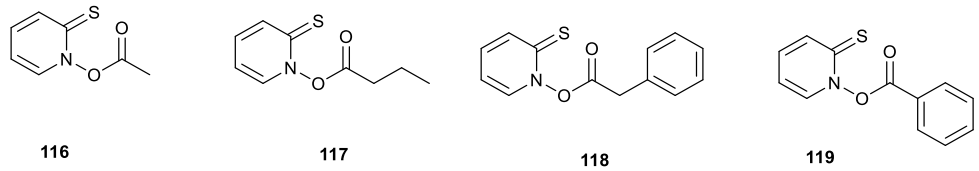

Figure 3.11 structures of newly synthesized pyrithione analogous. **116**; 2-sulfanylidene-1,2-dihydropyridin-1-yl acetate, **117**; 2-sulfanylidene-1,2-dihydropyridin-1-yl butanoate, **118**; 2-sulfanylidene-1,2-dihydropyridin-1-yl 2-phenylacetate, **119**; 2-sulfanylidene-1,2-dihydropyridin-1-yl benzoate.

Pyrithione (**104**) is a weak acid (pKa = -1.95), which is slightly soluble in water but completely dissolves in organic solvents (e.g., DCM, DMSO, benzene, $CHCl_3$, DMF and EtOAc) The *N*-oxide group can be easily modified via reaction with acyl chlorides. It is hypothesized that if the proposed mechanism of metal binding is taking place via N-oxide and thioketone, then the modified compounds (**Figure 3.11**) will have reduced efficacies compared to the original molecule (**104**) because of the modification of the *N*-oxide would obstruct the metal binding site.

3.3.1 Synthesis of 2-sulfanylidene-1,2-dihydropyridin-1-yl acetate (116)

Pyrithione (**104**) was reacted with acetyl chloride and a pyridine catalyst for 2 hrs in DCM at 0°C, this was followed by an aqueous workup and purification by column chromatography (**Scheme 3.1**).[44] Isolation of synthesise 2-sulfanylidene-1,2-dihydropyridin-1-yl acetate **116** was confirmed by identification of the molecular ion $[M+H]^+$ = 170.0280 (HRMS) and the appearance of a new peak at 2.48 ppm in the ^{1}H NMR spectrum which represent the methyl protons of the acetyl group.

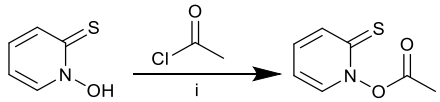

Scheme 3.1 Synthesis of 2-sulfanylidene-1,2-dihydropyridin-1-yl acetate (**116**) (Yield = 13%); i-Pyridine, DCM, 0 °C, 2 hrs.

3.2.2 Synthesis of 2-sulfanylidene-1,2-dihydropyridin-1-yl butanoate (117)

To access **117** pyrithione (**104**) was reacted with butyryl chloride and pyridine as a catalyst for 2hrs in DCM at 0 °C, followed by aqueous workshop and purification by column chromatography (**Scheme 3.2**). Synthesis of **117** was confirmed by identification of the molecular ion $[M+H]^+$ = 198.0592 (HRMS) and the appearance of new peaks at 1.10, 1.88, and 2.73 ppm in the ^{1}H NMR spectrum which coincide with the alkane chain.

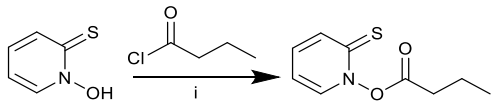

Scheme 3.2 Synthesis of 2-sulfanylidene-1,2-dihydropyridin-1-yl butanoate (**117**) (Yield = 22%); i-Pyridine, DCM, 0 °C, 2 hrs.

3.2.3 Synthesis of 2-sulfanylidene-1,2-dihydropyridin-1-yl 2-phenylacetate (118)

To access **118** pyrithione (**104**) was reacted with phenylacetyl chloride and pyridine as a catalyst for 2 hrs in DCM at 0 °C, followed by aqueous workup and purification by column chromatography (**Scheme 3.3**). Isolation of compound **118** was confirmed by HRMS ([M+H]+ = 246.0278) and the appearance of a new peak at 4.08 ppm in the ^{1}H NMR spectrum which represent the 2H of phenyl acetyl group.

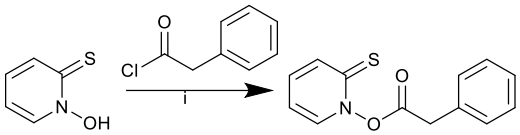

Scheme 3.3 Synthesis of 2-sulfanylidene-1,2-dihydropyridin-1-yl 2-phenylacetate (**118**) (Yield = 13%); i-Pyridine, DCM, 0 °C, 2 hrs.

3.2.4 Synthesis of 2-sulfanylidene-1,2-dihydropyridin-1-yl benzoate (119)

To prepare **119** pyrithione (**104**) was reacted with benzoyl chloride and pyridine as a catalyst for 2 hrs in DCM at 0 °C, followed by aqueous workup and purification by column chromatography (**Scheme 3.4**). Isolation of **119** was confirmed by identification of the molecular ion $[M+H]^+$ = 232.0451 in the HRMS and the appearance of new Ar-H peaks in the ^{1}H NMR spectrum corresponding to the benzoyl ring.

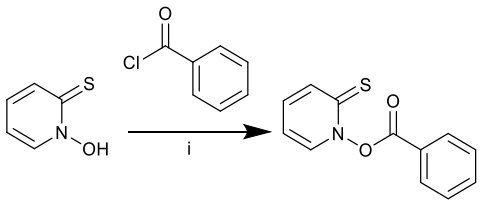

Scheme 3.4 Synthesis of 2-sulfanylidene-1,2-dihydropyridin-1-yl benzoate (**119**) (Yield = 34 %); i-Pyridine, DCM, 0 °C, 2 hrs.

Regarding the synthesis **116** to **119** the following points are worth noting. At first, the reactions were carried out on a smaller test scale (~20 mg), but it was found that the product was easily lost during work up and purification. The products were confirmed to be in the in the crude reaction mixtures but after purification they often seemed to degrade rapidly. Prep TLC plates were trialled for purification, instead of a standard column chromatography and this proved to be somewhat better in terms of product recovery. Simply scaling up (~200 mg) all the reactions seemed to go some way to solving the issues and the compounds were obtained using a standard column chromatography-purification approach when the synthesis was carried out a large scale.

It is also worth noting that **116** to **119** are believed to be light sensitive.[45] Hence, all the reactions were carried out with light excluded and in amber coloured containers, or containers covered with aluminium foil, to avoid degradation. A proposed mechanism of degradation of acyl thiohydroxamates through homolytic cleavage of the N-O bond, in the formation of the thiyl radical and acyloxy radical is shown in **Scheme 3.5.** Acyloxy radicals decarboxylate rapidly when R is an aliphatic moiety but are more persistent in the case of aromatic and conjugated acids.

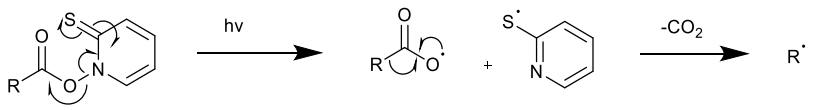

Scheme 3.5 Proposed mechanism for the degradation of synthetic targets in visible light.[45]

3.4 Evaluation of anti-leishmanial activity against *Leishmania mexicana*

Initial testing of the synthesized compounds **104** -**106** and **116** -**119**, involved a phenotypic screen against *L. mexicana* promastigotes and axenic amastigotes in a high throughput Alamar Blue® assay. Due to the fact that the compounds are light sensitive, they were handled with extra care while performing all the biological assays and repeats in the laboratory. The results obtained from this initial screen are summarised in **Table 3.1**. Compounds with promising activities were subjected to intracellular amastigotes assays as the next step. In addition to that, cytotoxicity against RAW 264.7 cells; macrophage-like cells, originating from Abelson leukaemia virus transformed cell line derived from BALB/c mice,[46] were determined to calculate selectivity index (SI) (**Table 3.1**). Physiochemical properties were predicted using Chem Axon software (**Table 3.2**). Later, the compounds considered as potential DUBs inhibitors with subjected to in gel fluorescence assays to identify the target DUB enzymes (collaboration with University of York).

All molecules (**104**-**106** and **116**-**119**) were first screened at a fixed concentration of 50 µM, following what has been previously done in the group. Percentages of viable *L. mexicana* promastigotes and axenic amastigotes after treatment are shown in the graph below (**Figure 3.12**). All four novel compounds (**116** to **119**), along with three commercially available drugs (**104** to **106**) investigated in this chapter, lead to *Leishmania* cell viabilities lower than 50% and as such they were continued to EC_{50} calculation.

The detailed experimental procedure for the biological screening can be found in **Chapter 7** (**Section 7.4.8**). However, in brief, compounds to be tested were added to 96-well microtiter plates containing *L. mexicana* promastigotes or amastigotes at 1 x 10^6 cells/ml concentration in triplicate and serial dilutions were carried out from 50 µM to 23 nM. Amphotericin B (**5**) and dimethyl sulfoxide (DMSO), which was used to prepare all the compound stock solutions, were used as positive and negative controls respectively. Then *L. mexicana* promastigotes were incubated for 20 hrs and axenic amastigotes were incubated for 44 hrs. The cell viability reagent, Alamar Blue® (10% v/v) was added to each well, incubated for another 4 hrs at the appropriate temperatures for the parasites; 26 °C for promastigotes and 33 °C for axenic amastigotes and, fluorescence was measured at 600 nm using the Biotek FL×800 plate reader.

.

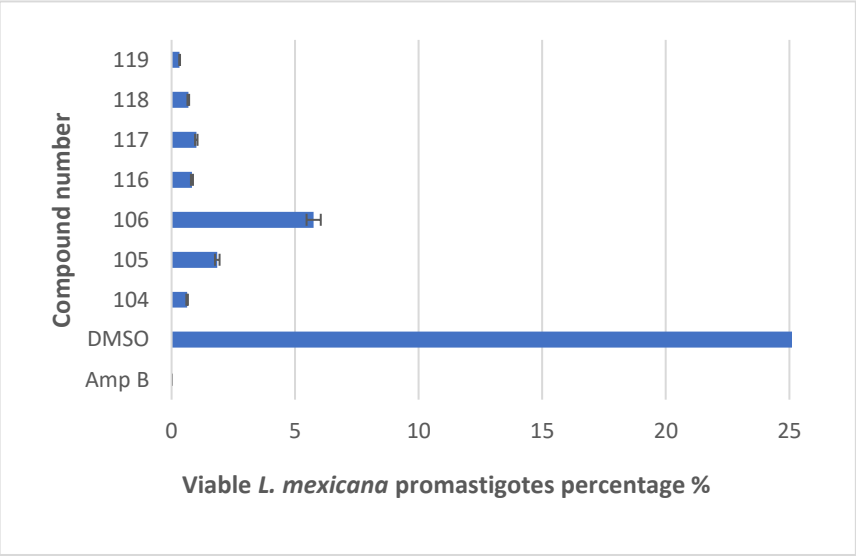

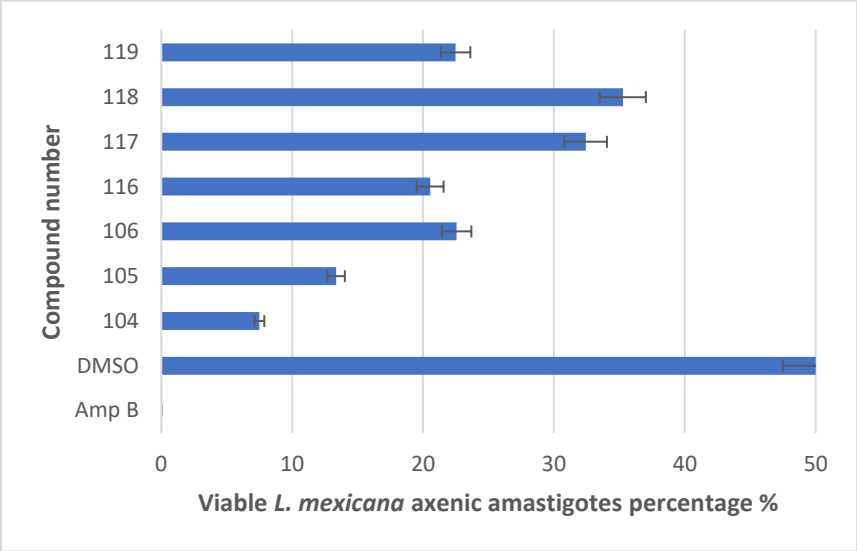

Figure 3.12 Results of initial screening of small molecules (**104** - **106**, **116** - **119**) at 50 µM against *L. mexicana* axenic amastigotes and promastigotes - (DMSO-negative control, Amp B-positive control). DMSO control has 100% cell viability, but x - axis was adjusted to a maximum of 25 and 50% in order to achieve a clear image of viable percentages of compounds screened (**104-106**, **116-119**).

Entry no.	Compound Number	*L. mexicana* axenic amastigotes		*L. mexicana* promastigotes		RAW 264.7 macrophages		Selectivity Index (SI)	*L. mexicana* intracellular amastigotes (infected stage)	
		EC_{50}/µM	95% CI	EC_{50}/µM	95% CI	CC_{50}/µM	95% CI		EC_{50}/µM	95% CI
1	**104**	0.0421	0.0255 to 0.0695	0.852	0.533 to 1.36	17.5	13.8 to 22.1	20.6	0.848	0.660 to 1.09
2	**105**	2.78	2.33 to 5.40	1.82	0.818 to 4.05	19.9	10.0 to 39.9	11.7	1.70	1.04 to 2.79
3	**106**	3.54	2.26 to 3.38	8.47	5.66 to 12.6	>100	(Very wide)	>86.2	1.16	0.785 to 1.71
4	**116**	0.0680	0.0437 to 0.105	0.774	0.479 to 1.25	6.76	4.59 to 9.95	5.00	1.35	0.837 to 2.19
5	**117**	0.241	0.0803 to 0.651	0.992	0.581 to 1.69	4.03	3.01 to 5.41	2.75	1.45	1.50 to 2.01
6	**118**	0.0633	0.0276 to 0.145	0.810	0.377 to 1.74	13.5	9.45 to 19.4	1.92	7.03	4.51 to 10.9
7	**119**	0.228	0.124 to 0.466	1.44	0.919 to 2.27	19.1	12.7 to 28.8	6.43	2.97	1.88 to 4.69

Table 3.1 Results of the screening carried out on compounds **104** - **106**, **116** - **119**, including the EC_{50} values and associated 95% confidence intervals for the axenic and intramacrophage amastigote assay and toxicity testing using RAW 264.7 cells. SI = CC_{50} (Raw 264.7) / EC_{50} (intracellular amastigotes)

All the compounds (**Table 3.1**) demonstrated low micromolar antiproliferative activities against *L. mexicana* axenic amastigotes and promastigotes which denote their high anti-leishmanial activities. Given the aforementioned activities of all the compounds, they were then subjected to intramacrophage and cytotoxicity assays to determine the ability of these compounds to inhibit the growth of parasites proliferating inside macrophages (**Table 3.1**) and to evaluate their toxicity towards mammalian cells. Murine macrophages, RAW 264.7 cells are considered as an appropriate model of macrophages and were selected in this project to determine the *in vitro* cytotoxic activity of test compounds. RAW 264.7 cells were seeded in a 96 well microtiter plate at 2.5 $\times 10^5$ cells/mL and incubated for 48 hrs before they were treated with test compounds in 3-fold dilutions from 100 µM to 0.41 µM concentrations, followed by a series of washing steps precisely described in **Chapter 7, Section 7.4.10**. Amphotericin B and DMSO were used as positive and negative controls. Then the cells were incubated for 24 hrs, before addition of 5 µL (10% v/v) of Alamar Blue® and fluorescence were measured at 600 nm using the Biotek FL×800 plate reader. Finally, Intramacrophage assays were executed as stated in **Chapter 2** and the elaborated protocol can be found in **Chapter 7** (**Section 7.4.11**).

Pyrithione (**104**) (**Table 3.1, Entry 1**) showed the highest anti-leishmanial activity against *L. mexicana* axenic amastigotes; EC_{50} 42.1 nM, compared to the other two drugs tested; Ciclopirox (**105**) (**Table 3.1, Entry 2**) (EC_{50}; 2.79 µM), Piroctone olamine (**106**) (**Table 3.1, Entry 3**) (EC_{50}; 3.55 µM) (**Table 3.1**). Furthermore, compound **104** (**Table 3.1, Entry 1**) is the most active compound against intracellular amastigotes with the selectivity index (SI) of 20.6. SI of the compounds were calculated by taking the ratio of Cytotoxicity (Raw 264.7) and EC_{50} (intracellular amastigotes).

$$Selectivity\ Index = \frac{\mathrm{CC_{50}(Raw264.7)}}{\mathrm{EC_{50}}(L.\,mexicana\ \text{intracellular amastigotes})}$$

In theory, the higher the SI value, the more effective and safer a drug would be. Selectivity indices greater than 10 suggest that their effects were on the parasite and not on the host cells. All the FDA approved tested in this chapter have SI values greater than 10. Efficacies of novel compounds against intracellular amastigotes can be listed as below; **116** > **117** > **119** > **118** (EC_{50}s; 1.35 µM, 1.45 µM, 2.97 µM and 7.03 µM respectively). Compound **118** (**Table 3.1, Entry 6**) has the highest anti-leishmanial activity against axenic amastigotes; 0.063 µM among newly synthesised compounds. However, **118** (**Table 3.1, Entry 6**) did not retain its activity particularly well in the infection assay displaying an EC_{50} of 7.03 µM against intracellular amastigotes. Overall, every compound in Table 3.1 has an EC_{50} < 4 µM against *L. mexicana* axenic amastigotes and most retained activity (10 µM >) in the infection assays, which is promising at this early stage of the drug discovery process.

Analysis of anti-leishmanial activities recorded for *L. mexicana* promastigotes highlighted the slightly improved activities of novel compounds **116** (**Table 3.1, Entry 4**) and **118** (**Table 3.1, Entry 6**) (0.774 µM and 0.810 µM respectively) compared to the original compound,**104** (**Table 3.1, Entry 1**). This was not the case with *L. mexicana* axenic amastigotes and intracellular amastigotes.

It is worth highlighting that considering all the EC_{50} values, CC_{50} values and Selectivity Indexes, compounds **104** (**Table 3.1, Entry 1**), **105** (**Table 3.1, Entry 2**) and **106** (**Table 3.1, Entry 3**) are promising starting points towards developing novel therapeutics against leishmaniasis.

The higher EC_{50} values obtained for the compounds in **Table 3.1** against *L. mexicana* promastigotes compared to axenic amastigotes stage parasite can be rationalised to some extent by considering the variations in *Leishmania* gene expression/transcription.[47] Stage specific expression in *Leishmania* has been reported previously for several genes, for example, *Imcpb* is a gene from *L. mexicana* that encodes a major cysteine proteinase in the parasite. *Imcpb* RNA levels are regulated with steady state levels being high in amastigotes, low in metacyclic promastigotes and undetectable in dividing promastigotes.[48] Statistical analysis of array hybridization data in *L. mexicana* revealed 288 genes (3.5% of all genes) whose steady state mRNA levels met the criteria for differential regulation between promastigotes and lesion derived amastigotes. Interestingly, sample comparison of promastigotes to axenic amastigotes resulted in only 0.2% differential regulation as a consequence of an increase in the magnitude of the transcript levels in cells under axenic conditions.[47]

Leishmania parasites express and assemble an enormous amount of distinctive glycoconjugates. Abundance, location, and uniqueness of these depends on the stage of life cycle; procyclic and metacyclic promastigotes carried by a sand fly vector and the amastigote stage which resides within the phagolysosome of macrophages.[49] Promastigotes are coated with a dense surface glycocalyx, composed mostly of molecules attached by glycosylphosphatidylinositol (GPI) anchors including proteins such as gp63, proteophosphoglycan (PPGs) and glycosylinositolphospholipids (GIPLs).[50] The major constituent is a large GPI anchored phosphoglycan called lipophosphoglycan (LPG). LPG on the promastigotes surface facilitates its attachment to the interior midgut wall and this stops the removal of parasites and mediates migration towards the anterior part of the sand fly's body. Amastigotes synthesize little or no LPG and it is not required for virulence, but there is substantial evidence that LPG is required for the survival of parasites during the initial stage of establishment in the macrophage.[51] Thus differences in cell membrane can also affect the binding ability of the compounds tested leading to changes in effective

concentrations. Apart from that, the potential effect of pH (initial pH difference in culture media and/or pH change due to metabolic activities in parasites), composition of the Schneider's insect medium, differences in incubation periods and the temperature differences can affect the stability and the accumulation of drug candidates, which ultimately result in different EC_{50} values.

In order to try and better understand the differences in the screening data obtained, physical properties (**Table 3.2**) related to Lipinski's rule of five parameters for the compounds were generated using Chemaxon software. The log *P* of pyrithione, (**104**) (**Table 3.2, Entry 1**) predicted is 0.9, and all the other compounds have log *P* values between 1 to 4. For comparison, log *P* values of drugs currently in use for the treatments of leishmaniasis, such as pentamidine (**4**) and miltefosine (**6**), were calculated (log *P* values are 2.32 and 2.25 respectively). Log *P* measures how hydrophobic or hydrophilic a chemical substance is, and this is useful in estimating the distribution of drugs within the body. If the drug is hydrophobic, they are mainly distributed in the lipid bilayers of cells. Conversely, hydrophilic drugs are found primarily in aqueous regions such as blood and serum. Hydrophobic compounds consist of hydrocarbons ($-CH_2-$ chains, rings) which lack the ability to form H bonds. Finally, it is worth noting that all four novel compounds (**116**, **117**, **118**, and **119**) have druglike properties in terms of molar mass and H bond donor/ acceptor capacity.

Entry no.	Compound	Lipinski's rule of five	Molar Mass g/mol	log *P*	H bond donor count	H bond acceptor count
1	**104**	✓	127.16	0.900	1	1
2	**105**	✓	207.27	2.21	1	2
3	**106**	✓	298.42	3.18	1	2
4	**116**	✓	169.20	1.04	0	1
5	**117**	✓	197.25	2.19	0	1
6	**118**	✓	245.30	2.88	0	1
7	**119**	✓	231.27	3.10	0	1

Table 3.2 List of physical properties fall within Lipinski's rule of five for the test compounds in Chapter 3.

Anti-fungal mechanisms of action for **104**, **105** and **106** are not clearly known and further analyses of potential targets are currently in progress. The Au(I) triphenylphospine complex of pyrithione (**115**) (**Figure 3.10**) previously mentioned was further studied by Marisol Vieites[33] to probe its potential interaction with DNA, and ultimately concluded that there is no significant binding, therefore DNA is assumed not to be the main target for the gold **115** complex. A significant increase in the inhibition of *T. cruzi* NADH-fumarate reductase was observed with respect to Pd(II) and Pt(II) complexes (**Figure 3.7**).[33] Furthermore, the Au(I) complex of pyrithione (**104**) was recently found to cause apoptosis *via* mitochondria-mediated cell death in lung cancer cells.[52]

Given that the three of the molecules (**104**, **105** and **106**) contain closely related functional groups involved in metal-binding, and that these groups are attached to a 6-membered heteroaromatic ring, it is highly likely that this core part of these molecules is essential for activity in all three cases. The lower efficacy of **105** and **106** (**Table 3.1, Entry 2,3**) observed against the axenic amastigotes (EC_{50}; 2.78 μM and 3.57 μM) and promastigotes (EC_{50}; 1.82 μM and 8.47 μM) could be due to the presence of bulkier side chains in these compounds. The presence of an oxygen atom in the place of sulphur may also reduce their affinity for metal ions, as the outermost electrons of the sulphur atom are less tightly

bound to the nucleus, making sulphur a stronger electron pair donor. However, given the fact that they are still efficient as anti-fungals and that their activity is potentially related to metal binding, **105** and **106** are probably still able to bind metals. Hence, it could be that **105** and **106** do not fit the specific target within the parasites or are less able to cross the parasite membrane and access the target. Nevertheless, they have shown increased activity in the intramacrophage assay (EC_{50}; 1.70 µM and 1.16 µM). One of the possibilities is that these might act as pro-drug molecules, converting into a more potent molecule once they are inside the macrophage by metabolic or physicochemical transformation.

3.5 Target identification and validation of seven potential DUB inhibitors.

To identify the targets of these molecules in L. mexicana promastigotes, a competition assay between the inhibitors and the activity-based ubiquitin probe (Cy5UbPRG) was performed. Experiments associated in this section was carried out by Mr Sergios Antoniou (PhD student) under the supervision of Professor Jeremy Mottram at University of York.

All the candidates (**104-106**, **116-119**) are potential DUB inhibitors and to probe this they were subjected to a gel-based assay in an attempt to validated DUBs as their target. Detailed experimental procedures that cover this part of the work can be found in **Chapter 7** (**Section 7.5.2**) and the workflow overview of the method is given in **Figure 3.13**. Briefly, the cell extracts/lysates of T7Cas9 *L. mexicana* promastigotes[13] were incubated with 30 µM of each candidate molecule for 1 hr at RT. Three controls were used in here, first, NI: no inhibitor was added but DMSO was added instead. Second, HB: HBX 41108 a non-specific DUB inhibitor. And lastly, FT: FT671 a molecule that does not inhibit any DUBs in *Leishmania*. Then the samples were incubated for another 5 mins with 1 µM of Cy5UbPRG probe and 2 µL of 50 mM NaOH. The reaction was then stopped by adding LDS buffer + DTT and incubating at 70°C for 10 mins. Finally, the samples were run on a NuPAGE™ 4-12% Bis-Tris protein gels, 1.5 mm, 10 well and imaged using the Amersham Typhoon with Excitation:635 nm, Filter: Cy5 670BP30 (**Figure 3.14**).

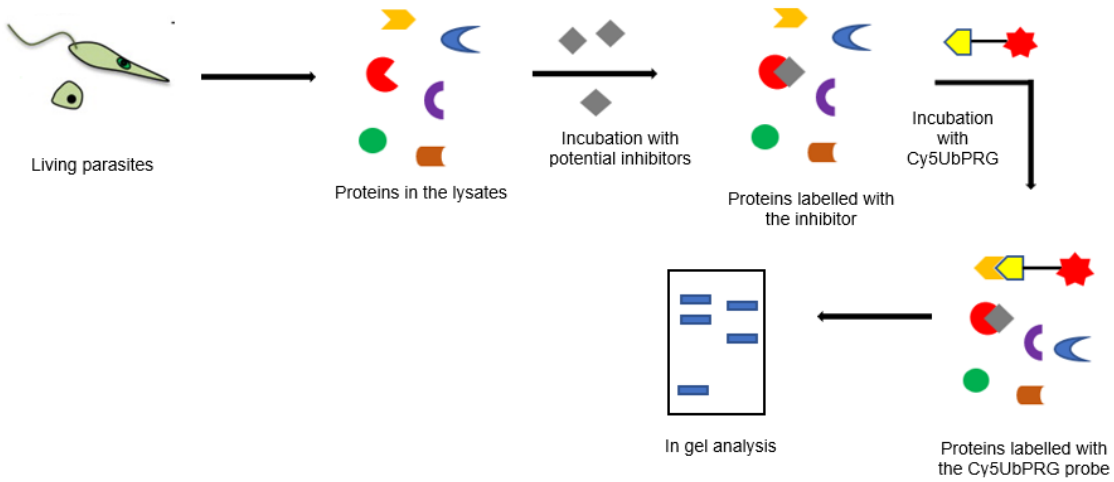

Figure 3.13 Workflow of the in-gel analysis for potential DUBs inhibitors.

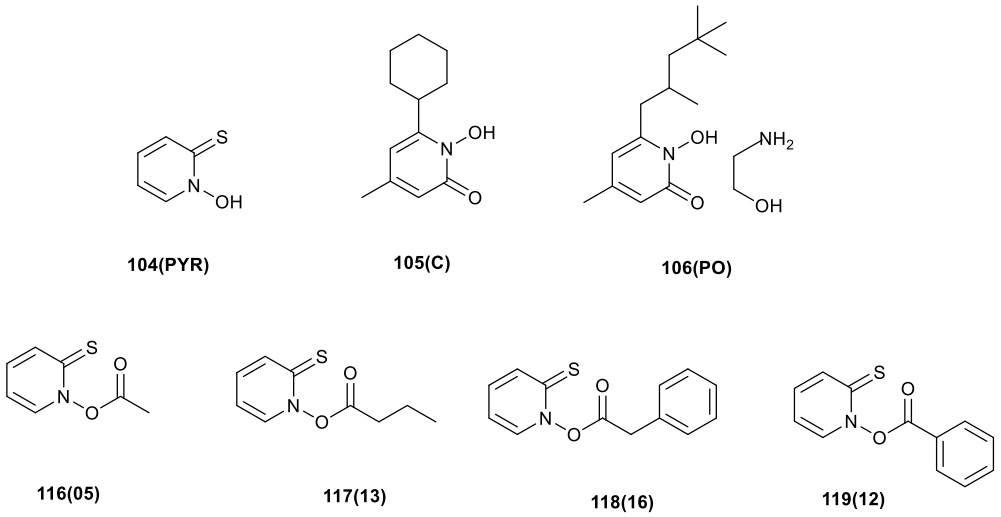

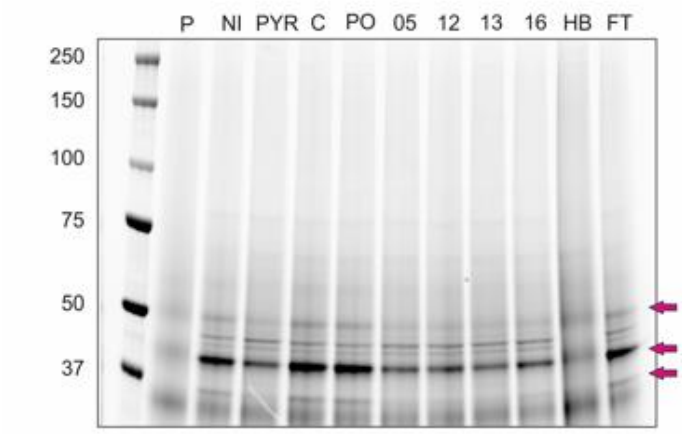

Figure 3.14. Chemical structures of potential DUB inhibitors (**104**, **105**, **106**, **116**, **117**, **118** and **119**) and SDS-PAGE analysis of *in vitro* competitive reaction of Cy5UbPRG and candidate inhibitors with DUBs in *L. mexicana*. Arrows indicate the three DUB enzymes inhibited by **104**, **116**, **117**, **118** and **119**. P: probe without lysate, NI: no inhibitor (control), HB: positive non-specific DUB inhibitor (control), FT: negative control.

As mentioned earlier, Cy5UbPRG is a fluorescent activity-based probe previously designed to react with active DUBs by forming a covalent attachement.[13] Active-site directed probes are a powerful tool in the study of enzymatic functions. Ubiquitin can covalently link through its C-terminal carboxylate to the N-terminal of a target protein. Ubiquitin was functionalized with propargylamine (Ub-PRG) by replacing Gly76 (C-terminal carboxylate of ubiquitin). This has shown a selective reaction with the active site cysteine residue of the DUB enzymes (**Figure 3.15**). Ub-PRG can be synthesized using a linear solid-phase peptide synthesis procedure. Cyanine 5 (Cy5) is a fluorophore label used for protein imaging and employed as the capturing agent in this study.[53] In the competitive activity-based assay, *L. mexicana* promastigotes lysates, which contain all the proteins including DUBs were first treated with the potential DUB inhibitors (in this case compounds **104** to **106** and **116** to **119**) and then the samples were treated with the Cy5UbPRG probe. If the candidate molecule targets/binds to DUB enzymes, when they undergo the probe treatment, the probe cannot establish a bond with the same DUB enzyme as the candidate because Cy5UbPRG probe is designed only to bind with active DUBs. Hence, the band which represents the relevant DUB enzyme disappears or decreases in intensity. DUBs which were inhibited with the candidate molecules are shown in purple colour arrows. Only pyrithione (**104**) and its derivatives (**116**-**119**) seem to inhibit DUBs and, more importantly, they all appear to target the same DUB enzymes (**Figure 3.14**). This suggests that the core of these molecule (pyrithione) must be responsible for forming a covalent attachment with the target protein and for the activity against the *L. mexicana* parasites.

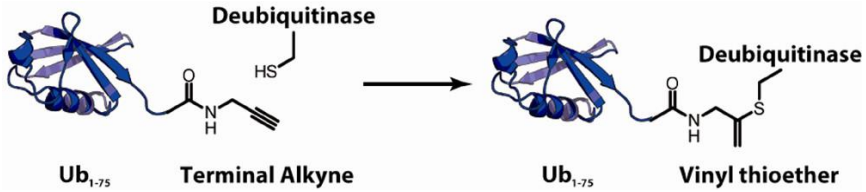

Figure 3.15. The reaction of Ub-PRG with the active-site cystine residue of the DUB enzyme.[53]

Absence of the active enzyme at the bottom of the gel is clearly noticeable compared to the other two DUBs indicated by the arrows (**Figure 3.14**). To identify the enzyme represented by the band disappeared at the bottom, DUB16 overexpressing *L. mexicana* cell line was used. Cells were treated as same way as explained above and another SDS-PAGE gel was run along with all the other samples (**Figure 3.16**). The high intense bad marked with the purple star is the band for DUB16 and the exact band was absent in each sample (**104**, **116**, **117**, **118** and **119**). This confirms that pyrithione (**104**) and its derivatives (**116** - **119**) inhibit DUB16 enzyme in *L. mexicana* promastigotes.

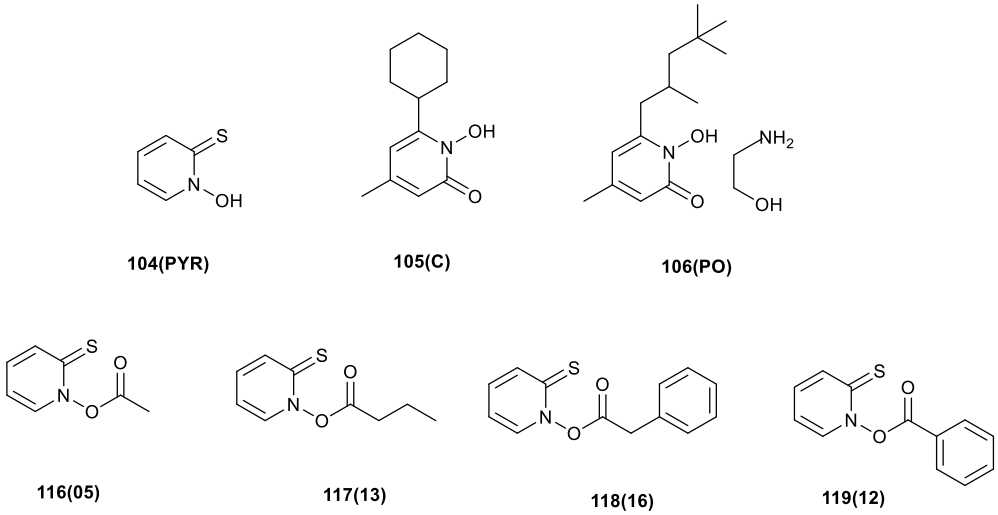

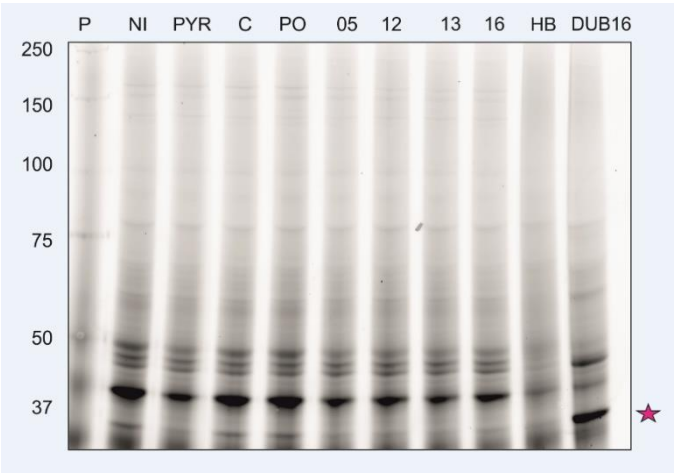

Figure 3.16. Chemical structures of potential DUB inhibitors (**104**, **105**, **106**, **116**, **117**, **118** and **119**) and SDS-PAGE analysis of *in vitro* competitive reaction of Cy5UbPRG and candidate inhibitors with DUBs in *L. mexicana.* P: probe without lysate, NI: no inhibitor (control), HB: positive non-specific DUB inhibitor (control), DUB16: DUB16 overexpressing cell line.

3.6 Further investigation of *L. mexicana* DUB16 overexpressing cells for their ability to develop resistance.

DUB16 is one of the essential proteins in *L. mexicana* promastigotes. Damianou *et al* have recently shown that it is impossible to generate a null mutant of DUB16, which indicates that *dub16* gene is essential for promastigote survival. To offer further evidence that *dub16* is essential and to overlook the possibility of a technical error in gene deletion, they successfully generated a facilitated null mutant line for DUB16 (*Δdub16[DUB16]*) by transfecting the parental Cas9 T7 cell line with a plasmid expressing DUB16.[13]

In an attempt to confirm that DUB16 inhibition is causing parasite death, a cell viability assay was performed between a DUB16 overexpressing *L. mexicana* cell line and *L. mexicana* T7/Cas9 parental cell line. If inhibitors **104**, **105**, **106**, **116**, **117**, **118** and **119** only target the DUB16 enzyme, then the DUB16 overexpressing cell line should be able to survive/show resistance amidst of the inhibition caused by the candidate drug molecules. *L. mexicana* promastigotes were grown in HOMEM medium supplemented with 10% heat-inactivated foetal calf serum (HIFCS) and 1% Penicillin/streptomycin solution at 25 °C. 50µL of promastigotes at 1×10^6 cells/mL and 50µL of drug diluted to appropriate concentrations (from 24 µM to 47 nM) were placed in 96 well plates and incubated at 25 °C for 20 hrs. The resorufin fluorescence (at 590 nm) was measured after adding Alamar Blue® 4 hrs before reading the plates. A detailed experimental protocol is provided in **Chapter 7** (**Section 7.5.3**). The *L. mexicana* T7/Cas9 cell line and DUB16 overexpressing cell line were exposed to the same procedure and the percentage survival was plotted against the compound concentrations in the same graph (**Figure 3.17**). Initially pyrithione (**104**) and compound **117** were studied and DMSO was used as a control. Miltefosine was used as a reference molecule since it is a drug already in use for the treatment of leishmaniasis. Several potential drug targets of miltefosine in *Leishmania* promastigotes have been reported recently, such as cytochrome-c oxidase and fatty acid and sterol mechanism.[54] However, no mechanism has been identified clearly and nothing is reported indicating it targeting DUBs. This explains the almost perfect overlap of the two different cell lines. By analysing the graphs, it is evident that DUB16 overexpressing cell line is not providing resistance over any of the compounds screened (**Figure 3.17**). If DUB16 is the only target for these molecules in *L. mexicana*, over expression of DUB16 would be likely to show tolerance at least to some extent and increase cell survival. But according to the data both *L. mexicana* T7/Cas9 cell line and DUB16 overexpressing cell lines behaved similarly (**Figure 3.17; a, b**).

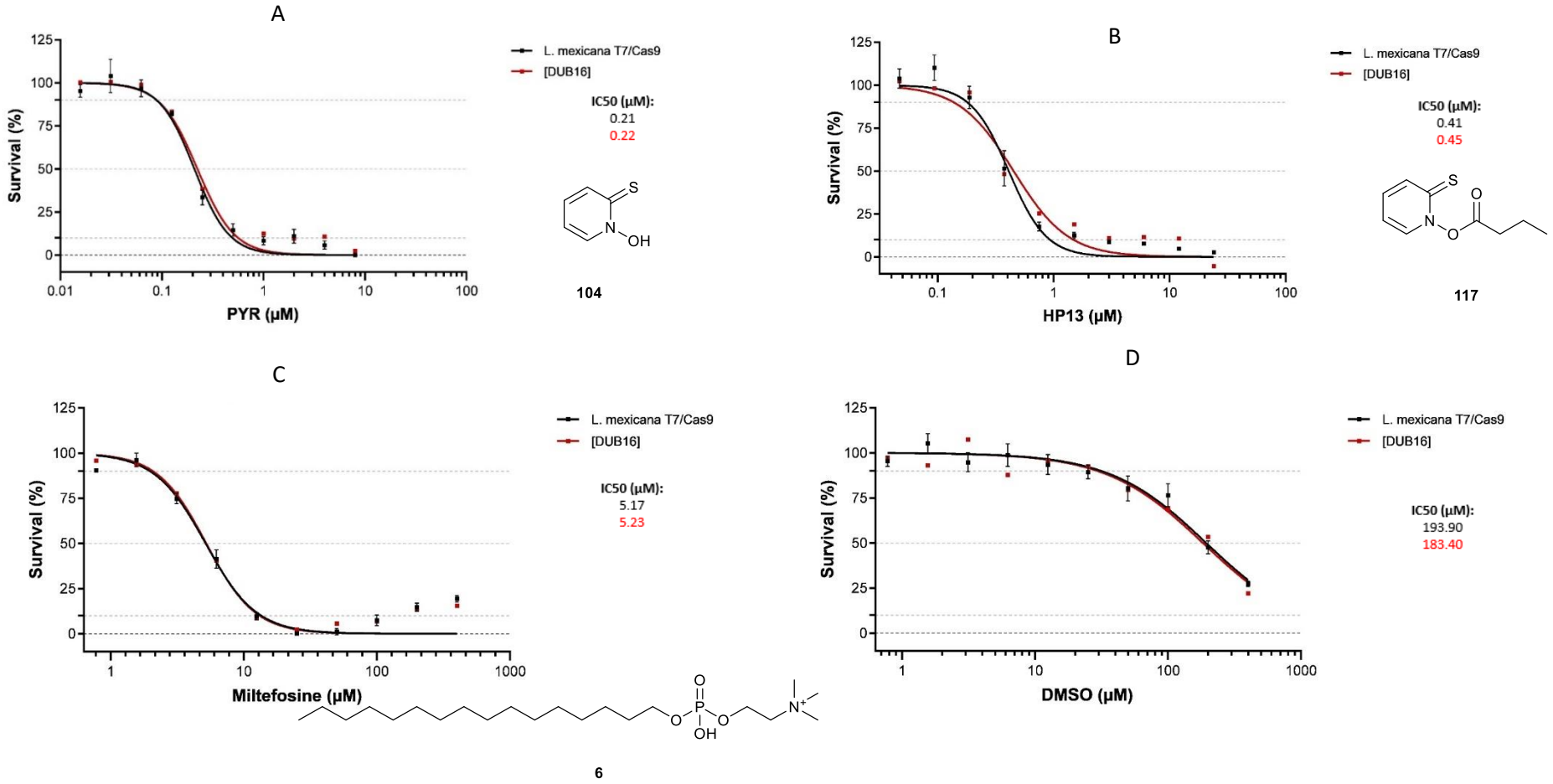

Figure 3.17. Analysis of resistance development in *L. mexicana* DUB16 overexpressing promastigotes. Percentage of survival was plotted against (**A**) Pyrithione (**104**), (**B**) 2-thioxopyridine-1(2H)-yl butyrate (**117**), (**C**) Miltefosine (**6**) and (**D**) DMSO concentrations (µM). *L. mexicana* T7/Cas9, [DUB 16] over-expressing cell line.

The lack of resistance towards **104** and **117** seen in the in overexpressed cell lines strongly indicated that while the pyrithione analogues can target DUB16 they likely exhibit their anti-parasitic activity via an alternative molecular target.

3.7 Chapter Summary

Three FDA approved drugs; pyrithione (**104**), ciclopirox (**105**) and piroctone olamine (**106**) were selected in this chapter to investigate their therapeutic repurposing as a treatment for leishmaniasis. Activity against *L. mexicana* was evaluated by carrying out growth inhibition assays against promastigote, axenic amastigote and intracellular amastigote stages of the parasite. The results obtained shown that all three drugs have the potential to be repurposed for the treatment of CL (**Table 3.1**). Additionally, four novel derivatives of pyrithione (**104**), compounds **116-119** were synthesized to a) try and improved bioactivity and b) to probe the role of metal chelation in the anti-parasitic activity of **104**. Compounds **116-119** were found to have nanomolar level EC_{50} values against *L. mexicana* (**Table 3.1**) suggesting that the activity of the parent compounds (**104**) is not associated with metal chelation. Being able to retain their anti-parasitic activity in infection assays (**Table 3.1**) and still possessing drug-like properties (**Table 3.2**) even after modification, is a very positive sign in terms of carrying out further studies on molecules with a pyrithione core and progressing them as potential drug leads. Furthermore, an In-gel fluorescence assay was carried out with the Cy5UbPRG probe to analyse if any of these molecules target DUBs enzymes. The Cy5UbPRG is a fluorescent activity-based probe previously designed to react with active DUBs (**Figure 3.14**). According to the results (**Figure 3.16**), it is evident that pyrithione (**104**) and the novel derivatives (**116-119**) inhibit DUB16 enzyme in *L. mexicana* promastigotes. DUB16 is an essential enzyme for the survival of *L. mexicana* promastigotes. Then, another assay was designed to further

evaluate a DUB16 overexpressing *L. mexicana* promastigotes cell line for its ability to develop resistance towards the inhibitors (**Figure 3.17**). It was evident from graphs A and B (**Figure 3.17**) that DUB16 overexpression does not provide any resistance towards the inhibition. However, this clarifies that DUB16 is not the only target for these inhibitors, and they may have other targets. Furthermore, it is worth noting that these inhibitors show increased selectivity towards DUB16 compared to the other two DUBs highlighted in **Figure 3.16**. Ciclopirox and piroctone olamine do not seem to target any of the DUBs in *Leishmania mexicana*, but they still show interesting anti-leishmanial activity. This again indicates that these candidate molecules may have a different mode of action.

3.8 References

1. Kaiser, M. *et al.* Antiprotozoal activity profiling of approved drugs: A starting point toward drug repositioning. *PLoS One* **10**, 1–16 (2015).

2. Chong, C. R. & Jr, D. J. S. *New uses for old drugs*. *Nature* vol. 448 (2007).

3. Baik, J. & Rosania, G. R. Macrophages Sequester Clofazimine in an Intracellular Liquid Crystal-Like Supramolecular Organization. *PLoS One* **7**, e47494 (2012).

4. Evans, A. T., Croft, S. L., Peters, W. & Neal, R. A. Antileishmanial effects of clofazimine and other antimycobacterial agents. *Ann. Trop. Med. Parasitol.* **83**, 447–454 (1989).

5. Domínguez-Asenjo, B. *et al.* Ex Vivo Phenotypic Screening of Two Small Repurposing Drug Collections Identifies Nifuratel as a Potential New Treatment against Visceral and Cutaneous Leishmaniasis. *ACS Infect. Dis.* **7**, 2390–2401 (2021).

6. Van Cutsem, J. The antifungal activity of ketoconazole. *Am. J. Med.* **74**, 9–15 (1983).

7. Alkhawajah, A. Recent trends in the treatment of cutaneous leishmaniasis. *Ann. Saudi Med.* **18**, 412–416 (1998).

8. Rifampicin-Drug bank. https://go.drugbank.com/drugs/DB01045 (2005).

9. Omeprazole-Drug bank. https://go.drugbank.com/drugs/DB00338 (2005).

10. Kochar, D. K. *et al.* A double blind, randomised placebo controlled trial of rifampicin with omeprazole in the treatment of human cutaneous leishmaniasis. *J. Vector Borne Dis.* **43**, 161–167 (2006).

11. Hughes, J. P., Rees, S. S., Kalindjian, S. B. & Philpott, K. L. Principles of early drug discovery. *Br. J. Pharmacol.* **162**, 1239–1249 (2011).

12. Zhao, C. *et al.* Repurposing an antidandruff agent to treating cancer: Zinc pyrithione inhibits tumor growth via targeting proteasome-associated deubiquitinases. *Oncotarget* **8**, 13942–13956 (2017).

13. Damianou, A. *et al.* Essential roles for deubiquitination in Leishmania life cycle progression. *PLoS Pathog.* **16**, e1008455 (2020).

14. Kirchhoff, L. V., Kim, K. S., Engman, D. M. & Donelson, J. E. Ubiquitin genes in trypanosomatidae. *J. Biol. Chem.* **263**, 12698–12704 (1988).

15. He, M. *et al.* The emerging role of deubiquitinating enzymes in genomic integrity, diseases, and therapeutics. *Cell Biosci.* **6**, 1–15 (2016).

16. Ravid, T. & Hochstrasser, M. Diversity of degradation signals in the ubiquitin-proteasome system. *Nat. Rev. Mol. Cell Biol.* **9**, 679–689 (2008).

17. Harrigan, J. A., Jacq, X., Martin, N. M. & Jackson, S. P. Deubiquitylating enzymes and drug discovery: Emerging opportunities. *Nat. Rev. Drug Discov.* **17**, 57–77 (2018).

18. Turcu Francisca E. Reyes, Ventii Karen H., W. K. D. W., Reyes-Turcu, F. E., Ventii, K. H. & Wilkinson, K. D. Nicotine-induced Upregulation of Nicotinic Receptors: Underlying Mechanisms. *Biochem Pharmacol* **78**, 756–765 (2009).

19. Azevedo, C. S. *et al.* Revealing a novel otubain-like enzyme from Leishmania

infantum with deubiquitinating activity toward K48-linked substrate. *Front. Chem.* **5**, 1–11 (2017).

20. Li, M., Brooks, C. L., Kon, N. & Gu, W. A dynamic role of HAUSP in the p53-Mdm2 pathway. *Mol. Cell* **13**, 879–886 (2004).

21. Colland, F. *et al.* Small-molecule inhibitor of USP7/HAUSP ubiquitin protease stabilizes and activates p53 in cells. *Mol. Cancer Ther.* **8**, 2286–2295 (2009).

22. Chauhan, D. *et al.* A Small Molecule Inhibitor of Ubiquitin-Specific Protease-7 Induces Apoptosis in Multiple Myeloma Cells and Overcomes Bortezomib Resistance. *Cancer Cell* **22**, 345–358 (2012).

23. Besteiro, S., Williams, R. A. M., Morrison, L. S., Coombs, G. H. & Mottram, J. C. Endosome sorting and autophagy are essential for differentiation and virulence of Leishmania major. *J. Biol. Chem.* **281**, 11384–11396 (2006).

24. Khare., S. *et al.* Proteasome inhibition for treatment of leishmaniasis, Chagas disease and sleeping sickness. *Nature* **537**, 229–233 (2016).

25. Wyllie, S. *et al.* Preclinical candidate for the treatment of visceral leishmaniasis that acts through proteasome inhibition. *Proc. Natl. Acad. Sci. U. S. A.* **116**, 9318–9323 (2019).

26. Nagle, A. *et al.* Discovery and Characterization of Clinical Candidate LXE408 as a Kinetoplastid-Selective Proteasome Inhibitor for the Treatment of Leishmaniases. *J. Med. Chem.* **63**, 10773–10781 (2020).

27. Chandler, C. J. & Segel, I. H. Mechanism of the antimicrobial action of pyrithione: effects on membrane transport, ATP levels, and protein synthesis. *Antimicrob. Agents Chemother.* **14**, 60–68 (1978).

28. Park, M., Cho, Y. J., Lee, Y. W. & Jung, W. H. Understanding the Mechanism of Action of the Anti-Dandruff Agent Zinc Pyrithione against Malassezia restricta. *Sci. Rep.* **8**, 1–11 (2018).

29. Reeder, N. L. *et al.* The antifungal mechanism of action of zinc pyrithione. *Br. J. Dermatol.* **165**, 9–12 (2011).

30. Krenn, B. M. *et al.* Antiviral Activity of the Zinc Ionophores Pyrithione and Hinokitiol against Picornavirus Infections. *J. Virol.* **83**, 58–64 (2009).

31. Vieites, M. *et al.* Potent in vitro anti-Trypanosoma cruzi activity of pyridine-2-thiol N-oxide metal complexes having an inhibitory effect on parasite-specific fumarate reductase. *J. Biol. Inorg. Chem.* **13**, 723–735 (2008).

32. Turrens, J. F. *et al.* Mercaptopyridine-N-oxide an NADH-fumarate reductase inhibitor blocks Trypanosoma cruzi growth in culture and in infected myoblasts. *FEMS Microbiol. Lett.* **175**, 217–221 (1999).

33. Vieites, M. *et al.* Synthesis and characterization of a pyridine-2-thiol N-oxide gold(I) complex with potent antiproliferative effect against Trypanosoma cruzi and Leishmania sp. insight into its mechanism of action. *J. Inorg. Biochem.* **103**, 1300–1306 (2009).

34. Roques, C., Brousse, S. & Panizzutti, C. In vitro antifungal efficacy of ciclopiroxolamine alone and associated with zinc pyrithione compared to ketoconazole against Malassezia globosa and Malassezia restricta reference strains. *Mycopathologia* **162**, 395–400 (2006).

35. Weir, S. J. *et al.* The repositioning of the anti-fungal agent ciclopirox olamine as a

novel therapeutic agent for the treatment of haematologic malignancy. *J. Clin. Pharm. Ther.* **36**, 128–134 (2011).

36. Feng, H. *et al.* Repurposing antimycotic ciclopirox olamine as a promising anti-ischemic stroke agent. *Acta Pharm. Sin. B* **10**, 434–446 (2020).

37. Carlson-Banning, K. M. *et al.* Toward Repurposing Ciclopirox as an Antibiotic against Drug-Resistant Acinetobacter baumannii, Escherichia coli, and Klebsiella pneumoniae. *PLoS One* **8**, e69646 (2013).

38. Kim, Y. *et al.* Increased In vivo efficacy of lenalidomide by addition of piroctone olamine. *In Vivo (Brooklyn).* **25**, 99–103 (2011).

39. Sigle, H. C., Schäfer-Korting, M., Korting, H. C., Hube, B. & Niewerth, M. In vitro investigations on the mode of action of the hydroxypyridone antimycotics rilopirox and piroctone on Candida albicans. *Mycoses* **49**, 159–168 (2006).

40. Couto, F. M. M. do. *et al.* Antifungal activity of the piroctone olamine in experimental intra-abdominal candidiasis. *Springerplus* **5**, 1–4 (2016).

41. Lu, D. *et al.* Activation of the Wnt signaling pathway in chronic lymphocytic leukemia. *Proc. Natl. Acad. Sci. U. S. A.* **101**, 3118–3123 (2004).

42. Panic, G., Vargas, M., Scandale, I. & Keiser, J. Activity profile of an FDA-approved compound library against Schistosoma mansoni. *PLoS Negl. Trop. Dis.* **9**, 1–15 (2015).

43. Albalawi, A. E. *et al.* Fe3O4@piroctone olamine magnetic nanoparticles: Synthesize and therapeutic potential in cutaneous leishmaniasis. *Biomed. Pharmacother.* **139**, 111566 (2021).

44. Barton, D. H. R. & Tachdjian, C. The Invention of Radical Reactions. Part XXVII. Modified Julia Synthesis of Olefins Using Radical Deoxygenation. *Tetrahedron* **48**, 7109–7120 (1992).

45. Barton, D. H. R., Chern, C. Y. & Jaszberenyi, J. C. The invention of radical reactions. Part XXXIV. Homologation of carboxylic acids to α-keto carboxylic acids by Barton-ester based radical chain chemistry. *Tetrahedron* **51**, 1867–1886 (1995).

46. Taciak, B. *et al.* Evaluation of phenotypic and functional stability of RAW 264.7 cell line through serial passages. *PLoS One* **13**, 1–13 (2018).

47. Holzer, T. R., McMaster, W. R. & Forney, J. D. Expression profiling by whole-genome interspecies microarray hybridization reveals differential gene expression in procyclic promastigotes, lesion-derived amastigotes, and axenic amastigotes in Leishmania mexicana. *Mol. Biochem. Parasitol.* **146**, 198–218 (2006).

48. Coombs, H., Mottram, J. C., Souza, E. & Waugh, S. Characterization of a multi-copy gene for a major stage-specific cysteine proteinase of Leishmania mexicana. *FEBS Lett.* **311**, 124–127 (1992).

49. Medina-Acosta, E., Karess, R. E. & Russell, D. G. Structually distinct genes for the surface protease of Leishmania mexicana are developmentally regulated. *Mol. Biochem. Parasitol.* **57**, 31–45 (1993).

50. Späth, G. F., Garraway, L. A., Turco, S. J. & Beverley, S. M. The role(s) of lipophosphoglycan (LPG) in the establishment of Leishmania major infections in mammalian hosts. *Proc. Natl. Acad. Sci. U. S. A.* **100**, 9536–9541 (2003).

51. Salvatore J. Turco, G. F. S. and & Beverley, S. M. Is lipophosphoglycan a

virulence factor? A surprising diversity between Leishmania species. *Trends Parasitol.* **17**, 223–226 (2001).

52. Li, X. *et al.* A new gold(I) complex-Au(PPh3)PT is a deubiquitinase inhibitor and inhibits tumor growth. *EBioMedicine* **39**, 159–172 (2019).

53. Ekkebus, R. *et al.* On Terminal Alkynes That Can React with Active-Site Cysteine Nucleophiles in Proteases. *J. Am. Chem. Soc.* **135**, 2867–2870 (2013).

54. Dorlo, T. P. C., Balasegaram, M., Beijnen, J. H. & Vries, P. J. D. Miltefosine: a review of its pharmacology and therapeutic efficacy in the treatment of leishmaniasis. *J. Antimicrob. Chemother.* **67**, 2576–2597 (2012).

4 Investigation of anti-parasitic properties of novel, diverse fluorinated molecules.

4.1 Introduction

Small organic molecules play an important role in drug discovery and development. They are typically characterized by molecular weights of <500g/mol, which allow them to easily penetrate cell membranes and reach target proteins or DNA. While traditional medicinal chemistry is often focused on the use of natural compounds or closely related derivatives, the incorporation of fluorine, an atom not typically found in natural products, in small-molecule drug discovery research programmes is widely seen. In fact despite the low abundance of fluoro-organic compounds in nature numerous fluorinated drugs have been developed as antimicrobial, antitumor and anti-inflammatory agents (**Figure 4.1**).[1] It is estimated that 25% of the small molecule drugs in the market are fluoro-pharmaceuticals.[2]

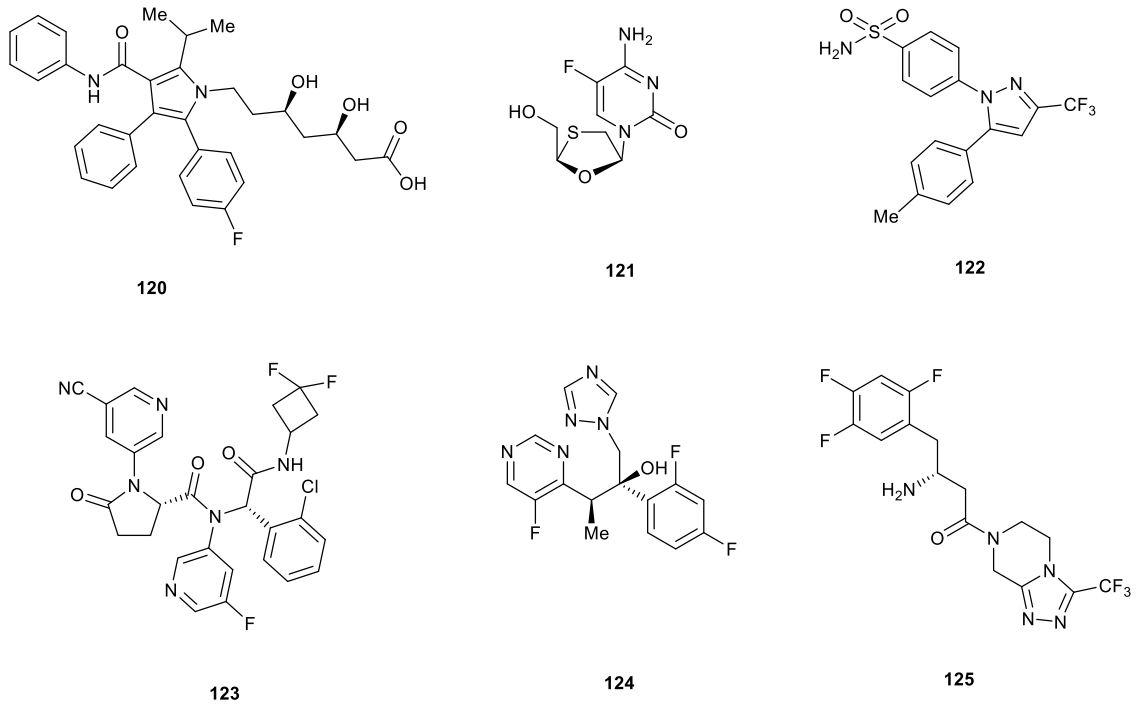

Figure 4.1 Selected examples of fluoro-pharmaceuticals with heterocycles. Lipitor; cardiovascular disease, 1997 (**120**) , emtricitabine; HIV, 2003 (**121**), celecoxib; an anti-inflammatory medication, 1999 (**122**), ivosidenib; an anti-cancer medication, 2018 (**123**), voriconazole; an anti-fungal medication, 2002 (**124**), and sitagliptin; diabetes, 2006 (**125**).[3]

Fluorine is a small atom (van der Waals radius 1.47 Å) with the highest electronegativity (3.98 Pauling scale). The relatively small size of the fluorine atom means that sterically it is comparable to a hydrogen (van der Waals radius of 1.20 Å) and as such it can be incorporated into a molecule with a low steric penalty. The low steric penalty means that fluorinated molecules are often processed in a similar way to their non-fluorinated analogues in terms of metabolism within biological systems.[4,5,6] Despite their similarities in size it is worth noting that the C-F bond is stronger (485 KJ/mol) than the C-H bond (416 KJ/mol), and this can be exploited in such a way as to use and H to F swap to make more resistant to metabolic degradation.[7] The first fluoro-pharmaceutical compound was fludrocortisone acetate (**126**) (**Figure 4.2**), which was marketed in 1954.[8] It is a synthetic corticosteroid that contains a fluorine atom at 9α-position. Pioneering work by Fried et al., on 9α-fluoro-hydrocortisone acetate revealed how introduction of fluorine into an existing biologically active compound enhanced its biological activity and improved versatility.[8] Fluoroquinolones, such as ciprofloxacin (**127**), norfloxacin (**128**) and levofloxacin (**129**) (**Figure 4.2**), were introduced in 1980s and act as potent antibacterial agents by inhibiting the activity of DNA gyrase and topoisomerase.[2]

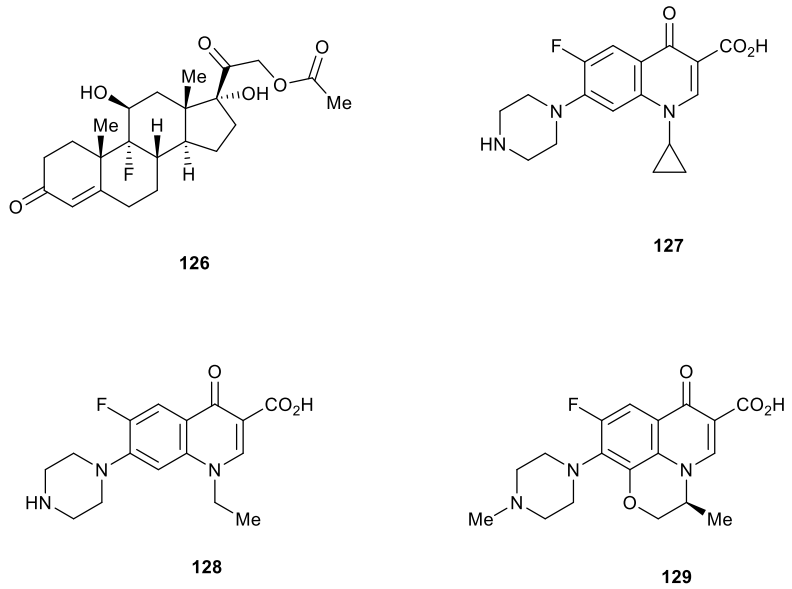

Figure 4.2 Chemical structures of fluorinated drugs developed in 1950s and 1980s. Florinef acetate, 1954 (**126**), ciprofloxacin, 1981 (**127**), norfloxacin, 1979 (**128**) and levofloxacin, 1993 (**129**).

As highlighted fluorine incorporation into small molecules has been extensively investigated in drug discovery research and some of the current applications of this strategy are discussed below.

Improved metabolic stability - Lipophilic compounds are susceptible to oxidative metabolism caused by liver enzymes, in particular cytochrome P450. Low metabolic stability is often found to limit bioavailability of compounds and is a recurring challenge in many drug-discovery projects.[1] One of the strategies is to block the metabolically reactive site with a fluorine substituent to prevent oxidation based on the fact that C-F bond is more resistant to attack than C-H bond.[9] Development of the cholesterol-absorption inhibitor Ezetimibe (**131**) from a moderately potent compound SCH48461 (**130**), is an example of the successful achievement of fluorine replacement (**Figure 4.3**).[10]

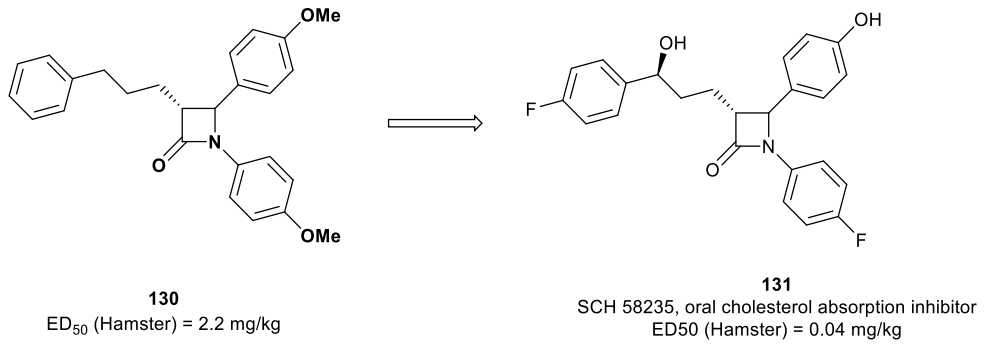

Figure 4.3 Development of Ezetimibe (**131**) by optimizing the lead, SCH4861(**131**).[10]

Altered physicochemical properties - The electronegativity of fluorine can affect the acidity or basicity of a compound. A change in the pK_a value of a molecule has a strong effect on its pharmacological properties and its binding affinity. For example, a highly basic group may be required to obtain a better binding affinity to the target protein, but at the same time it can limit the bioavailability of the compound. Finding an optimum condition while incorporating fluorine atoms can overcome these conflicts resulting a better

membrane permeability and thus improved bioavailability.[1] The work of van Niel et al., on novel fluorinated indole derivatives as selective 5-HT_{1D} receptor (involved in mechanisms which cause migraine) ligands, highlighted that the incorporation of fluorine has significantly reduced the pKa of the compounds (**Figure 4.4**).[11] This reduction of basicity associated with a weakening of the affinity to the receptor was shown to have a strong beneficial impact on oral absorption.[11]

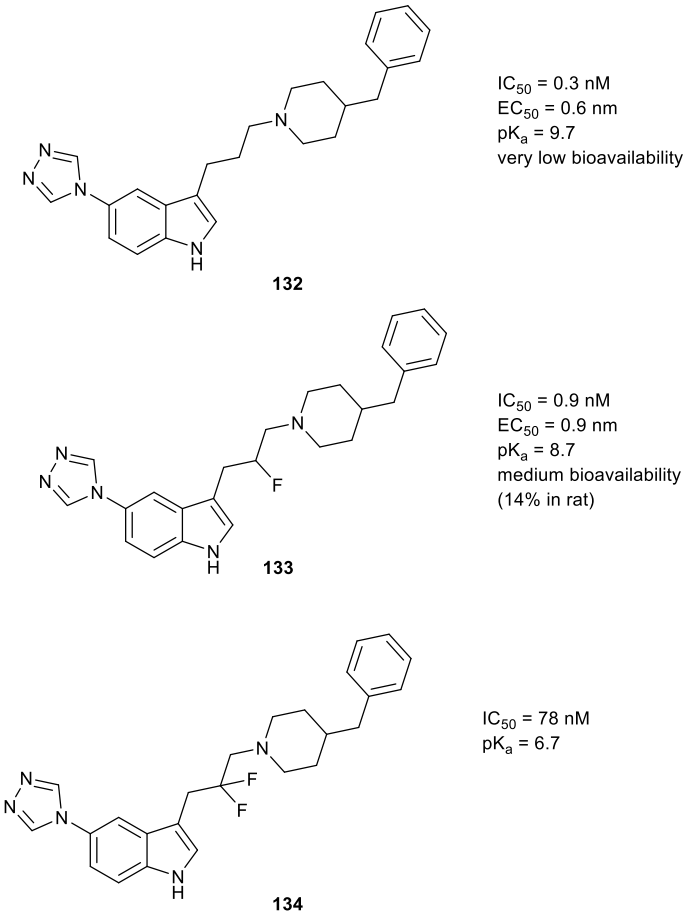

Figure 4.4 Effect of pKa value on the bioavailability. Monofluorinated molecule has a lower pKa that is still compatible with the receptor binding and increased bioavailability. The difluorinated molecule has a pKa < 7 and is no longer basic enough to bind with the receptor 5-HT_{1D}.[11]

Increased binding affinity: Fluorine can impose a significant effect on the binding affinity in ligand-protein complexes through direct interaction with the protein or indirect interaction by modulating the polarity of other groups of the ligand that link with the protein. For example, (napth-2-yl) difluoromethylphosphonic acid (**135**) has been found to inhibit

dephosphorylation of [^{32}P] insulin receptors by PTP-1B, a protein tyrosine phosphatase (PTPase), with ~88 % inhibition (35 - 40 μM IC_{50}), while non fluorinated compound (**136**) has no inhibition (**Figure 4.5**).[12] X-ray crystallographic and kinetic studies imply that this is due to direct interactions of at least one of the fluorine atoms with the enzyme active site and it is not linked to the pKa shifts.[13] The molecules shown in **Figure 4.5** have been synthesised as novel serine protease inhibitors with antithrombotic activities that differ just by one fluorine atom. It has been shown that the fluorinated compound (**137**) has a binding constant (K*i* = 0.26 μM) six times higher than the compound without fluorine (**138**) (K*i* = 1.6 μM) against thrombin.[1]

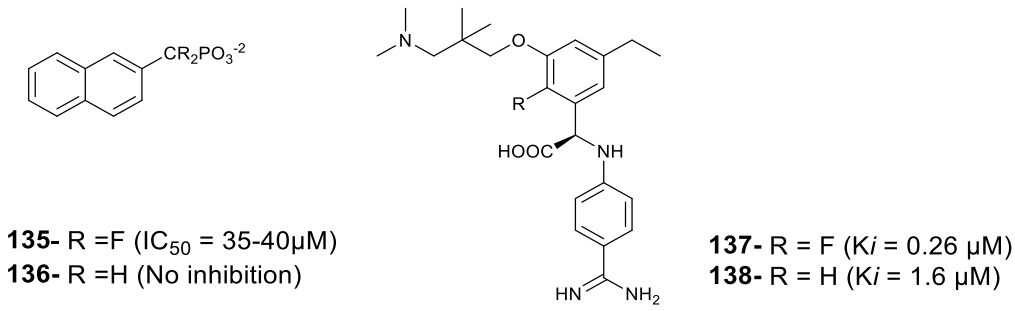

Figure 4.5 Structures, inhibition, and binding affinity of four compounds with and without fluorine substituent.

Fluorinated drug candidates have also been developed for the treatment of leishmaniasis and Chagas disease. Da Silva Maffei et al., have reported the anti-leishmanial activity of a series of copper (II) α-hydroxycarboxylate complexes (**Figure 4.6**) against *L. amazonensis* promastigotes.[14] The greatest activity against the parasites was found after a 72 hr incubation period and increased anti-leishmanial activity was observed in complexes $Cu(L1)_2$ (**139**) (297.2 ± 11.4 μM) and $Cu(L2)_2$ (**140**) (166.7 ± 18.3 μM) when CF_3 replaced the CH_3 moiety. It was suggested that the presence of CF_3 in the copper (II) complexes may induce higher anti-leishmanial activity due to enhanced parasite membrane penetration.[15,14]

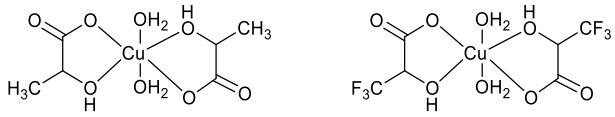

139 **140**

Figure 4.6 Chemical structures of $Cu(L1)_2$ (**139**) AND $Cu(L2)_2$ (**140**).

Curcumin (**141**) is a biologically active component of turmeric, a widely applied spice in Asian cuisine and a traditional medicine extracted from the roots of *Curcuma longa*. Recently, the activity of a fluorinated analogue of curcumin, (1E,6E)-4-[(3,4-difluorophenyl)-methylidene]-1,7-bis(4-hydroxy-3-methoxyphenyl) hepta-1,6-diene-3,5-dione (CDF) (**142**) (**Figure 4.7**) against *Leishmania major* (EC_{50} against promastigotes = 0.37 µM, EC_{50} against amastigotes = 0.35 µM) was calculated. It demonstrated significantly enhanced anti-parasitic activity compared to curcumin (EC_{50} against promastigotes = 103.2 µM).[16] Given the fact that CDF (**142**) has already been tested *in vivo* in female ICR-SCID mice [Institute of Cancer Research - Severe Combined immunodeficiency; ICR-SCID] where it was well tolerated and reported higher bioavailability than curcumin, it can be considered as a suitable drug candidate for parasitic diseases.[17]

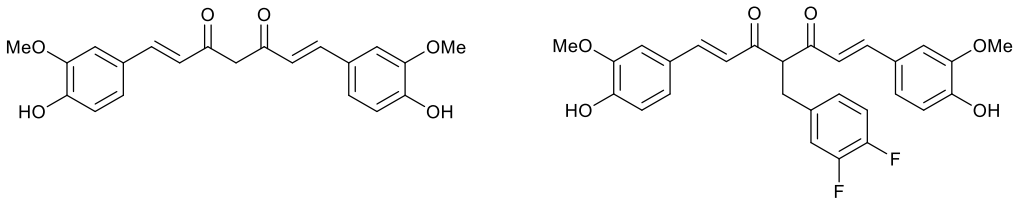

141 **142**

Figure 4.7 Chemical structures of Curcumin (**141**) and its semi-synthetic derivative, CDF (**142**).

Furthermore, 1,2,3-triazole-based tetrafluorophenoxymethyl ketone (**143**) (**Figure 4.8**), a nonpeptidic irreversible inhibitor of cruzain (a cysteine protease) was reported to be superior to the dipeptidyl vinyl sulfone (**144**) (peptidic inhibitor), which has been shown to

cure Chagas disease in animal models. While dipeptidyl vinyl sulfone is an effective inhibitor, it exhibits low oral bioavailability and a short circulating half-life due to its peptidic nature. Nonpeptidic 1,2,3-triazole-based tetrafluorophenoxymethyl ketone seem to successfully surpass those issues and completely eradicate parasites from the cells with no toxicity.[18]

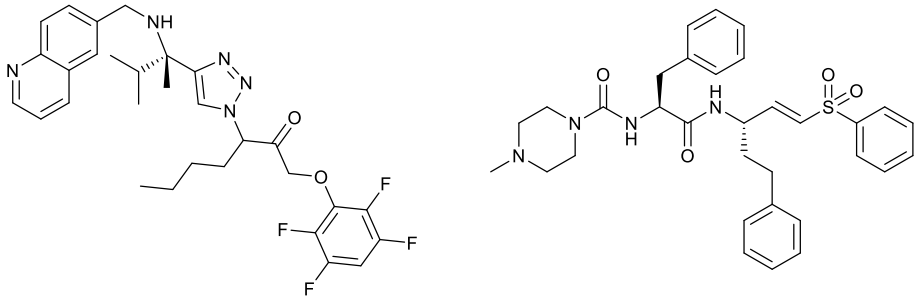

Figure 4.8 Chemical structures of 1,2,3-triazole-based tetrafluorophenoxymethyl ketone- Nonpeptidic inhibitor (**143**), dipeptidyl vinyl sulfone- peptidic inhibitor (**144**).

Manzano et al., have discovered that N1-(7-chloroquinolin-4-yl)-N3-(4-(5-fluorobenzo[b]thiophen-3-yl)benzyl)propane-1,3-diamine (**145**) (**Figure 4.9**) has promising antileishmanial activity against *Leishmania infantum*.[19] To gain further insights into the activity of this molecule, a second generation library was synthesized from **145** and their activity against *Leishmania infantum* parasites (*in vitro*- against promastigotes and *in vivo*- against intracellular amastigotes) were evaluated. Novel derivatives of **145** have slightly decreased yet promising antileishmanicidal activities (< 1.0 µM IC_{50} values).[20]

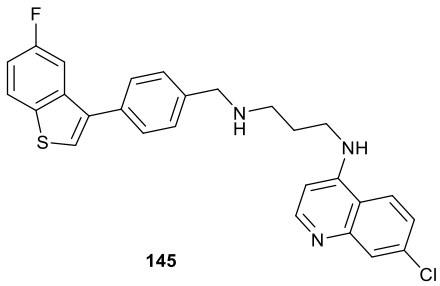

Figure 4.9 Structure of N1-(7-chloroquinolin-4-yl)-N3-(4-(5-fluorobenzo[b]thiophen-3-yl)benzyl)propane-1,3-diamine (**145**).

4.2 Evaluation of antiparasitic activity against *Leishmania mexicana* and *Trypanosoma cruzi.*

*The compound library screened in this chapter was synthesised by Dr Will D.G. Brittain (Cobb group) and Professor Graham Sandford's research group (**GS group**) at Durham University, UK. Biological testing associated with T. cruzi epimastigotes in this chapter was carried out at University of Sao Paulo, Brazil by Dr Richard Girard and Dr Flavia Damasceno under the supervision of Professor Ariel Silber. Anti-leishmanial assays with L. mexicana were carried out by the author of this thesis*.

Multi-functional pyridine derivatives and the construction of new heterocyclic drug systems can be readily derived from the highly reactive pentafluoropyridine core. Modification of pentafluoropyridine is most commonly achieved *via* nucleophilic aromatic substitution reactions. This reaction occurs firstly in the most activated 4-position of pentafluoropyridine, located para to ring nitrogen to give a range of 4-substituted tetrafluoropyridine systems (**Scheme 4.1**).[21]

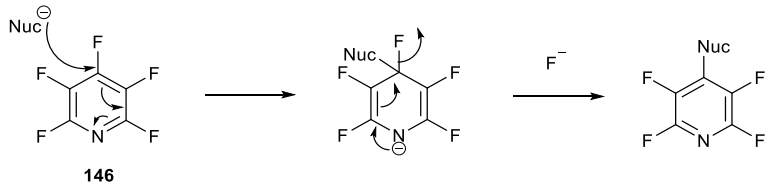

Scheme 4.1 S_NAr mechanism for pentafluoropyridine (**146**).

As part of an on-going research program in the Cobb group that is looking to utilise fluorine and more specifically pentafluoropyridine (**146**) in the design of biological relevant scaffolds (for fragment-based drug discovery), the first series of molecules were synthesized. Depending on the number of tetrafluoropyridines (TFPs) in the system, all 47 compounds screened in this chapter could broadly split into two distinct classes, Class One (**Table 4.1**) and Class Two (**Table 4.3**). The second series consists of 24 diverse, novel, fluorinated chemical scaffolds (**Figure 4.12**).

The libraries were stored at room temperature and once the stock solutions (10 mM) were prepared in DMSO, they were stored at -20 ºC. All the molecules were first screened against *L. mexicana* promastigotes and axenic amastigotes at a fixed concentration of 50 µM and compounds with poor activity were eliminated without progressing to EC_{50} determination as mentioned in Chapter 2. For *T. cruzi* the initial fixed concentration used was 5 µM. Therefore, the same library was again screened against *L. mexicana* at 5 µM to obtain similar data sets. The number of viable cells of *L. mexicana* as a survival percentage and the effect on *T. cruzi* epimastigotes, *L. mexicana* promastigotes and axenic amastigotes after the drug treatment at 5 µM were shown in **Table 4.1**, **Table 4.3** and **Table 4.5**.

Entry number	Compound Number	R	*L. mexicana* axenic amastigotes survival (%) at 50 µM	Effect on *L. mexicana* axenic amastigotes growth at 5µM	*L. mexicana* promastigotes survival (%) at 50 µM	Effect on *L. mexicana* promastigotes growth at 5µM	Effect on *T. cruzi* epimastigotes (CLB) growth at 5µM
1	**147**	1-*tert*-butyl-2-methylpyrrolidine-1,2, dicarboxylate	78	No	100	No	No
2	**148**	4-nitrophenoxy	89	No	89	No	No
3	**149**	3-methylphenoxy	94	No	100	No	No
4	**150**	2H-1-benzopyran-2-one	71	No	7	No	No
5	**151**	$C_6H_4NH_2$ (3-yloxy-aniline)	90	No	100	No	No
6	**152**	Biphenyl	67	No	3	No	No
7	**153**	benzonitrile	83	No	99	No	No
8	**154**	4-methoxyphenoxy	90	No	100	No	No
9	**155**	8-hydroxy-3a-methyl-1H,2H,3H,3aH,3bH,4H,5H,9bH,10H,11H,11aH-cyclopenta[a]phenanthren-3-one	84	No	86	No	No
10	**156**	1, benzyl-4-phenyl-1,2,3,triazole	81	No	48	No	No
11	**157**	4-iodophenoxy	100	No	100	No	No
12	**158**	4-methoxybiphenyl	100	No	100	No	No
13	**159**	4-[2-(4-hydroxyphenyl)propan-2-yl]-2-iodophenol	73	No	4	No	No
14	**160**	1-iodonaphthalene	72	No	4	No	No
15	**161**	[1,1‘-binaphthalene]-2-ol	73	No	4	No	No
16	**162**	4-[2-(4-hydroxyphenyl)propan-2-yl]-2,6-diiodophenol	44	No	24	No	No

17	**163**	4-((4'-methoxy-[1,1'-biphenyl]	82	No	55	No	No
18	**164**	5-[2-(4-hydroxyphenyl)propan-2-yl]-4'-methoxy-[1,1'-biphenyl]-2-ol	89	No	100	No	No
19	**165**	naphthalen-1-ol	77	No	79	No	No
20	**166**	naphthalen-2-ol	96	No	86	No	No
21	**167**	5-iodo-[1,1'-biphenyl]-2,2'-diol	67	No	5	No	No
22	**168**	3'-iodo-4'-methoxy-[1,1'-biphenyl]-4-ol	71	No	29	No	No
23	**169**	6-iodo-[1,1'-biphenyl]3-ol	73	No	44	No	No
24	**170**	2,6-dimethylphenoxy	100	No	100	No	No
25	**171**	3-ethynylphenoxy	100	No	100	No	No
26	**172**	pyridin-3-yloxy	98	No	100	No	No
27	**173**	2-tert-butylphenoxy	100	No	100	No	No
28	**174**	4-(trifluoromethyl)phenoxy	100	No	100	No	No
29	**175**	2-methylphenoxy	100	No	100	No	No
30	**176**	3-iodophenoxy	100	No	89	No	No
31	**177**	2-(1,1'-biphenyl)	4	No	8	No	No
32	**178**	4-(2-phenylpropan-2-yl)phenol	10	No	3	No	No
33	**179**	3-(1,1'-biphenyl)	33	No	23	No	No
34	**180**	4-(4-phenylmethyl)phenol	22	No	9	No	No
35	**181**	3'-iodo-4'-methoxy-[1,1'-biphenyl]	55	No	28	No	No
36	**182**	4-[1-(4-hydroxyphenyl)-1-phenylethyl]phenol	9	No	1	Yes(18%)	No
37	**183**	4-[(4-hydroxyphenyl)methyl]-2-iodophenol	10	No	4	No	No
38	**184**	2-bromo-4-[2-(4-hydroxyphenyl)propan-2-yl]phenol	33	No	8	No	No
39	**185**	4-[1-(4-hydroxyphenyl)-1-phenylethyl]-2-iodophenol	14	No	5	No	No

Table 4.1 Core structure of the Class One and the biological data against *L. mexicana* axenic amastigotes, promastigotes, and *T. cruzi* epimastigotes (No- not active against *T. cruzi).*

Most of the compounds screened in this initial library were not active against the parasite species tested but some were moderately active (**Table 4.7**). Compounds with low survival rate were selected to determine EC_{50} (compounds with less than 50% viable cells at 50 µM). For a better understanding of the screening data obtained, physiochemical properties associated with Lipinski's rule of five parameters were generated using Chemaxon software (**Table 4.2, Table 4.4** and **Table 4.6**).

Entry number	Compound number	Lipinski's rule of five	Molar Mass g/mol	log P	H bond donor count	H bond acceptor count
1	**147**	✓	394.32	2.66	0	4
2	**148**	✓	288.15	3.55	0	3
3	**149**	✓	257.18	4.13	0	1
4	**150**	✓	311.19	2.97	0	3
5	**151**	✓	258.17	2.78	1	2
6	**152**	×	319.25	5.26	0	1
7	**153**	✓	268.17	3.47	0	2
8	**154**	✓	273.18	3.45	0	2
9	**155**	×	405.39	5.69	0	2
10	**156**	×	400.33	5.41	0	3
11	**157**	×	349.28	5.10	0	2
12	**158**	✓	369.05	4.54	0	1
13	**159**	×	435.37	6.97	1	2
14	**160**	×	503.23	6.91	1	2
15	**161**	×	419.11	5.53	0	1
16	**162**	×	629.13	7.84	1	2
17	**163**	×	349.28	5.10	0	2
18	**164**	×	483.46	7.47	1	3
19	**165**	✓	293.22	4.60	0	1
20	**166**	✓	293.22	4.60	0	1
21	**167**	×	461.15	5.88	1	2

22	**168**	✓	335.25	4.95	1	2
23	**169**	×	475.18	6.03	0	2
24	**170**	✓	271.21	4.64	0	1
25	**171**	✓	267.18	3.76	0	1
26	**172**	✓	244.15	2.39	0	2
27	**173**	×	299.27	5.16	0	1
28	**174**	✓	311.16	4.49	0	1
29	**175**	✓	257.19	4.12	0	2
30	**176**	✓	369.06	4.54	0	1
31	**177**	✓	335.26	4.95	1	2
32	**178**	×	377.34	5.99	1	2
33	**179**	✓	335.26	4.95	1	2
34	**180**	×	526.39	7.93	0	2
35	**181**	×	349.28	5.99	1	2
36	**182**	×	475.18	6.03	0	2
37	**183**	×	439.41	7.12	1	2
38	**184**	×	475.18	6.33	1	2
39	**185**	×	456.23	6.75	1	2

Table 4.2 Physical properties of the **Class One** compounds fall within Lipinski's rule of five (i.e., a molecule with a molecular mass less than 500 Da, no more than 5 hydrogen bond donors, no more than 10 hydrogen bond acceptors, and partition coefficient log *P* not greater than 5). Physical properties were calculated using ChemAxon online service https://chemicalize.com/welcome.

Anti-parasitic activity of the library (**Table 4.1**) varies drastically despite all of the compounds having the same tetrafluoropyridine (TFP) core structure. This implies that the nature of the subunit on the 4-position of the core is what alters their biological activity the most. From the 39 compounds screened in the first series, 18 of them were active against either *L. mexicana* promastigotes or axenic amastigotes at 50 µM concentration and only one (**182**, **Table 4.1**, **Entry 36**) was active against *L. mexicana* promastigotes at 5 µM.

The synthesised molecules (**Table 4.1**) were also evaluated for their ability to inhibit *T. cruzi* epimastigote proliferation at 5 µM. Untreated and parasites treated with 20 µM Benznidazole were used as negative and positive controls, respectively. None of the compounds in this series (**Table 4.1**) of TFP analogues had any effect on *T. cruzi* epimastigotes.

Compound **152** (**Table 4.1, Entry 6**) has a biphenyl group attached to the 4-position of the TFP core and is highly active against *L. mexicana* promastigotes (3% survival). When a methoxy group is connected to the biphenyl group (compound **163**, **Table 4.1, Entry 17**) it reduces the anti-leishmanial activity, increasing their survival rate (from 3% to 55%). However, adding an iodine to the compound **163** (compound **168**, **Table 4.1, Entry 22**) slightly decreases the viable cell percentage (change from 55% to 29%). Methoxy (-O-CH_3) is an electron donating group by resonance, and the electronegativity of iodine in **168** (**Table 4.1, Entry 22**) might balance this effect finally causing the increased activity. Between compounds **167** (**Table 4.1, Entry 21**) and **177** (**Table 4.1, Entry 31**), incorporating an iodine has slightly increased the activity of **167** in *L. mexicana* promastigotes while the opposite effect is seen against axenic amastigotes. Additionally, having two iodine groups (compound **162**, **Table 4.1, Entry 16**) instead of a one iodine (compound **159**, **Table 4.1, Entry 13**), decreases activity against *L. mexicana* promastigotes. Besides the chemical structural differences between the molecules there are several other reasons that could explain the differences seen in the biological data in Table 4.1. Differences in cell membranes, pH of the media, media composition, and different incubation periods could all play a role (e.g., these points were previously discussed in Chapter 2). In an attempt to prove any relationships between physical properties and biological activity could be found, two graphs were plotted: log P vs Survival % (**Figure 4.10**). By analysing the scatter plot of *L. mexicana* promastigotes (**Figure 4.10 (A)**), it is notable that most of the active compounds with less than 50% survival have log

P values greater than 5 (log P; 5.5-8). However, according to Lipinski's rule of five, an oral drug should have a log P value <5 for a better oral and intestinal absorption.

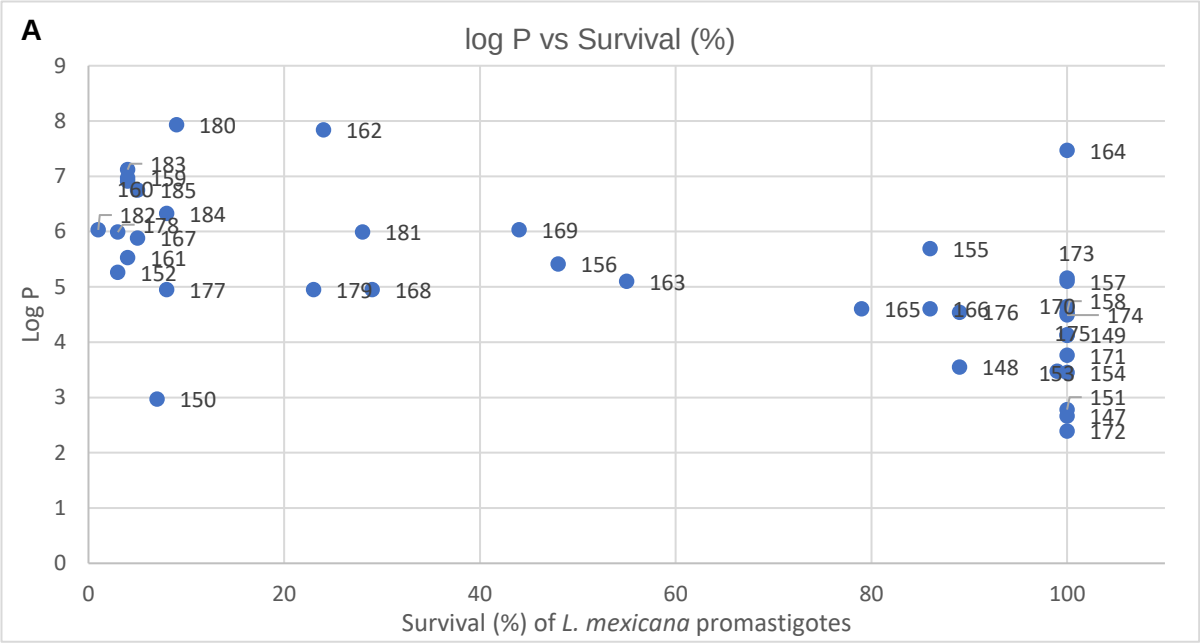

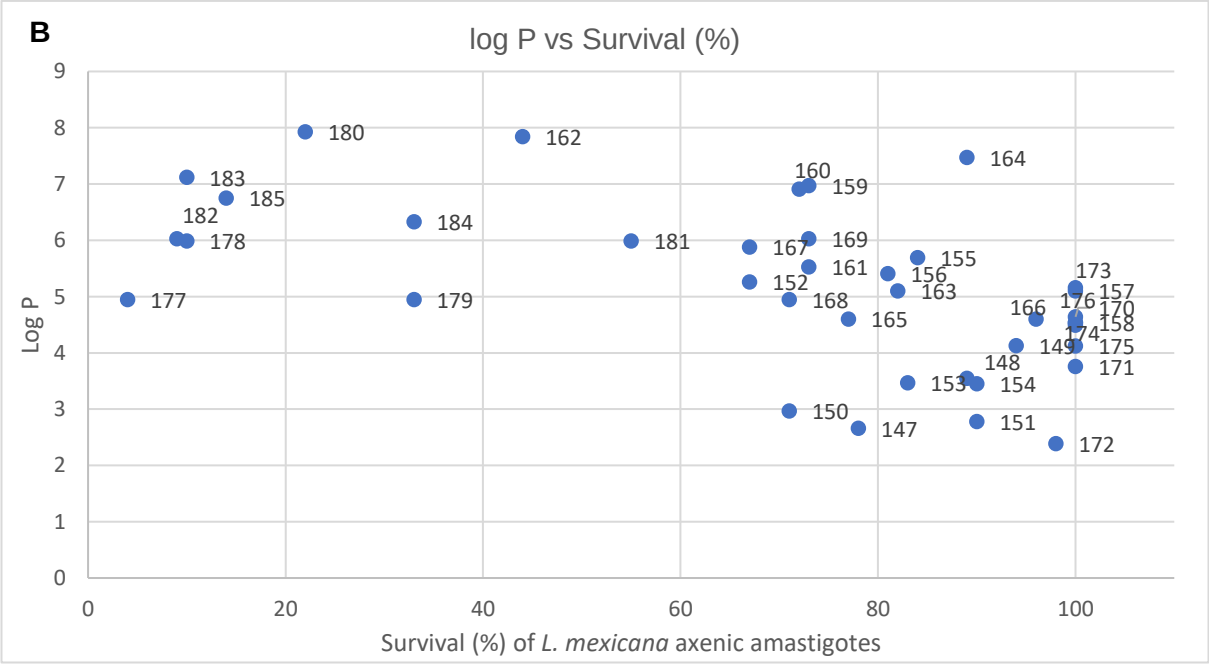

Figure 4.10 representation of log P vs survival % for the first series, Class One, (**A**) *L. mexicana* promastigotes, (**B**) *L. mexicana* axenic amastigotes.

The rule of 5 is based on a distribution of calculated physiochemical properties among thousands of drugs. Therefore, by definition, some drugs will lie outside the cut-off parameters and there are FDA approved drugs that violate one or two rules.[22,23] This may suggest that for a Class of compounds with a TFP core, designing molecules with higher log P values could be beneficial in future.

The same pattern can be seen in the plot of *L. mexicana* axenic amastigotes (**Figure 4.10 (B)**). All the active compounds have log P values between 4.5 - 8.0. But, unlike promastigotes, for axenic amastigotes, there are more inactive compounds with log Ps in the same range (log P 4.5 - 8.0).

Compound **193** (**Table 4.3, Entry 8**) is the only active compound against *L. mexicana* promastigotes and axenic amastigotes in the Class Two with two TFPs in it (**Table 4.3**). **189** (**Table 4.3, Entry 4**) and **190** (**Table 4.3, Entry 5**) are active against *L. mexicana* promastigotes with 40-45% survival.

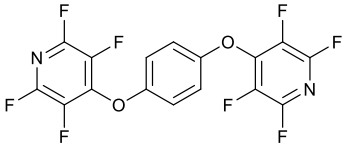

186

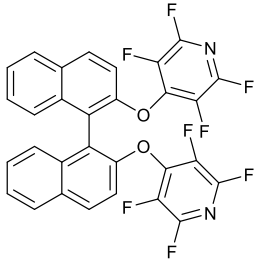

187

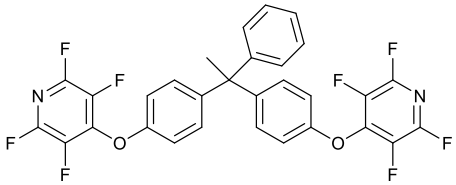

188

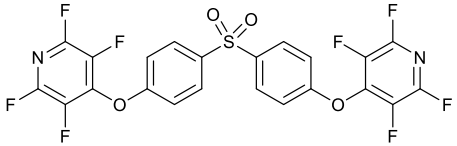

189

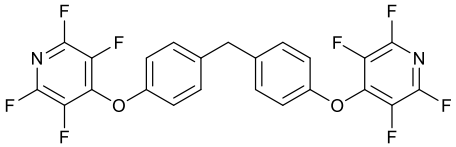

190

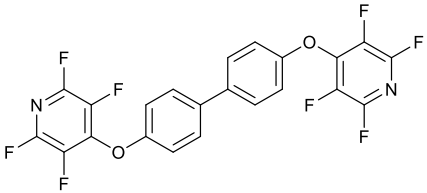

191

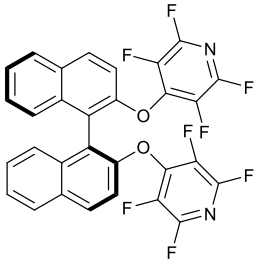

192

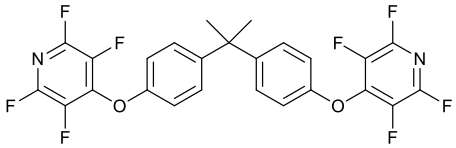

193

Entry No.	Com. No.	R	*L. mexicana* axenic amastigotes survival (%) at 50 µM	Effect on *L. mexicana* axenic amastigotes growth at 5µM	*L. mexicana* promastigotes survival (%) at 50 µM	Effect on *L. mexicana* promastigotes growth at 5µM	Effect on *T. cruzi* epimastigotes (CLB) growth at 5µM
1	**186**	C_6H_4	75	No	100	No	No
2	**187**	*1,1'-binaphthalene*	100	No	100	No	No
3	**188**	4-[1-(4-hydroxyphenyl)-1-phenylethyl]phenol	100	No	100	No	No
4	**189**	Diphenylsulfone	87	No	42	No	No
5	**190**	Diphenylmethane	88	No	45	No	No
6	**191**	Diphenyl	83	No	100	No	No
7	**192**	*1,1'-binaphthalene*	100	No	100	No	No
8	**193**	4-[2-(4-hydroxyphenyl)propan-2-yl]phenol	29	No	4	No	No

Table 4.3 Structures and biological data of Class Two compounds against *L. mexicana* axenic amastigotes, promastigotes, and *T. cruzi* epimastigotes (No-not active against *T. cruzi*).

Log P vs percentages of surviving cells of *L. mexicana* were plotted for Class Two as described for Class One (**Figure 4.11**). All the compounds have a log P > 5, but only three were active against *L. mexicana* promastigotes (**Figure 4.11(A)**) and only one was active against *L. mexicana* axenic amastigotes (**Figure 4.11(B)**).

Entry number	Compound number	Lipinski's rule of five	Molar Mass g/mol	log P	H bond donor count	H bond acceptor count
1	**186**	×	408.20	5.25	0	2
2	**187**	×	584.42	8.88	0	2
3	**188**	×	584.42	8.88	0	2
4	**189**	×	498.33	7.34	0	2
5	**190**	×	548.36	6.21	0	4
6	**191**	×	484.30	6.90	0	2
7	**192**	×	588.46	9.06	0	2
8	**193**	×	526.39	7.93	0	2

Table 4.4 Physical properties of the **Class Two** compounds fall within Lipinski's rule of five (i.e., a molecule with a molecular mass less than 500 Da, no more than 5 hydrogen bond donors, no more than 10 hydrogen bond acceptors, and log *P* not greater than 5). Physical properties were calculated using ChemAxon online service https://chemicalize.com/welcome..

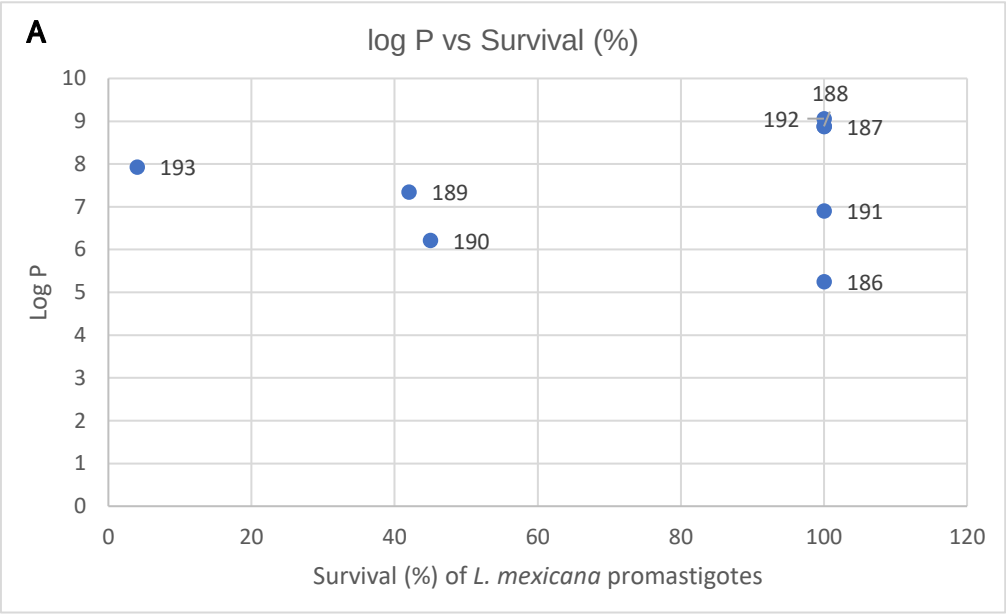

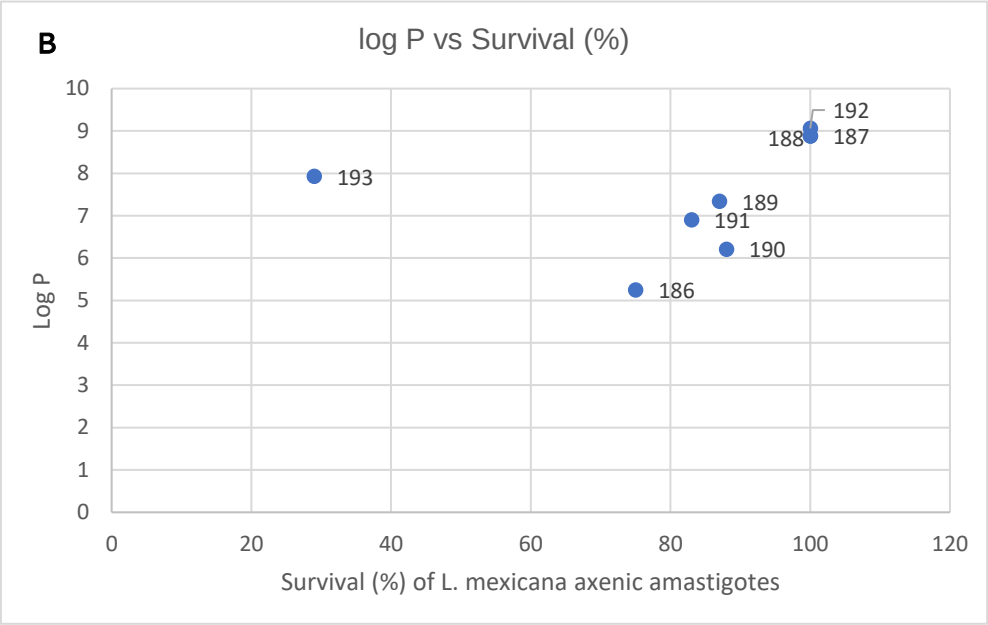

Figure 4.11 Representation of log P vs survival % for the first series -Class Two, (**A**) *L. mexicana* promastigotes, (**B**) *L. mexicana* axenic amastigotes.

The second library (GS group) screened in this chapter consists of 24 novel fluorinated compounds (**Figure 4.12** and **Table 4.5**). Only two compounds, **198** (**Table 4.5**, **Entry 5**) and **201** (**Table 4.5**, **Entry 8**) from this library were active against *L. mexicana* parasites and compound **198** was also active against *T. cruzi* epimastigotes.

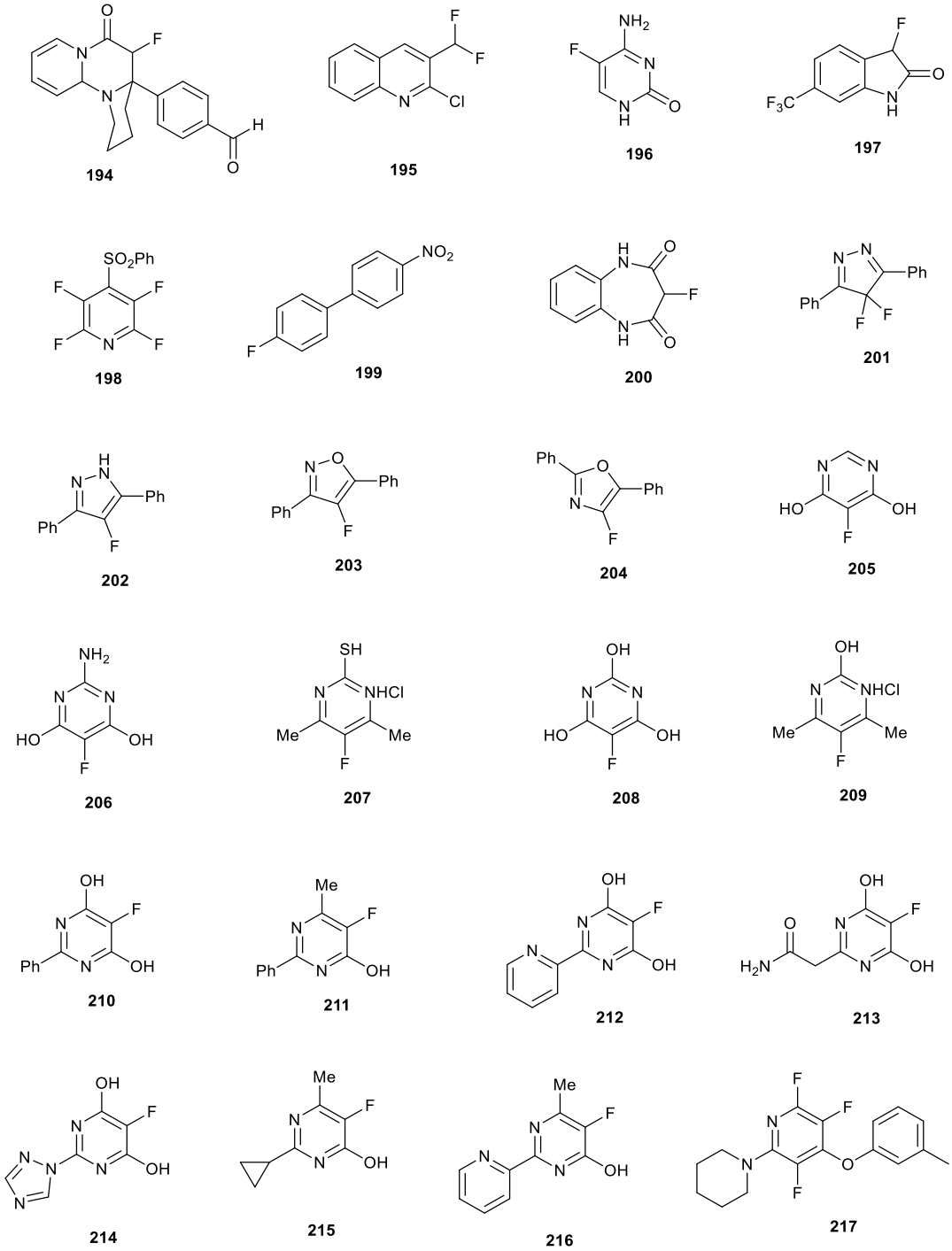

Figure 4.12 Chemical structures of the novel perfluoro-aromatic compound library- GS group.

Entry No.	Com No.	*L. mexicana* axenic amastigotes survival (%) at 50 µM	Effect on *L. mexicana* axenic amastigotes growth at 5µM	*L. mexicana* promastigotes survival (%) at 50 µM	Effect on *L. mexicana* promastigotes growth at 5µM	Effect on *T. cruzi* epimastigotes (CLB) growth at 5uM
1	**194**	100	No	100	No	No
2	**195**	100	No	100	No	No
3	**196**	100	No	100	No	No
4	**197**	59	No	100	No	No
5	**198**	3	Yes (3%)	2	Yes (3%)	Yes
6	**199**	42	No	100	No	No
7	**200**	100	No	100	No	No
8	**201**	1	Yes (18%)	2	Yes (6%)	No
9	**202**	100	No	100	No	No
10	**203**	100	No	100	No	No
11	**204**	72	No	100	No	No
12	**205**	100	No	100	No	No
13	**206**	97	No	100	No	No
14	**207**	50	No	100	No	No
15	**208**	82	No	100	No	No
16	**209**	79	No	100	No	No
17	**210**	100	No	100	No	No
18	**211**	100	No	100	No	No
19	**212**	100	No	100	No	No
20	**213**	96	No	100	No	No
21	**214**	74	No	100	No	No
22	**215**	76	No	100	No	No
23	**216**	29	No	67	No	No
24	**217**	67	No	97	No	No

Table 4.5 – Biological data of the second library (GS) against *L. mexicana* axenic amastigotes, promastigotes, and *T. cruzi* epimastigotes (No-Not active).

Scatter plot graphs in **Figure 4.13** shows that all the active compounds in second series have log P values below 5 and all of them score 4 out of 4 from the Lipinski's rule of five (**Table 4.6**). It is also worth noting that compounds with negative log P values are inactive against *L. mexicana*.

Entry number	Compound number	Lipinski's rule of five	Molar Mass g/mol	log P	H bond donor count	H bond acceptor count
1	**194**	✓	268.25	1.33	0	3
2	**195**	✓	213.61	3.34	0	1
3	**196**	✓	129.09	-1.45	2	3
4	**197**	✓	219.14	2.12	1	1
5	**198**	✓	291.22	3.06	0	3
6	**199**	✓	217.19	3.70	0	2
7	**200**	✓	194.17	0.47	2	2
8	**201**	✓	256.26	4.01	0	2
9	**202**	✓	238.27	4.02	1	1
10	**203**	✓	239.25	4.08	0	1
11	**204**	✓	239.25	4.04	0	1
12	**205**	✓	130.08	-1.25	1	3
13	**206**	✓	145.09	-2.00	2	4
14	**207**	✓	194.65	0.59	1	1
15	**208**	✓	146.08	-1.09	2	3
16	**209**	✓	178.59	-0.30	1	2
17	**210**	✓	206.18	1.06	2	4
18	**211**	✓	204.20	0.862	1	3
19	**212**	✓	207.16	-1.03	2	5
20	**213**	✓	187.13	-1.93	3	3
21	**214**	✓	197.13	-1.57	2	6
22	**215**	✓	168.17	-0.212	1	3
23	**216**	✓	205.19	0.03	1	4
24	**217**	×	322.33	5.14	0	2

Table 4.6 Physical properties of the **Second library** of compounds fall within Lipinski's rule of five (i.e., a molecule with a molecular mass less than 500 Da, no more than 5 hydrogen bond donors, no more than 10 hydrogen bond acceptors, and log *P* not greater than 5). Physical properties were calculated using ChemAxon online service https://chemicalize.com/welcome.

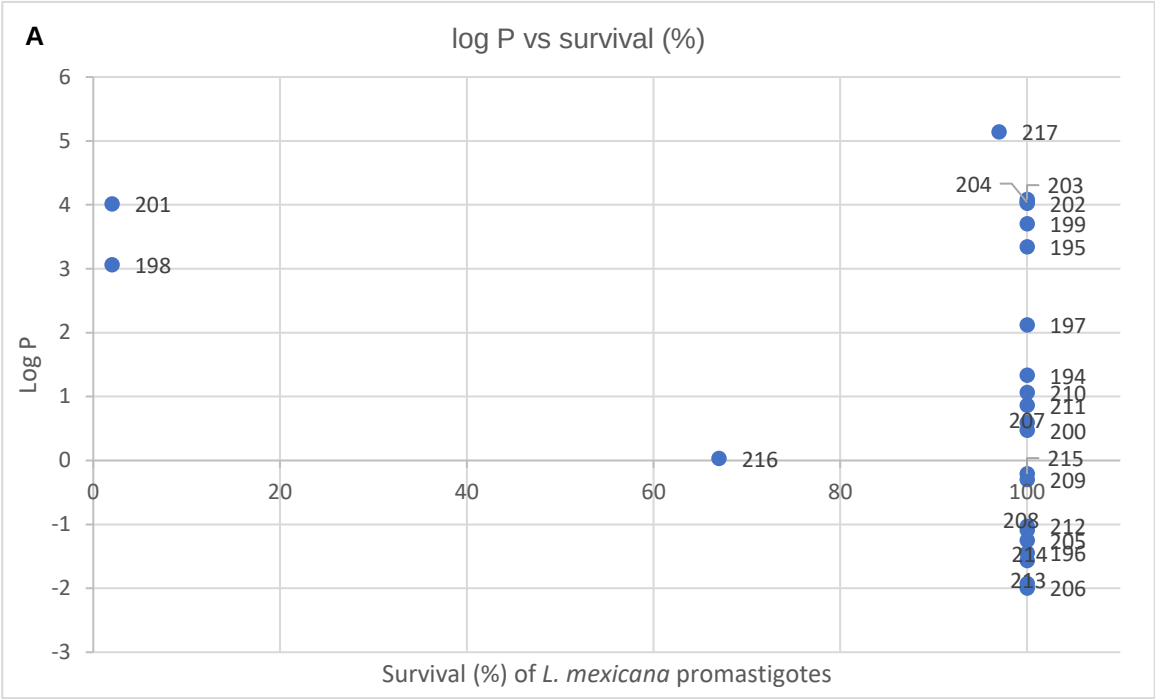

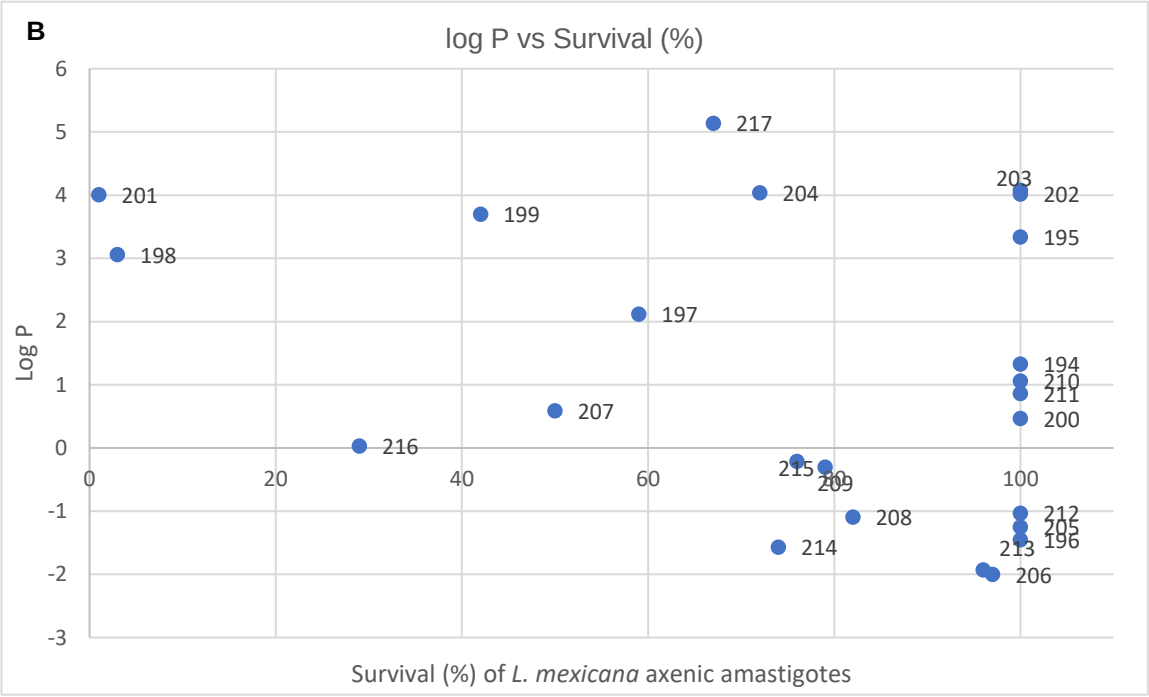

Figure 4.13 Representation of log P vs survival % for the second series, (A) *L. mexicana* promastigotes, (B) *L. mexicana* axenic amastigotes.

Preliminary screening was followed by a secondary screening to calculate EC_{50} values for the compounds with anti-parasitic activities. Detailed protocol for the dose response assays against *L. mexicana* can be found in **Chapter 7** (**Section 7.4.8**). In brief,

compounds to be tested were added to 96-well plates containing *L. mexicana* promastigotes or axenic amastigotes at 1 x 10^6 cells/ml concentration in triplicate and serial dilutions were carried out from 50 µM to 23 nM. DMSO and Amphotericin B were used as negative and positive controls.

Compound **150** (**Table 4.7, Entry 1**) had the most potent activity against *L. mexicana* promastigotes (EC_{50} = 1.14 µM) and met all the criteria mentioned in Lipinski's rule of 5. Nevertheless, it was not active against axenic amastigote form of the parasite. From the Class Two, **193** (**Table 4.7, Entry 17**) was the only active compound with 5.67 µM EC_{50} value against *L. mexicana* axenic amastigotes but fails in achieving two parameters in Lipinski's rule of 5 (MW; 526.39 g/mol and log P; 7.93).

183 (**Table 4.7, Entry 13**) and **198** (**Table 4.7, Entry 18**) both showed activities lower than 5 µM against *L. mexicana* axenic amastigotes (3.19 and 0.433 µM respectively). Compound **198**, 4-(benzenesulfonyl)-2,3,5,6-tetrafluoropyridine (**Table 4.5**, **Entry 5**), was also active against *L. mexicana* promastigotes (EC_{50}; 1.33 µM) and it was the only active compound against *T. cruzi* epimastigotes among the others (**Figure 4.14** and **Figure 4.15** represent the dose-response curves obtained from the data). Therefore, it was selected to assess its IC_{50} on epimastigote growth in order to measure its efficacy against *T. cruzi.*

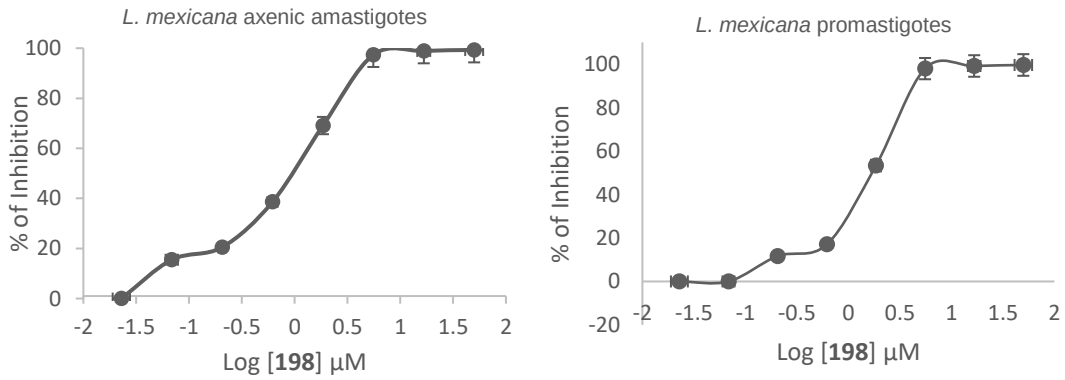

Figure 4.14 Dose-response curves for *L. mexicana* axenic amastigotes and promastigotes.

Detailed protocols for the dose response assays against *T. cruzi* can be found in **Chapter 7** (**Section 7.6.2**). In summary, the cell density of exponentially proliferating epimastigotes was adjusted to 2.5 x 10^6 cells/ml and transferred into 96-well plates. Epimastigotes proliferation at different concentrations of **198** was measured by reading the optical density (OD) at 620 nm every 24 hrs for 9 days. Compound **198** exhibited a dose-dependent epimastigotes growth inhibition with IC_{50}; 1.55 µM (**Table 4.7, Entry 18**) (**Figure 4.15**) in the exponential growth phase (5th day). The remaining molecules in this library were not studied further.

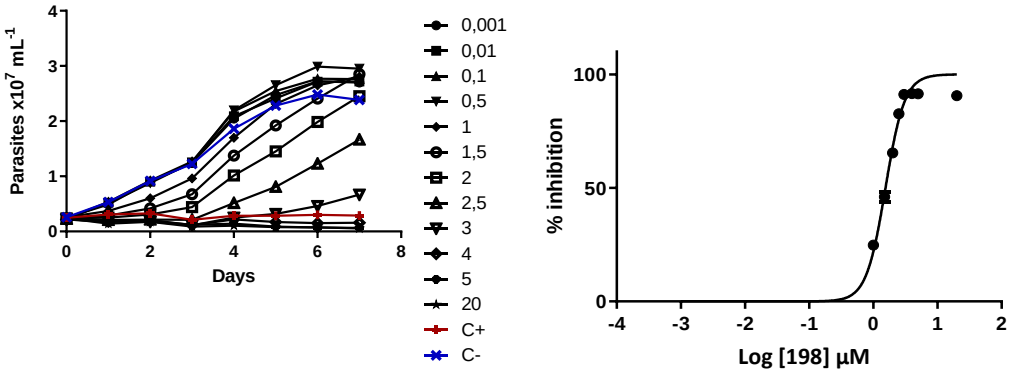

Figure 4.15 Proliferation curves of epimastigotes of *T. cruzi* in the presence of different concentrations of **198**, and the correspondent dose-response curves.

Entry no.	Compound no.	EC_{50} against *L. mexicana* axenic amastigotes (µM)	EC_{50} against *L. mexicana* promastigotes (µM)	IC_{50} against *T. cruzi* epimastigotes (µM)	CC_{50} (µM)
1	**150**	ND	1.145	ND	ND
2	**152**	ND	2.665	ND	ND
3	**161**	ND	2.817	ND	ND
4	**159**	ND	2.889	ND	ND
5	**160**	ND	3.295	ND	ND
6	**162**	ND	11.38	ND	ND
7	**167**	ND	1.53	ND	ND
8	**168**	ND	3.571	ND	ND
9	**169**	ND	7.57	ND	ND
10	**177**	29.65	ND	ND	ND
11	**180**	14.09	ND	ND	ND
12	**182**	7.43	ND	ND	ND
13	**183**	3.19	ND	ND	ND
14	**185**	7.95	ND	ND	ND
15	**189**	ND	7.825	ND	ND
16	**190**	ND	2.74	ND	ND
17	**193**	5.67	ND	ND	ND
18	**198**	0.433	1.33	1.55	16.8 µM on CHO-K_1 10.4 µM on Raw.264.7

Table 4.7 – Biological activity of selected active compounds from the two series screened in this chapter against *L. mexicana* axenic amastigotes, promastigotes, *T. cruzi* epimastigotes and cytotoxicity data (ND; not done).

4.3 Cytotoxicity of 4-(benzenesulfonyl)-2,3,5,6-tetrafluoropyridine (198) and Its activity against intracellular *T. cruzi* parasites.

It is estimated that 70% of pharmaceutical products in the market are based upon heterocyclic structures with favourable drug like properties. Lead generation and optimization require readily available core scaffolds that possess the ability to produce several distinct biological responses to synthesis structurally diverse compound libraries (**Chapter 5**).[24] Pentafluoropyridine (PFP) is potentially an excellent scaffold because it is highly reactive toward nucleophilic attack as a result of its electron deficient nature. This makes it highly amenable to chemical modifications and hence library analog generation.

In order to carry out further studies we need to prepare more 4-(benzenesulfonyl)-2,3,5,6-tetrafluoropyridine (**198, Scheme 4.1**) and this was achieved by reaction of pentafluoropyridine (PFP, **146**) with sodium phenylsulfinate in DMF.[25] There is no published work to prove the biological activity of **198** so far/as yet but it has been used as a probe to detect small molecule thiols with a simple ^{19}F platform. Biological thiols of cysteine (Cys), homocysteine (Hcy), glutathione (GSH) and hydrogen sulphide (H_2S) are involved in many cellular regulations and their eccentric levels are directly correlated with many different diseases. Thus, identification and quantification of these thiols would provide insights into related pathophysiological changes and pharmacokinetic information.[26]

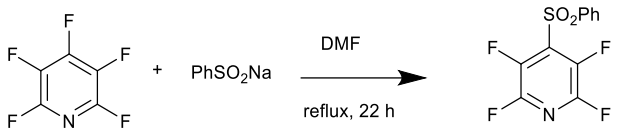

146 **198**

Scheme 4.1 Synthesis of 4-benzenesulfonyl-2,3,5,6-tetrafluoropyridine (**198**).

As compound **198** is the only molecule that was identified with promising activity against both parasite species, which cause leishmaniasis and Chagas disease, its cytotoxicity was determined against Raw 264.7 cells (as mentioned in Chapter 2) and CHO-K_1 cell lines (a cell line isolated from the ovary of an adult, female Chinese hamster[27]). CHO-K_1 cells were cultured or not (control) in the presence of different concentrations of **198** and the cytotoxicity (CC_{50}) was obtained by fitting a sigmoidal dose-response curves to the data (refer **Chapter 7**, **Section 7.6.3** for the detailed protocol). Compound **198** reported 16.8 µM CC_{50} on CHO-K_1 cells (**Figure 4.16**) and 10.4 µM CC_{50} on Raw 264.7 cells (**Figure 4.17**). Selectivity indices (SI) for **198** were calculated for *L. mexicana* axenic amastigotes (SI; 24) and *T. cruzi* epimastigotes (SI;10.83).

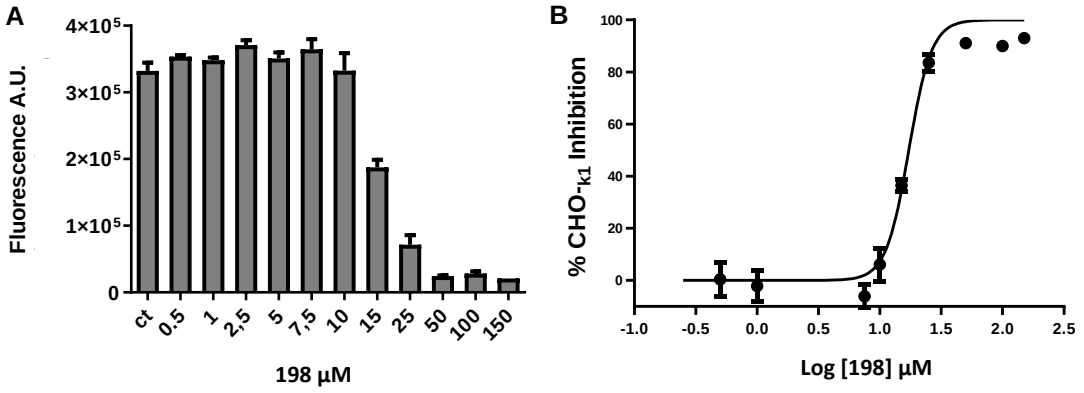

Figure 4.16 (**A**) The viability of CHO-K_1 cells treated with different concentrations of **198** for 48 hrs was assessed by Alamar Blue® assay. (**B**) The inhibition of proliferation was expressed as a percentage.

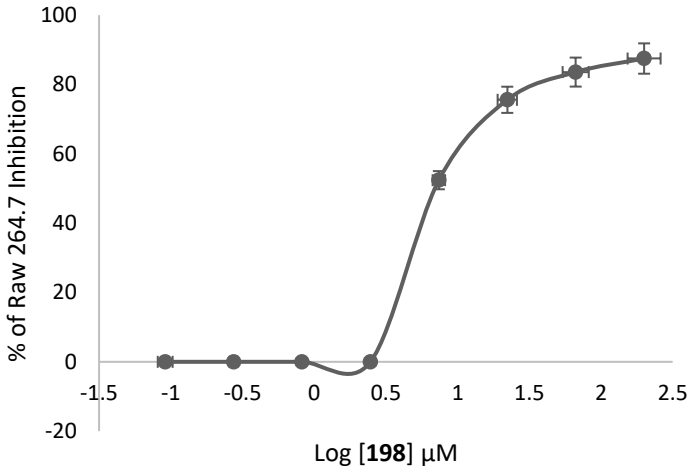

Figure 4.17 The inhibition of Raw 264.7 cell proliferation was expressed as a percentage.

Given the **198** showed low toxicity against mammalian cell lines, it was tested against the infected stages of *T. cruzi* parasites (**Figure 4.18**). CHO-K_1 cells were seeded in a 96-microtiter plate at 2.5 ×10^6 cells/mL and incubated for 24 hrs before they were incubated with trypomastigote form (2.5 ×10^6 cells per well) for 4 hrs. All the parasites remain in the supernatant was removed and the infected cells were treated with different concentrations of **198** (0.01 to 5 µM) for overnight. Then the plates were incubated at 33 ºC to allow parasites to complete the infection cycle. To measure the effect of **198** on amastigote replication, the trypomastigotes released from infected mammalian cell cultures (treated

or not (control)) were counted at the 5th day of post-infection (**Figure 4.18 (A)**). IC_{50} value (0.05 ± 0.051 µM) was calculated from the data obtained from the dose-response curve (**Figure 4.18 (B)**).

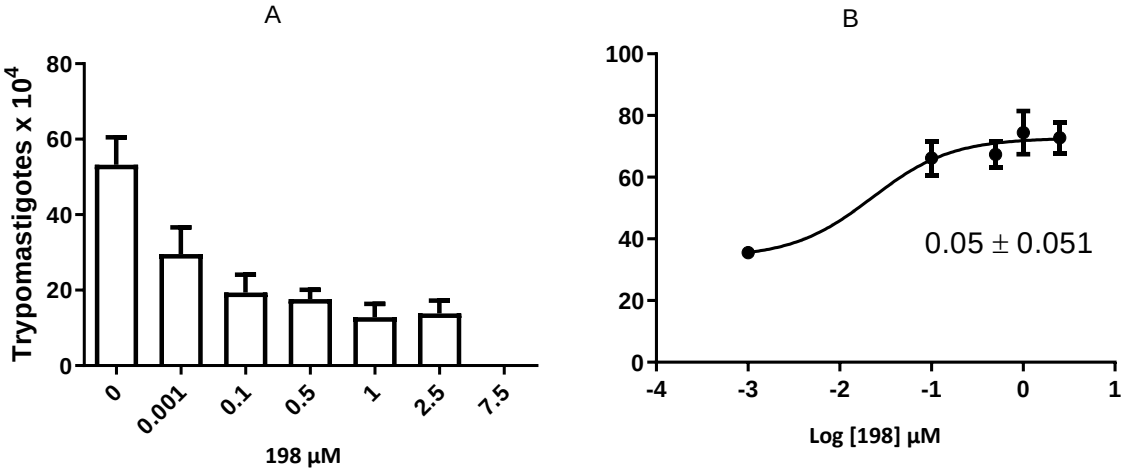

Figure 4.18 (**A**) Number of trypomastigotes released from infected mammalian cells at different concentration of **198** (**B**) Dose-response curve obtained from the data.

Based on the IC_{50} value obtained, a selectivity index (SI) was calculated for **198** (SI = 336). In order to verify that **198** diminished the release of trypomastigotes due to its effect on the amastigote proliferation, infected cells were treated with 0.05 µM **198** (IC_{50} for the trypomastigote release) or not (control) for two days after infection. After fixing and staining the infected cells, the effect of **198** on the total number of cells, the number of infected cells, and the number of amastigotes per infected cell were quantified. Compound **198** significantly diminished the infected cells by 50% (**Figure 4.19 (A)**) and the number of parasites per cell by 25% (**Figure 4.19 (B)**) which diminished the infection index (percentage of infected cells × the number of parasites per infected cell) by 50% ((**Figure 4.19 (C)**). Taking everything into consideration, these results indicate that **198** interferes the parasites proliferation and/or differentiation during the intracellular infection.

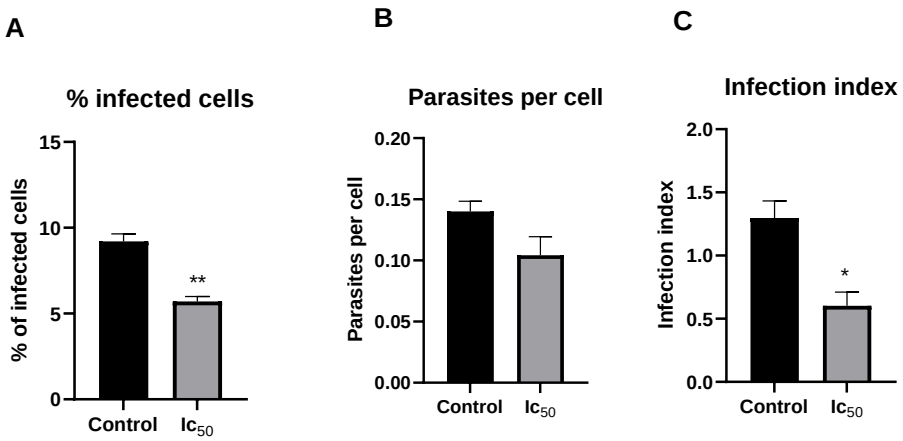

Figure 4.19 (**A**) Evaluation of the effect of **198** on the successful establishment of the infection (**B**) The number of intracellular amastigotes per infected cell (**C**) The infection index.

4.4 Investigation of the ability of 4-(benzenesulfonyl)-2,3,5,6-tetrafluoropyridine (198) to trigger programmed cell death in *T. cruzi* epimastigotes.

Experiments associated with T. cruzi in this section were carried out by Dr Richard Girard and Dr Flavia Damasceno under the supervision of Professor Ariel Silber at University of Sao Paulo.

Programmed cell death (PCD) was first proposed in 1964 by Lockshin and Williams, suggesting that cell death during development follows a sequence of controlled steps leading to locally and temporally defined self-destruction.[28] Cell death involves three main mechanisms; apoptosis, autophagy and necrosis. Initially, it was assumed that apoptosis arose with multicellularity. But in recent years it has become clear that similar mechanisms can be found in unicellular eukaryotic species including trypanosomatids of the genera *Trypanosoma spp*. (*T. brucei* and *T. cruzi*) and *Leishmania spp*. PCD is essential for the development, homeostasis and defence of multicellular organisms.[29] Different types of PCD have been described in unicellular parasites, including apoptosis and autophagic cell death, triggered in response to various stimuli. In trypanosomatids, apoptosis is induced by heat shock, reactive oxygen species (ROS), anti-parasitic drugs, prostaglandins, starvation, antimicrobial peptides, antibodies and mutations in cell-cycle regulated

genes.[28] Evidence has accumulated over the past couple of decades that have described morphological and biochemical events that occur during the apoptosis of trypanosomatids that share certain characteristics with mammalian apoptosis, such as production of reactive oxygen species, increase in cytosolic Ca^{2+} level,[30] changes in mitochondrial membrane potential (ΔΨm), cytochrome c release, protease activation, perturbances of the plasma membrane ('blebbing'), exposure of phosphatidylserine residues in the outer leaflet of the plasma membrane (indicative of a loss of membrane asymmetry), chromatin condensation and DNA fragmentation.[28]

It has been shown that mitochondria play a significant role in cell death decisions. In trypanosomatids, many apoptogenic agents or stresses are associated with a dysfunction of the mitochondrion indicated by changes in ΔΨm. The antiparasitic activity of many drugs is mediated by the loss of mitochondrial ΔΨm.[28,31] The electrochemical gradient in a normal cell is maintained by actively pumping H^+ during the electron transfer through the respiratory chain and the membrane potential maintains the integrity and function of mitochondria. Therefore, perturbations in the membrane potential (ΔΨm) could lead to decrease in ATP production, which ultimately results in apoptosis.[32] In *T. cruzi* epimastigotes, the trigger induces cytosolic Ca^{2+} elevation. Ca^{2+} enters the mitochondrion, inducing permeabilization of the inner mitochondrial membrane and the overload of Ca^{2+} resulted in the loss of ΔΨm.[33] Following the ΔΨm, ROS (superoxide anion) are generated by mitochondria via oxidative phosphorylation finally leading the apoptosis. This pathway has been reported when *T. cruzi* epimastigotes were exposed to fresh human serum.[30] Phosphatidylserine is predominantly located on the inner leaflet of the plasma membrane, and is translocated to outer leaflet when apoptosis is induced, in a process that resembles apoptosis of mammalian cells. This serves as a sensitive marker for early stages of apoptosis. It can be detected with annexin V, which binds to phosphatidylserine with high affinity in the presence of Ca^{2+}.[34,35] Treatment with higher concentrations of 3-Hydroxy-2-methylene-3-(4-nitrophenylpropanenitrile) (**MBHA3**) (**218**) (**Figure 4.20**) led to extensive

plasma membrane damage, loss of mitochondrion membrane potential, DNA fragmentation and acidification of the cytoplasm in *T. cruzi*.

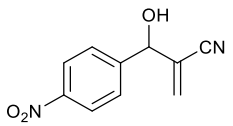

218

Figure 4.20 Chemical structure of MBHA3 (**218**).

With the purpose of investigating the ability of **198** to trigger a PCD in *T. cruzi* epimastigotes, the typical morphological, cellular, and biochemical PCD hallmarks such as variations in Ca^{2+} concentrations, mitochondrial inner membrane potential (ΔΨm), ATP level imbalance, exposure of phosphatidylserine residues from the inner to the outer leaflet of the plasma membrane and/or membrane permeabilization were evaluated in this chapter. Furthermore, the ability of **198** to interfere with the parasite cell cycle progression was also investigated. Detailed protocols can be found in the **Chapter 7** (**Section 7.6.5 - 7.6.9**).

To assess the exposure of phosphatidylserine and plasma membrane permeabilization, the *T. cruzi* epimastigotes were first treated with 1.5 µM and 3 µM of compound **198** (1× IC_{50} and 2×IC_{50} respectively) and then the parasites were incubated with annexin V-fluorescein isothiocyanate (FITC) and propidium iodide (PI), respectively. Next, the epimastigotes were analysed by flow cytometry. The data in **Figure 4.21** shows that **198**

triggers membrane permeabilization but did not solely induce the exposure of phosphatidylserine.

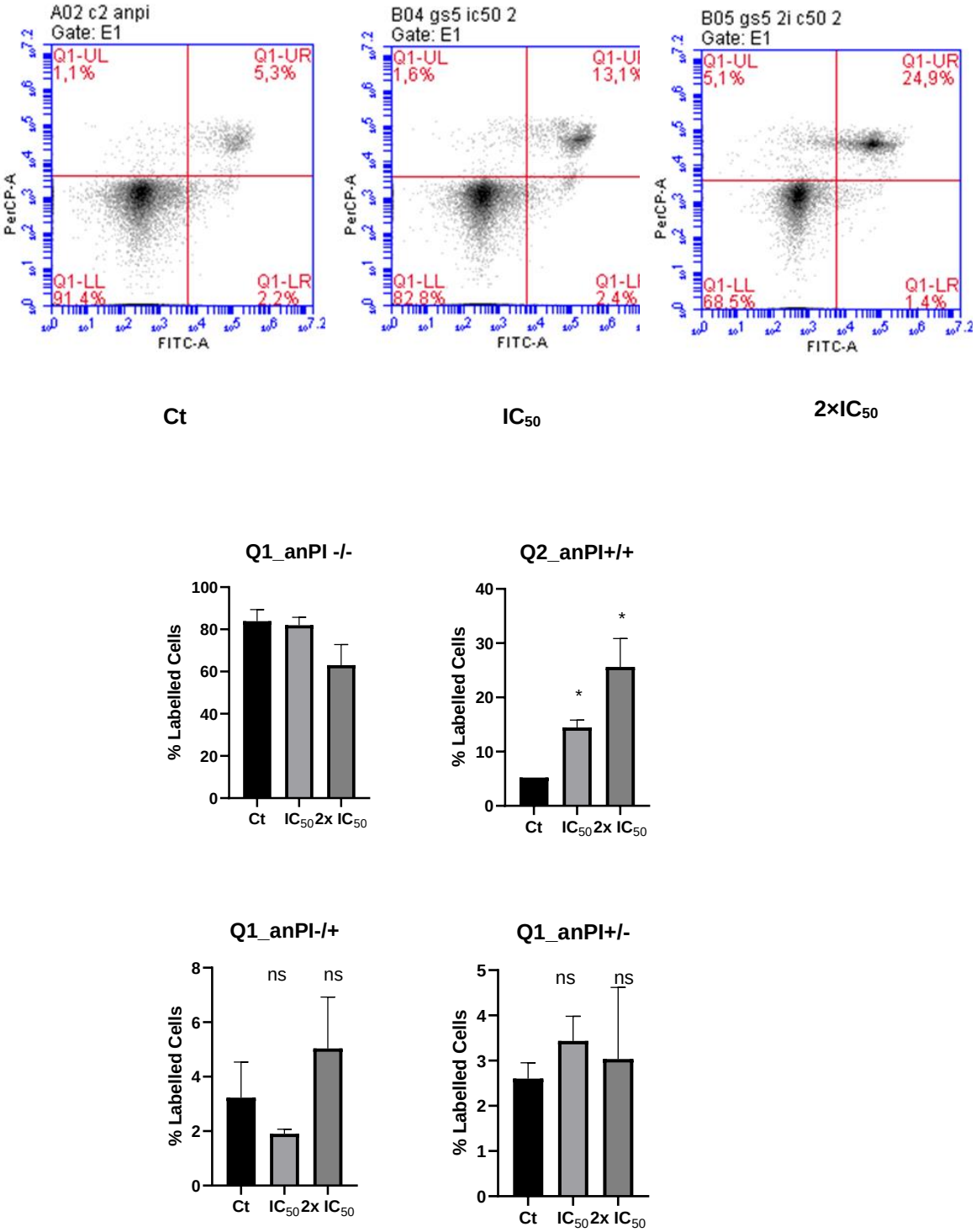

Figure 4.21 Analysis of cell death in *T. cruzi* epimastigotes treated with comp. **198** by assessing extracellular exposure of phosphatidylserine and plasma membrane integrity. Cells were treated with 1× IC_{50} and 2×IC_{50} of **198** for four days.

To measure the mitochondrial membrane potential (ΔΨm), first, *T. cruzi* epimastigotes were treated with 1.5 µM or 3 µM of compound **198** for 0, 1, 3, 6 hrs and 4 days, then parasites were stained with rhodamine 123 (Rh123) and analysed by flow cytometry. Trifluoromethoxy carbonylcyanide phenylhydrazone (FCCP) was used as the positive control and untreated parasites were considered as the negative control. **Figure 4.22** shows that **198** treated parasites exhibit a dose dependent short-term decrease in the fluorescence values obtained after 1hr incubation, indicating an alteration of ΔΨm.

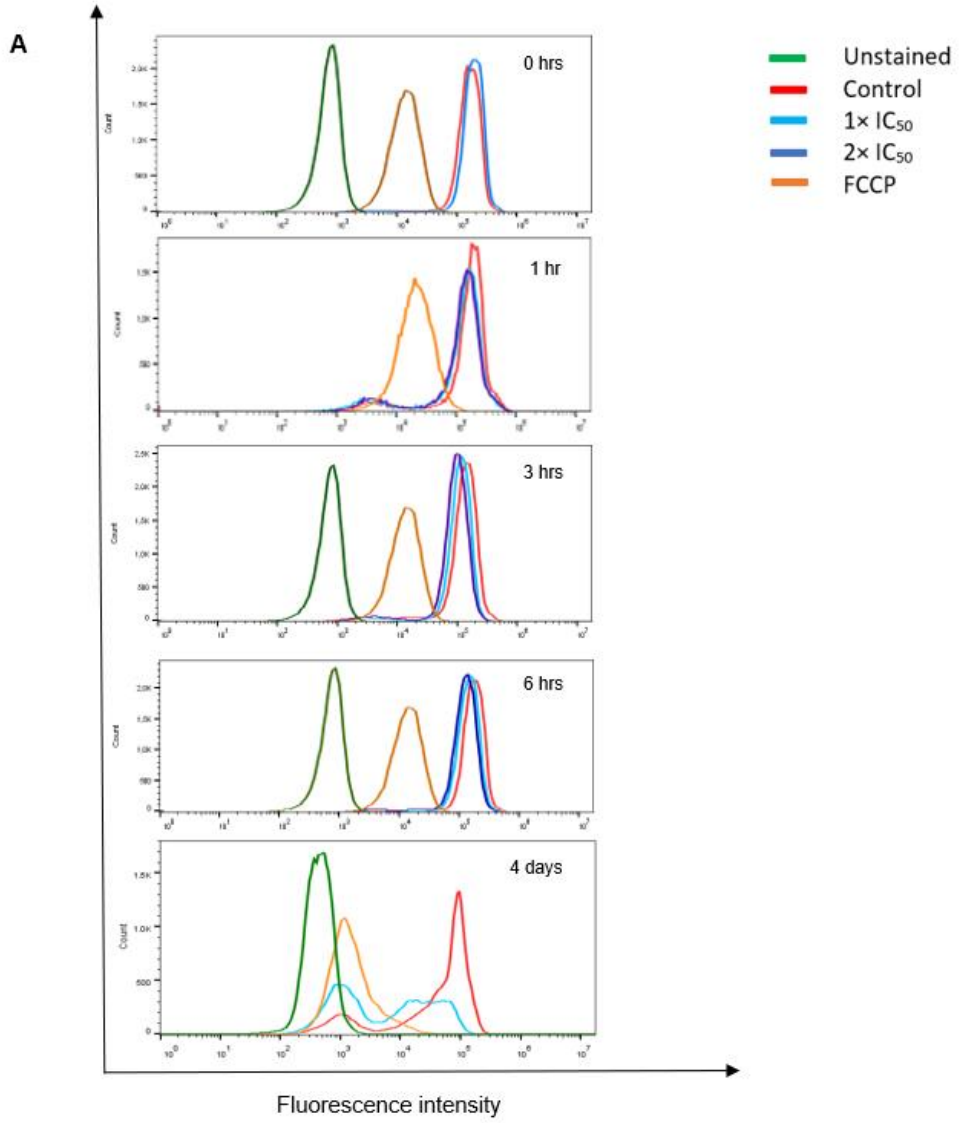

Figure 4.22 Evaluation of short-term and long-term effect of **198** on *T. cruzi* epimastigotes mitochondrial inner membrane potential, ΔΨm. **Panel A:** Histograms representing the distribution of fluorescence corresponding to ΔΨm for each treated population.

B

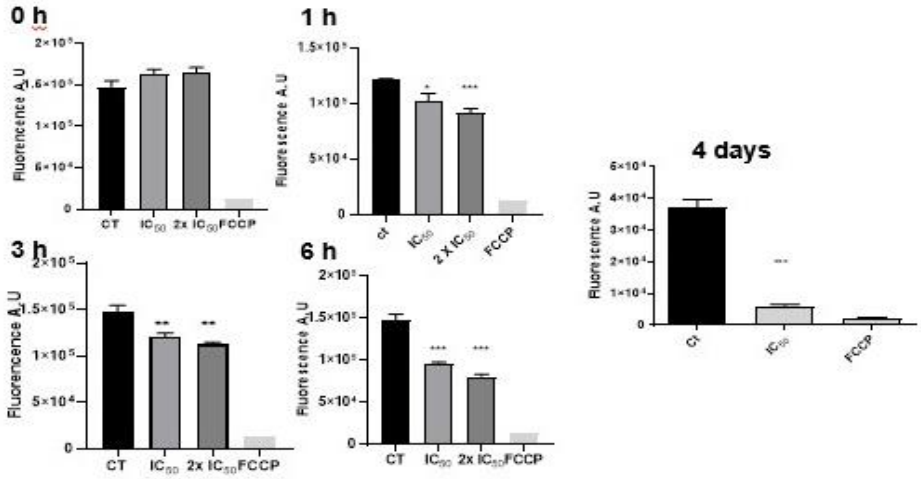

Figure 4.22, **Panel B**: The peaks of each population were plotted as a measurement of the average ΔΨm (Rh 123 - λ_{em} 588 nm).

To determine the possible variations of the intracellular Ca^{2+} concentrations, *T. cruzi* epimastigotes were treated with 1.5 µM (untreated cells were used as a control) for 0, 1, 3, 6 hrs and 4 days. After the treatment, parasites were incubated with Fluo-4 AM (a non-fluorescent acetoxymethyl ester, which cleaves to give fluorescent Fluo-4 inside the cell) and analysed by flow cytometry. The data obtained shows that intracellular Ca^{2+} concentration is starting to decrease from the 3-hour treatment onwards (**Figure 4.23**).

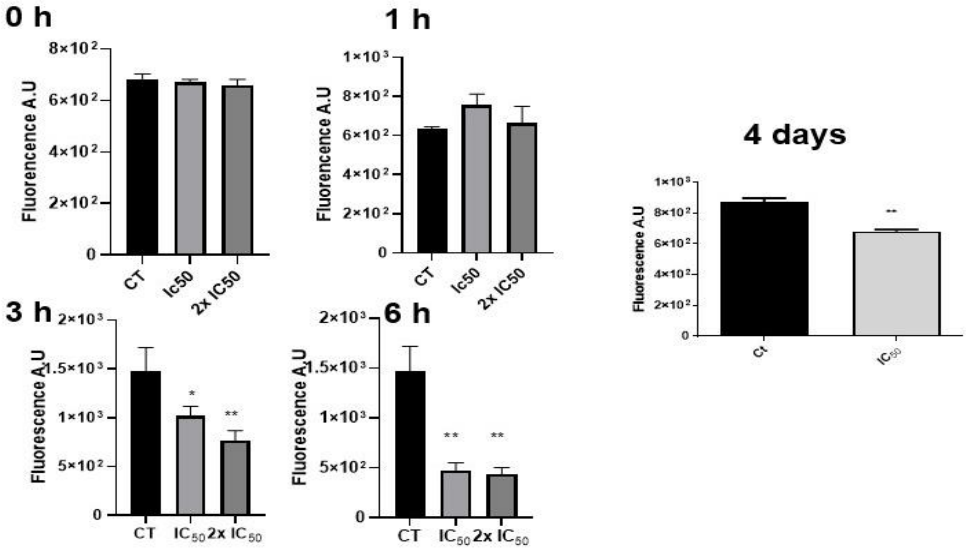

Figure 4.23 Short-term and long-term effect of compound **198** on the cytosolic Ca^{2+} of *T. cruzi* epimastigotes.

To evaluate the possible changes in the ATP level after the treatment with **198**, *T. cruzi* epimastigotes were treated with 1.5 µM or 3 µM for 4 days (untreated cells were used as a control) using a bioluminescent assay (570 nm). **Figure 4.24** shows that the treated parasites exhibit a disruption of the ATP level after 4 days of treatment.

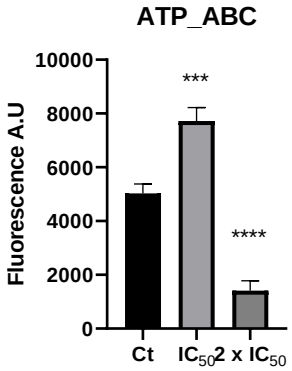

Figure 4.24 Quantification of cytoplasmic ATP levels.

Additionally, another experiment was carried out to investigate if the proliferation arrest was due to an interference with the *T. cruzi* cell cycle. To validate this hypothesis, *T. cruzi* epimastigotes were treated with 1.5 µM and 3 µM **198** for 4 days (untreated cells were used as a control). The cells were then labelled with PI and flow cytometry analysis of cell cycle progression was carried out. Interestingly, compound **198** triggered a significant decrease of cells in the G_0/G_1 phases at 2× IC_{50} concentration (**Figure 4.25**). These data stipulate that at a higher concentration, **198** also interfere with parasite cell cycle progression.

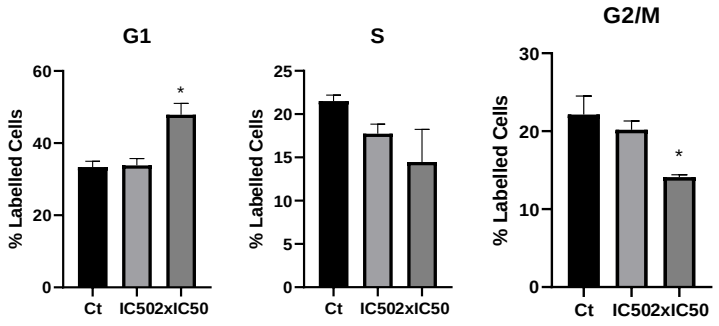

Figure 4.25 Effect of **198** on *T. cruzi* epimastigotes cell cycle.

4.5 Chapter Summary

With the purpose of identifying novel fluorinated scaffolds/starting points, we have screened two novel fluorinated libraries against *Leishmania mexicana* and *Trypanosoma cruzi* to determine their anti-parasitic activity. From a total of 71 compounds, only one, 4-(benzenesulfonyl)-2,3,5,6-tetrafluoropyridine (**198**) (**Table 4.7, Entry 18**), was found to be active against both parasite species [EC_{50} (*L. mexicana* promastigotes); 1.33 µM, EC_{50} (*L. mexicana* axenic amastigotes); 0.433 µM, IC_{50} (*T. cruzi* epimastigotes); 1.55 µM, EC_{50} (*T. cruzi* infected stage); 0.05 µM]. Additionally, the ability of **198** to trigger a programmed cell death (PCD) in *T. cruzi* epimastigotes was investigated by evaluating the exposure of phosphatidylserine in the external leaflet of the plasma membrane, plasma membrane permeabilization, mitochondrial inner membrane potential (Δψm), cytosolic Ca^{2+} concentration, ATP level imbalance and the effect on *T. cruzi* epimastigotes cell cycle. From the experiments carried out it is evident that **198** triggers plasma membrane permeabilization (**Figure 4.21**), alters the *T. cruzi* epimastigote's mitochondrial function by collapsing mitochondrial potential (**Figure 4.22**), decrease the intracellular Ca^{2+} concentration (**Figure 4.23**) and disrupt the intracellular ATP levels (**Figure 4.24**). Additionally, **198** also arrest the G_0 phase of cell cycle in *T. cruzi* at higher concentrations (**Figure 4.25**). In summary, all of the data gathered suggest that **198** could be an interesting lead compound to further develop with regards to identifying a new drug against *T. cruzi.*

4.6 References

1. Böhm, H. J. *et al.* Fluorine in medicinal chemistry. *ChemBioChem* **5**, 637–643 (2004).

2. Inoue, M., Sumii, Y. & Shibata, N. Contribution of Organofluorine Compounds to Pharmaceuticals. *ACS Omega* **5**, 10633–10640 (2020).

3. Han, J. *et al.* Next generation organofluorine containing blockbuster drugs. *J. Fluor. Chem.* **239**, 109639 (2020).

4. Cobb, S. L. & Murphy, C. D. 19F NMR applications in chemical biology. *J. Fluor. Chem.* **130**, 132–143 (2009).

5. Gimenez, D., Phelan, A., Murphy, C. D. & Cobb, S. L. 19F NMR as a tool in chemical biology. *Beilstein J. Org. Chem.* **17**, 293–318 (2021).

6. Hidde Boersma, F. G., Colin McRoberts, W., Cobb, S. L. & Murphy, C. D. A 19F NMR study of fluorobenzoate biodegradation by Sphingomonas sp. HB-1. *FEMS Microbiol. Lett.* **237**, 355–361 (2004).

7. Wakefield, B. Fluorinated Pharmaceuticals. *Innov. Pharm. Technol.* **74**, 74–78 (2003).

8. Josef Fried and Emily F. Sabo. Editor 1455. *J. Am. Chem. Soc* **2273**, 3–4 (1954).

9. Shah, P. & Westwell, A. D. The role of fluorine in medicinal chemistry. *J. Enzyme Inhib. Med. Chem.* **22**, 527–540 (2007).

10. Clader, J. W. The Discovery of Ezetimibe: A View from Outside the Receptor. *J. Med. Chem.* **47**, 1–9 (2004).

11. Van Niel, M. B. *et al.* Fluorination of 3-(3-(piperidin-1-yl)propyl)indoles and 3-(3-(piperazin- 1-yl)propyl)indoles gives selective human 5-HT(1D) receptor ligands with improved pharmacokinetic profiles. *J. Med. Chem.* **42**, 2087–2104 (1999).

12. Kole, H. K., Smyth, M. S., Russ, P. L. & Burke, T. R. Phosphonate inhibitors of protein-tyrosine and serine/threonine phosphatases. *Biochem. J.* **311**, 1025–1031 (1995).

13. Burke, T. R. *et al.* Small molecule interactions with protein-tyrosine phosphatase PTP1B and their use in inhibitor design. *Biochemistry* **35**, 15989–15996 (1996).

14. Da Silva Maffei, R., Yokoyama-Yasunaka, J. K. U., Miguel, D. C., Uliana, S. R. B. & Espósito, B. P. Synthesis, characterization and evaluation of antileishmanial activity of copper(II) with fluorinated α-hydroxycarboxylate ligands. *BioMetals* **22**, 1095–1101 (2009).

15. Ong, Y. C., Roy, S., Andrews, P. C. & Gasser, G. Metal Compounds against Neglected Tropical Diseases. *Chem. Rev.* **119**, 730–796 (2019).

16. Khan, T. A., Koko, W. S., Al Nasr, I. S., Schobert, R. & Biersack, B. Activity of Fluorinated Curcuminoids against Leishmania major and Toxoplasma gondii Parasites. *Chem. Biodivers.* **18**, 1–7 (2021).

17. Padhye, S. *et al.* Fluorocurcumins as Cyclooxygenase-2 Inhibitor: Molecular Docking, Pharmacokinetics and Tissue Distribution in Mice. *Pharm. Res.* **26**, 2438–2445 (2009).

18. Brak, K. *et al.* Nonpeptidic Tetrafluorophenoxymethyl Ketone Cruzain Inhibitors as Promising New Leads for Chagas Disease Chemotherapy. *J. Med. Chem.* **53**,

1763–1773 (2010).

19. Konstantinović, J. *et al.* Novel Aminoquinoline Derivatives Significantly Reduce Parasite Load in Leishmania infantum Infected Mice. *ACS Med. Chem. Lett.* **9**, 629–634 (2018).

20. Manzano, J. I. *et al.* 4-Aminoquinoline-based compounds as antileishmanial agents that inhibit the energy metabolism of Leishmania. *Eur. J. Med. Chem.* **180**, 28–40 (2019).

21. Beyki, K., Haydari, R. & Maghsoodlou, M. T. Reaction of hydroxylated naphtoquinones/antraquinones with pentafluoropyridine. *Springerplus* **5**, 1–4 (2016).

22. Pathania, S. & Singh, P. K. Analyzing FDA-approved drugs for compliance of pharmacokinetic principles: should there be a critical screening parameter in drug designing protocols? *Expert Opin. Drug Metab. Toxicol.* **17**, 351–354 (2021).

23. Protti, Í. F. *et al.* Do Drug-likeness Rules Apply to Oral Prodrugs? *ChemMedChem* **16**, 1446–1456 (2021).

24. Sandford, G., Slater, R., Yufit, D. S., Howard, J. A. K. & Vong, A. Tetrahydropyrido[3,4-b]pyrazine Scaffolds from Pentafluoropyridine. *J. Org. Chem.* **70**, 7208–7216 (2005).

25. Baron, A. *et al.* Polyfunctional Tetrahydropyrido [2 , 3- b] pyrazine Scaffolds from 4-Phenylsulfonyl Tetrafluoropyridine. *J. Org. Chem.* **70**, 9377–9381 (2005).

26. Chai, Z. *et al.* Simultaneous detection of small molecule thiols with a simple19F NMR platform. *Chem. Sci.* **12**, 1095–1100 (2021).

27. Xu, X. *et al.* The genomic sequence of the Chinese hamster ovary (CHO)-K1 cell line. *Nat. Biotechnol.* **29**, 735–741 (2011).

28. Smirlis, D. *et al.* Targeting essential pathways in trypanosomatids gives insights into protozoan mechanisms of cell death. *Parasites and Vectors* **3**, 1–15 (2010).

29. Bruchhaus, I., Roeder, T., Rennenberg, A. & Heussler, V. T. Protozoan parasites: programmed cell death as a mechanism of parasitism. *Trends Parasitol.* **23**, 376–383 (2007).

30. Irigoín, F. *et al.* Mitochondrial calcium overload triggers complement-dependent superoxide-mediated programmed cell death in Trypanosoma cruzi. *Biochem. J.* **418**, 595–604 (2009).

31. Dutta, A., Bandyopadhyay, S., Mandal, C. & Chatterjee, M. Aloe vera leaf exudate induces a caspase-independent cell death in Leishmania donovani promastigotes. *J. Med. Microbiol.* **56**, 629–636 (2007).

32. Sandes, J. M. *et al.* Trypanosoma cruzi cell death induced by the Morita-Baylis-Hillman adduct 3-hydroxy-2-methylene-3-(4-nitrophenylpropanenitrile). *PLoS One* **9**, 1–9 (2014).

33. Kessler, R. L., Soares, M. J., Probst, C. M. & Krieger, M. A. Trypanosoma cruzi Response to Sterol Biosynthesis Inhibitors: Morphophysiological Alterations Leading to Cell Death. *PLoS One* **8**, (2013).

34. Madeo, F., Fröhlich, E. & Fröhlich, K. U. A yeast mutant showing diagnostic markers of early and late apoptosis. *J. Cell Biol.* **139**, 729–734 (1997).

35. Matsuo, A. L. *et al.* In vitro and in vivo trypanocidal effects of the cyclopalladated

compound 7a, a drug candidate for treatment of Chagas' disease. *Antimicrob. Agents Chemother.* **54**, 3318–3325 (2010).

5 Design and biological evaluation of a 2nd generation library derived from, 4-benzenesulfonyl-2,3,5,6-tetrafluoropyridine.

5.1 Introduction

The drug discovery process has undergone many significant changes over the past few decades in order to decrease the high attrition rate of drug candidates.[1] Introduction of high-throughput screening in 1989 has provided a means but which hundreds of thousands of compounds can now be assessed for biological activity by a variety of *in vitro* assays within a short time frame.[2] The introduction of combinatorial chemistry techniques has allowed researchers to synthesise a collection of compounds comprising millions of different chemical entities for biological screening purposes.[3] However, the introduction of the aforementioned approaches has not led to the expected increase in the number of suitable candidates for hit-to-lead generation.[4,5] Thus, medicinal chemists have begun to pay closer attention to the structure and function of molecules synthesized and screened as drug candidates in order to recognize and hopefully predict *drug-like* entities. Molecular *drug-like* properties can be defined as a combination of favourable physiochemical (e.g., solubility, stability) and biological parameters (e.g., absorption, distribution, metabolism, elimination, and toxicity).[6,1]

Construction of libraries of appropriate *drug-like* molecules has been based on the concept of privileged structures.[7] These molecules possess versatile binding properties and can retain their selectivity for a variety of different biological receptors even after going through modification of various structural features. Once a suitable privileged structure has been identified, rapid analogue synthesis techniques (RAS) are used to produce arrays of compounds containing the required privileged structure as the ‘core’ of the molecule (**Figure 4.1**).[8]

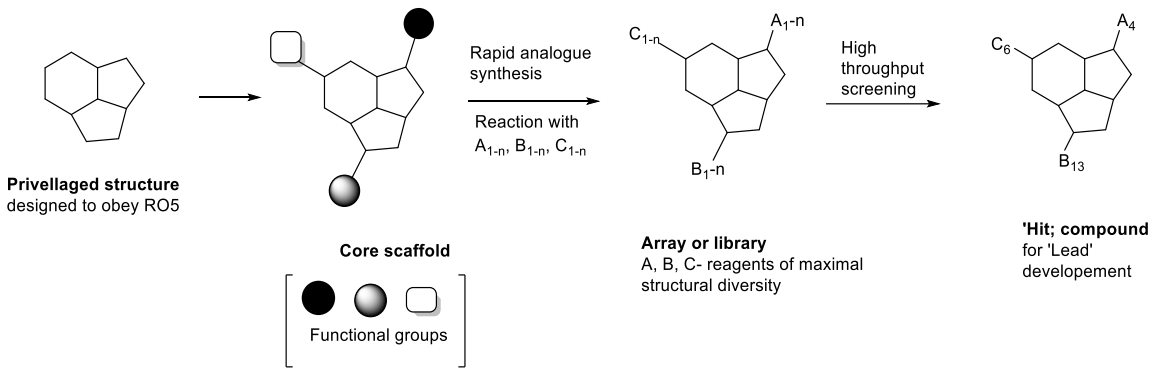

Figure 5.1 Privileged structures, core scaffolds and RAS in the drug discovery process.[9]

In this part of the project, 4-benzenesulfonyl-2,3,5,6-tetrafluoropyridine (**198**) (**Figure 4.2**) is considered as the privileged 'core' structure and a small library of novel molecules based on this core were synthesized. As described in the previous Chapter **198** was found to have an EC_{50} of 1.55 µM against *T. cruzi* epimastigotes and an EC_{50} of 0.433 µM against *L. mexicana* axenic amastigotes (**Chapter 4**, **Table 4.7**, **Entry 18**). This data combined with the determination of suitable CC_{50} values (>15µM) against mammalian cell lines (CHO-K_1, RAW 264.7) has stimulate the synthesis of a new library of compounds based on the **198** core.

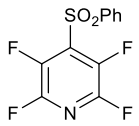

198

Figure 5.2 Chemical structure of 4-benzenesulfonyl-2,3,5,6-tetrafluoropyridine (**198**).

In 2017 Ranjbar-Karimi et.al. reported the antibacterial activity of quinoline derivatives that had some structurally similarities to **198**, 4-benzenesulfonyl-2,3,5,6 tetrafluoropyridine (N1-(7-chloroquinolin-4-yl)-N2-(3,5,6-trifluoro-4-(phenylsulfonyl)pyridin-2-yl)ethane-1,2-diamine (**219**) and 7-chloro-4-(4-(3,5,6-trifluoro-4-(phenylsulfonyl)pyridin-2-yl)piperazin-1-yl)quinoline (**220**) (**Figure 5.3**) against Gram positive *S. aureus* bacteria.[10] Compounds

219 and **220** were found to be moderately active against *S. aureus* with the same MIC, 400 µg/mL.[10] A search of the literature revealed that to date no biological activity for **198** has been reported.

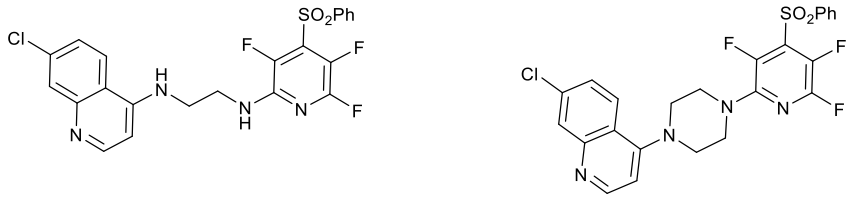

219 **220**

Figure 5.3 Chemical structures of **219** and **220**.

Reactions between pentafluoropyridine PFP (**146**) and nucleophiles are found to be regioselective in the majority of cases, with the initial nucleophilic aromatic substitution of the fluorine atom located at the 4-position of pentafluoropyridine via the corresponding Meisenheimer intermediate occurring as shown in **Scheme 5.1**.[9,11] The regioselectivity of this reaction is due to the presence of the ring nitrogen, which activates the *para* position preferentially and maximizing the number of activating fluorine atoms that are located *ortho* to the site of nucleophilic attack. Monosubstituted systems are still activated towards nucleophilic attack and all five fluorine atoms can be replaced with an excess quantity of suitable nucleophiles. This demonstrates the feasibility of using highly fluorinated heterocycles as scaffolds where C-F bond acts as readily substituted functional group.[9,12]

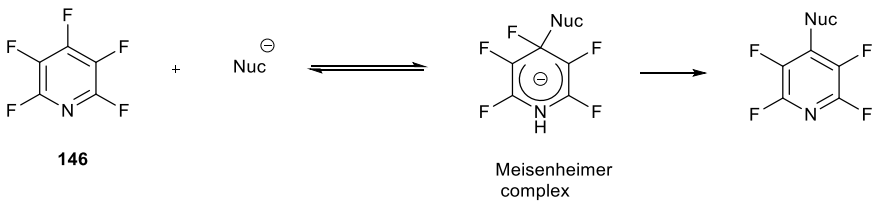

146

Meisenheimer complex

Scheme 5.1 Generation of Meisenheimer intermediate from pentafluoropyridine (**146**).[13]

For multiple reactions the order of nucleophilic attack on PFP (**146**) is found to be 4 > 2 > 3, for monosubstituted reactions and the order of substitution for a succession of five nucleophilic substitution steps can be postulated to occur as in **Scheme 5.2**.[13]

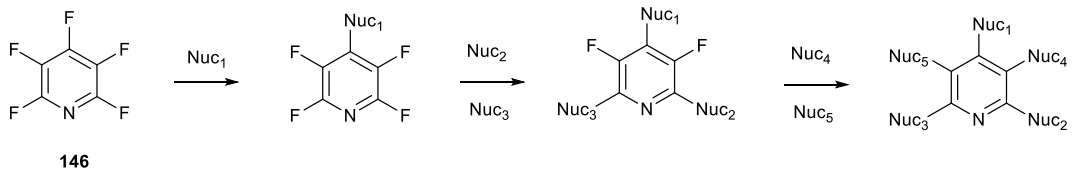

Scheme 5.2 Nucleophilic aromatic substitution of pentafluoropyridine (**146**).[13]

The reactivity profile established for pentafluoropyridine (PFP) (**146**), where the 4, 2-, 6-positions are substituted by a succession of oxygen-cantered nucleophiles, has allowed medicinal chemists to use PFP as a core scaffold for the synthesis of biologically active pyridine systems. For example, to prove that inhibition of the p38 MAP kinase protein could treat the underlying cause of chronic inflammatory diseases, Revesz et al. prepared a diverse set of 2,6-diamino-3,5-difluoropyridinyl substituted pyridinylimidazoles, -pyrroles, -oxazoles, and thiazoles. Inhibition of p38 MAP kinase reduce the production of pro-inflammatory cytokines, whose excessive production initiate inflammation and tissue destruction in the diseases namely rheumatoid arthritis. Pyridinylimidazole (**221**) was the most potent analogue with the inhibition of swelling in adjuvant induced arthritis rats (ED_{50}; 10 mg/kg b.i.d) and collagen induced arthritis rats (ED_{50}; 5 mg/kg b.i.d) (**Figure 5.4**).[14]

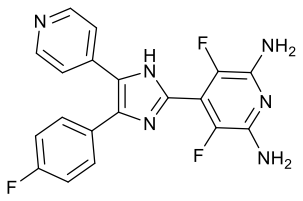

221

Figure 5.5 Chemical structure of Imidazole analogue (**221**).

5.2 Synthesis of 2,3,5,6-tetrafluoropyridin-4-yl benzenesulfinate (198).

In order to prepare a library of compounds for further investigation we first needed to access the core molecule **198**. This was achieved as follows in one step form commercial pentafluoropyridine (PFP, **146**). PFP (**146**) was reacted with phenylsulfinic acid sodium salt in DMF (25 mL) under reflux conditions for 20 hrs. Recrystallization of the precipitate with ethanol gave beige crystals of 4-benzenesulfonyl-2,3,5,6-6-tetrafluoropyridine (**198**) (**Scheme 5.3**).

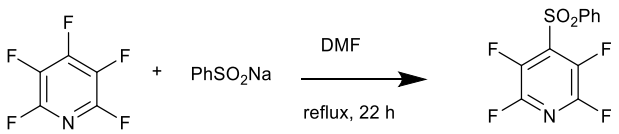

146 **198**

Scheme 5.3 Synthesis of 4-benzenesulfonyl-2,3,5,6-tetrafluoropyridine (**198**). Yield = 31%.

The production of 4-benzenesulfonyl-2,3,5,6-tetrafluoropyridine (**198**) was confirmed by a combination of NMR and mass spectral analysis. ^{19}F NMR showed that there were only two fluorine resonance for all four fluorine atoms, which indicated the presence of two *ortho* and two *meta* fluorine atoms as would be expected for **198** (**Figure 5.5**). Introducing an electron donating group by nucleophilic substitution deactivates the ring and prevents further attack on the fluoroaromatic core.[15] Phenylsulfonyl group however is strongly

electron withdrawing, and hence, it helps activate the fluoro-pyridine ring towards further nucleophilic substitutions.[16]

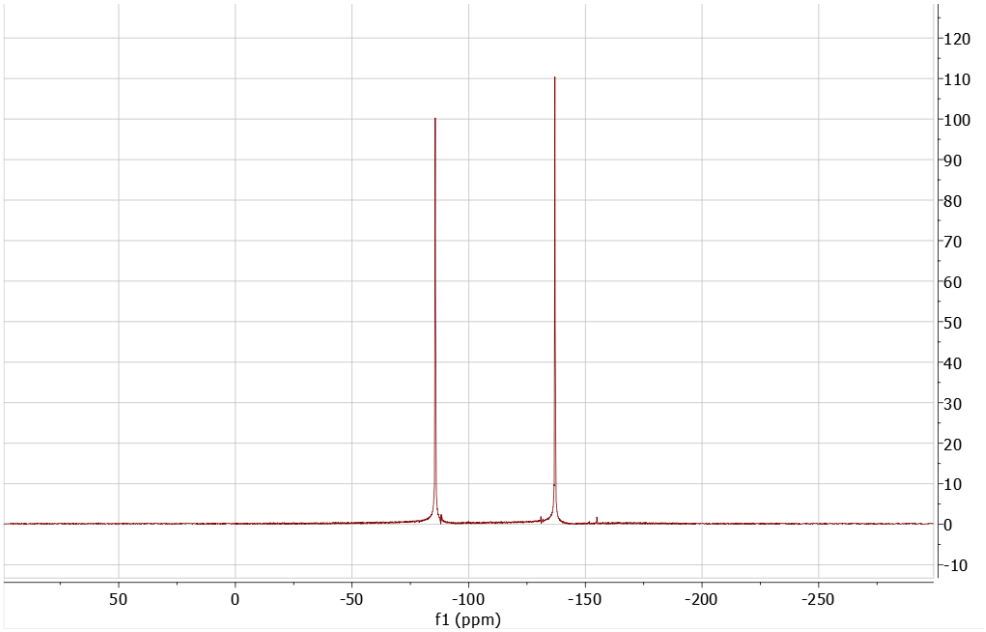

Figure 5.5 ^{19}F NMR spectrum of compound **198**.

5.3 Synthesis of 4-phenylsulfonyl tetrafluoropyridine derivatives

With 4-benzenesulfonyl-2,3,5,6-tetrafluoropyridine (**198**) in hand our attention turned towards derivatising this molecule via nucleophilic aromatic substitution to prepare a new library of compounds. **198** was heated to reflux with the required amine and potassium carbonate for 24 hrs in acetonitrile at 110 °C. The reaction product was purified by column chromatography. Full procedures for all of the reactions carried out can be found in **Chapter 7** and the compound library synthesised is given in **Table 5.1**. Reaction of amines with 4-benzenesulfonyl-2,3,5,6-tetrafluoropyridine (**198**) under reflux conditions, in some cases gave a mixture of mono- and di-substituted products (**Scheme 5.4**). Purification of all the compounds was carried out by column chromatography using Hexane: EtOAc solvent mixture. Substituted products and their possible isomers were identified by a combination of ^{19}F NMR, ^{1}H NMR, and mass spectral analysis.

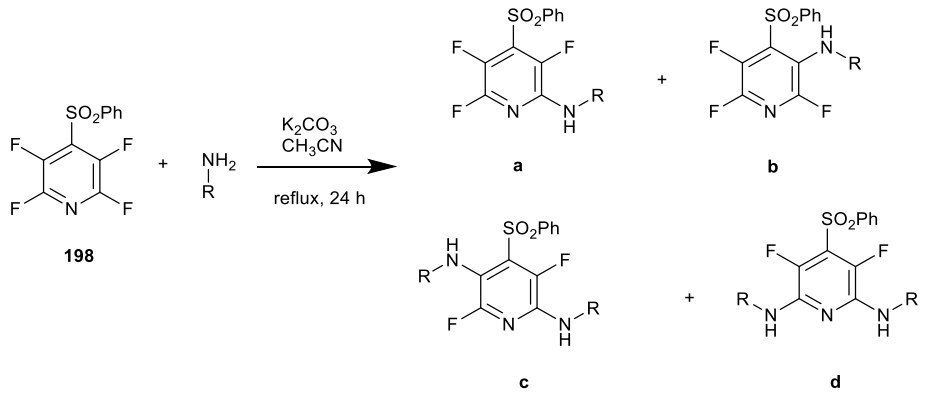

Scheme 5.4 Reaction of 4-phenylsulfonyl tetrafluoropyridine with amines.

Entry no.	Compound number	R	EC_{50} against *L. mexicana* axenic amastigotes/μM	CC_{50} against RAW 264.7/ μM
1	**222a** **222b**	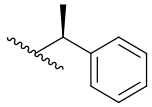	1.50 N/A	2.77 N/A
2	**223a**	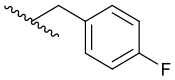	N/A	N/A
3	**224a** **224b**	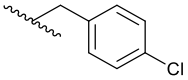	4.42 3.62	15.0 >100
4	**225a** **225b**	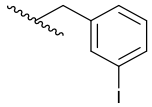	3.94 5.83	77.3 48.4
5	**226a** **226b**	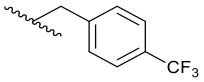	N/A N/A	N/A N/A
6	**227a** **227b**	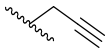	2.06 1.66	>100 26.6
7	**228a** **228b**	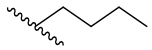	N/A 9.29	N/A 21.4

Table 5.1 Structures and isomers of the synthesised library of molecules and the results of the screening carried out, including EC_{50} values against *L. mexicana* axenic amastigotes and toxicity data using RAW 264. N/A – not active against *L. mexicana*.

A second set of compounds was synthesised by reacting 4-benzenesulfonyl-2,3,5,6-tetrafluoropyridine (**198**) with phenols (**Scheme 5.5**). Full procedures for these reactions can be found in **Chapter 7** and the library synthesised is listed in **Table 5.2**.

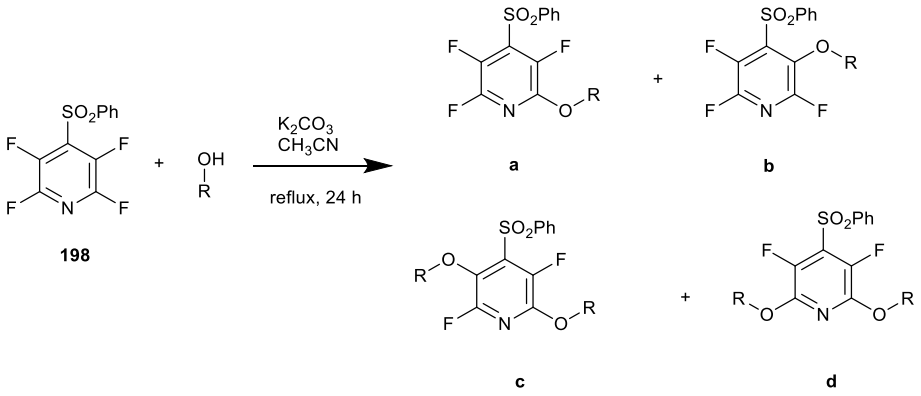

Scheme 5.5 Reaction of 4-phenylsulfonyl tetrafluoropyridine with phenols.

Entry no.	Compound number	R	EC_{50} against *L. mexicana* axenic amastigotes/µM	CC_{50} against RAW 264.7/ µM
1	**229**	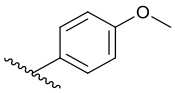	N/A	N/A
2	**230**	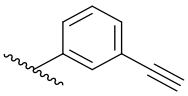	0.155	5.71
3	**231**	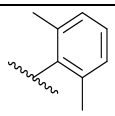	0.576	12.2
4	**232**	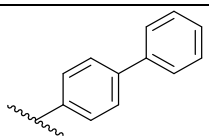	1.37	-
5	**233**	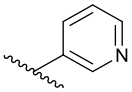	0.656	2.45
6	**234**	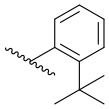	0.681	3.40
7	**235**	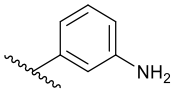	0.442	1.70
8	**236**	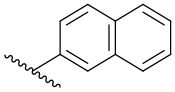	1.18	6.41
9	**237**	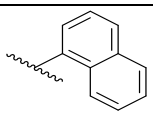	1.98	1.86

10	**238**	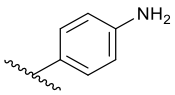	0.525	17.4
11	**239**	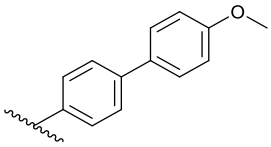	4.51	3.94
12	**240**	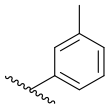	0.526	47.8

Table 5.2 Structures and isomers of the synthesised library of molecules and the results of the screening carried out, including EC_{50} values against *L. mexicana* axenic amastigotes and toxicity data using RAW 264.7. N/A – not active against *L. mexicana*.

5.4 Determination of biological activity against *Leishmania mexicana* and cytotoxicity assays.

Initial testing of compounds **222**-**240**, involved a phenotypic screen against *L. mexicana* axenic amastigotes in a high throughput Alamar Blue® assay. Compounds with promising activities were subjected to cytotoxicity assays as the next step. All of the molecules were first screened at a fixed concentration of 50 µM. Compounds which killed more than 50% of the cell population were selected to calculate EC_{50}.

The detailed experimental protocol for the biological screening carried out in this Chapter can be found in **Chapter 7** (**Section 7.4**). However, in brief, compounds to be tested were added to 96-well plates containing amastigotes 1 x 10^6 cells/ml in triplicate and serial dilutions were carried out from 50 µM to 23 nM. Amphotericin B and the solvent Dimethyl Sulfoxide (DMSO), which used to dissolve all the compounds were added to the plate as positive and negative controls, respectively. In addition, including wells containing only medium allow to correct the background fluorescence. After 44 hr incubation, the cell viability reagent Alamar Blue® (10% v/v) was added to each well and incubated for 4 hours at 33 °C. Alamar Blue® assay use the reducing activity of living cells to quantitatively determine cell viability via a fluorescent or colorimetric detection technique. The cell viability can be calculated by measuring the intensity of fluorescence emitted from cells and GraphPad Prism software was used to calculate EC_{50} values.

All the compounds (**222**-**240**) underwent the screening procedure describe above and EC_{50} values were calculated against *L. mexicana* axenic amastigotes. Most of the compounds tested found to have EC_{50} values of less than 10 µM. In this series of compounds, **230** (**Table 5.2, Entry 2**) was found to be the most effective with an EC_{50} of 0.155 µM against *L. mexicana* axenic amastigotes. Compounds **235** (**Table 5.2, Entry 7**) and **238** (**Table 5.2, Entry 10**) which have amine groups on their aromatic rings in the *meta* and *para* positions, have a slightly decreased EC_{50} value, 0.442 µM and 0.525 µM,

compared to **198**; 0.433 µM (parent compound) against *L. mexicana* axenic amastigotes. Compounds **232** (**Table 5.2, Entry 4**) and **239** (**Table 5.2, Entry 11**) have biphenyl groups attached to the -2 position of 4-benzenesulfonyl-2,3,5,6-tetrafluoropyridine (**198**). The difference between these two is that compound **239** (**Table 5.2, Entry 11**) has a methoxy group in the *para* position, which is assumed to cause a ~3 -fold reduction in activity; 4.51 µM compared to the EC_{50} of **232**; 1.37 µM. However, compound **229** (**Table 5.2, Entry 1**) was not active against *L. mexicana* axenic amastigotes even though it has a methoxy group in the *para* position of the phenyl ring attached to the -2 position.

Based on the structures and the reported EC_{50} values, the type of subunits (electron donating or electron withdrawing groups) on the aromatic ring seem to affect the biological activity. As an example, in the second set of compounds, **231** (**Table 5.2, Entry 3**) has two methyl groups on its aromatic ring in the *ortho* positions and it has an EC_{50} of 0.576 µM against *L. mexicana* axenic amastigotes but compound **239** (**Table 5.2, Entry 11**) which has an iodine group in the *para* position has an EC_{50} of 4.51 µM activity. A similar situation can be seen in the first set of compounds, **223a** (**Table 5.1, Entry 2**) and **226a** (**Table 5.1, Entry 5**) have fluorine and $-CF_3$ groups in their *para* positions and display no activity against *L. mexicana* axenic amastigotes and yet **224a** (**Table 5.1, Entry 3**), **235a** (**Table 5.1, Entry 4**) with chlorine and iodine substituents showing EC_{50} values of 4.42 µM and 3.94 µM, respectively.

As most of the compounds (**Table 5.1** and **5.2**) displayed low micromolar activities against *L. mexicana* axenic amastigotes they were subjected to cytotoxicity assays to eliminate off target effects of these drug candidates on human body (**Table 5.1** and **5.2**). RAW 264.7 cells were seeded at 2.5 $\times 10^5$ cells/mL and incubated 48 hours before they were treated with compounds in 3-fold dilutions from 25 µM to 0.195 µM, followed by series of washing steps precisely described in **Chapter 7**. The cells were incubated for further 24 hours including Alamar Blue® addition mentioned above and fluorescence were measured.

Though compounds **222** to **240** all displayed promising anti-parasitic activities, most of them have low CC_{50} values (e.g., high toxicity). For example, **230** (**Table 5.2, Entry 2**) is the most antiparasitic compound screened (EC_{50} = 0.155 µM, against *L. mexicana* axenic amastigotes) but it also has a high cytotoxic level, CC_{50}; 5.71 µM. Compounds **237** (**Table 5.2, Entry 9**), **239** (**Table 5.2, Entry 11**) and **222a** (**Table 5.1, Entry 1**) all have EC_{50} values and CC_{50} values that are similar. Analysing the anti-leishmanial activity and cytotoxicity together, **229b**, **225**, **227**, **238**, and **240** can be considered as the most promising compound to investigate further as potential leads.

5.5 Application of proteomics tools to identify target proteins for compound 230 in *L. mexicana* promastigotes.

Determination of both molecular targets and mode of action remain two of the most challenging areas in drug discovery. Chemical proteomics, an approach in which small molecule probes are used to covalently tag proteins in a function-dependent manner, has been introduced to address these challenges. The term 'proteomics' was first originated in 1995 and was defined as the large-scale characterization of the protein in a cell line, tissue, or organism with the goal of obtaining a more global and integrated view of biology by studying all the proteins in a cell rather than each one individually.[17] Proteomics tools allow the identification, analysis of expression levels, post-translational modifications (PTMs), interactions, structure, and subcellular distribution of proteins. Quantitative MS-based proteomics can divide into absolute and relative quantification methods and are based on stable isotope labelling strategies or label free quantification (LFQ). Absolute quantification measures the absolute protein abundance based on known protein/peptide standard concentrations. Relative quantification compares relative protein abundance between different biological conditions.[18] In the last decade, high-throughput screening of chemical libraries has enabled researchers to identify molecules involved in establishing leishmaniasis (among hosts, parasites and vectors), developing parasite resistance as

well as characterization of novel therapeutic targets.[19] Proteomics approaches also play a valuable role in drug development beyond the initial identification of a drug target; for example, proteomics can be applied to monitor therapeutic and toxic effects of newly developed compounds by particularly evaluating changes in the proteome of cell lines following treatment. Furthermore, proteomics can be used to analyse the interactions between the drug and the therapeutic target protein, which can subsequently enable modification of the drug molecule to improve drug affinity, efficiency, and efficacy. Evaluation of the specificity of a potential drug candidate using proteomic techniques can be used to chemically alter the drug to improve drug selectivity and reduce non-specific binding.[20]

In the 1980s, the first protein maps of *L tropica*, *L. mexicana* and *L. braziliensis* were published[21,22], even before the term 'proteomics' had been created[23]. *Leishmania* proteins were being largely identified by using SDS gel electrophoresis methods followed by MS analysis. The insight of all parasitic metabolic pathways, proteins involved in signalling systems and membrane will facilitate the development of new drugs with the help of bioinformatic tools.[22] Wright et al. used an in-house established approach for elucidating the global impact of N-myristoyl-transferase (NMT) dependent protein myristoylation in *L. donovani*.[24] In this work, a combination of an alkyne-tagged myristic acid analogue (**Figure 5.6**) and chemical knockdown experiments was used to identify NMT substrates and to quantify their relative abundance. [24]

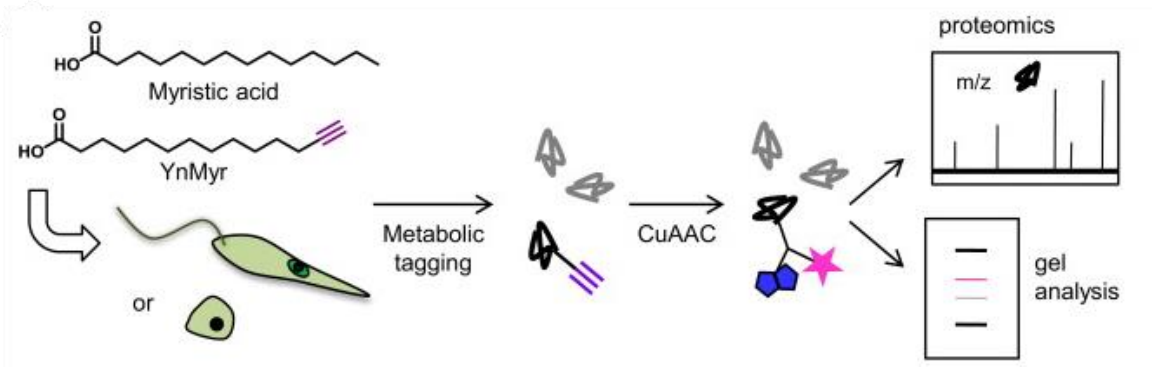

Figure 5.6 Overview of metabolic tagging of proteins with myristic acid analogue YnMyr and analysis following copper-catalyzed cycloaddition of an alkyne or azide (CuAAC).[24]

NMT-dependant protein myristoylation in *L. donovani* has been investigated and it indicated that a small-molecule mediated NMT inhibition (e.g., Inhibitor 1, **Figure 5.7**) may have extensive implications on *L. donovani* biology, impacting things such as signal transduction, transport, or degradation. However, additional experiments are necessary to further validate NMT as a leishmaniasis drug target.[24,25]

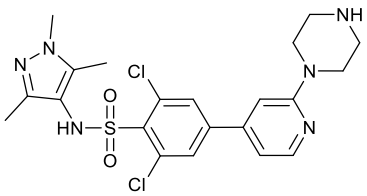

241

Figure 5.7 Chemical structure of Inhibitor 1 (2,6-dichloro-4-(2-(piperazin-1-yl)pyridin-4-yl)-N-(1,3,5-trimethyl-1H-pyrazol-4-yl)benzenesulfonamide) (**241**).[24]

5.5.1 In-gel fluorescence assays

A preliminary in-gel fluorescence screening assay was carried out to verify the positive labelling of proteins with **230, 227a, and 227b** (**Figure 5.8**). To facilitate the click reaction, it is necessary to have an alkyne group or an azide group within the structure. Since **230, 227a, and 227b** already have an alkyne group they were selected for the In-gel fluorescence assay and compound **228** was used as a negative control. Workflow for the

assay is given in **Figure 5.9**. Assays were performed as previously described with slight modifications.[26]

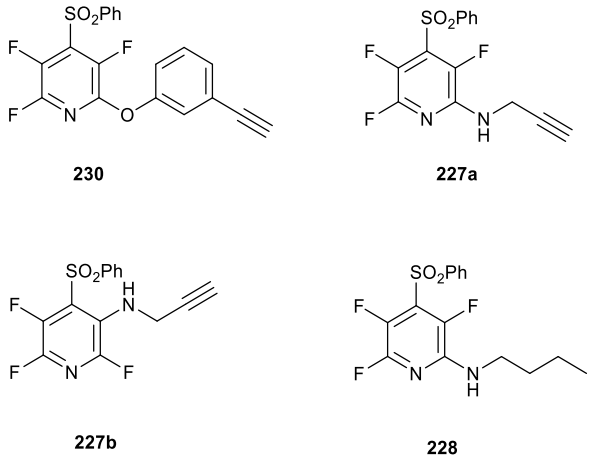

Figure 5.8 Chemical structures of the selected compounds (**230, 227a, 227b and 228**) for the in-gel fluorescence assay.

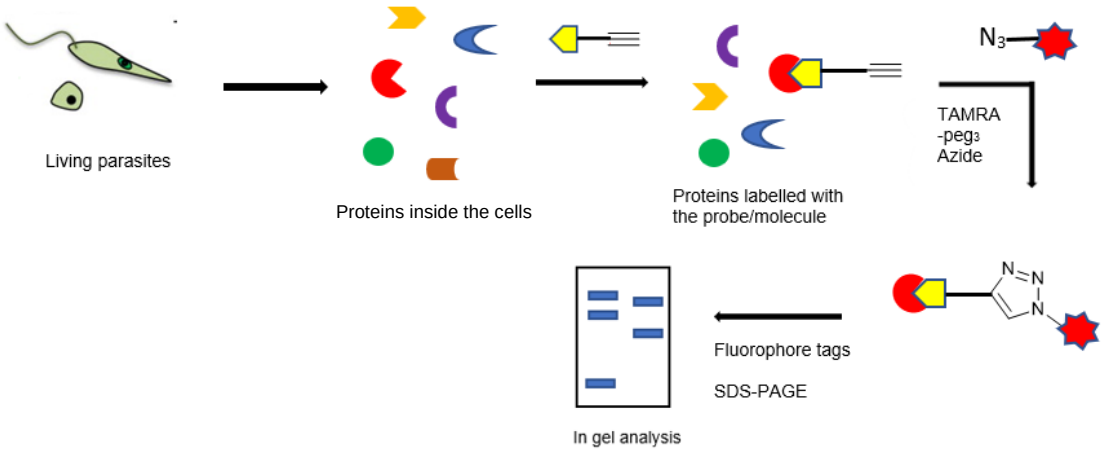

Figure 5.9 Workflow for the in-gel fluorescence assay.

Detailed protocols can be found in **Chapter 7** (**Section 7.7.6**). Briefly, *L. mexicana* promastigotes were treated with the preferred compound concentrations for 2 hrs at 26 ºC. After the treatment, cells were washed twice with PBS to ensure that there is no excess compound left and the cell lysates were prepared using the lysis buffer (50 mM HEPES pH 7.5, 150 mM NaCl, 4% SDS). Protein concentrations of the cell lysates were measured using the BCA assay to prepare 1 mg/mL proteins solutions for the click reaction. In the

click reaction, probe/compound labelled proteins were incubated with a mixture of $CuSO_4$, TAMRA-PEG_3-Azide (capture reagent), tris[2-carboxyethyl]phosphine (TCEP) solution and tris[{1-benzyl-4triazoyl}methyl]amine (TBTA) solution for 2 hours at room temperature. Proteins were precipitated by adding EDTA, ice cold methanol and storing overnight at -80 ºC. On the following day, protein pellets were collected and air dried before resuspending them in the lysis buffer. Then, the samples were mixed with 4X LDS loading buffer (10-20% β-mercaptoethanol in 4X Laemmli sample buffer) and boiled at 95 ºC for 8 mins before loading on 0.01% SDS gels. Gels were run in a gel electrophoresis equipment using 1X running buffer, approximate running time is 1-1.5 hrs and 180-200 voltage and scanned for fluorescence labelling using a GE typhoon 5400 gel scanner (**Figure 5.10**).

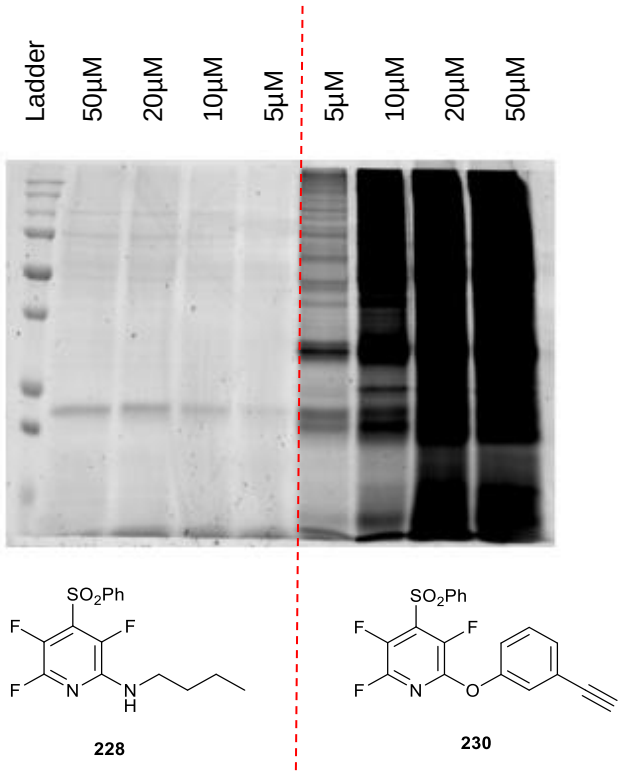

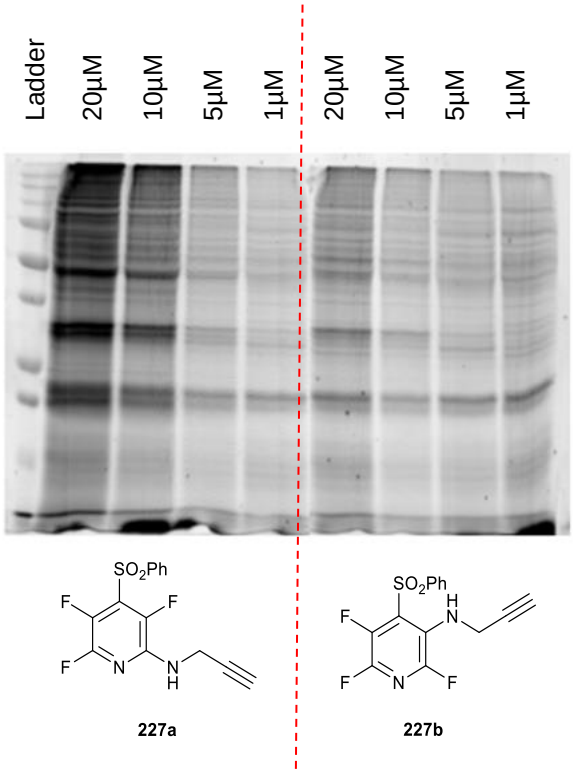

Figure 5.10 Scanned gel images which indicate positive and negative protein labelling in *L. mexicana* promastigotes.

Figure 5.10 clearly shows the positive protein labelling by the fluorinated compounds with alkyne handle (**230**, **227a** and **227b**) confirming the formation of covalent bonds between proteins and the compound/probe. It should be noted that that results do not confirm that compound **228** cannot also bind to proteins. The absence of an alkyne group in **228**, means that the click reaction cannot occur, and hence negative/ no protein labelling is observed.

A protease inhibitor cocktail is used with the lysis buffer to prevent the degradation of extracted proteins and to obtain the best possible protein yield and activity. cOmpleteTM, Mini, EDTA-free protease inhibitor cocktail inhibit a broad spectrum of serine and cysteine proteases as well as leave stability and the function of metal-dependent proteins unaffected. In a click chemistry reaction, Cu(I) is used to catalyse the 1,3-dipolar cycloaddition of an alkyne with an azide to form a 1,2,3-triazole. In this experiment, Copper (II) sulfate ($CuSO_4$) and TCEP (a reducing agent) was used as the source of Cu(I). However, Cu (I) is thermodynamically unstable and readily oxidizes to inactive Cu (II).

Thus, it usually requires a Cu(I) stabilizing ligand, TBTA. This leads to a more reliable click reaction by avoiding the oxidation of Cu(I) by dissolved oxygen.

5.5.2 Effect of fluorine in protein labelling

From the compounds studied, 2-(3-ethynylphenoxy)-3,5,6-trifluoro-4-(phenylsulfonyl) pyridine (**230**) was found to be the most active compound (EC_{50} = 0.155 µM) against *L. mexicana* axenic amastigotes among the three compounds analysed (**230**, **227a** and **227b**) and therefore selected for further studies. To evaluate the effect of fluorine on protein labelling, a molecule similar to **246** was synthesised where the fluorine atoms were replaced with hydrogen, 2-(3-ethynylphenoxy)-4-(phenylsulfonyl)pyridine (**246**).

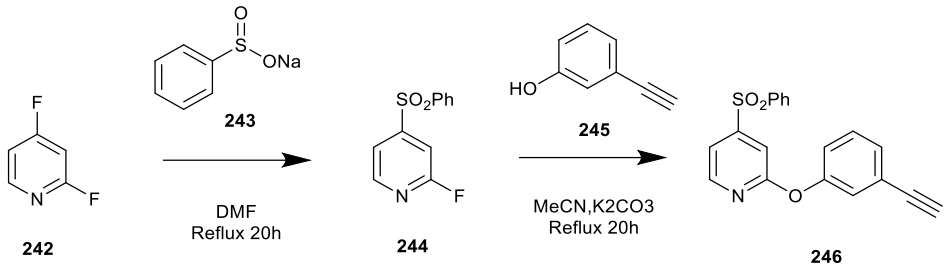

Scheme 5.6 Synthesis of non-fluorinated compound **246** (2-(3-ethynylphenoxy)-4-(phenylsulfonyl)pyridine). Yield = 19%.

The same reaction protocol outlined in **Section 5.5.1** was followed to generate cell lysates from *L. mexicana* promastigotes (**Figure 5.11**), Raw 264.7 and MCF-7 cells (**Figure 5.12**) treated with **230** and **246**. The fluorescence images obtained after running the gels (**Figure 5.11** and **5.12**) confirmed that fluorine is essential for protein binding. A gradient of labelled proteins was noticed with the concentrations and some non-specific binding can be seen in the gel with non-fluorinated **246**.

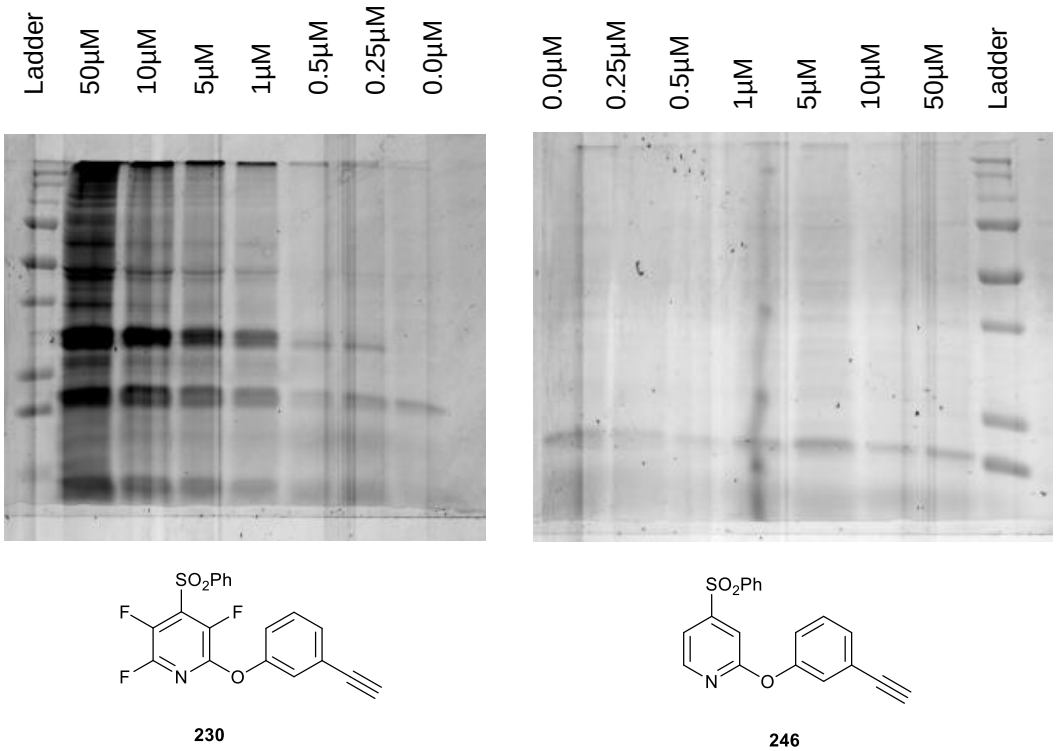

Figure 5.11 Scanned gel images which represent positive and negative protein labelling of **230** and **246** in *L. mexicana* promastigotes.

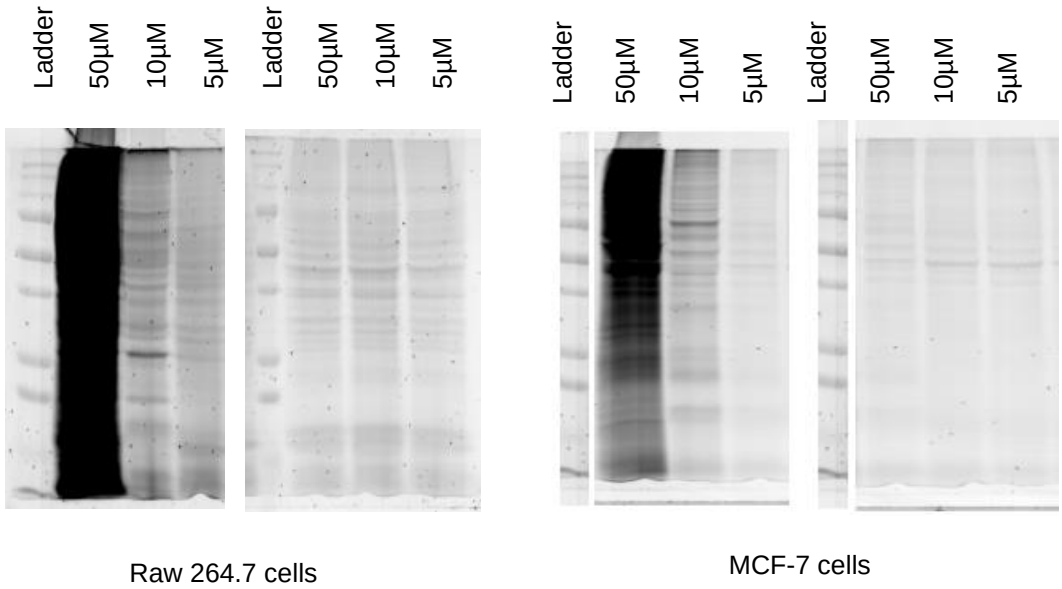

Figure 5.12 Scanned gel images which represent positive and negative protein labelling of **230** and **246** in Raw 264.7 and MCF-7 cells.

5.5.3 Competition assay between fluorinated (230) and non-fluorinated (246) molecules

Non-specific binding is one of the main limitations of affinity-based protein profiling (ABPP) strategies. Application of competitive-ABPP is gaining increasing attention as a strategy to overcome this problem. In competitive binding, a proteome is pre-incubated with the parent compound and subsequently with the activity-based probes, thus reducing the binding of the probe with the target proteins by competing for the common active site.[27]

L. mexicana promastigotes were treated with the **230** at a 50 µM concentration for 1 hour, followed by the addition of **246** at a 5 µM concentration and incubated further for 2 hours. A detailed experimental method is provided in **Chapter 7** (**Section 7.7.6.6**). The scanned gel image is shown in **Figure 5.13,** and it shows that there is no significant difference in protein labelling compared to the DMSO control. This result implies that that **230** is not competing with **246** the active site of a protein/enzyme target. It is possible that the compounds screened may have separate target proteins or different binding sites on the same target.

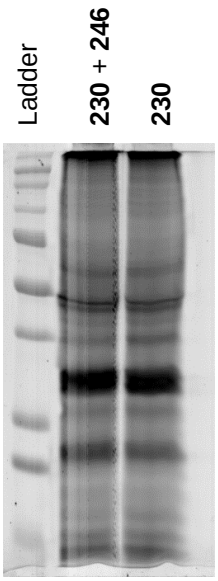

Figure 5.13 Scanned gel image for the competitive-ABPP assay of compound **230** and **246** for the *L. mexicana* promastigotes proteome.

5.5.4 Reaction of compound 198 with Glutathione (GSH)

In an attempt to probe how **198** might be reacting in a biological context a simple reactivity experiment was designed with glutathione. Glutathione is a small molecule made from the amino acids glycine, cysteine, and glutamic acid and exists in either its reduced (GSH) (**247**) or oxidised form (GSSG) (**248**) (**Figure 5.14**).

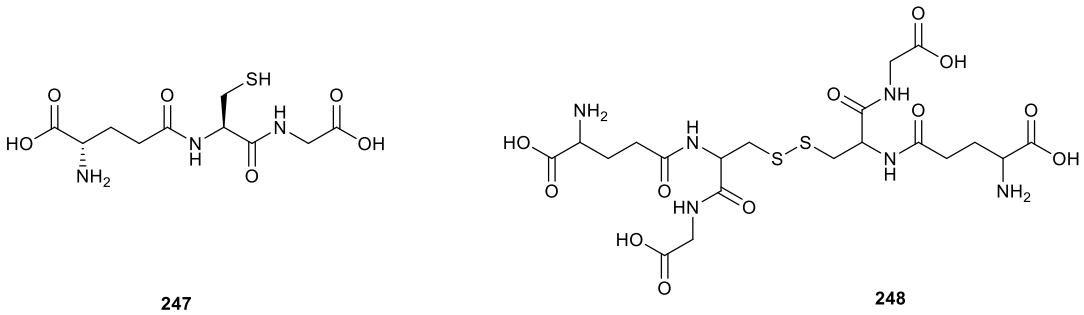

Figure 5.14 Chemical structures of reduced (**247**) and oxidized (**248**) forms of glutathione.

The reaction between glutathione (**247**) and **198** was carried out in PBS buffer at a 1:5 ratio (**198**:**247**). The reaction was monitored by mass spectrometry at time intervals of 0, 0.5, 1.0, 2.0, 3.0, 24, 48, 72 hrs. After 48 hours, mass spectrometry indicated the replacement of the phenyl sulfonyl group in **198** by glutathione (e.g., a mass of 456.7 g/mol was detected).

Given that the reaction carried out in aqueous medium was relatively slow, different types of solvents were tried (e.g., DMSO, MeCN: H_2O, DMF) to optimise the reaction rate and to get better yields of the displacement product for analysis. DMSO was found to be the best solvent for the reaction (almost a complete conversion within 24 hrs), but due to the difficulties in removing DMSO, we finally decided to carry out the reaction in DMF (**Scheme 5.7**).

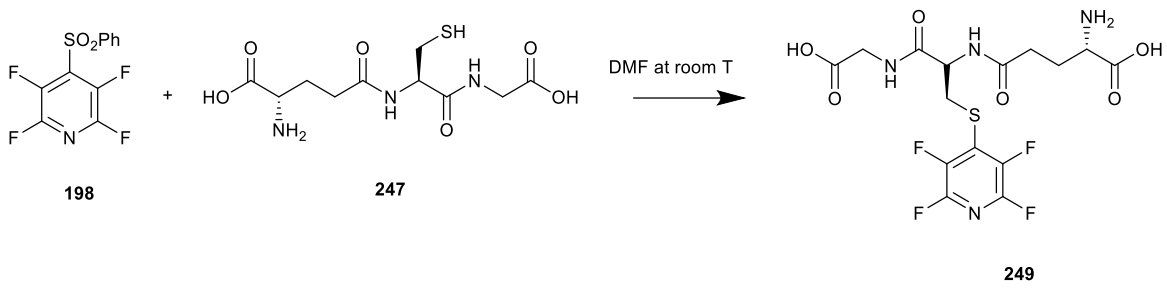

Scheme 5.7 Reaction of **198** with glutathione (**247**) in DMF.

Figure 5.15 shows the ^{19}F NMR spectra taken in DMSO-d_6. The initial ^{19}F NMR shows the peaks of **198** in DMSO-d_6 (**Figure 5.15 (A)**) and the 2nd NMR shows the peaks for the reaction of **198** and glutathione in DMSO-d_6 after 24 hrs (**Figure 5.15 (B)**). The 3rd NMR spectrum represent the same reaction carried out in DMF and the NMR taken in DMSO-d_6 for the comparison (**Figure 5.15 (C)**). DMF was removed by co-evaporated with toluene.

The ^{19}F NMR spectra (**Figure 5.15**) clearly demonstrate the peaks shift and there is no change in the number of peaks. This and the mass detected in MS spectrum (**Figure 5.15 (D)**) proves that glutathione replaces the phenyl sulfonyl group in the **198**. The end product (**249**) was purified by HPLC.

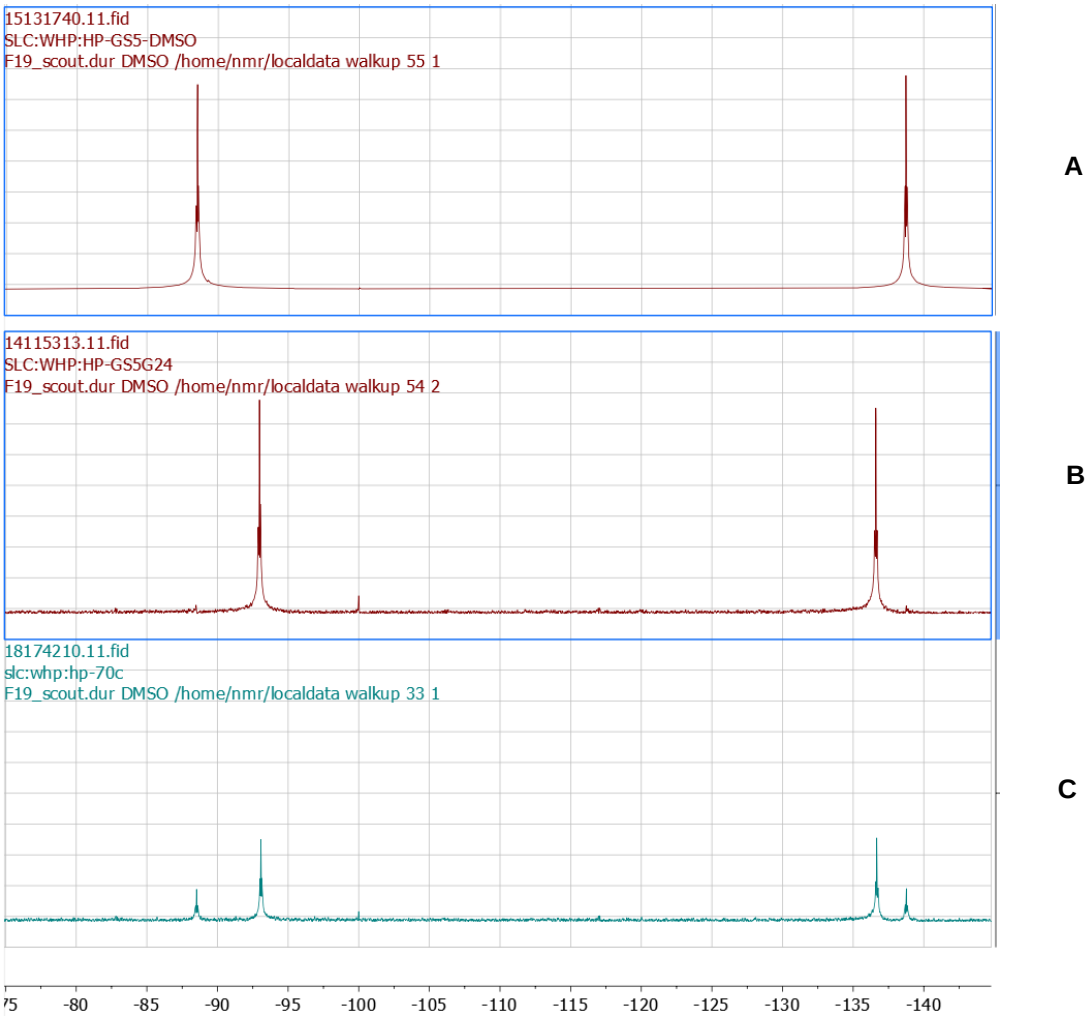

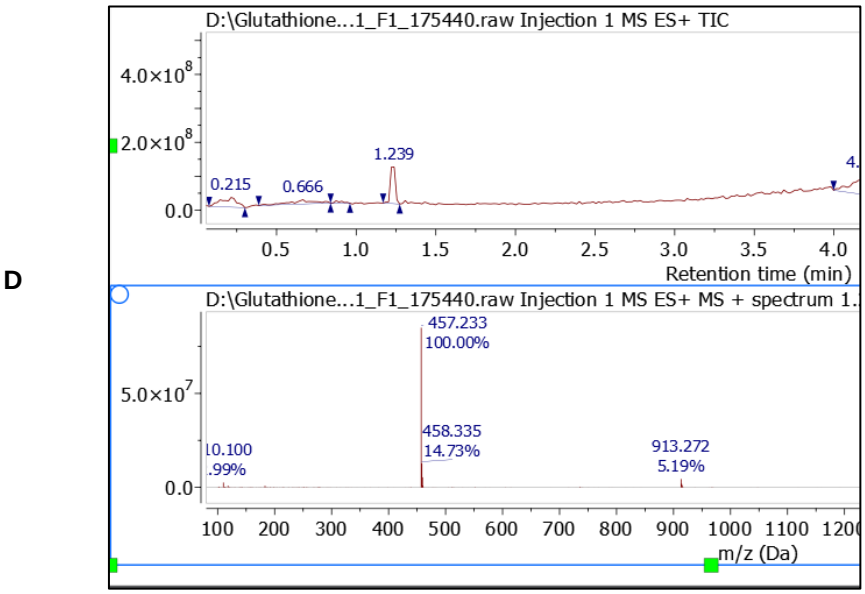

Figure 5.15 ^{19}F NMR shifts. NMRs were taken in DMSO-d_6. **A** - ^{19}F NMR of compound **198** in DMSO-d_6. **B** - ^{19}F NMR of **198** + GSH reaction carried out in DMSO-d_6. **C** -^{19}F NMR of **198** + GSH reaction carried out in DMF (NMR taken in DMSO-d_6). **D** - MS spectrum of **249** $[M+H]^+$ = 457.

5.5.5 Mass-Spectrometry based proteomics studies with compound 230

Based on the anti-parasitic activity and further studies on the importance of fluorine in protein labelling the decision was made to subject **230** to mass spectrometry-based proteomics assays.

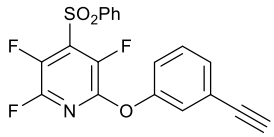

230

Detailed protocols are provided in **Chapter 7** (**Section 7.7.7**) and a schematic diagram of the process that was undertaken is shown in **Figure 5.16**. Assays were performed with slight modifications to the original protocol reported.[28] Briefly, *L. mexicana* promastigotes were treated with **230** at a 5 µM concentration for 2 hours at 26 ºC and after the treatment, cell lysates were prepared as mentioned in the Chapter 7, **Section 7.7.4**. To facilitate the click reaction, probe/compound labelled proteins were incubated with a mixture of $CuSO_4$, Biotin-Azide (capture reagent), tris[2-carboxyethyl]phosphine (TCEP) solution and tris[{1-benzyl-4triazoyl}methyl]amine (TBTA) solution for 3 hours at room temperature. And then proteins were precipitated by adding EDTA, ice cold methanol and storing overnight at -80 ºC. On the following day, protein pellets were collected and air dried before resuspending them in PBS with 0.1% SDS. For the affinity enrichment, collected supernatant from the above was combined with freshly washed NeutrAvidin-agarose beads and the mixture was then incubated at room temperature for 1.5 hrs using an end-to-end shaker. Afterwards, the beads were collected and washed with a 1% SDS solution in PBS and PBS respectively.

Furthermore, on bead reduction and alkylation of proteins were achieved by treating the agarose beads with TCEP, iodoacetamide respectively followed by series of washing steps with triethylamine bicarbonate (TEAB) buffer. TCEP is a reducing agent which used

to breaks the disulphide bonds between cysteine amino acids and iodoacetamide prevent re-formation of disulphide bonds. Then the beads were incubated with trypsin at 37 ºC for 12-16 hrs for the tryptic digestion of proteins. Formic acid (FA) was used to acidify the peptide mixture (pH 3>) after the incubation period and the supernatant was collected. The samples were evaporated to complete dryness using a speed vacuum. Finally, the samples were desalted using Sep-Pak C_{18} columns with buffer A (98% MiliQ H_2O, 2% Acetonitrile and 0.1% FA) and then peptides were eluted using buffer B (35% MiliQ H_2O, 65% Acetonitrile and 0.1% FA). Eluted solutions were evaporated to complete dryness using a speed vacuum. Desalted tryptic peptide solutions in water with 0.1% formic acid were analysed on an Acquity UPLC M-Class nano-LC system (Waters Corporation) interfaced to a Xevo G2-XS Quadrupole Time-of-flight (Tof) tandem mass spectrometer.

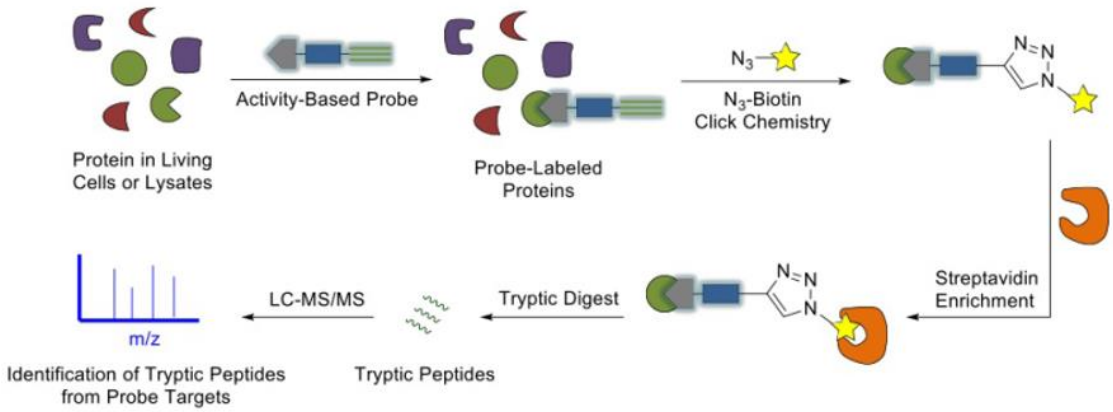

Figure 5.16 Schematic diagram of MS based proteomics.

Initially, the same protocols for label free protein labelling were followed as Kalesh et al. described in their recent study.[28] From these initial experiments, there were no proteins to identify in the MS analysis stage. The reason that no proteins were identified could be due to the fact that the covalent bond formed between the protein and the drug molecule was not strong enough to go through all the harsh washing conditions in the protocol. Therefore, the protocol was modified by reducing the number of washing steps (the

modified protocols are listed in the Chapter 7, **Section 7.7.7.5**) to see if it yielded any positive result. After the aforementioned changes to the protocol, the processed mass spectrometry data identified 117 proteins and 510 peptides in *L. mexicana* promastigotes. However, due to the changes in the protocols that were used, there are limited number of proteins which showed preferential enrichment in the sample (*L. mexicana* promastigotes treated with compound number **230**) compared with the DMSO treated sample. 19 of the most abundant proteins identified in *Leishmania mexicana* strain MHOM/GT/2001/U1103 are listed below.

- Putative 60S ribosomal protein
- Glucose transporter
- Putative ATPase alpha subunit
- Glyceraldehyde-3-phosphate dehydrogenase
- Putative 60S ribosomal protein L2
- GTP-binding nuclear protein
- Putative 60S ribosomal protein L23a
- Nucleoside diphosphate kinase
- Putative ubiquitin-conjugating enzyme e2
- Peptidyl-prolyl cis-trans isomerase
- Elongation factor 2
- Tryparedoxin peroxidase
- Putative heat-shock protein hsp70
- Putative 40S ribosomal protein S10
- Activated protein kinase c receptor (LACK)_guanine nucleotide-binding protein beta subunit-like protein
- Putative mitochondrial phosphate transporter
- Elongation of fatty acids protein
- Heat shock protein 83-1
- Uncharacterized protein

The gene ontology (GO) is a public resource that develop organism independent ontologies which provide a uniform vocabulary for representing domain knowledge. It is the most widely used ontology for specifying cellular location/components, molecular function, and biological process participation of human and other model organism genes. The ontology represents the relationship between GO terms and GO terms are associated with genes as a form of annotation. The GO annotation shows the list of all annotated genes linked to ontology terms describing those genes.[29] From the data obtained in this part of the project a gene ontology (GO) enrichment analysis was carried out. Scatter plots were generated for biological processes (**Figure 5.17**), cellular components (**Figure 5.18**) and molecular functions (**Figure 5.19**) using TriTrypDB database and REVIGO web server. The list of GO terms and their P-values for each scatter plot is mentioned with respective plots. P-value is the probability of seeing the genes annotated to a particular GO term in the user's list out of the total genes in the whole genome that are annotated to that GO term. The closer the p value to zero, the more significant the particular GO term is.[30]

The axes in these plots have no intrinsic importance. Revigo uses multidimensional scaling (MDS) to reduce the dimensionality of a matrix of the GO terms pairwise semantic similarities. The values associated with GO terms represent P values in the plots. Molecular function terms (**Figure 5.19**) describe the activities in *L. mexicana* promastigotes at molecular level performed by the gene products (e.g., a protein) we have identified. Then, **Figure 5.17** represent the biological processes/programs accomplished by multiple molecular activities listed in **Figure 5.19**. Finally, cellular components of *L. mexicana* promastigotes highlighted in **Figure 5.18** reveal the locations relative to cellular structures in which proteins perform their functions.

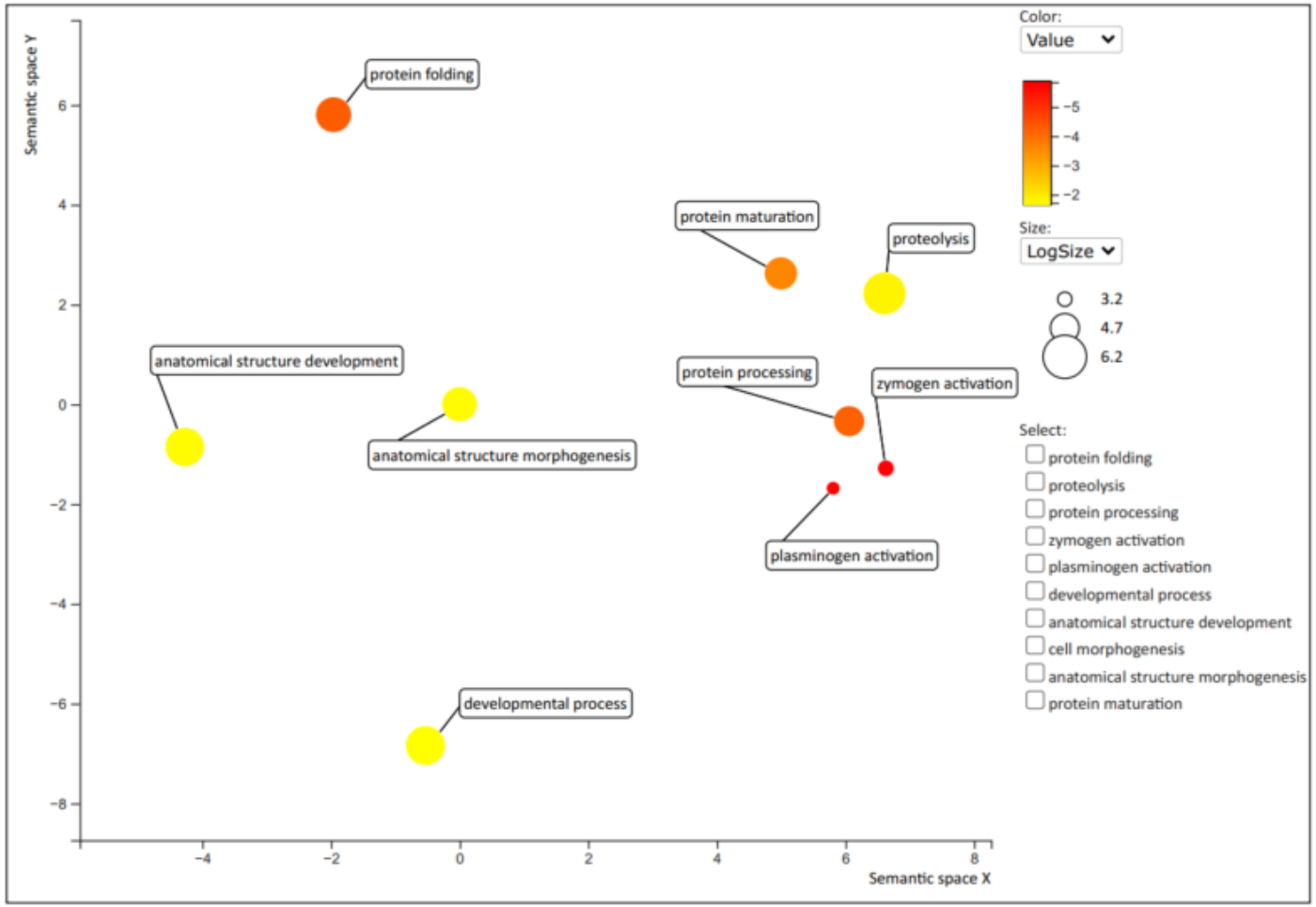

GO term	P-value
plasminogen activation	1.39e-6
zymogen activation	1.39e-6
protein folding	4.42e-5
protein processing	5.00e-5
protein maturation	2.11e-4
proteolysis	1.29e-2
anatomical structure development	1.67e-2
anatomical structure morphogenesis	1.67e-2
developmental process	1.93e-2

Figure 5.17 Scatter plot representing the biological processes of the genes identified and the list of GO terms with their respective p-values.

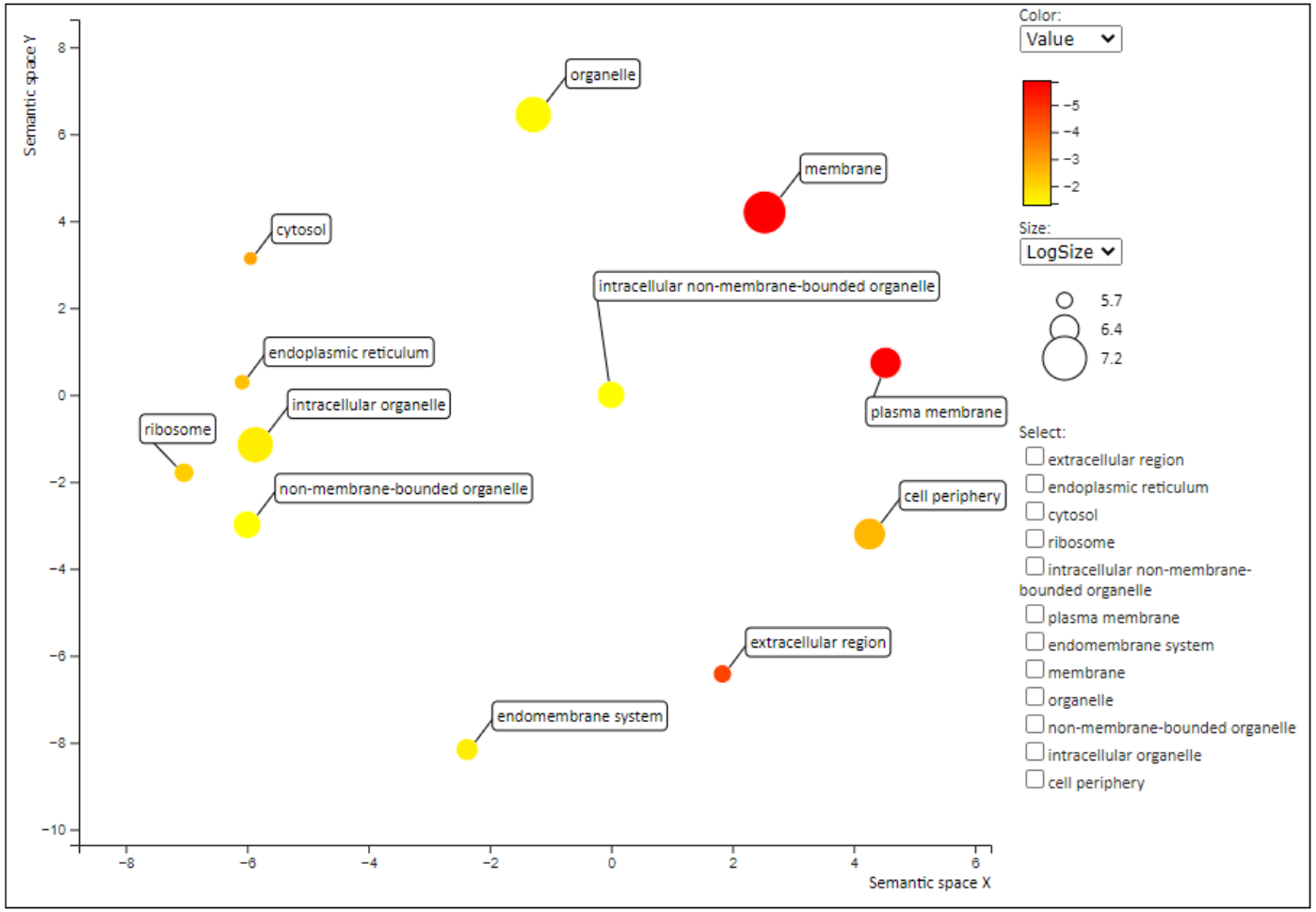

GO term	P-value
extracellular region	2.09e-5
cytosol	1.12e-3
plasma membrane	4.42e-5
cell periphery	2.39e-3
endoplasmic reticulum	3.52e-3
ribosome	5.66e-3
endomembrane system	2.11e-2
intracellular organelle	2.21e-2
organelle	3.43e-2
intracellular non-membrane-bounded organelle	4.36e-2
non-membrane-bounded organelle	4.36e-2

Figure 5.18 Scatter plot representing the cellular components of the genes identified and the list of GO terms with their respective p-values.

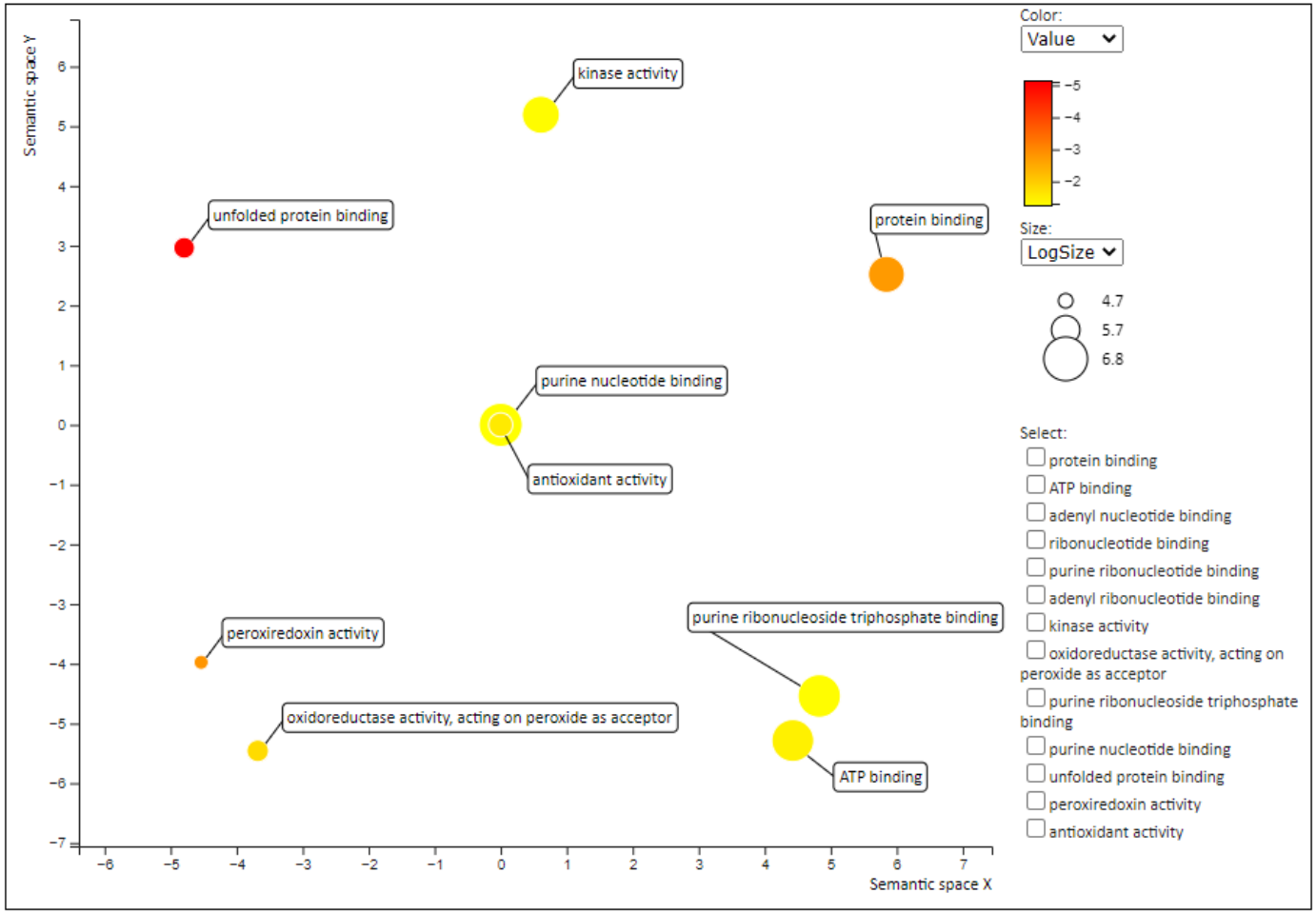

GO term	P-value
unfolded protein binding	7.75e-6
peroxiredoxin activity	1.29e-3
protein binding	1.55e-3
oxidoreductase activity, acting on peroxide as acceptor	1.42e-2
antioxidant activity	2.43e-2
ATP binding	3.07e-2
kinase activity	4.42e-2
purine ribonucleoside triphosphate binding	4.55e-2
purine nucleotide binding	4.92e-2

Figure 5.19 Scatter plot representing the molecular function of the genes identified and the list of GO terms with their respective p-values.

5.6 Chapter Summary

A library of fluorinated molecules (second generation library based on the 4-phenylsulfonyl tetrafluoropyridine, **198** core) was synthesised, and their anti-parasitic activity determined against *L. mexicana* axenic amastigotes. In some cases, it was challenging to purify molecules prepared in the second-generation library, because of the mixture of mono- and di-substituted products in the crude samples. The compound 2-(3-ethynylphenoxy)-3,5,6-trifluoro-4-(phenylsulfonyl) pyridine (**230**) had the lowest EC_{50} value (0.155 µM) against *L. mexicana* axenic amastigotes. From the full library of 25 compounds, 18 compounds which had promising biological activity were then subjected to cytotoxicity assays. The outcome of the cytotoxicity assays confirmed that nearly half of the compounds are toxic (less than 10µM CC_{50} values) to mammalian/host cells.

To investigate the mode of action and potential molecular target of the compounds screen proteomics tools were then employed in the target identification studies. First, in-gel fluorescence assays were performed with *L. mexicana* promastigotes, RAW 264.7 and MCF-7 cell lysates to confirm the covalent binding of the selected molecules (**227a**, **227b**, and **230**) with the proteins. The scanned gel images obtained (**Figure 5.10** and **5.11**) showed that positive labelling between the selected candidate molecules and the proteins had occurred. The essential requirement for fluorine atoms on the core pyridine structure in protein labelling was confirmed in the by the lack of labelling seen in the gel image in **Figure 5.10** and **5.11** when the non-fluorinated version of **230**, compound **247** was investigated. Investigation of the competitive binding of **230** and **247** showed a negative result, which indicated that **247** is not competing with **230** for the same binding site of the target proteins (**Figure 5.10**). Additionally, 4-phenylsulfonyl tetrafluoropyridine (**198**) was reacted with reduced glutathione (GSH) to probe the mechanism by which **198** is binding to proteins. NMR (both ^{1}H and ^{19}F) and mass spectrometry data (**Figure 5.15**) confirmed that glutathione reacts with **198** to displaces the sulphonyl group within the molecule (**Scheme 5.7**). MS-based proteomics analysis (Label free) identified a list of (19 proteins)

potential target proteins for **230.** The first run of MS-based proteomics did not show any labelled proteins. Therefore, we had to optimise the method assuming that a covalent bond between the protein and the candidate molecule is not strong enough to withhold all the harsh washing conditions. Having obtained a list of target proteins, gene ontology (GO) enrichment has generated GO terms for biological processes (**Figure 5.17**), cellular components (**Figure 5.18**) and molecular functions (**Figure 5.19**) of the identified genes/proteins. Collectively, these scatter plots show the molecular activities of the *L. mexicana* proteins (in promastigotes) we discovered, biological processes executed by these activities and the cellular compartments where these functions take place. This needs to be repeated to get more statistically accurate results.

5.7 References

1. Sugiyama., Y. Druggability: selecting optimized drug candidates. *Drug Discovery Today* vol. 10 1577–1579 (2005).

2. Horton, D. A., Bourne, G. T. & Smythe, M. L. The combinatorial synthesis of bicyclic privileged structures or privileged substructures. *Chem. Rev.* **103**, 893–930 (2003).

3. Walters, W. P., Murcko, A. & Murcko, M. A. Recognizing molecules with drug-like properties. *Curr. Opin. Chem. Biol.* **3**, 384–387 (1999).

4. Bailey, D. & Brown, D. High-throughput chemistry and structure-based design: Survival of the smartest. *Drug Discov. Today* **6**, 57–59 (2001).

5. Leach, A. R. & Hann, M. M. The in silico world of virtual libraries. *Drug Discov. Today* **5**, 326–336 (2000).

6. Walters, W. P. & Murcko, M. A. Prediction of 'drug-likeness'. *Adv. Drug Deliv. Rev.* **54**, 255–271 (2002).

7. DeSimone, R., Currie, K., Mitchell, S., Darrow, J. & Pippin, D. Privileged Structures: Applications in Drug Discovery. *Comb. Chem. High Throughput Screen.* **7**, 473–493 (2004).

8. Mason, J. S. *et al.* New 4-point pharmacophore method for molecular similarity and diversity applications: Overview of the method and applications, including a novel approach to the design of combinatorial libraries containing privileged substructures. *J. Med. Chem.* **42**, 3251–3264 (1999).

9. Ojima, I. *Fluorine in medicinal chemistry and Chemical Biology*. (John Wiley & Sons, Ltd., Publication, 2009). doi:10.1016/bs.pmch.2014.11.001.

10. Ranjbar-Karimi, R. & Poorfreido, A. Incorporation of Fluorinated Pyridine in the Side Chain of 4-Aminoquinolines: Synthesis, Characterization and Antibacterial Activity. *Drug Res. (Stuttg).* **68**, 17–22 (2018).

11. Amii, H. & Uneyama, K. C-F bond activation in organic synthesis. *Chem. Rev.* **109**, 2119–2183 (2009).

12. Baron, A. *et al.* Polyfunctional Tetrahydropyrido [2 , 3- b] pyrazine Scaffolds from 4-Phenylsulfonyl Tetrafluoropyridine. *J. Org. Chem.* **70**, 9377–9381 (2005).

13. Reza, R.-K. & Mousavi, M. Regiochemistry of nucleophilic substitution of 4-phenylsulfonyl tetrafluoropyridine with unequal bidentate nucleophiles. *J. Fluor. Chem.* **131**, 587–591 (2010).

14. Revesz, L. *et al.* SAR of 2,6-diamino-3,5-difluoropyridinyl substituted heterocycles as novel p38 MAP kinase inhibitors. *Bioorganic Med. Chem. Lett.* **12**, 2109–2112 (2002).

15. Chambers, R. D. *Fluorine in Organic Chemistry*. (CRC Press, 2004). doi:10.1021/ed053pa271.2.

16. Banks, R. E. *et al.* Heterocyclic Polyfluoro-compounds. Part XI2 Synthesis and Some Reactions of 2,3,5,6-Tetrafluoropyridine-4-aldehyde and -4-nitrile. *J. Chem. Soc.* 2089–2091 (1967).

17. Graves, P. R. & Haystead, T. A. J. Molecular Biologist's Guide to Proteomics. *Microbiol. Mol. Biol. Rev.* **66**, 39–63 (2002).

18. Capelli-Peixoto, J.´ına., Mule, S. N., Tano, F. T., Palmisano, G. & Stolf, B. S. Proteomics and Leishmaniasis Potential Clinical Applications. *Proteomics Clin. Appl.* **13**, 1800136 (2019).

19. Veras, P. S. T. & De Menezes, J. P. B. Using proteomics to understand how Leishmania parasites survive inside the host and establish infection. *Int. J. Mol. Sci.* **17**, 1270 (2016).

20. Moseley, F. L., Bicknell, K. A., Marber, M. S. & Brooks, G. The use of proteomics to identify novel therapeutic targets for the treatment of disease. *J. Pharm. Pharmacol.* **59**, 609–628 (2010).

21. Handman, E., Hocking, R. E., Mitchell, G. F. & Spithill, T. W. Isolation and characterization of infective and non-infective clones of Leishmania tropica. *Mol. Biochem. Parasitol.* **7**, 111–126 (1983).

22. Negrão, F., Eberlin, M. N. & Giorgio, S. Proteomic approaches for drug discovery against tegumentary leishmaniasis. *Biomed. Pharmacother.* **95**, 577–582 (2017).

23. Paape, D. & Aebischer, T. Contribution of proteomics of Leishmania spp. to the understanding of differentiation, drug resistance mechanisms, vaccine and drug development. *J. Proteomics* **74**, 1614–1624 (2011).

24. Wright, M. H. *et al.* Global analysis of protein N-myristoylation and exploration of N-myristoyltransferase as a drug target in the neglected human pathogen leishmania donovani. *Chem. Biol.* **22**, 342–354 (2015).

25. Ehrmann, M., Kaschani, F. & Kaiser, M. Chemical proteomics versus Leishmaniasis. *Chem. Biol.* **22**, 309–310 (2015).

26. Kalesh, K. & Denny, P. W. A boncat-itraq method enables temporally resolved quantitative profiling of newly synthesised proteins in leishmania mexicana parasites during starvation. *PLoS Negl. Trop. Dis.* **13**, 1–26 (2019).

27. Wang, S. *et al.* Advanced activity-based protein profiling application strategies for drug development. *Front. Pharmacol.* **9**, 1–9 (2018).

28. Kalesh, K., Sundriyal, S., Perera, H., Cobb, S. L. & Denny, P. W. Quantitative Proteomics Reveals that Hsp90 Inhibition Dynamically Regulates Global Protein Synthesis in Leishmania mexicana. *mSystems* **6**, 1–15 (2021).

29. Tomczak, A. *et al.* Interpretation of biological experiments changes with evolution of the Gene Ontology and its annotations. *Sci. Rep.* **8**, 1–10 (2018).

30. GO enrichment analysis. http://geneontology.org/docs/go-enrichment-analysis/ (1999).

6 Conclusions and Future work

Leishmaniasis and Chagas disease are neglected tropical diseases (NTDs) which affect millions of people around the world. These diseases are more frequent among impoverished communities and available drugs are limited in number and have various side effects. Hence, there is an urgent need for novel, more effective, safe, and convenient drugs/treatments. The overarching aim of this work was to identify suitable compounds that could be used for the development of new therapeutics for leishmaniasis and Chagas disease. Alongside this there was a desire to study the mode of action and potential molecular targets of any identified leads.

In Chapter 2, the anti-leishmanial activity of a library of molecules with highly diverse chemical space was evaluated with the purpose of identifying novel chemical entities for future development. From a library of 53 compounds in total, we identified around 18 compounds that were shown to have potent activity against *L. mexicana* (M379) axenic amastigotes. Compound **40** (**Table 2.2, Entry 1**) in Class One (9,10-phenanthrenedione derivatives) and **64** (**Table 2.5, Entry 5**) in Class Two (Phenanthrolines) have the lowest EC_{50} values against *L. mexicana* axenic amastigotes, 0.214 µM and 0.175 µM respectively. While it was promising to discover compounds with nanomolar activity against *L. mexicana* axenic amastigotes, they have slightly decreased activity against intracellular amastigotes. However, most of the compounds screened were found to have high toxicity values against HeLa cells compared to their activity against intracellular amastigotes and this make them less convincing as suitable starting points for development. For example, compound **40** has a 6 µM CC_{50} against HeLa cells, and 3.12 µM EC_{50} against *L. mexicana* intracellular amastigotes (**Table 2.2, Entry 1**) and compound **64** has a 10 µM CC_{50} against HeLa cells, 3.27 µM EC_{50} against *L. mexicana* intracellular amastigotes (**Table 2.5, Entry 5**). Selecting the most active compounds from this library and structurally modifying them to be less cytotoxic is an obvious area for future studies.

Additionally, it is possible to develop chemical probes from the active molecules and continue with target identification studies using proteomics as in Chapter 5. Given the high degree of novelty in terms of chemical space within this library this might be a fruitful area of study, and it has the potential to uncover new, unexplored molecular targets in *L. mexicana.*

Chapter 3 highlights the work that has been carried out to investigate the activity of three, FDA approved anti-fungals, pyrithione (**104**), ciclopirox (**105**) and piroctone olamine (**106**) against *Leishmania mexicana* (M379). Each of these compounds displayed anti-leishmanial activities against both the promastigote and axenic amastigote forms of the *L. mexicana* parasite. Additionally, they were subjected to *L. mexicana* intracellular assays to test if they could retain their activity inside host cells and their SI values were calculated (**Table 3.1**). Having EC_{50} values lower than 2 µM (**Table 3.1**) and SI values greater than 10 (**Table 3.1**) proved their ability to retain activity inside macrophages and be considered realistic developable hits for drug repurposing. **104** contains an N-oxide group adjacent to a thiocarbonyl and compounds **105** and **106** contain an N-oxide group adjacent to a carbonyl. Given their structural properties **104**, **105** and **106** are known metal chelators but surprisingly their exact mode of antifungal activity remains unknown. It is possible that **104**, **105** and **106** could potentially inhibit the *Leishmania* parasites *via* a metal-dependant mechanism but further studies were needed to confirm this. Of the three compounds **104** had shown the lowest EC_{50} value; 42.11nM against axenic amastigotes (**Table 3.1**) and as such this was selected to test the metal binding theory. In order to test the theory that metal chelation may play a role in the mechanism of **104**, this compound was modified by appending different acyl group to the N-oxide. The synthesise and characterisation of four modified compounds, **116**, **117**, **118** and **119** was achieved. Biological evaluation showed that modification of the N-oxide functionality did not significantly change the activity of the compounds against *L. mexicana* axenic and intracellular amastigotes. This seems to suggest that a metal-dependent mode of action is not in operation for compound **104** in

terms of its anti-leishmanial properties. **116**, **117**, **118** and **119** displayed reduced but still highly promising anti-parasitic activity with EC_{50} values less than 10 µM against *L. mexicana* intracellular amastigotes (**Table 3.1, Entry 4, 5, 6, and 7**). On the other hand, they reported SI values of less than 10 (**Table 3.1**), making them challenging to consider as appropriate hits. The in-gel fluorescence assays (**Figure 3.13**) carried out for further exploration of enzymatic targets displayed that pyrithione (**104**) and the novel derivatives (**116**-**119**) inhibit DUB16 enzyme in *L. mexicana* promastigotes (**Figure 3.16**). However, it was evident from the resistance development assays carried out that DUB16 is not the only target which causes the parasitic cell death (**Figure 3.17**). Therefore, further studies regarding target identification are essential. Furthermore, it is worth noting that these inhibitors show increased selectivity towards DUB16 compared to the other two DUBs highlighted in **Figure 3.15**. This suggests that pyrithione (**104**) and its novel derivatives (**116-119**) can be developed and optimised as chemical-biology probes which specifically target DUB16 in the future. Finally, pyrithione (**104**), ciclopirox (**105**) and piroctone olamine (**106**) are anti-fungal drugs already on the market, all the pharmacokinetic and safety profiles are available. Hence, they can be promptly evaluated in phase II clinical trials. However, it is crucial to achieve *in vivo* data against mouse models infected with *L. mexicana* for these candidate molecules (**104**, **105**, and **106**) in future.

In Chapter 4, the initial tetrafluoro-pyridine (TFP) compound library (**Table 4.1** and **4.3**) yielded no compounds with activity against *T. cruzi* parasites. In the second library (**Table 4.5**), synthesized by Prof. Graham Sandford's research group, one active compound, 4-(benzenesulfonyl)-2,3,5,6-tetrafluoropyridine (**198**) was identified to have activity against both *L. mexicana* and *T. cruzi* species [EC_{50} (*L. mexicana* promastigotes); 1.33 µM, EC_{50} (*L. mexicana* axenic amastigotes); 0.433 µM, IC_{50} (*T. cruzi* epimastigotes); 1.55 µM, EC_{50} (*T. cruzi* infected stage); 0.05 µM] (**Table 4.7**). The key objective of chapter was to identify novel fluorinated chemical entities with anti-parasitic activity and to determine how these can trigger programmed cell death (PCD) in the parasites. Programmed cell death in *T.*

cruzi epimastigotes was investigated (collaboration with Professor Ariel Sliber) by typical morphological, cellular, and biochemical PCD hallmarks as such as Ca^{2+}, mitochondrial inner membrane potential (ΔΨm) and ATP level imbalance. Results indicated that compound **198** triggers plasma membrane permeabilization (**Figure 4.21**) and alters the *T. cruzi* epimastigote's mitochondrial function by collapsing mitochondrial potential (**Figure 4.22**), decreasing the intracellular Ca^{2+} concentration (**Figure 4.23**) and disrupting the intracellular ATP levels (**Figure 4.24**). Furthermore, **198** also arrest the G_0 phase of cell cycle at higher concentrations (**Figure 4.25**). This suggest that **198** could be an interesting lead compound against *T. cruzi.* Performing the same PCD experiments for *L. mexicana* should be the next step in this section and then it is essential to carry out *in vivo* testing with infected mouse models.

In Chapter 5, a second-generation library derived from 4-phenylsulfonyl tetrafluoropyridine core (compound **198**) was synthesised to facilitate a structure activity relationship (SAR) analysis and identify more compounds with anti-parasitic activities. Proteomics tools were used to try and identify the target proteins of selected, active compounds. The library was screened against *L. mexicana* axenic amastigotes and then active compounds were subjected to cytotoxicity assays. 2-(3-ethynylphenoxy)-3,5,6-trifluoro-4-(phenylsulfonyl) pyridine (**230**) had the lowest EC_{50} value (0.155 µM) (**Table 5.2, Entry 2**) against axenic amastigotes. However, nearly half of the compounds were found to have high toxicity towards mammalian/host cells. For the proteomics analysis, compounds that already contained an alkyne functional group were selected. This allowed the click reaction (required as part of the workflow **Figure 5.9**) to be performed without having to modify the original compound to attach an alkyne group or an azide group to facilitate the click reaction. Initially the in-gel fluorescence (TAMRA-peg3-azide fluorescence tag) assays were performed with *L. mexicana* promastigotes, RAW 264.7 and MCF-7 cell lysates to confirm the covalent binding of the selected molecules with the bind. The scanned gel images obtained (**Figure 5.10** and **5.12**) clearly indicate that positive labelling between

the selected candidate molecules and proteins had occurred. Additionally, it was possible to confirm that fluorine atoms on the core ring structure are essential for the protein labelling seen by **246**. This was achieved by synthesising the non-fluorinated version of **246** and re-running the gels with this molecule, compound **230** (**Figure 5.11**). Furthermore, 4-phenylsulfonyl tetrafluoropyridine (**198**) was reacted (outside the cell) with reduced glutathione to evaluate how **198** is interacting with the proteins and it was confirmed by NMR (both ^{1}H and ^{19}F) and mass spectrometry data (**Figure 5.15**) that glutathione replaces the sulphonyl group within **198** (**Scheme 5.7**). Mass spectrometry-based proteomics analysis has discovered 19 potential target proteins of **230** in *L. mexicana* promastigotes. Then, a GO enrichment was run using the tritrypBD database and it has generated information regarding the molecular activities of *L. mexicana* proteins identified (**Figure 5.19**), biological programs achieved by the molecular activities (**Figure 5.17**), and the cellular components where these functions occur in the *L. mexicana* promastigotes (**Figure 5.18**). This whole proteomics assay needs to be repeated to get more statistically accurate results. Considering the results obtained to date, there are three future goals that should be addressed in relation to this series of compounds; 1) screening of the second-generation library against *T. cruzi*, 2) perform the proteomics experiments with *T. cruzi* epimastigotes lysates, 3) develop probes with the most active compounds in this library to continue with the proteomics assays.

In summary, compounds, **40** (**Table 2.2, Entry 1**), **64** (**Table 2.5, Entry 1**) from Chapter 2, compounds **104**, **105**, **106**, **116**, **117**, **118** and **119** (**Table 3.1**) from Chapter 3, compound **198** (**Table 4.7**) from Chapter 4 and compounds **224(b)**, **225**, **227**, **238** and **240** (**Table 5.1** and **5.2**) from Chapter 5 were identified as potential 'Lead' molecules for further development with regards to leishmaniasis. The work carried out on target identification in *L. mexicana* promastigotes discovered that compound **104**, **116**, **117**, **118** target the DUB 16 enzyme (amongst other target molecules). Furthermore, compound **198** (Chapter 4) shows anti-parasitic activity against both *L. mexicana* and *T. cruzi* species (**Table 4.7**).

198 can trigger programmed cell death (PCD) in *T. cruzi* epimastigotes by altering plasma membrane permeability (**Figure 4.21**), mitochondrial function (**Figure 4.22**), intracellular Ca^{2+} concentration (**Figure 4.23**) and intracellular ATP levels (**Figure 4.24**). Additionally, 19 potential target proteins of **230** (a compound in the 2nd generation library derived from **198**) in *L. mexicana* promastigotes were identified in Chapter 5. Given the aforementioned points the project has met its initial aims.

.

7 Experimental

General experimental

All starting materials and reagents were bought from commercial sources and used as received. All column chromatography was carried out using silica purchased from Sigma Aldrich using the solvent system noted in the experimental methods. ^{1}H NMR spectra were recorded at 400 and 700 MHz using Bruker Avance III and Varian VNMRS-700 spectrometers. ^{13}C NMR spectra were recorded at 101,151 and 176 MHz using Bruker Avance III, Varian VNMRS-600 and VNMRS-700 spectrometer. ^{19}F NMR spectra were recorded at 376 MHz using a Bruker Avance III spectrometer. All coupling constants are reported in Hertz (Hz). Chemical shifts are reported in ppm and are referenced to residual solvent peaks; $CDCl_3$ (^{1}H 7.24 ppm, ^{13}C 77ppm). Mass spectra were collected on a Waters TQD mass spectrometer and accurate mass spectra was collected using a Waters LCT Premier XE mass spectrometer.

7.1 Synthetic Procedures – Chapter 3

7.1.1 General procedure for the synthesis of *N*-oxy-Pyridinethione

Due to the light sensitivity of the products, reactions were carried out in the dark. Pyrithione (**104**) (1 equiv.) was dissolved in DCM (1 mL) and the temperature lowered to 0°C using an ice bath. Pyridine (1.31 equiv.) and the required acyl chloride (3.14 equiv.) were added to the reaction flask which was then stirred at 0°C for 2 hrs. The reaction was monitored after 2 hrs by TLC showing full consumption of pyrithione (**104**). The reaction mixture was washed with water (3 x 2 portions), dried with $MgSO_4$, filtered and the solvent was removed *in vacuo*. The product was purified by column chromatography (silica gel, hexane: EtOAc, 1:1).

7.1.2 Synthesis of 2-thioxopyridin-1(2H)-yl acetate (116)

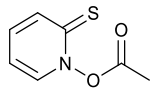

Synthesised according to the general procedure for the synthesis of *N*-oxy-Pyridinethiones from pyrithione (**104**) (0.13 g, 1.05 mmol), pyridine (0.10 mL, 1.38 mmol) and acetyl chloride (0.24 mL, 3.30 mmol) to give 2-thioxopyridin-1(2H)-yl acetate (**116**) (0.02 g, 13%) as a yellow powder.

^{1}H NMR (400 MHz, $CDCl_3$) δ 7.72 (ddd, *J* = 8.8, 1.8, 0.6, 1H, Ar*H*), 7.60 (ddd, *J* = 6.9, 1.6, 0.6, 1H, Ar*H*), 7.24 (ddd, *J* = 8.8, 6.9, 1.6, 1H, Ar*H*), 6.67 (td, *J* = 6.9, 1.8, 1H, Ar*H*), 2.48 (s, 3H, CH_3)

^{13}C NMR (101 MHz, $CDCl_3$) δC 175.9, 166.0, 137.6, 137.5, 133.6, 112.6, 18.5

HRMS ESI$^+$ Calculated for $[M+H]^+$ $C_7H_7NO_2S^+$ = 170.0215 Found 170.0280

The physical and spectroscopic data obtained matched that previously reported in the literature.[1]

7.1.3 Synthesis of 2-thioxopyridin-1(2H)-yl butyrate (117)

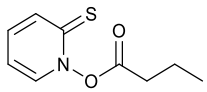

Synthesised according to the general procedure for the synthesis of *N*-oxy-Pyridinethiones from Pyrithione (**104**) (0.10 g, 0.78 mmol), pyridine (0.08 mL, 1.02 mmol) and butyryl chloride (0.25 mL, 2.44 mmol) to give 2-thioxopyridin-1(2H)-yl butyrate (**117**) (0.03 g, 22%) as a yellow powder.

^{1}H NMR (400 MHz, $CDCl_3$) δ 7.72 (ddd, *J* = 8.8, 1.8, 0.6, 1H, Ar*H*), 7.58 (ddd, *J* = 6.9, 1.6, 0.6, 1H, Ar*H*), 7.23 (ddd, *J* = 8.8, 6.9, 1.6, 1H, Ar*H*), 6.66 (td, *J* = 6.9, 1.8, 1H, Ar*H*), 2.73 (t, *J* = 7.4, 2H, CH_2), 1.88 (h, *J* = 7.4, 2H, CH_2), 1.10 (t, *J* = 7.4, 3H, CH_3)

^{13}C NMR (101 MHz, $CDCl_3$) δC 175.9, 170.0, 137.7, 137.5, 133.6, 112.6, 33.4, 18.0, 13.6

HRMS ESI$^+$ Calculated for $[M+H]^+$ $C_9H_{11}NO_2S^+$ = 198.0587 found 198.0592

The physical and spectroscopic data obtained matched that previously reported in the literature.[2]

7.1.4 Synthesis of 2-thioxopyridin-1(2H)-yl 2-phenylacetate (118)

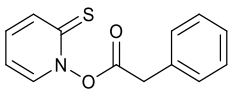

Synthesised according to the general procedure for the synthesis of *N*-oxy-Pyridinethiones from Pyrithione (**104**) (0.05 g, 0.47 mmol), pyridine (0.05 mL, 0.62 mmol) and phenylacetyl chloride (0.19 mL, 1.47 mmol) to give 2-thioxopyridin-1(2H)-yl 2-phenylacetate (**118**) (0.01 g, 13%) as a yellow powder.

^{1}H NMR (400 MHz, $CDCl_3$) δ 7.73 (dd, *J* = 8.8, 1.8 Hz, 1H, Ar*H*), 7.58 - 7.51 (m,1H, Ar*H*), 7.47 - 7.35 (m, 5H, Ar*H*), 7.23 (ddd, *J* = 8.8, 6.9, 1.6 Hz, 1H, Ar*H*), 6.64 (td, *J* = 6.9, 1.8 Hz, 1H, Ar*H*), 4.08 (s, 2H, CH_2)

^{13}C NMR (101 MHz, $CDCl_3$) δC 175.6, 167.3, 137.5, 137.4,133.6, 131.4, 129.6, 128.9, 127.9, 112.7, 38.5

HRMS ESI$^+$ Calculated for $[M+H]^+$ $C_{13}H_{11}NO_2S^+$ = 246.0256 Found 246.0278

The physical and spectroscopic data obtained matched that previously reported in the literature.[3]

7.1.5 Synthesis of 2-thioxopyridin-1(2H)-yl benzoate (119)

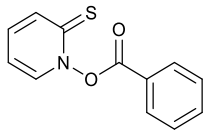

Synthesised according to the general procedure for the synthesis of *N*-oxy-Pyridinethiones from Pyrithione (**104**) (0.12 g, 1.49 mmol), pyridine (0.10 mL, 1.95 mmol) and benzoyl chloride (0.43 mL, 4.68 mmol) to give 2-thioxopyridin-1(2H)-yl benzoate (**119**) (0.12 g, 34%) as a green powder.

^{1}H NMR (400 MHz, $CDCl_3$) δ 8.30 - 8.26 (m, 2H, Ar*H*), 7.79 - 7.76 (m, 1H, Ar*H*), 7.75 - 7.69 (m, 2H, Ar*H*), 7.61 - 7.55 (m, 2H, Ar*H*), 7.31 - 7.25 (m,1H, Ar*H*), 6.72 (td, *J* = 6.9, 1.8, 1H, Ar*H*)

^{13}C NMR (101 MHz, $CDCl_3$) δC 175.9, 162.7, 138.0, 137.5, 135.0, 133.6, 130.8, 130.2, 129.0, 112.7

HRMS ESI$^+$ Calculated for $[M+H]^+$ $C_{12}H_9NO_2S^+$ = 232.0434 Found 232.0451

The physical and spectroscopic data obtained matched that previously reported in the literature.[4]

7.2 Synthetic procedures – Chapter 4

The synthetic procedures required to prepare the compounds provided by Dr Will D.G. Brittain (Cobb group) and Prof. Graham Sandford's research group (GS group) can be found in the references listed (**Table 7.1**, **7.2** and **7.3**). Were the compounds have been reported previously a literature reference is provided.

Comp. No.	Structure	ref	Comp. No.	Structure	ref
147	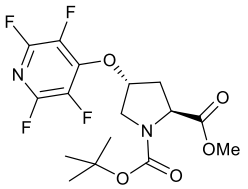	-	**167**	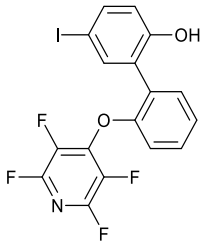	5
148	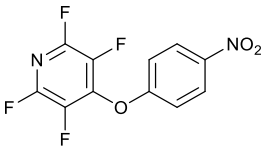	6	**168**	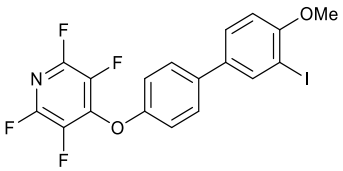	5
149	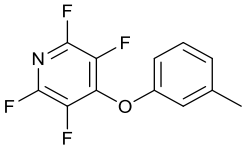	6	**169**	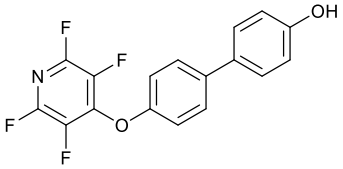	5
150	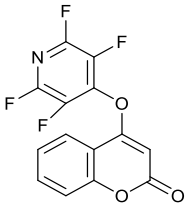	-	**170**	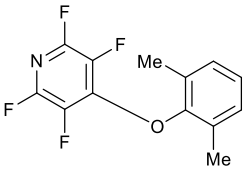	6
151	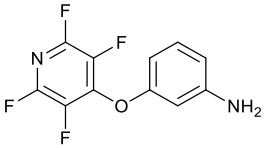	6	**171**	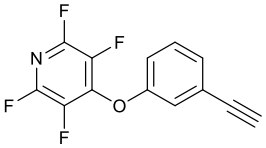	6
152	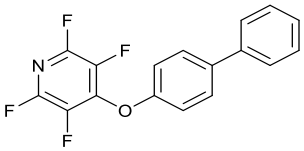	6	**172**	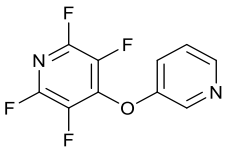	6
153	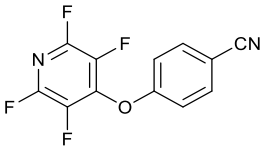	6	**173**	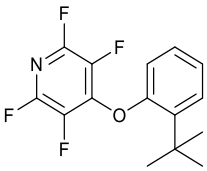	6
154	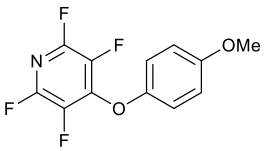	6	**174**	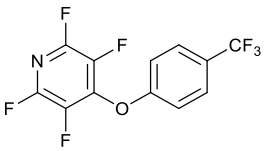	6
155	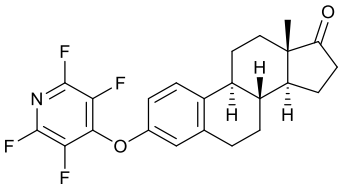	6	**`175**	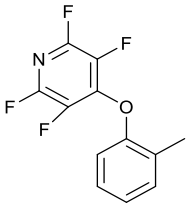	6

156	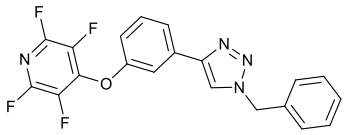	6	**176**	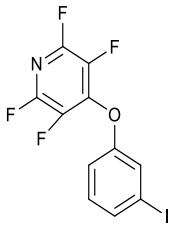	6
157	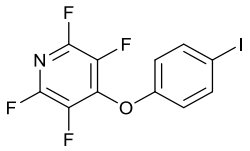	6	**177**	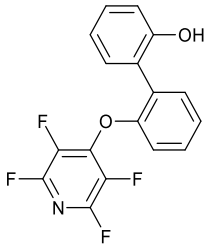	5
158	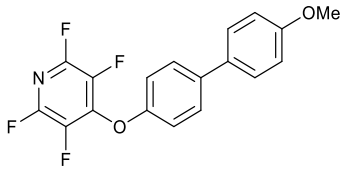	5	**178**	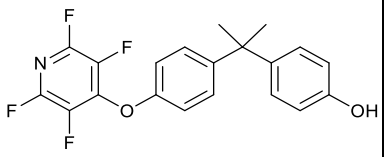	5
159	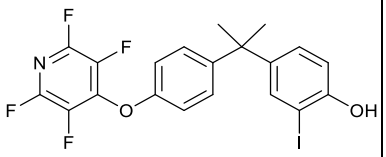	5	**179**	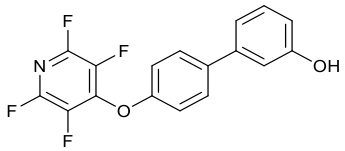	-
160	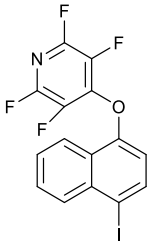	5	**180**	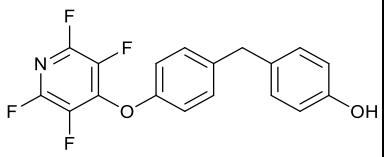	5
161	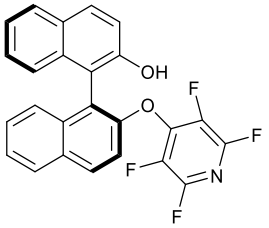	5	**181**	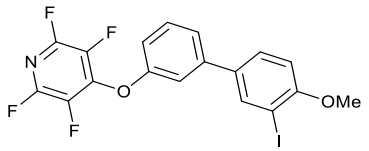	5
162	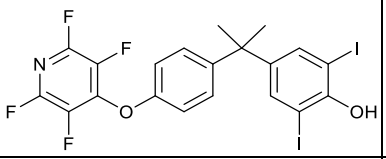	5	**182**	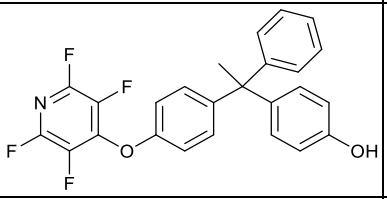	5
163	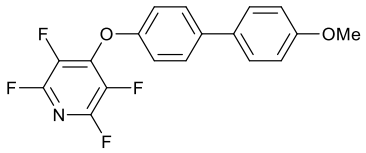	5	**183**	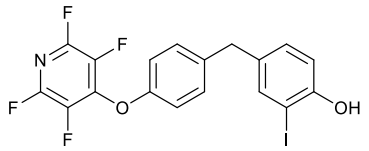	5

164	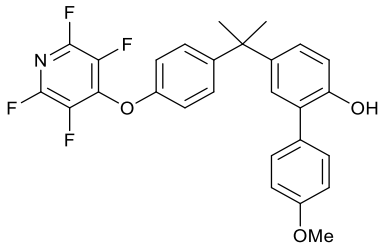	5	**184**	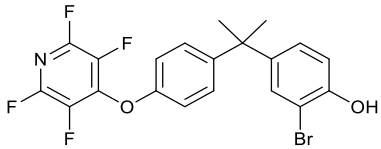	5
165	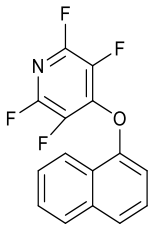	7	**185**	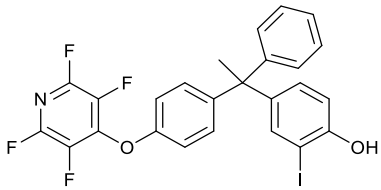	5
166	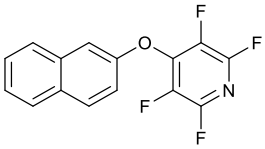	7			

Table 7.1 Chemical structures of Class One compounds in the first library in Chapter 4 and the references available for their synthetic procedure.

Comp. No.	Structure	ref
186	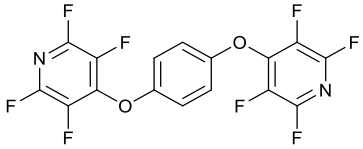	Commercially available
187	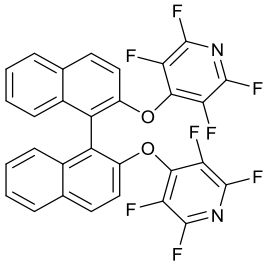	
188	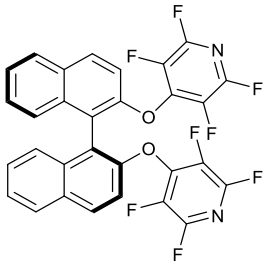	

189	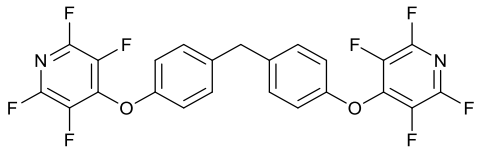	
190	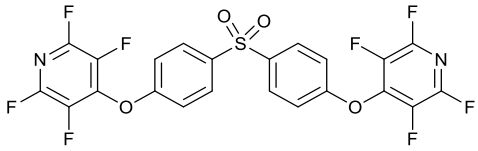	
191	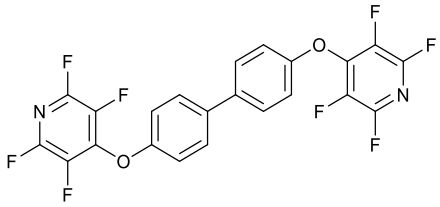	
192	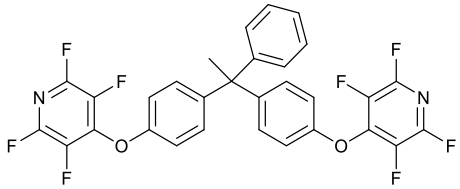	
193	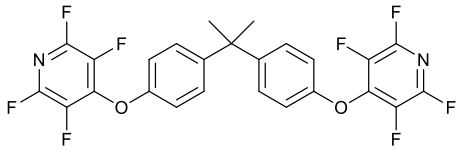	

Table 7.2 Chemical structures of Class Two compounds in the first library in Chapter 4 and the references available for their synthetic procedure.

Comp .no.	Structure	ref	Comp . no.	Structure	ref
194	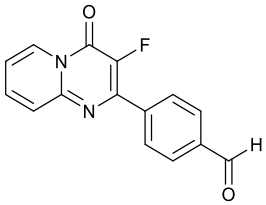	8	**205**	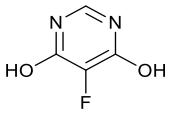	9
95	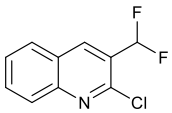	WO2010/30027, 2010, A1	**206**	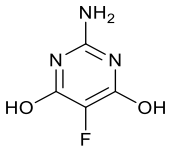	10
196	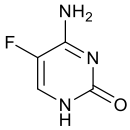	11	**207**	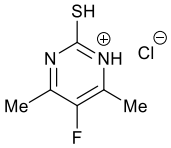	-
197	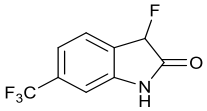	12	**208**	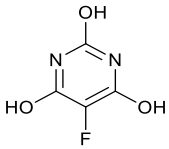	WO2011/50200, 2011, A1
198	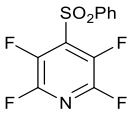	13	**209**	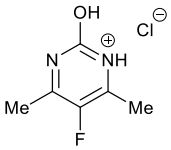	-
199	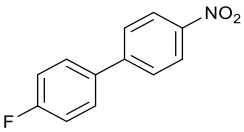	14	**210**	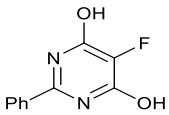	15
200	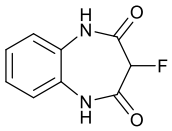	16	**211**	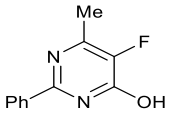	17

201	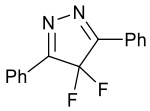	18	**212**	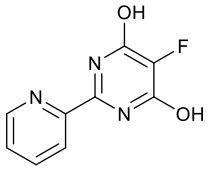	Commercially available
202	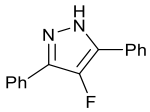	18	**213**	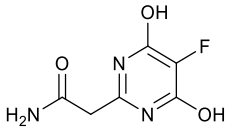	Commercially available
203	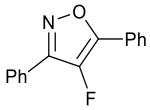	19	**214**	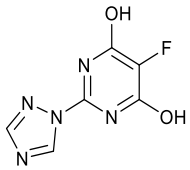	-
204	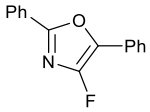	Commercially available	**215**	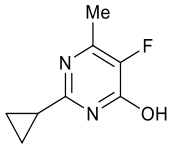	Commercially available
			216	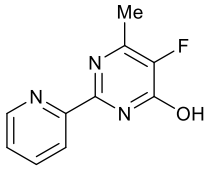	20

Table 7.3 Chemical structures of the second library in Chapter 4 and the references available for their synthetic procedure.

7.3 Synthetic procedures- Chapter 5

7.3.1 Synthesis of 2,3,5,6-tetrafluoropyridin-4-yl benzenesulfinate (198)

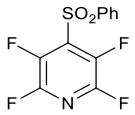

Pentafluoropyridine (**146**) (5.30 g, 31.6 mmol) was added to a solution of phenylsulfinic acid sodium salt (4.90 g, 30.4 mmol) in DMF (25 mL). The reaction mixture was heated to reflux for 20 hrs. At this time TLC analysis indicated complete conversion of starting material. The reaction mixture was cooled to room temperature and poured into water (250 mL) and the resulting precipitate was separated by filtration. Recrystallization from ethanol gave 4-benzenesulfonyl-2,3,5,6-tetrafluoropyridine (**198**) (2.70 g, 31%) as a beige powder.

^{1}H NMR (400 MHz, $CDCl_3$) δ 8.14 (d, *J* = 7.9, 2H, Ar*H*), 7.85 - 7.76 (m, 1H, Ar*H*), 7.68 (t, *J* = 7.9, 2H, Ar*H*)

^{13}C NMR (101 MHz, $CDCl_3$) δ 143.2 - 142.5 (m), 139.2, 137.7 - 136.9 (m), 135.7, 133.4 - 132.9 (m), 129.9, 128.5

^{19}F NMR (376 MHz, $CDCl_3$) δ -85.15 – -86.16 (2F, m), -136.58 – -137.37 (2F, m)

HRMS ESI$^+$ Calculated for $[M-H]^-$ $C_{11}H_5NO_2SF_4^-$ = 287.9942 Found 287.9935

The physical and spectroscopic data obtained matched that previously reported in the literature.[21]

7.3.2 General procedure for reactions of 4-Benzenesulfonyl-2,3,5,6-tetrafluoropyridine with amines.

The required amine (1.1 equiv.) and potassium carbonate (5 equiv.) were added to MeCN (150 mL). Compound **198** (1 equiv.) was added, and the resulting solution was heated to reflux for 24 hrs. Reaction progress was monitored after 24 hrs by TLC. The reaction was cooled to room temperature and the reaction mixture was filtered. The reaction mixture was concentrated *in vacuo* and the product was purified by column chromatography (silica gel, hexane: EtOAc 1:9).

7.3.3 Synthesis of 2,3,5-trifluoro-6-[(1-phenylethyl)amino]pyridin-4-yl benzenesulfinate (222)

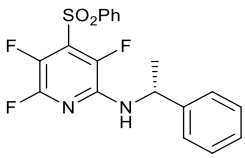

222a

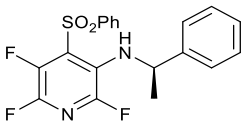

222b

Synthesised according to the general procedure for reactions of 4-benzenesulfonyl-2,3,5,6-tetrafluoropyridine with amines from phenylethylamine (0.22 g, 1.89 mmol), potassium carbonate (1.20 g, 8.60 mmol) and compound **198** (0.50 g, 1.72 mmol). The reaction mixture was purified by column chromatography (silica gel, hexane: EtOAc 1:9) to give 2,3,5-trifluoro-6-[(1-phenylethyl)amino]pyridin-4-yl benzenesulfinate **222a** (0.24 g, 36%) and 2,3,6-trifluoro-5-[(1-phenylethyl)amino]pyridin-4-yl benzenesulfinate **222b** (0.08 g, 13%).

222a - ^{1}H NMR (400 MHz, $CDCl_3$) δ 8.10 (dd, *J* = 8.0, 1.5, 2H, Ar*H*), 7.76 – 7.70 (m, 1H, Ar*H*), 7.64 – 7.59 (m, 2H, Ar*H*), 7.36 (d, *J* = 4.4, 4H, Ar*H*), 7.31 – 7.28 (m, 1H, Ar*H*), 5.08 (d, *J* = 4.2, 1H), 1.58 (d, *J* = 6.4, 3H, CH_3)

^{19}F NMR (376 MHz, $CDCl_3$) δ -88.48 – -91.00 (1F, m), -138.96 – -141.98 (1F, m), -155.16 – -158.93 (1F, m)

HRMS ESI$^+$ Calculated for $[M+H]^+$ $C_{19}H_{16}N_2O_2SF_3^+$ = 393.0885 Found 393.0876

222b- ^{1}H NMR (400 MHz, $CDCl_3$) δ 7.88 (dt, *J* = 8.6, 1.4, 2H, Ar*H*), 7.74 - 7.70 (m, 1H, Ar*H*), 7.60 - 7.55 (m, 2H, Ar*H*), 7.39 - 7.29 (m, 5H, Ar*H*), 5.03 (m, 1H, CH), 1.67 (dd, *J* = 6.8, 1.0, 3H, CH_3)

^{19}F NMR (376 MHz, $CDCl_3$) δ -69.78 – -72.66 (1F, m), -101.17 – -104.05 (1F, m), -137.08 – -139.97 (1F, m)

HRMS ESI$^+$ Calculated for $[M+H]^+$ $C_{19}H_{16}N_2O_2SF_3^+$ = 393.0885 Found 393.0893

7.3.4 Synthesis of 2,3,5-trifluoro-6-{[(4-fluorophenyl)methyl]amino}pyridin-4-yl benzenesulfinate (223)

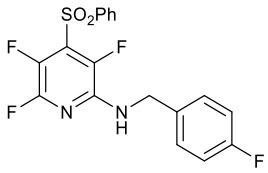

Synthesised according to the general procedure for reactions of 4-benzenesulfonyl-2,3,5,6-tetrafluoropyridine with amines from 4-fluorobenzylamine (0.24 g, 1.89 mmol), potassium carbonate (1.20 g, 8.60 mmol) and compound **198** (0.50 g, 1.72 mmol). The product was purified by column chromatography (silica gel, hexane: EtOAc 1:9) to give 2,3,5-trifluoro-6-[(1-phenylethyl)amino]pyridin-4-yl benzenesulfinate **223** (0.24 g, 35%).

223 - ^{1}H NMR (400 MHz, $CDCl_3$) δ 8.13 – 8.08 (m, 2H, Ar*H*), 7.77 – 7.72 (m, 1H, Ar*H*), 7.65 – 7.60 (m, 2H, Ar*H*), 7.34 – 7.29 (m, 2H, Ar*H*), 7.08 – 7.01 (m, 2H, Ar*H*), 5.13 (s, 1H), 4.54 (d, *J* = 5.6, 2H, CH_2)

^{19}F NMR (376 MHz, $CDCl_3$) δ -87.73 – -91.87 (1F, m), -112.09 – -117.11 (1F, m), -138.59 – -143.61 (1F, m), -154.28 – -159.30 (1F, m)

HRMS ESI$^+$ Calculated for $[M+H]^+$ $C_{18}H_{13}N_2O_2SF_4^+$ = 397.0634 Found 397.0630

7.3.5 Synthesis of 2-{[(4-chlorophenyl)methyl]amino}-3,5,6-trifluoropyridin-4-yl benzenesulfinate (224)

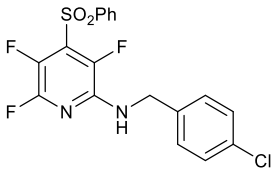

224a

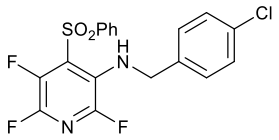

224b

Synthesised according to the general procedure for reactions of 4-benzenesulfonyl-2,3,5,6-tetrafluoropyridine with amines from 4-chlorobenzylamine (0.27 g, 1.89 mmol), potassium carbonate (1.20 g, 8.60 mmol) and compound **198** (0.50 g, 1.72 mmol). The reaction mixture was purified by column chromatography (silica gel, hexane: EtOAc 1:9) to give 2-{[(4-chlorophenyl)methyl]amino}-3,5,6-trifluoropyridin-4-yl benzenesulfinate **224a** (0.27 g, 38%), and 5-{[(4-chlorophenyl)methyl]amino}-2,3,6-trifluoropyridin-4-yl benzenesulfinate **224b** (0.37 g, 53%).

224a- ^{1}H NMR (400 MHz, $CDCl_3$) δ 8.10 (dd, *J* = 7.9, 1.5, 2H, Ar*H*), 7.78 - 7.71 (m, 1H, Ar*H*), 7.65 - 7.58 (m, 2H, Ar*H*), 7.36 – 7.21 (m, 4H, Ar*H*), 5.21 (s, 1H), 4.55 (d, *J* = 5.7, 2H, CH_2)

^{19}F NMR (376 MHz, $CDCl_3$) δ -87.73 – -90.24 (1F, m), -138.21 – -141.47 (1F, m), -155.54 – -158.05 (1F, m)

HRMS ESI$^+$ Calculated for $[M+H]^+$ $C_{18}H_{13}N_2O_2SClF_3^+$ = 413.0338 Found 413.0342

224b- ^{1}H NMR (400 MHz, $CDCl_3$) δ 7.83 (dd, *J* = 8.7, 1.4, 2H, Ar*H*), 7.76 - 7.70 (m, 1H, Ar*H*), 7.58 (dd, *J* = 8.4, 7.5, 2H, Ar*H*), 7.40 – 7.36 (m, 2H, Ar*H*), 7.31 (d, *J* = 8.4, 2H, Ar*H*), 5.32 (s, 1H), 4.60 (dd, *J* = 6.5, 3.4, 2H, CH_2)

^{19}F NMR (376 MHz, $CDCl_3$)δ -71.03 – -75.55 (1F, m), -100.41 – -104.93 (1F, m), -135.82 – -139.97 (1F, m)

HRMS ESI$^+$ Calculated for $[M+H]^+$ $C_{18}H_{13}N_2O_2SClF_3^+$ = 413.0338 Found 413.0331

7.3.6 Synthesis of 2,3,5-trifluoro-6-{[(3-iodophenyl)methyl]amino}pyridin-4-yl benzenesulfinate (225)

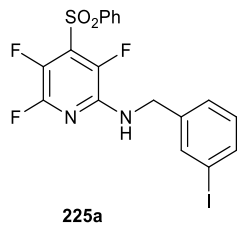

225a

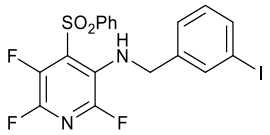

225b

Synthesised according to the general procedure for reactions of 4-benzenesulfonyl-2,3,5,6-tetrafluoropyridine with amines from 3-iodobenzylamine (0.44 g, 1.89 mmol), potassium carbonate (1.20 g, 8.60 mmol) and compound **198** (0.50 g, 1.72 mmol). The reaction mixture was purified by column chromatography (silica gel, hexane: EtOAc 1:9) to give 2,3,5-trifluoro-6-{[(3-iodophenyl)methyl]amino}pyridin-4-yl benzenesulfinate **225a** (0.24 g, 28%) and 2,3,6-trifluoro-5-{[(3-iodophenyl)methyl]amino}pyridin-4-yl benzenesulfinate **225b** (0.23 g, 27%).

225a- ^{1}H NMR (400 MHz, $CDCl_3$) δ 8.10 (dd, *J* = 7.7, 1.5, 2H, Ar*H*), 7.76 – 7.71 (m, 1H), Ar*H*), 7.69 – 7.60 (m, 4H, Ar*H*), 7.30 (ddd, *J* = 7.7, 1.8, 1.0, 1H, Ar*H*), 7.08 (t, *J* = 7.8, 1H, Ar*H*), 5.23 (d, *J* = 7.2, 1H), 4.52 (d, *J* = 5.8, 2H, C*H₂*)

^{19}F NMR (376 MHz, $CDCl_3$) δ -88.10 – -90.99 (1F, m), -138.60 – -141.99 (1F, m), -155.18 – -158.44 (1F, m)

HRMS ESI$^+$ Calculated for $[M+H]^+$ $C_{18}H_{13}N_2O_2SF_3I^+$ = 504.9695 Found 504.9717

225b- ^{1}H NMR (400 MHz, $CDCl_3$) δ 7.99 - 7.88 (m, 2H, Ar*H*), 7.77 - 7.71 (m, 2H, Ar*H*), 7.68 (dt, *J* = 7.9, 1.4, 1H, Ar*H*), 7.64 - 7.59 (m, 2H, Ar*H*), 7.35 (dt, *J* = 7.7, 1.3, 1H, Ar*H*), 7.13 (t, *J* = 7.8, 1H, Ar*H*), 4.58 (d, *J* = 3.6, 2H, CH_2)

^{19}F NMR (376 MHz, $CDCl_3$) δ -71.90 – -74.66 (1F, m), -100.41 – -105.31 (1F, m), -135.83 – -139.98 (1F, m)

HRMS ESI$^+$ Calculated for $[M+H]^+$ $C_{18}H_{13}N_2O_2SF_3I^+$ = 504.9695 Found 504.9690

7.3.7 Synthesis of 2,3,5-trifluoro-6-({[4-(trifluoromethyl) phenyl]methyl}amino) pyridin-4-yl benzenesulfinate (226)

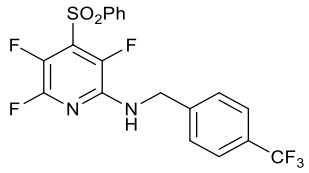

Synthesised according to the general procedure for reactions of 4-Benzenesulfonyl-2,3,5,6-tetrafluoropyridine with amines from 4-(trifluoromethyl)benzylamine (0.14 g, 1.89 mmol), potassium carbonate (1.20 g, 8.60 mmol) and Compound **198** (0.50 g, 1.72 mmol). The product was purified by column chromatography (silica gel, hexane: EtOAc 1:9) to give 2,3,5-trifluoro-6-({[4-(trifluoromethyl)phenyl]methyl}amino)pyridin-4-yl benzenesulfinate **226** (0.31 g, 40%) as yellow crystals.

^{1}H NMR (400 MHz, $CDCl_3$) δ 7.89 (dq, *J* = 7.2, 1.4, 2H, Ar*H*), 7.76 - 7.71 (m, 1H, Ar*H*), 7.67 (d, *J* = 8.0, 2H, Ar*H*) 7.67 - 7.55 (m, 2H, Ar*H*), 7.51 (d, *J* = 8.0, 2H, Ar*H*), 7.43 - 7.35 (m, 1H, Ar*H*), 4.71 (dd, *J* = 6.7, 3.5, 2H, CH_2)

^{19}F NMR (376 MHz, $CDCl_3$) δ -61.10 – -65.37 (3F, m), -72.03 – -75.92 (1F, m), -100.54 – -105.31 (1F, m), -136.21 – -140.86 (1F, m)

HRMS ESI$^+$ Calculated for $[M+H]^+$ $C_{19}H_{13}N_2O_2SF_6^+$ = 447.062 Found 447.0591

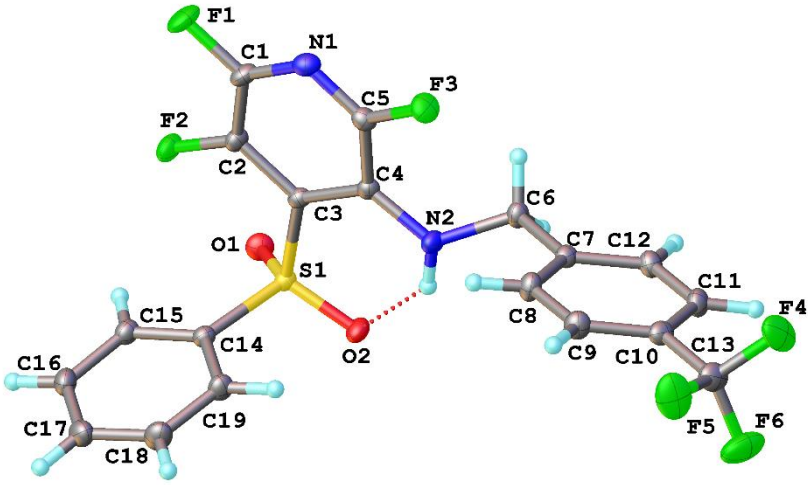

Figure 7.1: Crystal structure of 2,3,5-trifluoro-6-({[4-(trifluoromethyl)phenyl]methyl}amino)pyridin-4-yl benzenesulfinate **226**. Crystal structure reported with a 50% thermal ellipsoid probability.

7.3.8 Synthesis of 2,3,5-trifluoro-6-[(prop-2-yn-1-yl)amino]pyridin-4-yl benzenesulfinate (227)

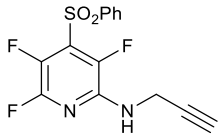

227a

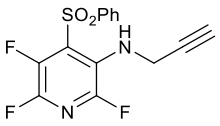

227b

Synthesised according to the general procedure for reactions of 4-benzenesulfonyl-2,3,5,6-tetrafluoropyridine with amines from propargylamine (0.10 g, 1.89 mmol), potassium carbonate (1.20 g, 8.60 mmol) and compound **198** (0.50 g, 1.72 mmol). The reaction mixture was purified by column chromatography (silica gel, hexane: EtOAc 1:9) to give 2,3,5-trifluoro-6-[(prop-2-yn-1-yl)amino]pyridin-4-yl benzenesulfinate **227a** (0.18

g, 33%) and 2,3,6-trifluoro-5-[(prop-2-yn-1-yl)amino]pyridin-4-yl benzenesulfinate **227b** (0.17 g, 30%).

227a- ^{1}H NMR (400 MHz, $CDCl_3$) δ 8.13 - 8.09 (m, 2H, Ar*H*), 7.77 - 7.72 (m, 1H, Ar*H*), 7.65 - 7.60 (m, 2H, Ar*H*), 5.0 (s, 1H), 4.19 (dd, *J* = 5.6, 2.5, 2H, CH_2), 2.20 (s, 1H)

^{19}F NMR (376 MHz, $CDCl_3$) δ -87.72 – -91.87 (1F, m), -138.22 – -141.99 (1F, m), -154.30 – -157.31 (1F, m)

HRMS ESI$^+$ Calculated for $[M+H]^+$ $C_{14}H_{10}N_2O_2SF_3^+$ = 327.0415 Found 327.0405

227b- ^{1}H NMR (400 MHz, $CDCl_3$) δ 8.08 (dt, *J* = 8.6, 1.4, 2H, Ar*H*), 7.78 - 7.70 (m, 1H, Ar*H*), 7.65 - 7.59 (m, 2H, Ar*H*), 7.16 (s, 1H), 4.24 (d, *J* = 3.6, 2H, CH_2), 2.39 -2.20 (m, 1H)

^{19}F NMR (376 MHz, $CDCl_3$) δ -71.90 – -74.66 (1F, m), -98.78 – -102.05 (1F, m), -135.83 – -140.35 (1F, m)

HRMS ESI$^+$ Calculated for $[M+H]^+$ $C_{14}H_{10}N_2O_2SF_3^+$ = 327.0415 Found 327.0415

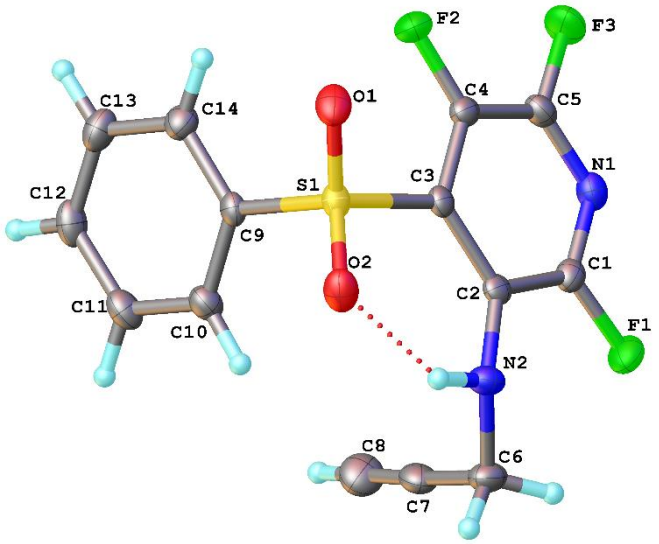

Figure 7.2: Crystal structure of 2,3,6-trifluoro-5-[(prop-2-yn-1-yl)amino]pyridin-4-yl benzenesulfinate **227(b)**. Crystal structure reported with a 50% thermal ellipsoid probability.

7.3.9 Synthesis of 2-(butylamino)-3,5,6-trifluoropyridin-4-yl benzenesulfinate (228)

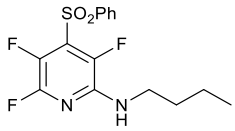

228a

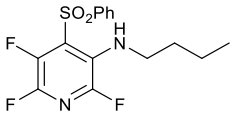

228b

Synthesised according to the general procedure for reactions of 4-benzenesulfonyl-2,3,5,6-tetrafluoropyridine with amines from butylamine (0.14 g, 1.89 mmol), potassium carbonate (1.20 g, 8.60 mmol) and compound **198** (0.50 g, 1.72 mmol). The reaction mixture was purified by column chromatography (silica gel, hexane: EtOAc 1:9) to give 2-(butylamino)-3,5,6-trifluoropyridin-4-yl benzenesulfinate **228a** (0.33 g, 55%) and 5-(butylamino)-2,3,6-trifluoropyridin-4-yl benzenesulfinate **228b** (0.15 g, 25%).

228a- ^{1}H NMR (400 MHz, $CDCl_3$) δ 8.12 - 8.00 (m, 2H, Ar*H*), 7.72 (td, *J* = 7.2, 1.4, 1H, Ar*H*), 7.61 (dd, *J* = 8.6, 7.2, 2H, Ar*H*), 4.88 (s, 1H), 3.37 (td, *J* = 7.3, 5.6, 2H, CH_2), 1.58 (tt, *J* = 7.9, 6.2, 2H, CH_2), 1.42 – 1.31 (m, 2H, CH_2), 0.94 (t, *J* = 7.3, 3H, CH_3)

^{19}F NMR (376 MHz, $CDCl_3$) δ -88.48 – -91.87 (1F, m), -138.60 – -143.62 (1F, m), -156.81 – -163.09 (1F, m)

HRMS ESI$^+$ Calculated for $[M+H]^+$ $C_{14}H_{16}N_2O_2SF_3^+$ = 345.0863 Found 345.0885

228b- ^{1}H NMR (400 MHz, $CDCl_3$) δ 8.02 (dt, *J* = 7.2, 1.4, 2H, Ar*H*), 7.78 - 7.68 (m, 1H, Ar*H*), 7.65 - 7.57 (m, 2H, Ar*H*), 6.91 (t, *J* = 5.9, 1H), 3.48 (tt, *J* = 7.1, 5.0, 2H, CH_2), 1.66 (dq, *J* = 14.1, 7.1, 2H, CH_2), 1.53 - 1.43 (m, 2H, CH_2), 1.00 (t, *J* = 7.1, 3H, CH_3)

^{19}F NMR (376 MHz, $CDCl_3$) δ -72.66 – -76.30 (1F, m), -103.68 – -106.57 (1F, m), -136.71 – -140.73 (1F, m)

HRMS ESI$^+$ Calculated for $[M+H]^+$ $C_{16}H_{10}N_2O_2SF_3^+$ = 345.0885 Found 345.0885

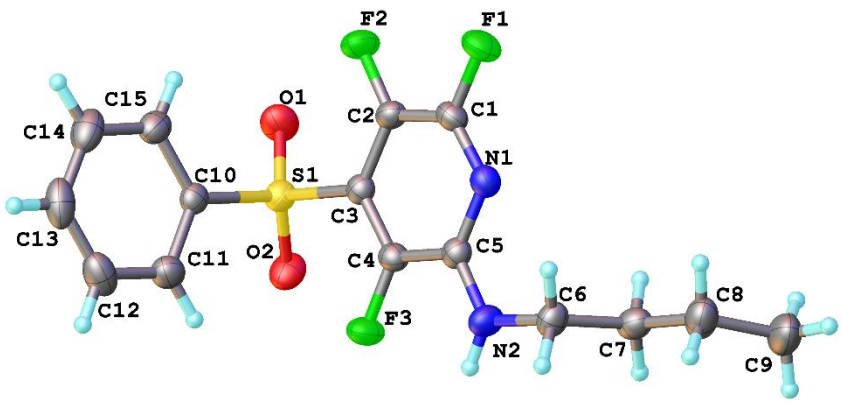

Figure 7.3: Crystal structure of 2-(butylamino)-3,5,6-trifluoropyridin-4-yl benzenesulfinate **228(b)**. Crystal structure reported with a 50% thermal ellipsoid probability.

7.3.10 General procedure for reactions of 4-Benzenesulfonyl-2,3,5,6-tetrafluoropyridine with phenols.

The required phenol (1.1 equiv.) and potassium carbonate (5 equiv.) were added to MeCN (150 mL). Compound **198** (1 equiv.) was added, and the resulting solution was heated to reflux for 24 hrs. Reaction progress was monitored after 24 hrs by TLC. The reaction was cooled to room temperature and the reaction mixture filtered. The reaction mixture was concentrated *in vacuo* and the product was purified by column chromatography (silica gel, hexane: EtOAc 1:9).

7.3.11 Synthesis of 2,3,5-trifluoro-6-(4-methoxyphenoxy)-4-(phenylsulfonyl) pyridine (229)

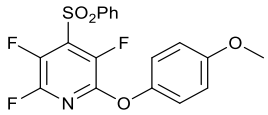

Synthesised according to the general procedure for reactions of 4-benzenesulfonyl-2,3,5,6-tetrafluoropyridine with phenols from 4-methoxyphenol (0.24 g, 1.89 mmol), potassium carbonate (1.20 g, 8.60 mmol) and compound **198** (0.50 g, 1.72 mmol). The product was purified by column chromatography (silica gel, hexane: EtOAc 1:9) to give 2,3,5-trifluoro-6-(4-methoxyphenoxy)-4-(phenylsulfonyl) pyridine **229** (0.23 g, 34%) as yellow crystals.

^{1}H NMR (400 MHz, $CDCl_3$) δ 8.21 - 8.13 (m, 2H, Ar*H*), 7.83 - 7.74 (m, 1H, Ar*H*), 7.72 - 7.63 (m, 2H, Ar*H*), 7.09 – 7.01 (m, 2H, Ar*H*), 6.98 – 6.89 (m, 2H, Ar*H*), 3.83 (s, 3H)

^{19}F NMR (376 MHz, $CDCl_3$) δ -87.24 – -87.56 (1F, m), -135.12 – -135.41 (1F, m), -144.94 – -145.20 (1F, m)

HRMS ESI$^+$ Calculated for $[M+H]^+$ $C_{18}H_{12}NO_4SF_3^+$ = 396.0501 Found 396.0517

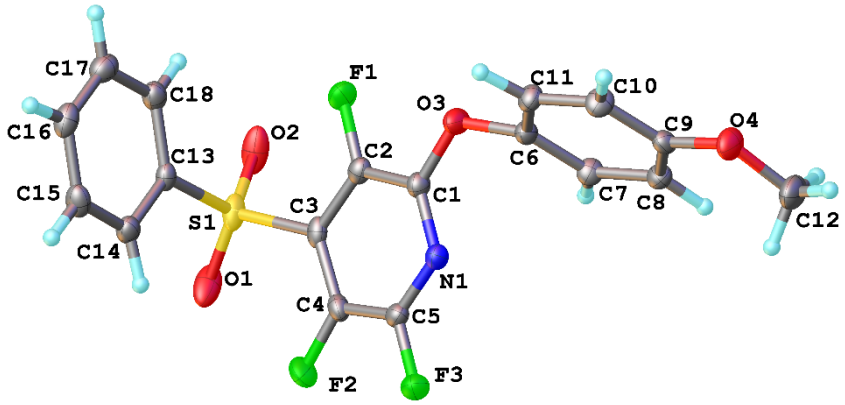

Figure 7.4: Crystal structure of 2,3,5-trifluoro-6-(4-methoxyphenoxy)-4-(phenylsulfonyl) pyridine **229**. Crystal structure reported with a 50% thermal ellipsoid probability.

7.3.12 Synthesis of 2-(3-ethynylphenoxy)-3,5,6-trifluoro-4-(phenylsulfonyl) pyridine (230)

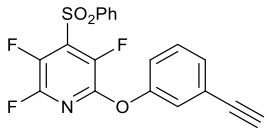

Synthesised according to the general procedure for reactions of 4-benzenesulfonyl-2,3,5,6-tetrafluoropyridine with phenols from 3-hydroxyphenylacetalyne (0.22 g, 1.89 mmol), potassium carbonate (1.20 g, 8.60 mmol) and compound **198** (0.50 g, 1.72 mmol). The product was purified by column chromatography (silica gel, hexane: EtOAc 1:9) to give 2-(3-ethynylphenoxy)-3,5,6-trifluoro-4-(phenylsulfonyl) pyridine **230** (0.28 g, 42%) as light brown crystals.

^{1}H NMR (400 MHz, $CDCl_3$) δ 8.20 - 8.14 (m, 2H, Ar*H*), 7.82 - 7.75 (m, 1H, Ar*H*), 7.71 - 7.63 (m, 2H, Ar*H*), 7.44 – 7.34 (m, 2H, Ar*H*), 7.26 – 7.23 (m, 1H, Ar*H*), 7.15 – 7.10 (m, 1H, Ar*H*), 3.13 (s, 1H)

^{19}F NMR (376 MHz, $CDCl_3$) δ -86.84 – -87.17 (1F, m), -134.52 – -134.81 (1F, m), -143.26 – -143.53 (1F, m)

HRMS ESI$^+$ Calculated for $[M+H]^+$ $C_{18}H_{12}NO_3SF_3^+$ = 390.0402 Found 390.0412

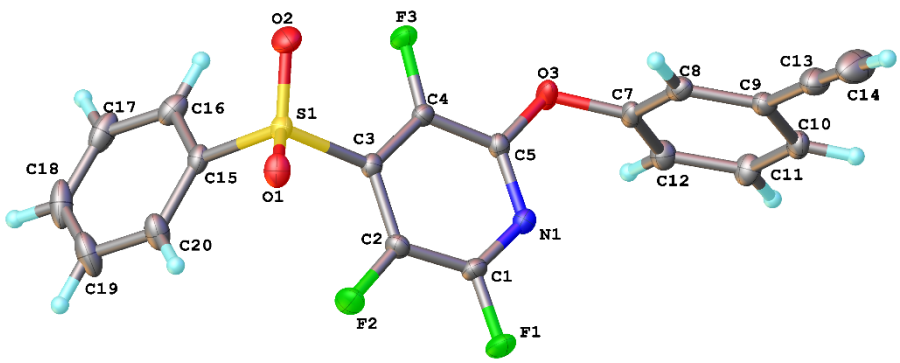

Figure 7.5: Crystal structure of 2-(3-ethynylphenoxy)-3,5,6-trifluoro-4-(phenylsulfonyl) **230**. Crystal structure reported with a 50% thermal ellipsoid probability.

7.3.13 Synthesis of 2-(2,6-dimethylphenoxy)-3,5,6-trifluoro-4-(phenylsulfonyl) pyridine (231)

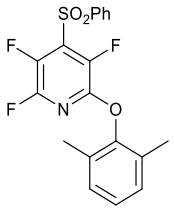

Synthesised according to the general procedure for reactions of 4-benzenesulfonyl-2,3,5,6-tetrafluoropyridine with phenols from 2,6-dimethylphenol (0.23 g, 1.89 mmol), potassium carbonate (1.20 g, 8.60 mmol) and compound **198** (0.50 g, 1.72 mmol). The product was purified by column chromatography (silica gel, hexane: EtOAc 1:9) to give 2-(2,6-dimethylphenoxy)-3,5,6-trifluoro-4-(phenylsulfonyl) pyridine **231** (0.53 g, 78%) as a light-yellow coloured powder.

^{1}H NMR (400 MHz, $CDCl_3$) δ 8.25 - 8.16 (m, 2H, Ar*H*), 7.86 - 7.74 (m, 1H, Ar*H*), 7.73 - 7.64 (m, 2H, Ar*H*), 7.16 – 7.07 (m, 3H, Ar*H*), 2.11 (d, *J* = 0.7, 6H)

^{19}F NMR (376 MHz, $CDCl_3$) δ -87.40 – -88.02 (1F, m), -135.66 – -136.29 (1F, m), -145.03 – -145.66 (1F, m)

HRMS ESI$^+$ Calculated for $[M+H]^+$ $C_{19}H_{14}NO_3SF_3^+$ = 390.0719 Found 390.0725

7.3.14 Synthesis of 2-([1,1'-biphenyl]-4-yloxy)-3,5,6-trifluoro-4-(phenylsulfonyl) pyridine (232)

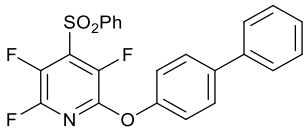

Synthesised according to the general procedure for reactions of 4-benzenesulfonyl-2,3,5,6-tetrafluoropyridine with phenols from 4-phenylphenol (0.32 g, 1.89 mmol), potassium carbonate (1.20 g, 8.60 mmol) and compound **198** (0.50 g, 1.72 mmol). The product was purified by column chromatography (silica gel, hexane: EtOAc 1:9) to give 2-([1,1'-biphenyl]-4-yloxy)-3,5,6-trifluoro-4-(phenylsulfonyl) pyridine **232** (0.40 g, 53%) as a yellow powder.

^{1}H NMR (400 MHz, $CDCl_3$) δ 8.21 - 8.17 (m, 2H, Ar*H*), 7.82 - 7.77 (m, 1H, Ar*H*), 7.72 - 7.67 (m, 2H, Ar*H*), 7.66 – 7.62 (m, 2H, Ar*H*), 7.62 – 7.58 (m, 2H, Ar*H*), 7.50 – 7.45 (m, 2H, Ar*H*), 7.41 – 7.36 (m, 1H, Ar*H*), 7.22 – 7.18 (m, 2H, Ar*H*)

^{19}F NMR (376 MHz, $CDCl_3$) δ -86.11 – -88.22 (1F, m), -133.68 – -136.10 (1F, m), -143.08 – -143.12 (1F, m)

HRMS ESI$^+$ Calculated for $[M+H]^+$ $C_{23}H_{14}NO_3SF_3^+$ = 442.0704 Found 442.0725

7.3.15 Synthesis of 2,3,5-trifluoro-4-(phenylsulfonyl)-6-(pyridin-3-yloxy) pyridine (233)

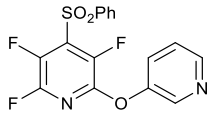

Synthesised according to the general procedure for reactions of 4-benzenesulfonyl-2,3,5,6-tetrafluoropyridine with phenols from 3-hydroxypyridine (0.18 g, 1.89 mmol), potassium carbonate (1.20 g, 8.60 mmol) and compound **198** (0.50 g, 1.72 mmol). The product was purified by column chromatography (silica gel, hexane: EtOAc 1:9) to give 2 ,3,5-trifluoro-4-(phenylsulfonyl)-6-(pyridin-3-yloxy) pyridine **233** (0.31 g, 49%) as brown crystals.

^{1}H NMR (400 MHz, $CDCl_3$) δ 8.55 (dd, *J* = 4.7, 2H, Ar*H*), 8.50 (d, *J* = 2.8, 1H, Ar*H*), 8.16 (dd, *J* = 7.8, 2H, Ar*H*), 7.83 – 7.74 (m, 1H, Ar*H*), 7.67 (dd, *J* = 8.5, 2H, Ar*H*), 7.60 – 7.49 (m, 1H, Ar*H*), 7.44 – 7.36 (m, 1H, Ar*H*)

^{19}F NMR (376 MHz, $CDCl_3$) δ -86.05 – -88.33 (1F, m), -133.07 – -135.84 (1F, m), -141.94 – -143.91 (1F, m)

HRMS ESI$^+$ Calculated for $[M+H]^+$ $C_{16}H_9N_2O_3SF_3^+$ = 367.0365 Found 367.0364

7.3.16 Synthesis of 2-(2-(tert-butyl) phenoxy)-3,5,6-trifluoro-4-(phenylsulfonyl) pyridine (234)

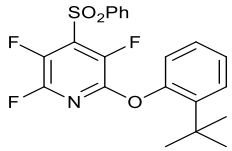

Synthesised according to the general procedure for reactions of 4-benzenesulfonyl-2,3,5,6-tetrafluoropyridine with phenols from 2-tert-butylphenol (0.28 g, 1.89 mmol), potassium carbonate (1.20 g, 8.60 mmol) and compound **198** (0.50 g, 1.72 mmol). The product was purified by column chromatography (silica gel, hexane: EtOAc 1:9) to give 2-(2-(tert-butyl) phenoxy)-3,5,6-trifluoro-4-(phenylsulfonyl) pyridine **234** (0.34 g, 47%) as a yellow oil.

^{1}H NMR (400 MHz, $CDCl_3$) δ 8.22 - 8.15 (m, 2H, Ar*H*), 7.84 - 7.76 (m, 1H, Ar*H*), 7.73 - 7.65 (m, 2H, Ar*H*), 7.48 – 7.43 (m, 1H, Ar*H*), 7.25 - 7.16 (m, 2H, Ar*H*), 6.95 – 6.87 (m, 1H, Ar*H*), 1.36 (s, 9H)

^{19}F NMR (376 MHz, $CDCl_3$) δ -86.37 – -87.22 (1F, m), -135.34 – -135.97 (1F, m), -143.81 – -144.44 (1F, m)

HRMS ESI$^+$ Calculated for $[M+H]^+$ $C_{21}H_{18}NO_3SF_3^+$ = 421.1057 Found 421.1038

7.3.17 Synthesis of 3-((3,5,6-trifluoro-4-(phenylsulfonyl)pyridin-2-yl)oxy)aniline (235)

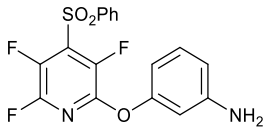

Synthesised according to the general procedure for reactions of 4-benzenesulfonyl-2,3,5,6-tetrafluoropyridine with phenols from 3-aminophenol (0.21 g, 1.89 mmol), potassium carbonate (1.20 g, 8.60 mmol) and compound **198** (0.50 g, 1.72 mmol). The product was purified by column chromatography (silica gel, hexane: EtOAc 1:9) to give 3-((3,5,6-trifluoro-4-(phenylsulfonyl)pyridin-2-yl)oxy)aniline **235** (0.26 g, 40%) as yellow crystals.

^{1}H NMR (400 MHz, $CDCl_3$) δ 8.19 - 8.14 (m, 2H, Ar*H*), 7.81 - 7.75 (m, 1H, Ar*H*), 7.70 - 7.63 (m, 2H, Ar*H*), 7.20 – 7.13 (m, 1H, Ar*H*), 6.60 - 6.54 (m, 1H, Ar*H*), 6.49 – 6.44 (m, 1H, Ar*H*), 6.43 – 6.40 (m, 1H, Ar*H*), 3.78 (s, 2H)

^{19}F NMR (376 MHz, $CDCl_3$) δ -86.74– -87.59 (1F, m), -134.41 – -135.09 (1F, m), -144.07 – -144.83 (1F, m)

HRMS ESI$^+$ Calculated for $[M+H]^+$ $C_{17}H_{11}N_2O_3SF_3^+$ = 380.0515 Found 380.0521

7.3.18 Synthesis of 2,3,5-trifluoro-6-(naphthalen-2-yloxy)-4-(phenylsulfonyl) pyridine (236)

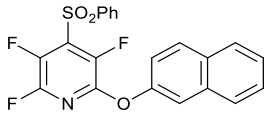

Synthesised according to the general procedure for reactions of 4-benzenesulfonyl-2,3,5,6-tetrafluoropyridine with phenols from 2-napthanol (0.27 g, 1.89 mmol), potassium carbonate (1.20 g, 8.60 mmol) and compound **198** (0.50 g, 1.72 mmol). The product was purified by column chromatography (silica gel, hexane: EtOAc 1:9) to give 2,3,5-trifluoro-6-(naphthalen-2-yloxy)-4-(phenylsulfonyl) pyridine **236** (0.33 g, 46%) as a beige powder.

^{1}H NMR (400 MHz, $CDCl_3$) δ 8.22 - 8.16 (m, 2H, Ar*H*), 7.93 - 7.86 (m, 2H, Ar*H*), 7.83 - 7.77 (m, 2H, Ar*H*), 7.71 – 7.64 (m, 2H, Ar*H*), 7.58 (d, *J* = 2.4, 1H, Ar*H*), 7.55 – 7.50 (m, 2H, Ar*H*), 7.29 – 7.23 (m, 1H, Ar*H*)

^{19}F NMR (376 MHz, $CDCl_3$) δ -86.74 – -87.58 (1F, m), -134.45 – -135.29 (1F, m), -143.73 – -144.41 (1F, m)

HRMS ESI$^+$ Calculated for $[M+H]^+$ $C_{21}H_{12}NO_3SF_3^+$ = 416.0562 Found 416.0568

7.3.19 Synthesis of 2,3,5-trifluoro-6-(naphthalen-1-yloxy)-4-(phenylsulfonyl) pyridine (237)

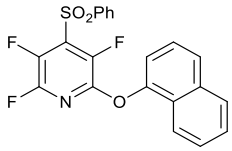

Synthesised according to the general procedure for reactions of 4-benzenesulfonyl-2,3,5,6-tetrafluoropyridine with phenols from 1-napthanol (0.27 g, 1.89 mmol), potassium carbonate (1.20 g, 8.60 mmol) and compound **198** (0.50 g, 1.72 mmol). The product was purified by column chromatography (silica gel, hexane: EtOAc 1:9) to give 2,3,5-trifluoro-6-(naphthalen-1-yloxy)-4-(phenylsulfonyl) pyridine **237** (0.24 g, 34%) as yellow crystals.

^{1}H NMR (400 MHz, $CDCl_3$) δ 8.24 - 8.19 (m, 2H, Ar*H*), 7.94 - 7.88 (m, 2H, Ar*H*), 7.82 - 7.77 (m, 2H, Ar*H*), 7.72 – 7.66 (m, 2H, Ar*H*), 7.58 - 7.46 (m, 3H, Ar*H*), 7.29 – 7.22 (m, 2H, Ar*H*)

^{19}F NMR (376 MHz, $CDCl_3$) δ -85.72 – -88.98 (1F, m), -133.45 – -136.71 (1F, m), -141.99 – -146.13 (1F, m)

HRMS ESI$^+$ Calculated for $[M+H]^+$ $C_{21}H_{12}NO_3SF_3^+$ = 416.0550 Found 416.0568

7.3.20 Synthesis of 4-((3,5,6-trifluoro-4-(phenylsulfonyl)pyridin-2-yl)oxy)aniline (238)

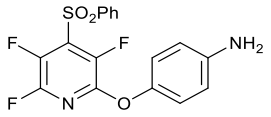

Synthesised according to the general procedure for reactions of 4-benzenesulfonyl-2,3,5,6-tetrafluoropyridine with phenols from 4-aminophenol (0.21 g, 1.89 mmol), potassium carbonate (1.20 g, 8.60 mmol) and compound **198** (0.50 g, 1.72 mmol). The product was purified by column chromatography (silica gel, hexane: EtOAc 1:9) to give 4-((3,5,6-trifluoro-4-(phenylsulfonyl) pyridin-2-yl) oxy) aniline **238** (0.35 g, 54%) as a yellow powder.

^{1}H NMR (400 MHz, $CDCl_3$) δ 8.22 - 8.10 (m, 2H, Ar*H*), 7.83 - 7.72 (m, 1H, Ar*H*), 7.69 - 7.58 (m, 2H, Ar*H*), 6.95 – 6.85 (m, 2H, Ar*H*), 6.75 - 6.63 (m, 2H, Ar*H*), 3.71 (s, 2H)

^{19}F NMR (376 MHz, $CDCl_3$) δ -87.37– -87.73 (1F, m), -135.23 – -135.55 (1F, m), -145.44 – -145.74 (1F, m)

HRMS ESI$^+$ Calculated for $[M+H]^+$ $C_{17}H_{11}N_2O_3SF_3^+$ = 381.0521 Found 381.0511

7.3.21 Synthesis of 2,3,5-trifluoro-6-((4'-methoxy-[1,1'-biphenyl]-4-yl)oxy)-4-(phenylsulfonyl) pyridine (239)

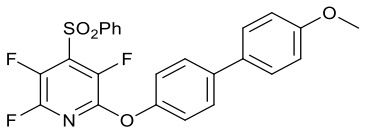

Synthesised according to the general procedure for reactions of 4-benzenesulfonyl-2,3,5,6-tetrafluoropyridine with phenols from 4hydroxy-4'-methoxybiphenyl (0.38 g, 1.89 mmol), potassium carbonate (1.20 g, 8.60 mmol) and compound **198** (0.50 g, 1.72 mmol) The product was purified by column chromatography (silica gel, hexane: EtOAc 1:9) to give 2,3,5-trifluoro-6-((4'-methoxy-[1,1'-biphenyl]-4-yl)oxy)-4-(phenylsulfonyl) pyridine **239** (0.054 g, 7%) as a yellow powder.

^{1}H NMR (400 MHz, $CDCl_3$) δ 8.21 - 8.16 (m, 2H, Ar*H*), 7.82 - 7.76 (m, 1H, Ar*H*), 7.71 - 7.64 (m, 2H, Ar*H*), 7.61 – 7.56 (m, 2H, Ar*H*), 7.54 – 7.50 (m, 2H, Ar*H*), 7.19 – 7.15 (m, 2H, Ar*H*), 7.02 – 6.98 (m, 2H, Ar*H*), 3.88 (s, 3H)

^{19}F NMR (376 MHz, $CDCl_3$) δ -87.06– -87.38 (1F, m), -134.63 – -134.91 (1F, m), -144.13 – -144.39 (1F, m)

HRMS ESI$^+$ Calculated for $[M+H]^+$ $C_{24}H_{16}NO_4SF_3^+$ = 472.0824 Found 472.0830

7.3.22 Synthesis of 2,3,5-trifluoro-4-(phenylsulfonyl)-6-(m-tolyloxy) pyridine (240)

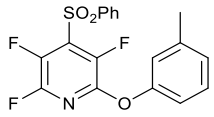

Synthesised according to the general procedure for reactions of 4-benzenesulfonyl-2,3,5,6-tetrafluoropyridine with phenols from m-cresol (0.20 g, 1.89 mmol), potassium carbonate (1.20 g, 8.60 mmol) and compound **198** (0.50 g, 1.72 mmol). The product was purified by column chromatography (silica gel, hexane: EtOAc 1:9) to give 2,3,5-trifluoro-4-(phenylsulfonyl)-6-(m-tolyloxy)pyridine **240** (0.37 g, 57%) as a yellow powder.

^{1}H NMR (400 MHz, $CDCl_3$) δ 8.21 - 8.09 (m, 2H, Ar*H*), 7.81 - 7.72 (m, 1H, Ar*H*), 7.71 - 7.61 (m, 2H, Ar*H*), 7.34 - 7.24 (m, 1H, Ar*H*), 7.12 – 7.05 (m, 1H, Ar*H*), 6.93 - 6.86 (m,2H, Ar*H*), 2.38 (s, 3H)

^{19}F NMR (376 MHz, $CDCl_3$) δ -86.87– -87.63 (1F, m), -134.51 – -135.92 (1F, m), -144.10 – -144.80 (1F, m)

HRMS ESI$^+$ Calculated for $[M+H]^+$ $C_{18}H_{12}NO_3SF_3^+$ = 380.0568 Found 380.0554

7.2.22 Synthesis of 4-(benzenesulfonyl)-2-fluoropyridine (244)

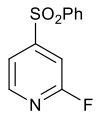

2,4-Difluoropyridine (**242**) (1.80 g, 15.70 mmol) was added to a solution of phenylsulfinic acid sodium salt (2.50 g, 15.20 mmol) in DMF (25 mL). The reaction mixture was heated to reflux for 20 h. At this point TLC analysis indicated full conversion of starting material. The reaction mixture was cooled to room temperature and poured into water (250 mL) and the formed precipitate was separated by filtration. Recrystallization from ethanol gave 4-(benzenesulfonyl)-2-fluoropyridine (**244**) as clear crystals and was confirmed by NMR, LCMS an X-ray crystallographic structure. Crude material was directly used in next step without further purification.

^{1}H NMR (400 MHz, $CDCl_3$) δ 8.14 (d, *J* = 7.9, 2H, Ar*H*), 7.85 - 7.76 (m, 1H, Ar*H*), 7.68 (t, *J* = 7.9, 2H, Ar*H*)

^{19}F NMR (376 MHz, $CDCl_3$) δ - 62.97 (F, s)

LCMS – found mass for $[M+H]^+$ $C_{11}H_8FNO_2S^+$ = 273.03

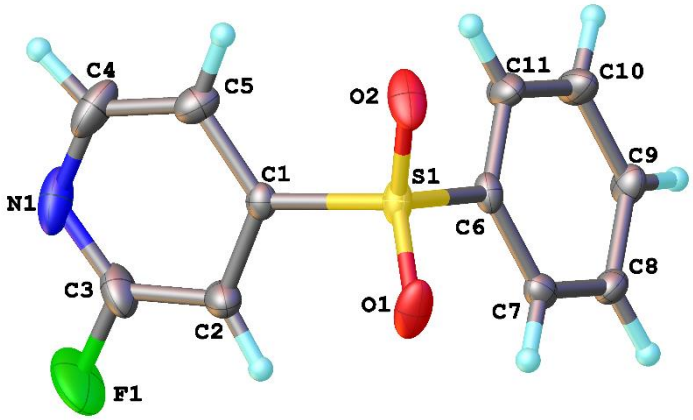

Figure 7.6: Crystal structure of 4-(benzenesulfonyl)-2-fluoropyridine **244**. Crystal structure reported with a 50% thermal ellipsoid probability.

7.3.23 Synthesis of 4-(benzenesulfonyl)-2-(3-ethynylphenoxy)pyridine (246)

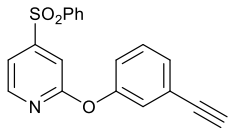

3-Hydroxyphenylacetalyne (**245**) (0.11 g, 0.93 mmol) and potassium carbonate (0.59 g, 4.26 mmol) were added to MeCN (50 mL). Compound **244** (0.25 g, 1.05 mmol) was added, and the resulting solution was heated to reflux for 24 hrs. The reaction was cooled to room temperature and the reaction mixture was filtered. The reaction mixture was concentrated *in vacuo* and the product was purified by column chromatography (silica gel, hexane: EtOAc 1:9) to give 4-(benzenesulfonyl)-2-(3-ethynylphenoxy)pyridine **246** (0.06 g, 19%).

^{1}H NMR (400 MHz, $CDCl_3$) δ 8.34 – 8.32 (m, 1H, Ar*H*), 8.03 – 8.00 (m, 2H, Ar*H*), 7.72 – 7.67 (m, 1H, Ar*H*), 7.64 – 7.58 (m, 2H, Ar*H*), 7.45 (d, *J* = 4.6, 2H, Ar*H*), 7.41 – 7.37 (m, 2H, Ar*H*), 7.26 (dt, *J* = 2.2, 0.9, 1H, Ar*H*), 7.17 – 7.11 (m, 1H, Ar*H*), 3.12 (s, 1H)

^{13}C NMR (101 MHz, $CDCl_3$) δ 164.0, 153.3, 153.0, 149.3, 139.5, 134.3, 129.8, 129.7, 129.3, 128.3, 125.0, 123.8, 122.2, 115.4, 109.6, 82.7, 78.2

HRMS ESI$^+$ Calculated for $[M-H]^-$ $C_{11}H_5NO_2SF_4^-$ = 336.0694 Found 336.0689

7.4 Biological assays - Chapter 2, 3, 4 and 5

7.4.1 Culturing of *Leishmania mexicana*

Leishmania mexicana (MNYC/BZ/62/M379*)* promastigotes were thawed at 37 °C and immediately transferred into Schneider's insect medium (Sigma-Aldrich) supplemented with 0.4 g/L $NaHCO_3$, 0.6 g/L anhydrous $CaCl_2$, 15% (v/v) heat inactivated foetal bovine serum (FBS) (Gibco) and 1% (v/v) penicillin/streptomycin (P/S) solution (Gibco), pH 7. The culture was incubated at 26 °C for 2-3 days until parasites were growing well and then inoculated into fresh media at a concentration of 5 x 10^5 cells/mL. Subsequently, parasites were maintained at log phase by splitting to 5 x 10^5 cells/mL every 3 days. Cells were counted using a Neubauer Improved Haemocytometer.[22]

L. mexicana log phase promastigotes were differentiated to axenic amastigotes[22] by transferring to Schneider's insect medium supplemented with 0.4 g/L $NaHCO_3$, 0.6 g/L anhydrous $CaCl_2$ 20% heat inactivated FBS, pH 5.5 and 1% (v/v) P/S (Gibco) at 5 x 10^5 cells/mL and incubating at 26 °C for 5-6 days until they reach metacyclic stage. Parasites were then seeded at 5 x 10^5 cells/mL in the same medium and incubated at 33 °C. After additional 5-7 days incubation, parasites should be in the amastigotes stage and ready for the infection of the host cells. *L. mexicana* axenic amastigotes were maintained at 33 °C by subculturing at a concentration of 5 x 10^5 cells/mL every 5-7 days.[22]

7.4.2 Culturing of RAW 264.7 murine macrophages

RAW 264.7 macrophages were rapidly thawed at 37 °C and transferred to 4 mL of Dulbecco's Modified Eagle's $Medium_{10}$ ($DMEM_{10}$) high glucose with GlutaMax (Gibco), supplemented with 10% (v/v) heat inactivated FBS and 1% (v/v) P/S. This cell suspension was then immediately centrifuged for 5 mins at 1500 rpm to remove DMSO (the cryoprotectant). The supernatant was discarded, and the cell pellet was resuspended in 10.0 mL of $DMEM_{10}$ (pre warmed to 37 °C) in a vented cap T75 flask. Next, cells were incubated at 37 °C, with 5% CO_2 and passaged until they reached 80% confluence. For

each passage the media was removed, and cells were rinsed with sterile phosphate saline buffer (PBS) (Sigma-Aldrich) to remove all the serum (trypsin inhibiting properties). 2.0 to 3.0 mL of 0.25% (w/v) Trypsin-0.53 mM EDTA solution was then added followed by a 5-15 mins incubation at 37 °C to detach cells. Finally, 6.0 to 8.0 mL of $DMEM_{10}$ culture media was added after the incubation of maximum 15 mins. If the cells are still not detached cell scrapers (STARLAB) was used to gently lift cells from the bottom of the flasks. Cells were counted using a Neubauer Improved Haemocytometer and seeded at a density of 1×10^6 cells/mL in 10.0 mL of $DMEM_{10}$ for the passage.

7.4.3 Preparation of frozen stocks

L. mexicana promastigotes were grown to log phase. Then 500 µL of parasite culture (about 0.5-1 x 10^7 cells/mL) was added to 500 µL of freezing culture medium (10% DMSO, 60% Schneider's insect medium, 30% heat inactivated FBS). This was then transferred into cryovials (STARLAB) and frozen slowly by incubating at 4 °C, -20 °C and -80 °C for 2 hrs each before transferring to a labelled box for long-term storage at -150 °C.

Frozen stocks of RAW 264.7 murine macrophages were prepared in the same manner but were instead frozen at a concentration of 4×10^6 cells/mL in $DMEM_{10}$ with 10% DMSO (Sigma-Aldrich). All cells were frozen at a low passage number.

7.4.4 Preparation of test compounds and amphotericin B stock solutions

All the purified compounds and amphotericin B (Sigma-Aldrich) were prepared at 10 mM in DMSO (Sigma-Aldrich). The stocks were then stored at -20 ºC between uses and before each use stock was thoroughly defrosted, and vortexed.

7.4.5 Cell counting and concentration.

Cells were counted using a Neubauer Improved Haemocytometer under a light microscope (×40 magnification). 10 µL of cell culture was loaded into each of the two counting chambers and for dense cultures a dilution (1:10) of cells in medium was required to allow a better cell separation. The medium sized squares in the 1 mm^2 area at the centre of the 3×3 grid was selected for counting (1×10^{-4} mL volume per square) (**Figure 7.7**).

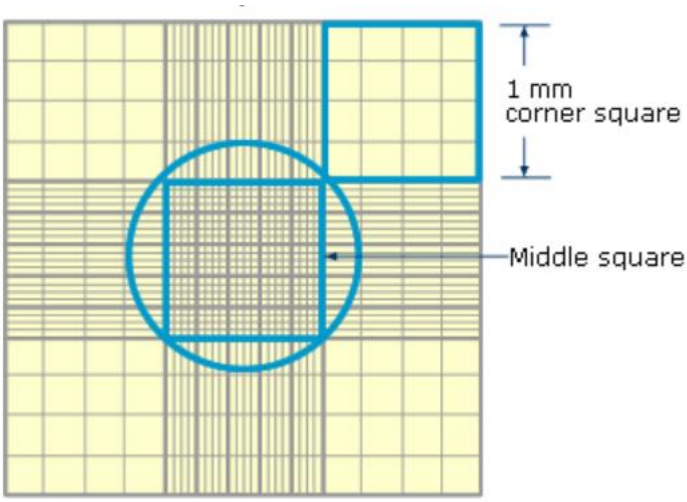

Figure 7.7 Standard Haemocytometer chamber
(https://www.dlsweb.rmit.edu.au/Toolbox/Laboratory/laboratory/studynotes/SNHaemo.htm)

The number of cells per mL was counted as follows:

$$Cell\ density = \frac{(number\ of\ cells\ counted)(dilution\ factor)}{(number\ of\ squares\ counted)(volume\ of\ a\ square)}$$

7.4.6 Assay validation for *L. mexicana* promastigotes and axenic amastigotes

Two 96-well microtiter plates were set up by adding 100 µL of Schneider's insect medium (pH 7.0, 15% FBS, 1% P/S) containing *L. mexicana* promastigotes at the following concentrations: 2×10^6 cells/mL, 1×10^6 cells/mL, 5×10^5 cells/mL, 2.5×10^5 cells/mL, 1.25×10^5 cells/mL, 6.25×10^4 cells/mL, 3.125×10^4 cells/mL, and 1.562×10^4 cells/mL.

The above concentrations were achieved by carrying out a 2-fold serial dilution from a 2 × 10^6 cells/mL culture and each dilution was done in triplicates. 100 µL of culture media was added to all the empty wells to measure the background fluorescence. One plate was incubated for 20 hrs at 26 ºC and the next plate was incubated for 44 hrs at 26 ºC. Then, 10 µL (10% v/v) of resazurin solution (5mg dissolved in 40mL of sterile PBS, 0.0125% w/v; Sigma-Aldrich) was added to each well and incubated for a further 4 hrs at 26 ºC. Fluorescence was measured using the Biotek microplate reader (Biotek FLx800, λ_{ex} 560 nm, λ_{em} 600 nm).

Assay validation for *L. mexicana* axenic amastigotes were carried out using the same protocol as above, but instead using Schneider's insect medium (pH 5.5, 20% FBS, 1% P/S) and incubation temperature of 33 °C.

7.4.7 Preliminary screen at 50 µM concentration against *L. mexicana* promastigotes and axenic amastigotes

199 µL of Schneider's insect medium (pH 7.0 and pH 5.5) containing cells at 1 x 10^6 cells/mL were seeded into a 96-well microtiter plate. Test compounds (1.0 µL of 10 mM stock in DMSO) and controls (DMSO used as a negative control and amphotericin B used as a positive control) were added to the corresponding wells in triplicate. Promastigotes containing plates were incubated at 26 °C for 20 hrs and axenic amastigotes were incubated for 44 hrs at 33 °C. Then, 20 µL (10% v/v) of resazurin solution (0.0125% w/v; Sigma-Aldrich) was added to each well and incubated for a further 4 hrs at respective temperatures. Plates were read using the Biotek microplate reader (Biotek FLx800, λ_{ex} 560 nm, λ_{em} 600 nm). Percentage of cell viability was calculated using MS excel data sheets and two bar charts were created to present the viable cell percentage of each test compound at 50 µM.

7.4.8 Dose-response assays with *L. mexicana* promastigotes and axenic amastigotes

1 x 10^6 cells/mL *L. mexicana* promastigotes in Schneider's insect medium (pH 7.0, 15% FBS, 1% P/S) (200 µL/well) with a serial drug dilution were seeded into a 96 well plates. Serial drug dilutions of eight 3-fold dilution steps covering a range from 50 – 23 nM were prepared in triplicates. Amphotericin B was used as a positive control (100 µM final concentration) and DMSO was used as the negative control (2% final concentration. Plates were incubated at 26 °C for 20 hrs. Then, 20 µL (10% v/v) of resazurin solution (0.0125% w/v; Sigma-Aldrich) (5mg resazurin dissolved in 40mL of sterile PBS) was added to each well and incubated for a further 4 hrs at respective temperatures. Plates were read using a plate reader (Biotek FLx800, λ_{ex} 560 nm, λ_{em} 600 nm).

Dose response assays using *L. mexicana* axenic amastigotes were carried out using the same protocol as above, but instead using Schneider's insect medium (pH 5.5, 20% FBS, 1% P/S) and incubating at 33 °C for 44 hrs before the addition of resazurin solution (0.0125% w/v; Sigma-Aldrich).

Data were analysed using the GraphPad software and decrease of fluorescence (equals to inhibition) was expressed as percentage of the fluorescence of control cultures and plotted against the drug concentrations. From the sigmoidal inhibition curves the EC_{50} values were calculated.

7.4.9 MTT assay - Chapter 2

HeLa cells were seeded in the 96 well plates at the density of 1x10^4 cells/well in DMEM supplemented with 10% FCS and 1% P/S. After 24 hr of incubation at 37°C, 5% CO_2, the medium was removed and the cells were treated with various concentrations of the compounds and incubated for 72 hr at 37°C, 5% CO_2. Thereafter, 15 µl of the MTT reagent were given in each well. For a positive control, Triton X-100 (1%) was added in some wells

before treating them with the MTT reagent. After 3 hr of incubation the cells were lysed using the Stop Solution to release the blue-purple formazan. The cell viability was determined by measuring the absorbance of the resulting formazan at 595 nm using a plate reader.

7.4.10 Cytotoxicity assays with RAW 264.7 macrophages - Chapter 3, 4 and 5

The RAW 264.7 cells were grown at 37 °C with 5% CO_2 in Gibco™ Dulbecco's Modified Eagle's $Medium_{10}$ ($DMEM_{10}$) high glucose supplemented with 10% (v/v) heat inactivated FBS and 1% (v/v) P/S. On day 1, 50 µL of RAW 264.7 cell suspension in $DMEM_{10}$ was added to each well in a 96 well plate at a concentration of $2.5x10^5$ cells/mL followed by an incubation of 24 hrs at 37 °C, 5% CO_2. On day 2, $DMEM_{10}$ was removed using the Vacuboy Hand Operator (Integra Biosciences) and cells were washed once with 100 µL $DMEM_2$ supplemented with 2% (v/v) heat inactivated FBS and 1% (v/v) P/S. 50 µL $DMEM_2$ was then added to each well before incubation for a further 24 hrs. On day 3, media was removed, and cells were washed three times with 50 µL $DMEM_2$ to remove any non-adherent cells before adding 50 µL/well of fresh $DMEM_2$ to each well. Test compounds with a serial dilution (range from 100 to 0.41 µM) and positive and negative controls (amphotericin B and DMSO respectively) were prepared in $DMEM_2$ and added to the corresponding wells (50 µL/well) for an incubation for 20 hrs at 37 °C, 5% CO_2. On day 4, 5 µL (10% v/v) of resazurin solution (0.0125% w/v; Sigma-Aldrich) was added to each well before a 4-hr incubation at 37 °C, 5% CO_2, prior to assessing cell viability using the Biotek FLx800 fluorescence microplate reader as before (Biotek FLx800, λ_{ex} 560 nm, λ_{em} 600 nm).

7.4.11 RAW 264.7 intramacrophage amastigote assay- Chapter 2 and 3

On day 1, 200 µL of cell solution (or 200 µL $DMEM_{10}$ for the *L. mexicana* control wells) was added to each well of a 96 well plate at a concentration of $2.5x10^5$ cells/mL in $DMEM_{10}$, and incubated for 24 hrs at 37 °C, 5% CO_2 to allow cells to adhere. On day 2, the RAW cells were carefully washed once with 50 µL $DMEM_2$. Addition of 200 µL of *L. mexicana* M379 amastigotes at $2.5x10^6$ cells/mL in $DMEM_2$ (10 amastigotes per macrophage) followed by an incubation for 24 hrs at 37 °C, 5% CO_2. of $2.5x10^6$ parasites/mL. 200 µL $DMEM_2$ was added to the RAW 264.7 control wells. On day 3, infected RAW cells were carefully washed five times with 50 µL of $DMEM_2$, followed by addition of 100 µL of $DMEM_2$ per well. Appropriate serial solutions of the test compounds and control solutions were prepared in $DMEM_2$ and added to corresponding wells (100 µL/well) in triplicate for an incubation for 24 hrs at 37 °C, 5% CO_2. On day 4, The media was then removed and infected and treated cells were carefully washed three times with 50 µL of serum free Schneider's insect medium, pH7.0 (SIM). 0.05% (v/v) sodium dodecyl sulfate (SDS) solution was then prepared (10 µL of 20% SDS in 4 mL of SIM) and lysis of the macrophages, three rows at a time was then carried out as follows. 20 µL of SDS (0.05% v/v) was added to the wells for 30 seconds, with gentle agitation of the plate during the incubation time before addition of 180 µL of Schneider's insect medium, 15% FBS, pH7. After lysis of macrophages in all wells, plates were wrapped with parafilm and incubated for 44 hrs at 26 °C. On day 6, 20 µL (10% v/v) of resazurin solution (0.0125% w/v; Sigma-Aldrich) was then added to each well, before rewrapping plates and incubating at 26 °C for 4 hrs. Plates were then read with the Biotek FLx800 microplate reader (Biotek FLx800, λ_{ex} 560 nm, λ_{em} 600 nm).

To ensure the collection of a robust data set, test compounds were screened in triplicate in each assay, and a minimum of three independent assays were carried out for each set of compounds.

7.5 Validation of DUB Inhibitors - Chapter 3

Screening of *L. mexicana* parasites for potential DUB inhibitors outlined below was carried out at the Department of Biosciences, University of York by Sergios Antoniou (PhD student in Professor Jeremy Mottram's group).

7.5.1 Culture of *Leishmania* (York)

Leishmania mexicana (MNYC/BZ/62/M379) were grown in HOMEM (Gibco) supplemented with 10% (v/v) heat inactivated foetal calf serum (HIFCS) (Gibco) and 1% (v/v) P/S solution (Sigma-Aldrich) at 25 °C. Mid-log phase parasites were defined as between 4-8 $\times 10^6$ cells/mL and stationary phase parasites between 1.5-2.5 $\times 10^7$ cells/mL.[23,24]

7.5.2 Competition assay between the inhibitors and Cy5UbPRG probe

3×10^7 cells from a log phase *L. mexicana* culture were spun at 1,000 × g and washed three times with 1mL of ice-cold Tris-buffered saline (TSB) wash buffer (44 mM NaCl, 5 mM KCl, 3 mM NaH_2PO_4, 118 mM sucrose and 10 mM glucose, pH 7.4). Next, the cells were lysed using a newly prepared ice-cold lysis buffer (50 mM Tris-HCl pH 7.4, 120 mM NaCl, 1% NP40 lysis buffer (Sigma-Aldrich) and freshly added in order: 1µg/mL pepstatin, 1 × cOmplete ULTRA tablets [Mini, EASY pack Protease inhibitor cocktail, Roche], 1 mM Dithiothreitol (DTT), 1mM phenylmethylsulfonyl fluoride (PMSF), 0.01 mM E64). Samples were incubated at 4 °C for 15 mins. Afterwards, samples were centrifuged at 17,000 × g for 15 mins and the supernatant discarded. Protein concentration of the samples were adjusted to 1 mg/mL in a total volume of 25 µL. These protein samples were then incubated with 30 µM of each test compound for 1hr at RT and three controls were used, first, NI: no inhibitor was added but DMSO was added instead. Second, HB: HBX 41108 a non-specific DUB inhibitor. At last, FT: FT671 a molecule that does not inhibit any DUBs

in *Leishmania*. 2 µL of 50mM NaOH and 1µM of Cy5UbPRG (UbiQ) were added. Lysis buffer was used to top up to a final volume of 25µL. The reaction mixture was then incubated at room temperature for 5 mins and the reaction was stopped by addition of 3 × loading dye (LDS buffer + DTT) followed by an incubation at 70 °C for 10 mins. 12 µL of each sample were then analysed in a gradient 4-12% NuPage Bis-Tris protein gel, for exactly 90 mins at 200V. The gel was then washed with water and imaged with Amersham Typhoon with Excitation: 635nm, filter: Cy5 670BP30 (GE Healthcare Life sciences).[23,24]

7.5.3 Evaluation of resistance development in *L. mexicana* DUB16 overexpressing cell line

L. mexicana promastigotes were grown in HOMEM medium (Gibco) (10% HI-FCS, 1% P/S, pH 7.0) at 25 °C. To assess the survival of *L. mexicana* and *L. mexicana* [DUB16] (DUB16 overexpressing *L. mexicana* cell line), 200µL of culture medium with 5×10^5 cells/mL promastigotes with a serial drug dilution (from 24 µM to 47 nM) were seeded in 96 well plates. After 20 hrs of incubation at 25 °C, 20 µL of Alamar Blue®, were added to each well and plates were incubated for another 4 hrs. Resorufin fluorescence ($579_{Ex}/584_{Em}$) was measured using a POLARstar Omega plate reader (BMG Labtech).

7.6 Biological assays against *T. cruzi*. - Chapter 4

7.6.1 Culturing *T. cruzi* parasites and CHO-K_1 cells

T. cruzi epimastigotes (CL strain clone 14) were maintained in exponential phase by subculturing the parasites every 48 hr in Liver Infusion Tryptose (LIT) medium at 28ºC. The Chinese Hamster Ovary cell line CHO-K_1 was cultivated in RPMI-1640 medium supplemented with 10% heat-inactivated Fetal Calf Serum (FCS), 0.15% (w/v) $NaHCO_3$, 100 units/mL penicillin and 100 mg/mL streptomycin at 37 ºC in a humidified atmosphere containing 5% CO_2.[25] Intracellular trypomastigotes, were obtained by infection of CHO-K_1

cells with trypomastigotes.[26] Infected cells were maintained at 37ºC in the presence of 10% FCS. After 24 hr, the cells were maintained at 33 ºC and 2% FCS. Trypomastigotes were collected from the extracellular medium five days after infection.

7.6.2 *In vitro* inhibition of proliferation assays on *T. cruzi* epimastigotes

The cell density of exponential phase epimastigotes (approximately 5×10^7 parasites/mL) was adjusted to 2.5×10^6 cells/mL. The parasites were then transferred into 96-well plates (200 µL/well). Epimastigote proliferation was measured by reading the optical density (OD) at 620 nm every 24 hr for 8 days (which allowed us to have readings through the exponential and stationary phases). The OD values were converted to cell density values (cells/mL) by using a calibration curve obtained by measuring the OD values at 620 nm of parasite suspensions at different known densities. The half-maximal inhibitory concentrations (IC_{50}) were determined from cell density data obtained at the 4th proliferation day, which corresponded to the mid exponential proliferation phase. Data were analysed by a non-linear regression to a sigmoidal dose-response curve using GraphPad Prism (v.6). DMSO-dissolved benznidazole (final concentration of 20 µM) and untreated parasites grown in the presence of the same volume of DMSO used for the benznidazole treatment, were used as positive and negative controls, respectively. The compounds were evaluated in quadruplicate in each experiment, and the results correspond to three independent experiments.

7.6.3 The effect of the compounds on mammalian cell viability

The viability of CHO-K_1 cells was evaluated by assessing the irreversible reduction of resazurin (7-hydroxy-3H-phenoxazine-3-one-10-oxide) to resorufin (7-hydroxy-3H phenoxazine-3-one), a redox fluorometric indicator. CHO-K_1 cells ($1.0\text{x}10^5$ cells/well) in 100 µL of RPMI medium supplemented with FCS (10%) were seeded in 96-well plates

with or without (control) different concentrations of the tested compounds. After 48 hrs, the cell viability was determined by the resazurin assay, the cells were incubated in the presence of 0.125 µg/µl resazurin for 3 hrs at 37 ºC in the absence of light. The fluorescence signal was measured in a Spectra Max M3 fluorometer (Molecular Devices) at λ_{exc} 560 nm and λ_{em} 590 nm. The IC_{50} values were determined by fitting a sigmoidal dose-response curve to the data using GraphPad Prism (v.6). Each assay was developed in triplicate and the results correspond to the mean of three independent experiments.

7.6.4 Effect of 198 on *T. cruzi* amastigote replication and trypomastigote release

CHO-K_1 cells (1.0 x 10^4 per well) were seeded in 96-well plates in RPMI medium supplemented with 10% FCS at 37 ºC for 24 hrs. Then, the cells were incubated with 5.0×10^5 trypomastigotes per well for 4 hrs. After this period, parasites in the supernatant were removed by washing the plates twice with PBS, and the cells were incubated overnight in RPMI medium supplemented with 10% FCS at 37 ºC in the presence of different concentrations of **198** (0.01 to 5 µM) or left untreated (control). After 24 hrs, the plates were incubated at 33 ºC and RPMI 2% FCS with the same different **198** concentrations to allow the parasites to complete the infection cycle. To measure the effect on amastigote replication, after 48 h the CHO-K_1 cells and parasites were fixed with 4% paraformaldehyde and stained with Hoechst 33342. Images were taken by fluorescence microscopy. Cells, parasites, and infected cells were counted using ImageJ software. The infection index (percentage of infected cells × the number of parasites per cell) was calculated. The effect of **198** on *T. cruzi* trypomastigotes release was determined on the fifth day post-infection, by counting the trypomastigotes released in the extracellular medium, using a Neubauer chamber. Each condition was assayed in three independent biological experiments.

In order to verify that **198** diminished the release of trypomastigotes due to its effect on the amastigote proliferation, infected cells were treated with 0.05 µM **198** (IC_{50} for the trypomastigote release) or not (control) for two days after infection. After fixing and staining the infected cells with 4% paraformaldehyde and stained with Hoechst 33342, the effect of **198** on the total number of cells, the number of infected cells, and the number of amastigotes per infected cell were quantified.

7.6.5 Analysis of phosphatidylserine exposure and Plasma membrane integrity

Epimastigotes (2.5 x10^6 cell/mL) were incubated for four days in the presence or absence (control) of 1.5 µM and 3.0 µM **198** (concentrations corresponding to 1 or 2 times the IC_{50}, respectively). To determine the exposure of phosphatidyl serine, the cells (1.0x10^6) were labelled with propidium iodide (PI) and Annexin-V FITC (Molecular Probes) according to the manufacturer's instructions. As positive controls for plasma membrane permeabilization and extracellular exposure of phosphatidylserine, the parasites were treated with 150 µM digitonin for 30 min. The cells were analysed by flow cytometry on a BD Accuri™ C6 Plus, each condition was run in three biological independent replicas with 10,000 events collected and analysed using BD CSampler Plus Software (v 1.0.27.1) and FlowJo software (v07).

7.6.6 Analysis of mitochondrial inner membrane potential (ΔΨm)

Epimastigotes (2.5x10^6 cell/mL) were incubated at different times for short-term (0, 1, 3 and 6hrs) and long-term (4 days) measurements of ΔΨm in the presence or absence (control) of 1.5µM and 3.0 µM **198** (concentrations corresponding to 1 or 2 times the IC_{50}, respectively). For determining variations in ΔΨm, cells were aliquoted in fractions at densities of 5.0x10^6 cells/mL and the parasites were washed twice in PBS by

centrifugation (2,700 x *g* for 5 min). The positive control was incubated for 15 min with 10 µM carbonyl cyanide-4-(trifluoromethoxy) phenylhydrazone (FCCP) in PBS. Then, all samples were centrifuged for 10 min at 2,700 x *g* and resuspended in PBS. The cells were labelled, or not for the unstained control, by the addition of 256 nM Rhodamine 123 (Rho123) for 20 min at 28 ºC. The cells were twice in washed with cytomix buffer (25 mM HEPES-KOH, 120 mM KCl, 0.15 mM $CaCl_2$, 2 mM EDTA, 5 mM $MgCl_2$, 10 mM K_2HPO_4/KH_2PO_4 buffer, pH 7.6, and 10 µM FCCP if indicated) and resuspended in 500 µL of the same buffer. Changes in the cell's fluorescence labelled with Rho123 were analysed by flow cytometry on a BD Accuri™ C6 Plus. Each condition was run in three biological independent replicas with 10,000 events collected and analysed using BD CSampler Plus Software (v 1.0.27.1) and FlowJo software (v07).

7.6.7 Analysis of intracellular Ca^{2+} levels

Epimastigotes (2.5 x 10^6 cell/mL) were incubated at different times for short-term (0, 1, 3 and 6 hrs) and long-term (four days) measurements of intracellular Ca^{2+} levels in the presence or absence (control) of 1.5 µM or 3.0 µM **198** (approximately 1 x IC_{50} and 2 x IC_{50}) (only 1.5 µM was used in the long-term assay). Then the parasites (1.0x10^7 cells) were washed with Phosphate Buffered Saline (PBS) and incubated with 5 µM Fluo-4 AM (Invitrogen) for one hour at 28 ºC, washed twice with HEPES glucose (50 mM HEPES, 116 mM NaCl, 5.4 mM KCl, 0.8 mM $MgSO_4$, 5.5 mM glucose and 2 mM $CaCl_2$, pH 7.4), resuspended in the same buffer and aliquoted into 96-well plates (2.5x10^7 per well). Readings were performed on a Spectra Max I3 fluorometer, (Molecular Devices) at λ_{exc} 490 nm and λ_{em} 518 nm. Each assay was developed in triplicate and the results correspond to the mean of three independent experiments.

7.6.8 Determination of *T. cruzi* intracellular ATP levels

Epimastigotes (2.5 x 10^6 cell/mL) were incubated for 4 days for the long-term measurements of ATP levels in the presence or absence (control) of 1.5 μM and 3.0 μM **198** (concentrations corresponding to approximately 1 x and 2 x IC_{50}, respectively). Intracellular ATP levels were measured by using a bioluminescent assay kit according to the manufacturer's instructions (Sigma-Aldrich). Briefly, 50 μL PBS was added to 100 μL cellular ATP-releasing reagent and added to a 50 μL suspension of 5.0x10^6 parasites, treated or not treated (control). Light emission levels were measured on a Spectra Max I3 fluorometer at 570 nm. Each assay was developed in triplicate and the results correspond to the mean of three independent experiments.

7.6.9 Analysis of Cell cycle

Epimastigotes (2.5x10^6 cells/mL) were incubated (or not, negative control) in the presence of 1.5 and 3.0 μM **198** for four days. Then, the cells (1.0x10^7 cells/mL) were collected by centrifugation (2,700 x *g* for 5 min), washed in PBS and fixed in 70% ethanol for 4 hrs. The parasites were washed twice in PBS and incubated with 10 μg/mL RNase A (Thermo Scientific) for 30 min at 37 ºC. To measure the DNA content, the cells were stained with 40 μg/mL propidium iodide (Molecular Probes/Invitrogen) and analysed by flow cytometry on a BD Accuri™ C6 Plus, with 50,000 events collected from three biological independent experiments. Histograms (number of counts by FL2 area), scatter plots (side scatter [SSC] area by forward scatter [FSC] area) and gates for each cell cycle phase were analysed using BD CSampler Plus Software (v 1.0.27.1) and FlowJo software (v07). Cell cycle data were fitted by a model included in the FlowJo software (v07).

7.6.10 Data treatment and statistical analysis

Curve adjustments, regressions, and statistical analyses were performed with the GraphPad Prism 7 analysis tools. All assays were performed at least in biological triplicates.

7.7 Proteomics - Chapter 5

7.7.1 Cell culturing

Detailed protocols for the maintenance of *L. mexicana* promastigotes, amastigotes and RAW 264.7 cells have been outlined in sections **7.3.1**. and **7.3.2**. Detailed protocol for culturing Hep G2 cells is stated in section **7.5.1.4**.

7.7.2 Culturing of Hep G2 cells

Hep G2 cells were thawed rapidly (approximately within 2 mins) by gentle agitation in a 37 ºC water bath. Then the vial content was transferred to a centrifuge tube containing ~5.0 mL of Dulbecco's Modified Eagle's $Medium_{10}$ ($DMEM_{10}$) high glucose with GlutaMax (Gibco), supplemented with 10% (v/v) heat inactivated FBS and 1% (v/v) P/S and centrifuged at 1000 rpm for 5 mins. Cell pellet was next resuspended in fresh, pre warmed 10.0 mL of $DMEM_{10}$ and dispensed into a T-75 flask before incubating at 37 ºC with 5% CO_2.

Once cells reach to a 70-80% confluence, the old medium was removed, and cells were washed 2 times with PBS. 2.0-3.0 mL of 0.25% (w/v) Trypsin-0.53 mM EDTA solution was added to the flask and incubated at 37 ºC for 5-15 mins to facilitate dispersal. Flask was observed under a microscope to check if the cells are detached. Then, 6.0-8.0 mL of fresh culture medium was added to the flask and cells were aspirated by gentle pipetting. Finally,

subcultures were made using 1:3 ratio and incubated at 37 ºC with 5% CO_2. Media was renewed every 2-3 days until next subculture.

7.7.3 Compound treatment

In gel fluorescence assays; Individual flasks containing 10.0 mL of cell cultures (*L. mexicana* promastigotes and axenic amastigotes. RAW 264.7 cells and Hep G2 cells were used at their 80% confluence in a T-75 flask) at a concentration of 5×10^6 cells/mL were prepared. Then the cells were treated with different compound concentrations ranging from 50 - 0.025 µM for 2 hrs. DMSO (sigma-Aldrich) was used as the negative control.

7.7.4 Preparation of lysates

After the 2-hr treatment, cell suspensions were centrifuged at 3260 rpm for 3-5 mins. Cell pellets were washed twice with 10.0 mL of sterile 1X PBS buffer (Sigma-Aldrich) (1 tablet was dissolved in 200mL Milli-Q water) and cells were collected every time by using the same centrifuge conditions. Then, 4.75 mL of lysis buffer (50mM HEPES (Sigma-Aldrich), 150mM NaCl (Fisher Scientific), 4% SDS (Fisher Scientific) in Milli-Q water, pH 7.5) and 0.25 mL of cOmplete™, Mini, EDTA-free protease inhibitor cocktail (Sigma-Aldrich) (dissolve one tablet in 0.50 mL lysis budder) were mixed to make the' lysis buffer solution'. Next, 300-500 µL of 'lysis buffer solution' was added to the cell pellet and incubated at room temperature for 5 mins. If necessary, a needle can be used to completely lyse the cells. Thereafter, lysate was transferred to microcentrifuge tubes and centrifuged at 10,000 rpm (or the maximum speed) for 10 mins to remove cell debris, supernatant was transferred to a new tube. Lysates were stored at -80 ºC until further analysis.[27,28]

7.7.5 Determination of Protein concentration – BCA assay

For the standard curve, 2mg/mL bovine serum albumin (BSA) stock solution was prepared in the same lysis buffer used to make lysates. Dilution scheme for microtiter plate procedure is listed in **Table 7.4**.

Vial	Volume of the diluent (µL)	Volume and source of BSA (µL)	Final BSA concentration (µg/mL)
A(stock)	0	300 (stock)	2,000
B	31.2	93.8 (stock)	1,500
C	50.0	50.0 (stock)	1,000
D	50.0	50.0 (vial B solution)	750
E	50.0	50.0 (vial C solution)	500
F	50.0	50.0 (vial E solution)	250
G	50.0	50.0 (vial F solution)	125
H	80.0	20.0 (vial G solution)	25
I	100	0	0

Table 7.4 Dilution scheme for microtiter plate procedure.

Unknown samples were diluted, 1:10 or accordingly, and three vials were prepared each containing 30µL of diluted sample. Pierce Rapid Gold BCA working reagent (WR); required volume of WR was prepared by mixing 50 parts of Rapid Gold BCA Reagent A with one part of Rapid Gold BCA Reagent B (50:1, Reagent A:B) (Pierce™ Rapid Gold BCA Protein Assay Kit-thermoscientific).

20 µL of each standard or unknown sample replicate were pipetted into a 96-well microtiter plate (Plate arrangement is shown in **Figure 7.8**). 200 µL of WR was added to each well (sample to WR ratio 1:10) and mixed well by gently shaking. Subsequently, plate was incubated for 5 mins at room temperature before measuring the absorbance at 480 nm using the Biotek FLx800 microplate reader. Plates should be read within 20-30 mins to ensure colour development of the top standard is not out of instrument linearity.

	A		S1	b							
	B		S1	b							
	C		S1	b							
	D										
	E		S2	b							
	F		S2	b							
	G		S2	b							
	H										

Figure 7.8 96-well microtiter plate arrangement. (A-H; standard series, S1; sample 1, S2; sample 2 and b; blank (I)).

7.7.6 Proteomics- In-gel fluorescence assay

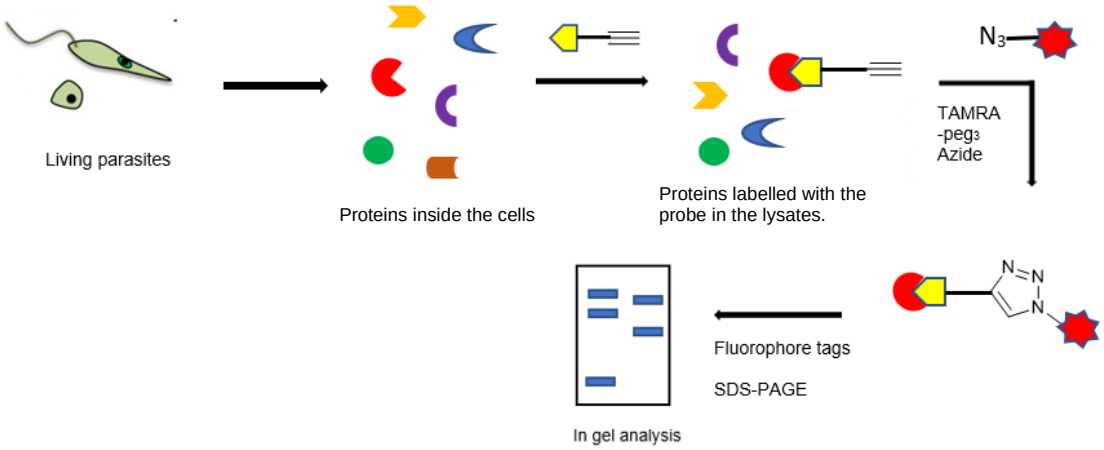

Figure 7.9 Workflow for the in-gel fluorescence assay.

7.7.6.1 Click chemistry.

Cell lysates at a 1 mg/mL protein concentration were treated with freshly premixed click chemistry reaction cocktail (100 µM capture reagent [TAMRA-PEG$_3$-Azide (Jena Bioscience); 10mM stock solution in DMSO], 1 mM $CuSO_4$ (Sigma-Aldrich) solution [50mM stock solution in Milli-Q water], 1mM tris[2-carboxyethyl]phosphine (Sigma-Aldrich) solution [TCEP solution; 50mM stock solution in Milli-Q water], and 100 µM tris[{1-benzyl-4triazoyl}methyl]amine (Sigma-Aldrich) solution [TBTA solution; 10 mM stock solution in DMSO]) for 2 hrs at room temperature. Then, EDTA solution (80 mM stock solution in Milli-

Q water) was added to the lysates (1:10, EDTA: lysate). Proteins were precipitated by adding ice cold methanol (9 volumes) (Sigma-Aldrich, LC-MS grade), and storing overnight at -80 ºC. To collect proteins, samples were centrifuged at 12,000 rpm for 15 mins at 4 ºC. The protein precipitates were washed twice with ice cold methanol (10 volumes), collected by centrifugation at 12,000 rpm for 5 mins at 4 ºC, and the supernatants were discarded. The protein pellets were air dried at room temperature for 20-30 mins and stored in a -80 ºC freezer.

7.7.6.2 Preparation of 0.01% SDS Tris HCl gels

Gel apparatus was set up with cleaned glass slides (Milli-Q water was used to clean). The solutions and volumes required for one SDS gel was listed below. Solutions were gently mixed by inverting the falcon tubes. Resolving gel solution was poured first and allowed to set for ~20 mins (Isopropanol was used to remove the air bubbles formed). Top layer of the gel was washed with Milli-Q water to remove isopropanol added previously. Then, stacking gel solution was poured between the glass slides on top of the resolving gel. This was followed by placing a comb (10 wells) on the stacking gel and allowing its solidification.

	Resolving Gel (8.0 mL)	**Stacking Gel (5.0 mL)**
• Milli-Q water	3.4 mL	3.1 mL
• 40% Acrylamide (Alfa Aesar)	2.4 mL	0.5 mL
• 1.5 M Tris HCl (Alfa Aesar)	2.0 mL	1.25 mL
• 10% SDS	80 µL	50 µL
• 10% APS (Ammonium Per sulfate)	80 µL	50 µL
• TEMED	8 µL	5µL

7.7.6.3 Preparation of 10X running buffer

30.0 g of Tris base (Sigma-Aldrich), 144.0 g of Glycine (Sigma-Aldrich) and 10.0 g of SDS (Fisher Scientific) was first dissolved in 700 mL of Milli-Q water and stirred well until completely dissolved. Then topped it up to 1.0 L.

10X was diluted to make a 1X running buffer to run the SDS-PAGE.

7.7.6.4 In-gel fluorescence scanning

The air-dried protein pellets were resuspended in lysis buffer (50mM HEPES, 150mM NaCl, 4% SDS in Milli-Q water, pH 7.5) to a 1.33 mg/mL final concentration. Then, 4X Laemmli sample buffer (Bio-Rad) (10-20% β-mercaptoethanol in 4X Laemmli sample buffer) was added to make the final protein concentration 1 mg/mL. The samples were vortexed and spun down for 1 min at 4000 rpm. Subsequently, samples were boiled at 95 ºC for 8 mins and allowed to cool down to room temperature. Then again samples were vortexed well and spun down for 1-2 mins at 4000 rpm before loading 20 µL each into the gel. 6.0 µL of Precision Plus Protein™ All Blue Pre-Stained Protein standards (Bio-Rad) was loaded next to the samples. The proteins were resolved by SDS-PAGE (gels were run in a gel electrophoresis equipment using 1X running buffer, approximate running time is 1-1.5 hrs and 180-200 voltage). The gels were scanned for fluorescence labelling using a GE typhoon 5400 gel scanner.

7.7.6.5 Coomassie brilliant blue staining

After scanning the gel, it was taken out from the glass slides and placed in a clean gel staining tray. First, the gel was washed with Milli-Q water for 10 mins and then activated GelCode™ Blue Safe Protein Stain was added enough to cover the gel. The tray was then placed on a shaker for 1-2 hrs to stain and later the stain was removed and replaced by Milli-Q water to de-stain the gel for 1-2 hrs or overnight.

7.7.6.6 Competitive binding assay with the fluorinated probe (230) and non-fluorinated probe (246)

Compound treatment: Two flasks containing 10.0 mL of *L. mexicana* promastigotes at a concentration of 5×10^6 cells/mL were prepared. First, the cells were treated with 50 µM of compound, **246** for 1 hr and then with 5 µM **230** for 2 hrs. DMSO (sigma-Aldrich) was used as the negative control. Then, protocols given in **sections, 7.5.3, 7.5.4,** and **7.5.5** were followed to prepare the lysates and carry out the in-gel fluorescence scan for the Competition assay.

7.7.6.7 Investigation of protein-drug interaction using glutathione (GSH)

Selected compound (**198**) was separately mixed with glutathione (GSH) at a 1:5 molar ratio. Different types of solvents were tested, such as, D_2O, DMSO-d_6, MeCN: H2O (1: 1), DMF and the reactions were monitored by taking mass spectrums at distinct time intervals (0, 0.5, 1, 3, 24, 48 hrs).

The change of fluorine peaks while **198** react with GSH were observed under two reaction conditions. All the ^{19}F NMR samples were run in DMSO-d_6 including the parent compound **198**.

Compound 198 in DMSO-d_6;

^{19}F NMR (376 MHz, DMSO-d_6) δ; -88.52 (td, *J* = 34.5, 14.3 Hz), -138.74 (tt, *J* = 36.5, 15.9 Hz).

(i) Reaction of 198 + GSH in DMSO-d_6. ^{19}F NMR taken after 24 hr incubation at room temperature;

^{19}F NMR (376 MHz, DMSO-d_6) δ; -92.70 – -93.25 (m), -136.33 – -136.88 (m), -166.34.

(ii) Reaction of 198 + GSH in DMF. ^{19}F NMR taken after 24 hr incubation at room temperature;

^{19}F NMR (376 MHz, DMSO-d$_6$) δ; -88.53 (d, *J* = 8.0 Hz), -91.60 – -97.60 (m), -136.50 – -137.99 (m), -138.76 (q, *J* = 26.7 Hz).

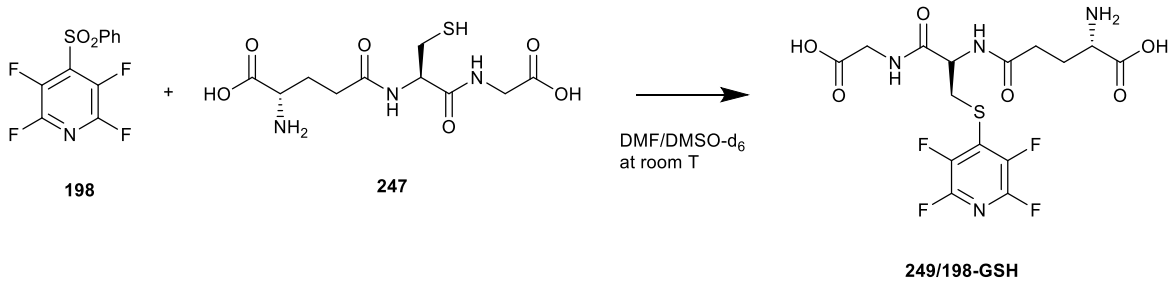

Scheme 7.1 Reaction of **198** with glutathione (**247**) in DMF/DMSO-d$_6$.

7.7.6.8 Purification of 198-GSH analogue using Preparative high-performance liquid chromatography (HPLC)

The crude mixture of **198**-GSH was dissolved in ~10 mL (50: 50 *v/v*% H_2O: MeCN) and purified by preparative RP-HPLC on a Discovery Bio wide pore C_{18}-5 column from Supelco (5 µm, 25 cm × 10 mm), using a Perking-Elmer 200 lc pump coupled to a Waters 486 tuneable absorbance detector recording at λ = 220 nm. An initial typical linear gradient was commonly employed where eluent A rose linearly from 0-100% of solvent B at a flow rate of 2 mL min^{-1} over a period of 60 minutes. Then the flow was maintained isocratically for 5 minutes at 100% of solvent B before returning to initial conditions (solvent A = 95: 5: 0.1 *v/v*% H_2O: MeCN: TFA; solvent B = 5: 95: 0.1 *v/v*% H_2O: MeCN: TFA). When needed and depending on the sequence, further optimization of the purification conditions was performed by either applying longer gradient times (0-100 *v/v*% solvent B over 110 minutes) or ideally by adjusting the gradient window to the product elution conditions (i.e.

0-50 *v/v*% solvent B in 60 minutes). Fractions corresponding to a single chromatographic peak were collected together, lyophilised and their identity and purity analysed by QToF-LC/MS and analytical HPLC.

7.7.7 Proteomics- MS/MS based analysis

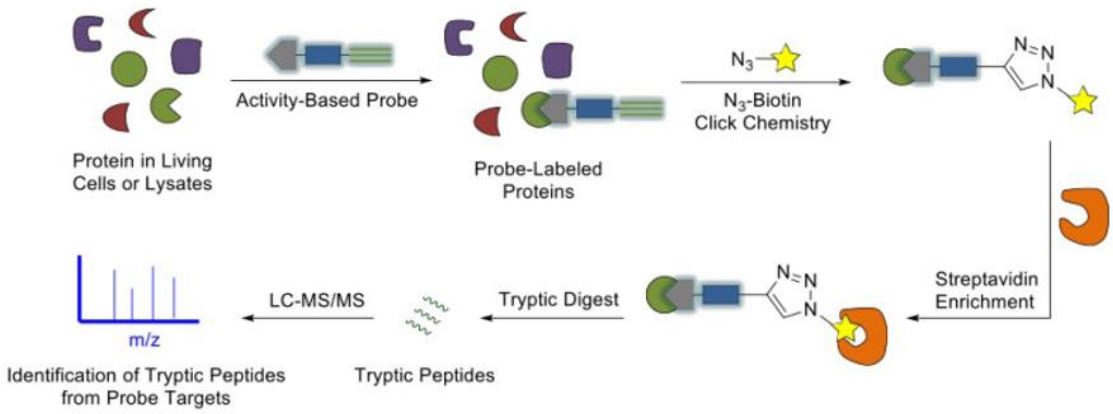

Figure 7.10 Schematic diagram of MS based proteomics.

7.7.7.1 Compound 230 and DMSO treatment

Mass spectrometry-based analysis; Two flasks containing 30.0 mL of cell cultures* at a concentration of 5×10^7 cells/mL were prepared. Cells were treated with the compound **230** at 5/10 µM concentration and with DMSO as the negative control.

Cell cultures* - *L. mexicana* promastigotes and amastigotes. Raw 264.7 cells and Hep G2 cells were used at their 80% confluence in a T-75 flask.

7.7.7.2 Lysates preparation and protein concentration determination

Sections **7.5.3**. and **7.5.4** were followed to prepare cell lysates and to determine the protein concentrations.

7.7.6.3 Click Chemistry

Cell lysates at a 1 mg/mL protein concentration were treated with freshly premixed click chemistry reaction cocktail (150 µM capture reagent [Biotin-Azide (Jena Bioscience); 10mM stock solution in DMSO], 1 mM $CuSO_4$ (Sigma-Aldrich) solution [50mM stock solution in Milli-Q water], 1mM tris[2-carboxyethyl]phosphine (Sigma-Aldrich) solution [TCEP solution; 50mM stock solution in Milli-Q water], and 150 µM tris[{1-benzyl-4triazoyl}methyl]amine (Sigma-Aldrich) solution [TBTA solution; 10 mM stock solution in DMSO]) for 3 hrs at room temperature. Then, EDTA solution (80 mM stock solution in Milli-Q water) was added to the lysates (1:10 ratio of EDTA: lysate). Proteins were precipitated by adding ice cold methanol (9 volumes) (Sigma-Aldrich, LC-MS grade), and storing overnight at -80 ºC. To collect proteins, samples were centrifuged at 12,000 rpm for 15 mins at 4 ºC. The protein precipitates were washed twice with ice cold methanol (10 volumes), collected by centrifugation at 12,000 rpm for 5 mins at 4 ºC, and the supernatants were discarded. The protein pellets were air dried at room temperature for 20-30 mins and stored in a -80 ºC freezer.[27]

7.7.7.4 Affinity enrichment

The air-dried protein pellets acquired after click reactions and protein precipitation were resuspended in PBS with 2% SDS to a 5mg/mL concentration by sonication [In a typical affinity enrichment experiment, 300 µg of cell lysate is subjected to click reaction and protein pellets were dissolved in 50 µL of 2%SDS in PBS]. The samples were then diluted 20-fold with PBS to adjust the final SDS amount to 0.1%. Afterwards, the samples were centrifuged at 2000 rpm for 5 mins at room temperature to remove the cell debris and the clear supernatant was used for the affinity enrichment. Generally, 30 µL of NeutrAvidin-agarose beads (Thermo Scientific), freshly washed three times with 0.1% SDS in PBS, was added to each of the sample, and the samples were mixed for 1.5 hrs at room temperature using an end-to-end rotating shaker. The agarose beads were then washed

two times with 1% SDS in PBS and two times with PBS. Each washing step used 20 volumes of the washing solutions with respect to the bead volume, and to collect the beads after each washing, the samples were centrifuged at 4000 rpm for 1 min at room temperature.[27]

7.7.7.5 On-bead reduction, Alkylation, and Tryptic digestion

After all the meticulous washing steps in affinity enrichment step, the beads were resuspended in 150 µL of 50 mM triethylammonium bicarbonate buffer (TEAB, Sigma-Aldrich) and treated with 10mM TCEP (200mM stock solution in 50mM TEAB) for 1 hr at room temperature. Then, beads were washed once with 50mM TEAB (~ 1.0mL) and collected by centrifuging at 4000 rpm for 1min at room temperature. The beads were resuspended in 150 µL of 50 mM TEAB buffer and treated with 20 mM iodoacetamide (200 mM stock solution in Milli-Q water) under dark conditions for 30-40 mins at room temperature. After the treatment, the beads were collected, washed once with 50 mM TEAB, and collected again by spinning them down at 4000 rpm for 1min at room temperature. Later, 200 µL of fresh 50 mM TEAB buffer was added to the beads and treated with 5 µg of sequencing grade modified trypsin (a vial of 20 µg trypsin was dissolved in 500 µL of 50 mM TEAB buffer) at 37 ºC for 16 hrs. After the incubation period, 2 µL of formic acid was added to the bead mixture and pH was checked using a pH paper to verify that pH is below 3. The samples were centrifuged at 5000 rpm for 5 mins at room temperature to collect the supernatant. The beads were washed once with 50 % v/v acetonitrile (MeCN) containing 0.1% v/v formic acid (use 100 - 200 µL) and mixed with the supernatant previously collected. Acidity of the supernatant was checked using pH papers (pH<3). The collected tryptic peptides were evaporated to dryness using the speed vac SPD120 machine (Thermoscientific; vacuum concentrator).[27]

7.7.7.6 Desalting

Buffer solutions required for the desalting process were listed below.

Buffer A	Buffer B
98% Milli-Q water	35% Milli-Q water
2% J (HPLC grade)	65% Acetonitrile (HPLC grade)
0.1% Formic acid	0.1% Formic acid

The peptides were re-dissolved in 500 µL of buffer A and Sep-Pak C_{18} (Waters- Sep-Pak C_{18} Classic Cartridge, 360 mg Sorbent per Cartridge, 55-105 µm- WAT051910) columns were used for desalting the samples. To equilibrate the C_{18} columns, first, 3.0-4.0 mL of buffer B was slowly flushed through the column. Then ~6.0 mL of buffer A was slowly passed through the columns without letting them dry. Peptide solutions were vortexed well and spined down at 4000 rpm for 1 min before carefully loading it to the C_{18} column 200 µL at a time. Then, the column was gently washed with 3.0-4.0 mL of buffer A, and the elute was discarded. The columns were moved to fresh 2.0 mL low binding tubes (Thermoscientific). The columns were flushed with 800-1000 µL of buffer B to elute the peptides, and then peptides were evaporated to dryness using the speed vac SPD120 machine (Thermoscientific; vacuum concentrator).[27]

7.7.7.7 LC-MS/MS analysis and proteomics data analysis

Desalted tryptic peptide solutions in water with 0.1% formic acid were analysed on an Acquity UPLC M-Class nano-LC system (Waters Corporation) interfaced to a Xevo G2-XS Quadrupole Time-of-flight (Tof) tandem mass spectrometer. Samples (5 µL) were applied to an on-line LC trap pre-column (Symmetry C18, 100Å 5 µm, 180 µm x 20 mm, Waters Corporation) by partial loop injection with the aid of the autosampler component of the Acquity M-Class system. Peptides were eluted from the pre-column trap and separated

on a nano flow UPLC column (HSS T3 1.8 µm, 75 µm x 250 mm, Waters Corporation) with a 60-minute linear gradient of 3 to 40% mobile phase B (acetonitrile with 0.1% formic acid) and mobile phase A (water with 0.1% formic acid). The column temperature was 35 °C. The eluted peptides were introduced into the mass spectrometer on-line via a nano electrospray source with temperature set at 80 °C and capillary voltage 3.2 kV. The mass spectrometer quadrupole was set to efficiently transmit ions with m/z > 300 and the Tof to detect ions in the 50-2000 m/z range in a scanning quadrupole-based data independent acquisition (DIA) mode (SONAR). The collision energy was 5 eV (low energy function) and 19 eV to 45 eV (elevated energy function) and the resolution was 35,000 FWHM.

The LC-MS/MS raw data were analysed with Progenesis QI for proteomics (Nonlinear Dynamics) software platform. Peptides were identified with the ion accounting identification method from searching a non-redundant *Leishmania mexicana* database, which contained 8,524 protein entries. The search allowed for a maximum of one trypsin missed peptide cleavage, static modification of cysteine (carbamidomethylation), and variable modification of methionine (oxidation). The peptide false discovery rate was set to less than 5%. Identified proteins were displayed according to the protein grouping method. The identified proteins were quantified across the different experimental conditions (probe-treatment versus DMSO-treatment) in Progenesis QI for proteomics with the Hi-N method. In the Hi-N method, after peptide and protein identification, the abundance of each peptide is calculated from all its constituent peptide ions. For each protein, the N most abundant peptides have their abundances averaged to provide a reading for the protein signal. A ranking of peptide abundance is carried out based on the integrated value across all runs, allowed by the lack of missing values and accurate alignment. This gives added confidence in the peptide selection, taking all runs into account to make the ranking robust. This averaged reading allows relative quantitation of the same protein across runs.

7.7.7.8 Gene Ontology (GO) Analysis

The gene ontology terms (biological process, cellular components, and molecular function) significantly enriched in the nascent proteins synthesized under the inhibition conditions of **230** in *L. mexicana* promastigotes relative to the predicted whole proteome of the organism were derived using TriTrypDB. REVIGO software was used to refine and visualize the enriched gene ontology terms.

7.8 References

1. Barton, D. H. R. & Tachdjian, C. The Invention of Radical Reactions. Part XXVII. Modified Julia Synthesis of Olefins Using Radical Deoxygenation. *Tetrahedron* **48**, 7109–7120 (1992).

2. Barton, D. H. R., Chern, C. Y. & Jaszberenyi, J. C. The invention of radical reactions. Part XXXIV. Homologation of carboxylic acids to α-keto carboxylic acids by Barton-ester based radical chain chemistry. *Tetrahedron* **51**, 1867–1886 (1995).

3. Aveline, Bc. M., Kochevar, I. E. & Redmond, R. W. Photochemistry of N-Hydroxypyridine-2-thione Derivatives: Involvement of the 2-Pyridylthiyl Radical in the Radical Chain Reaction Mechanism. *J. Am. Chem. Soc.* **117**, 9699–9708 (1995).

4. Blom, P., Xiang, A. X., Kao, D. & Theodorakis, E. A. Design, synthesis, and evaluation of N-aroyloxy-2-thiopyridones as DNA photocleaving reagents. *Bioorganic Med. Chem.* **7**, 727–736 (1999).

5. Brittain, W. D. G. & Cobb, S. L. Protecting Group-Controlled Remote Regioselective Electrophilic Aromatic Halogenation Reactions. *J. Org. Chem.* **85**, 6862–6871 (2020).

6. Brittain, W. D. G. & Cobb, S. L. Tetrafluoropyridyl (TFP): a general phenol protecting group readily cleaved under mild conditions. *Org. Biomol. Chem.* **17**, 2110–2115 (2019).

7. Zhu, Z. & Koltunov, K. Y. Ionic hydrogenation of naphthyl tetrafluoropyridin-4-yl ethers as a new route to 5,6,7,8-tetrahydronaphthols. *Mendeleev Commun.* **30**, 190–191 (2020).

8. Heeran, D. *et al.* Synthesis of polyfunctional fluoro-quinoline and fluoro-pyridopyrimidinone derivatives. *J. Fluor. Chem.* **249**, 109830 (2021).

9. Neelamkavil, S. F. *et al.* Discovery of MK-8282 as a Potent G-Protein-Coupled Receptor 119 Agonist for the Treatment of Type 2 Diabetes. *ACS Med. Chem. Lett.* **9**, 457–461 (2018).

10. Harsanyi, A. & Sandford, G. Fluorine gas for life science syntheses: Green metrics to assess selective direct fluorination for the synthesis of 2-fluoromalonate esters. *Green Chem.* **17**, 3000–3009 (2015).

11. Dietz, J.-P. *et al.* Synthesis of 5-Fluorocytosine Using 2-Cyano-2-fluoroethenolate as a Key Intermediate. *Eur. J. Org. Chem.* **2019**, 5519–5526 (2019).

12. Harsanyi, A., Sandford, G., Yufit, D. S. & Howard, J. A. K. Syntheses of fluorooxindole and 2-fluoro-2-arylacetic acid derivatives from diethyl 2-fluoromalonate ester. *Beilstein J. Org. Chem.* **10**, 1213–1219 (2014).

13. Baron, A. *et al.* Polyfunctional Tetrahydropyrido[2,3-b]pyrazine Scaffolds from 4-Phenylsulfonyl Tetrafluoropyridine. *J. Org. Chem.* **70**, 9377–9381 (2005).

14. Zhou, B. & Li, Y. Q. Palladium nanoparticles immobilized on poly(vinyl chloride)-supported pyridinium as an efficient and recyclable catalyst for suzuki-miyaura cross-coupling reaction. *E-Journal Chem.* **8**, 1490–1497 (2011).

15. Sambaiah, M. *et al.* Tandem Schiff-Base Formation/Heterocyclization: An Approach to the Synthesis of Fused Pyrazolo–Pyrimidine/Isoxazolo-Pyrimidine Hybrids. *Synlett* **30**, 586–592 (2019).

16. Ishikawa, N., Takaoka, A. & Ibrahim, M. K. Preparation of 2-fluoromalonic esters and related compounds from hexafluoropropene. *J. Fluor. Chem.* **25**, 203–212 (1984).

17. Lan, Y. *et al.* Synthesis and biological evaluation of novel sigma-1 receptor antagonists based on pyrimidine scaffold as agents for treating neuropathic pain. *J. Med. Chem.* **57**, 10404–10423 (2014).

18. Breen, J. R., Sandford, G., Patel, B. & Fray, J. Synthesis of 4,4-Difluoro-1 H - pyrazole Derivatives. *Synlett* **26**, 51–54 (2015).

19. Sato, K. *et al.* Synthesis of new fluorescent molecules having an aggregation-induced emission property derived from 4-fluoroisoxazoles. *Beilstein J. Org. Chem.* **16**, 1411–1417 (2020).

20. Zhang, P. *et al.* Pyridinylpyrimidines selectively inhibit human methionine aminopeptidase-1. *Bioorganic Med. Chem.* **21**, 2600–2617 (2013).

21. Baron, A. *et al.* Polyfunctional Tetrahydropyrido [2 , 3- b] pyrazine Scaffolds from 4-Phenylsulfonyl Tetrafluoropyridine. *J. Org. Chem.* **70**, 9377–9381 (2005).

22. Bates, P. A. The Developmental Biology of Leishmania Promastigotes. *Exp. Parasitol.* **79**, 215–218 (1994).

23. Jones, N. G., Catta-Preta, C. M. C., Lima, A. P. C. A. & Mottram, J. C. Genetically Validated Drug Targets in Leishmania: Current Knowledge and Future Prospects. *ACS Infect. Dis.* **4**, 467–477 (2018).

24. Damianou, A. *et al.* Essential roles for deubiquitination in Leishmania life cycle progression. *PLoS Pathog.* **16**, e1008455 (2020).

25. Cuevas-Hernández, R. I., Girard, R. M. B. M., Krstulović, L., Bajić, M. & Silber, A. M. An aromatic imidazoline derived from chloroquinoline triggers cell cycle arrest and inhibits with high selectivity the trypanosoma cruzi mammalian host-cells infection. *PLoS Negl. Trop. Dis.* **15**, e0009994 (2021).

26. Almeida-de-Faria, M., Freymüller, E., Colli, W. & Alves, M. J. M. Trypanosoma cruzi: Characterization of an intracellular epimastigote- like form. *Exp. Parasitol.* **92**, 263–274 (1999).

27. Kalesh, K., Sundriyal, S., Perera, H., Cobb, S. L. & Denny, P. W. Quantitative Proteomics Reveals that Hsp90 Inhibition Dynamically Regulates Global Protein Synthesis in Leishmania mexicana. *mSystems* **6**, 1–15 (2021).

28. Kalesh, K. & Denny, P. W. A boncat-itraq method enables temporally resolved quantitative profiling of newly synthesised proteins in leishmania mexicana parasites during starvation. *PLoS Negl. Trop. Dis.* **13**, 1–26 (2019).

Appendices

A1. Supplementary information

Electronic supplementary information is available for this report, containing physical properties of all compounds tested, detailed results of biological assays and structures of all the compounds tested.

A2. Chemical structures for compounds reported in Chapter 2

Class One

Compound Number	X number	Structure
40	X5747	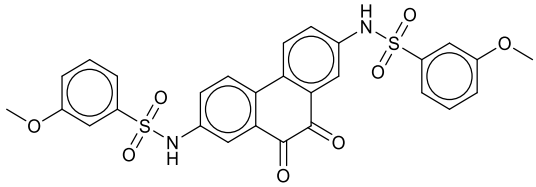
41	X4119	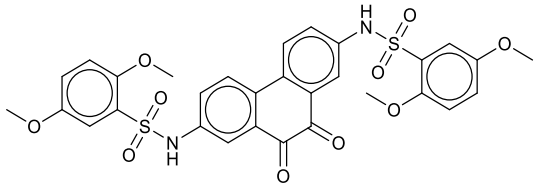
42	X4118	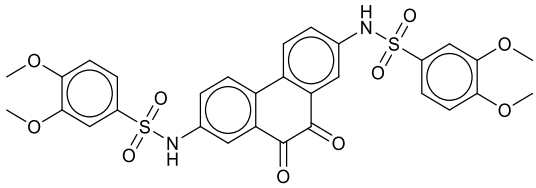
43	X4101	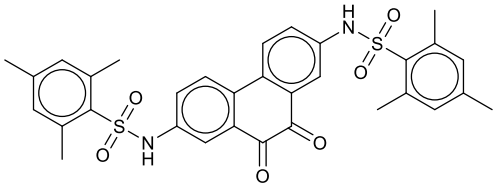
44	X4111	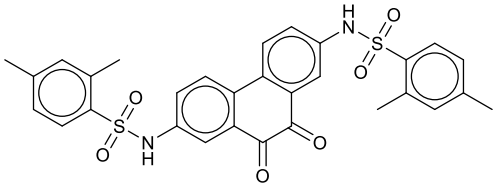

45	X4117	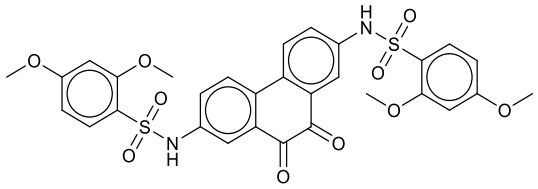
46	X5746	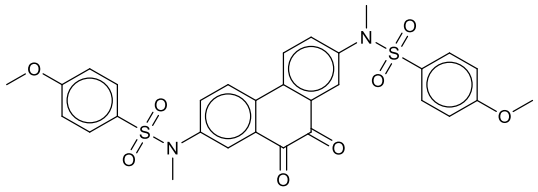
47	X499	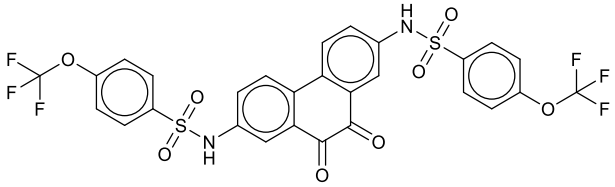
48	X4109	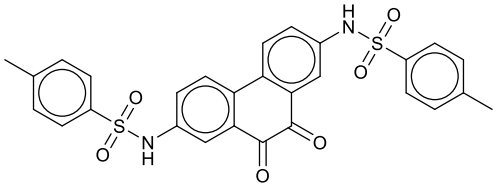
49	X4133	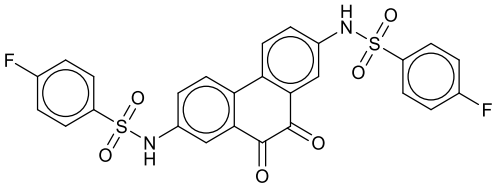
50	X5743	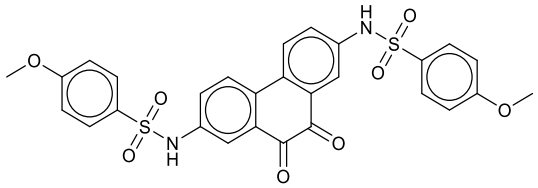
51	X5211	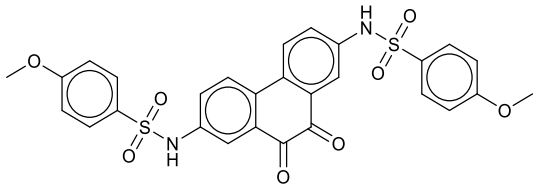
52	X4150	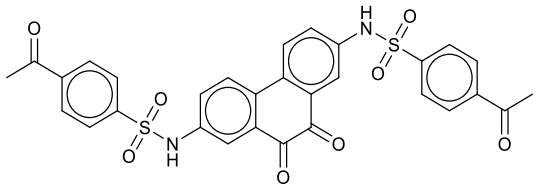
53	X4103	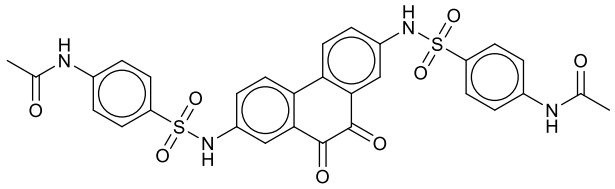

54	X5752	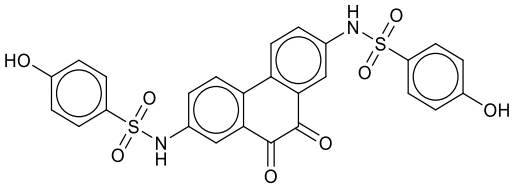
55	X4149	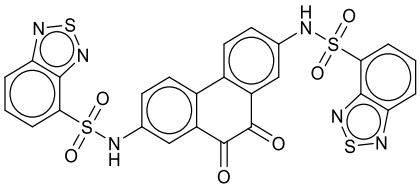

Class Two

Compound Number	X number	Structure
60	X6150	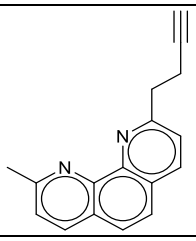
61	X3009	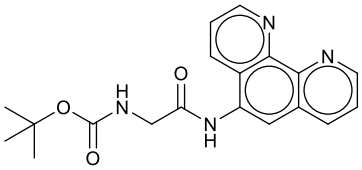
62	X8019	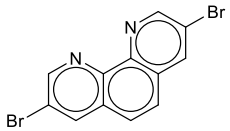
63	X7628	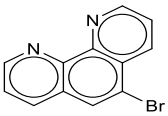
64	X9266	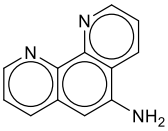
65	X9580	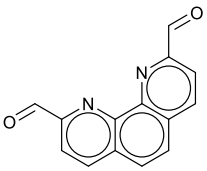

66	X8581	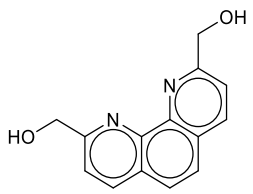
67	X11228	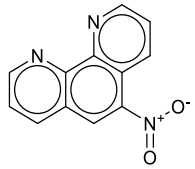

Class Three

Compound Number	X number	Structure
70	X5526	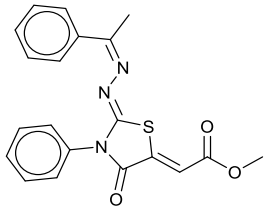
71	X5527	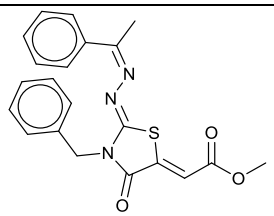
72	X5528	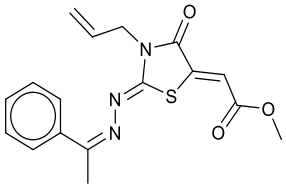
73	X5529	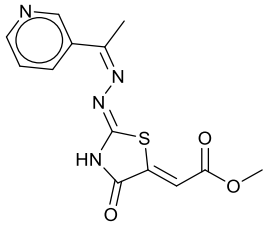

74	X5524	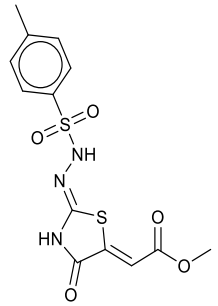
75	X5525	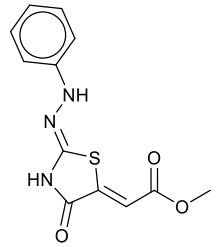
76	X5519	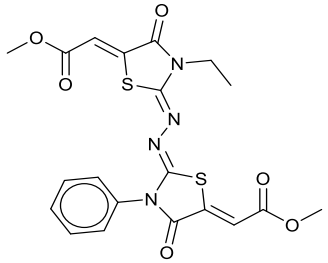
77	X5520	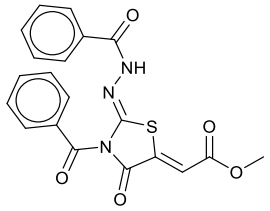
78	X5521	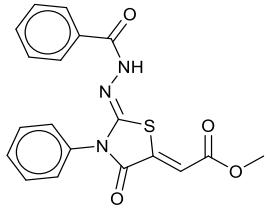
79	X5522	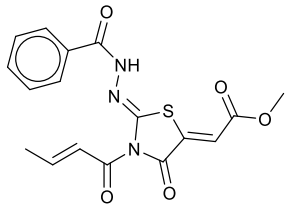
80	X5508	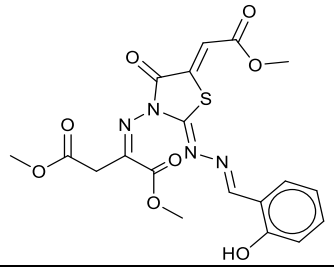

81	X5509	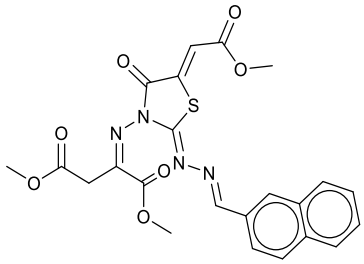
82	X5511	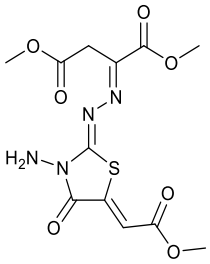

Class Four

Compound Number	X number	Structure
83	X2103	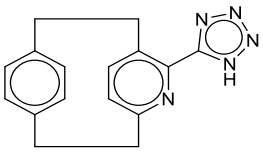
84	X2119	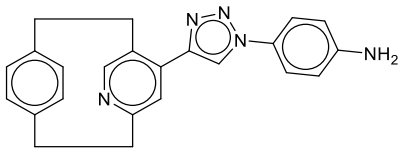
85	X2123	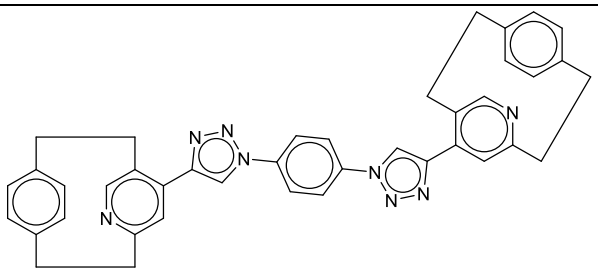
86	X2124	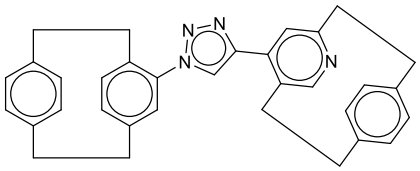
87	X2130	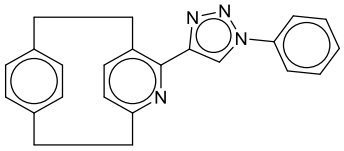

88	X2132	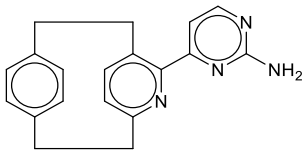
89	X2133	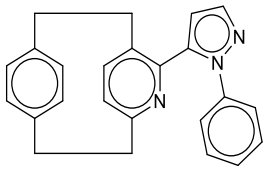
90	X2134	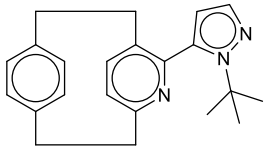
91	X2137	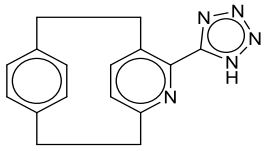
92	X2142	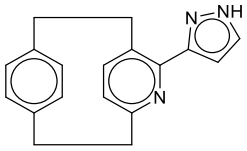
93	X2145	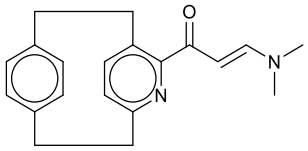
94	X2150	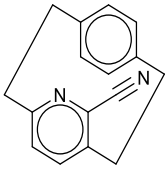
95	X2143	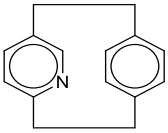

Class Five

Compound Number	X number	Structure
95	X1627	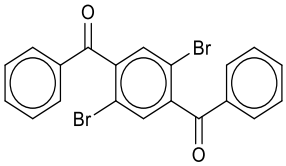

96	X1834	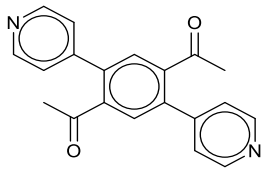
97	X8022	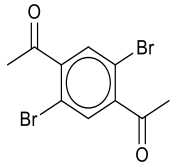

A 3: Crystal Structure Data

A 3.1 Sample Analysis

For X-Ray crystallography, single crystals were taken and analysed at 120 K. Samples were collected using a Bruker D8 Venture, the radiation source was Mo Kα (λ = 0.71073). Structures were solved by direct method and refined by full-matrix least squares on F^2 using Olex2, the refinement program was SHELXL 2017/1 (Sheldrick 2015) and the solution program was XS (Sheldrick 2008).

All sample analysis and refinement were performed by Dr Dmitry Yufit, Durham University.

A 3.2 Crystal Structure Determination of 226

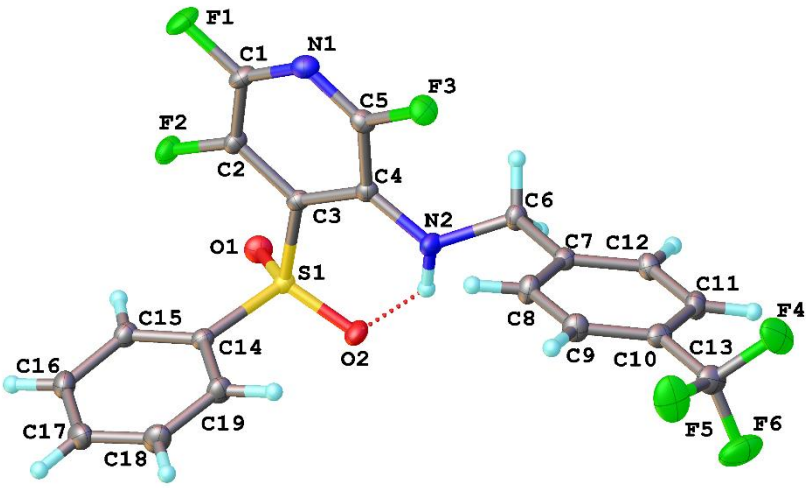

Figure A 1.1: Crystal structure of 2,3,5-trifluoro-6-({[4-(trifluoromethyl)phenyl]methyl}amino)pyridin-4-yl benzenesulfinate **226**. Crystal structure reported with a 50% thermal ellipsoid probability.

Identification code	21srv348
Empirical formula	$C_{19}H_{12}F_6N_2O_2S$
Formula weight	446.37
Temperature/K	120.0
Crystal system	monoclinic
Space group	$P2_1/c$
a/Å	13.2164(3)
b/Å	18.0963(4)
c/Å	7.5773(2)
α/°	90
β/°	92.0340(10)
γ/°	90
Volume/Å^3	1811.11(7)
Z	4
ρ_{calc}g/cm^3	1.637
μ/mm^{-1}	0.259
F(000)	904.0
Crystal size/mm^3	0.21 × 0.2 × 0.06
Radiation	Mo Kα (λ = 0.71073)
2Θ range for data collection/°	3.818 to 59.994
Index ranges	-18 ≤ h ≤ 18, -25 ≤ k ≤ 25, -10 ≤ l ≤ 10
Reflections collected	43079
Independent reflections	5276 [R_{int} = 0.0439, R_{sigma} = 0.0240]
Data/restraints/parameters	5276/0/319
Goodness-of-fit on F^2	1.051
Final R indexes [I>=2σ (I)]	R_1 = 0.0352, wR_2 = 0.0867
Final R indexes [all data]	R_1 = 0.0405, wR_2 = 0.0898
Largest diff. peak/hole / e Å^{-3}	0.48/-0.36

Table A 1.1: Crystal data and refinement properties of compound **226**.

A 3.3 Crystal Structure Determination of 227

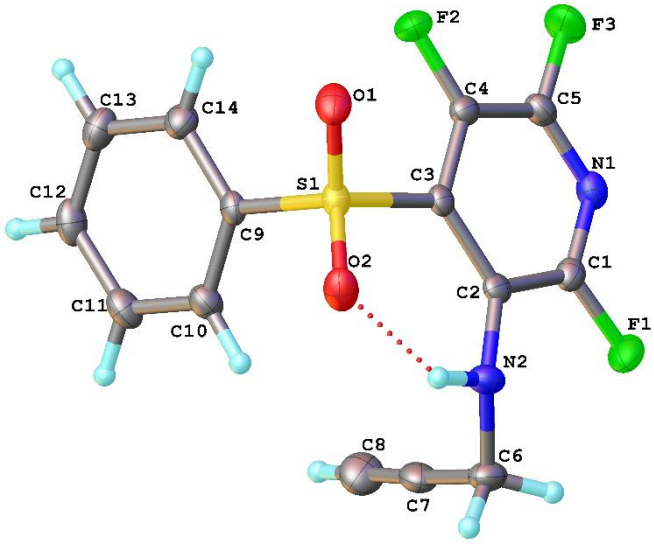

Figure A 1.2: Crystal structure of 2,3,6-trifluoro-5-[(prop-2-yn-1-yl)amino]pyridin-4-yl benzenesulfinate **227(b)**. Crystal structure reported with a 50% thermal ellipsoid probability.

Identification code	21srv349
Empirical formula	$C_{14}H_9F_3N_2O_2S$
Formula weight	326.29
Temperature/K	120.0
Crystal system	monoclinic
Space group	$P2_1/c$
a/Å	17.1271(4)
b/Å	8.9033(2)
c/Å	19.2218(5)
α/°	90
β/°	112.3700(10)
γ/°	90
Volume/Å^3	2710.51(11)
Z	8
ρ_{calc}g/cm^3	1.599
μ/mm^{-1}	0.283
F(000)	1328.0
Crystal size/mm^3	0.32 × 0.12 × 0.11

Radiation	MoKα (λ = 0.71073)
2Θ range for data collection/°	4.318 to 60
Index ranges	-24 ≤ h ≤ 24, -12 ≤ k ≤ 12, -27 ≤ l ≤ 27
Reflections collected	45349
Independent reflections	7883 [R_{int} = 0.0595, R_{sigma} = 0.0426]
Data/restraints/parameters	7883/0/469
Goodness-of-fit on F^2	1.031
Final R indexes [I>=2σ (I)]	R_1 = 0.0395, wR_2 = 0.0897
Final R indexes [all data]	R_1 = 0.0541, wR_2 = 0.0973
Largest diff. peak/hole / e $Å^{-3}$	0.37/-0.42

Table A 1.2: Crystal data and refinement properties of compound **227**.

A 3.4 Crystal Structure Determination of 228

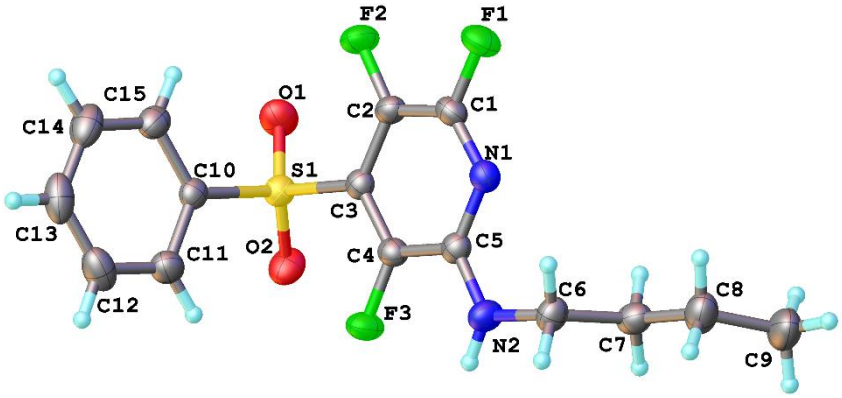

Figure A 1.3: Crystal structure of 2-(butylamino)-3,5,6-trifluoropyridin-4-yl benzenesulfinate **228(a)**. Crystal structure reported with a 50% thermal ellipsoid probability.

Identification code	21srv351
Empirical formula	$C_{15}H_{15}F_3N_2O_2S$
Formula weight	344.35
Temperature/K	200.0
Crystal system	monoclinic
Space group	$P2_1/c$
a/Å	10.7907(3)
b/Å	16.5089(4)
c/Å	8.9315(2)
α/°	90
β/°	105.8654(9)
γ/°	90
Volume/Å^3	1530.47(7)
Z	4
ρ_{calc}g/cm^3	1.494
μ/mm^{-1}	0.254
F(000)	712.0
Crystal size/mm^3	0.13 × 0.11 × 0.02
Radiation	Mo Kα (λ = 0.71073)
2Θ range for data collection/°	4.636 to 59.996
Index ranges	-15 ≤ h ≤ 15, -23 ≤ k ≤ 23, -12 ≤ l ≤ 12
Reflections collected	25917

Independent reflections	4461 [R_{int} = 0.0436, R_{sigma} = 0.0351]
Data/restraints/parameters	4461/0/268
Goodness-of-fit on F^2	1.059
Final R indexes [I>=2σ (I)]	R_1 = 0.0431, wR_2 = 0.0905
Final R indexes [all data]	R_1 = 0.0630, wR_2 = 0.0996
Largest diff. peak/hole / e $Å^{-3}$	0.30/-0.34

Table A 1.3: Crystal data and refinement properties of compound **228(a)**.

A 3.5 Crystal Structure Determination of 229

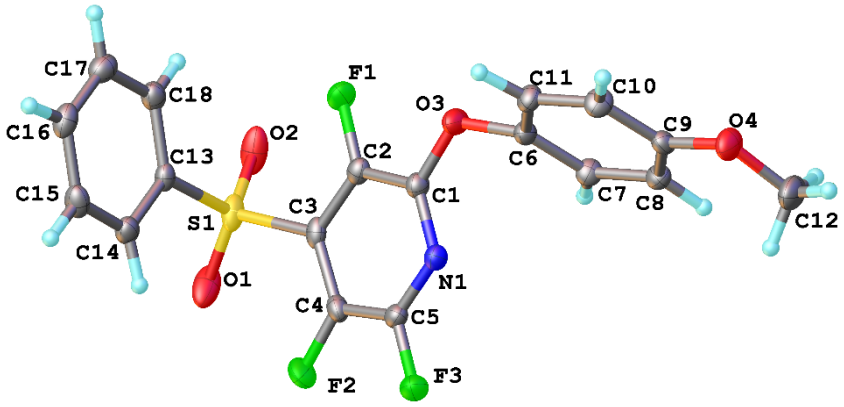

Figure A 1.4: Crystal structure of 2,3,5-trifluoro-6-(4-methoxyphenoxy)-4-(phenylsulfonyl) pyridine **229**. Crystal structure reported with a 50% thermal ellipsoid probability.

Identification code	21srv350
Empirical formula	$C_{18}H_{12}F_3NO_4S$
Formula weight	395.35
Temperature/K	120.0
Crystal system	orthorhombic
Space group	$Pca2_1$
a/Å	11.0571(3)
b/Å	8.8032(2)
c/Å	17.4211(4)
α/°	90
β/°	90
γ/°	90
Volume/Å^3	1695.73(7)
Z	4
ρ_{calc}g/cm^3	1.549
μ/mm^{-1}	0.248
F(000)	808.0
Crystal size/mm^3	0.15 × 0.12 × 0.02
Radiation	Mo Kα (λ = 0.71073)
2Θ range for data collection/°	4.676 to 59.98
Index ranges	-15 ≤ h ≤ 15, -12 ≤ k ≤ 12, -24 ≤ l ≤ 24
Reflections collected	27668

Independent reflections	4929 [R_{int} = 0.0463, R_{sigma} = 0.0372]
Data/restraints/parameters	4929/1/293
Goodness-of-fit on F^2	1.041
Final R indexes [I>=2σ (I)]	R_1 = 0.0342, wR_2 = 0.0675
Final R indexes [all data]	R_1 = 0.0442, wR_2 = 0.0722
Largest diff. peak/hole / e $Å^{-3}$	0.20/-0.29
Flack parameter	0.40(8)

Table A 1.4: Crystal data and refinement properties of compound **229**

A 3.6 Crystal Structure Determination of 230

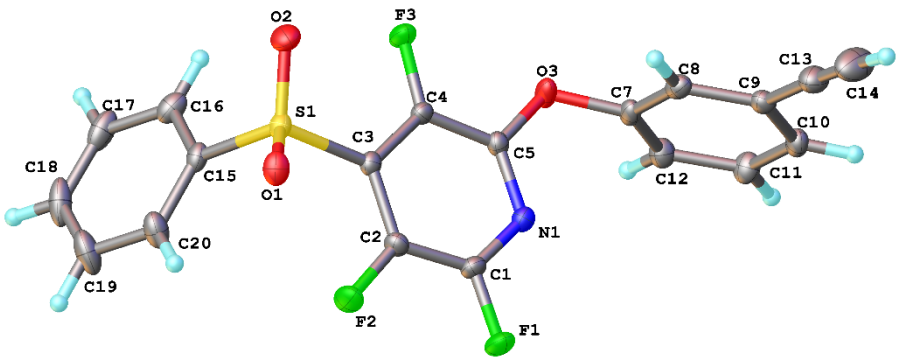

Figure A 1.5: Crystal structure of 2-(3-ethynylphenoxy)-3,5,6-trifluoro-4-(phenylsulfonyl) **230**. Crystal structure reported with a 50% thermal ellipsoid probability.

Identification code	21srv325
Empirical formula	$C_{19}H_{10}F_3NO_3S$
Formula weight	389.34
Temperature/K	120.0
Crystal system	monoclinic
Space group	$P2_1/n$
a/Å	11.2928(3)
b/Å	9.2624(3)
c/Å	16.2285(5)
α/°	90
β/°	98.3583(11)
γ/°	90
Volume/Å^3	1679.45(9)
Z	4
ρ_{calc}g/cm^3	1.540
μ/mm^{-1}	0.245
F(000)	792.0
Crystal size/mm^3	0.24 × 0.19 × 0.16
Radiation	MoKα (λ = 0.71073)
2Θ range for data collection/°	5.078 to 59.984
Index ranges	$-15 \leq h \leq 15$, $-13 \leq k \leq 13$, $-22 \leq l \leq 22$
Reflections collected	27850
Independent reflections	4863 [R_{int} = 0.0292, R_{sigma} = 0.0211]

Data/restraints/parameters	4863/0/284
Goodness-of-fit on F^2	1.042
Final R indexes [I>=2σ (I)]	R_1 = 0.0337, wR_2 = 0.0835
Final R indexes [all data]	R_1 = 0.0393, wR_2 = 0.0868
Largest diff. peak/hole / e $Å^{-3}$	0.37/-0.43

Table A 1.5: Crystal data and refinement properties of compound **230**

A 3.7 Crystal Structure Determination of 244

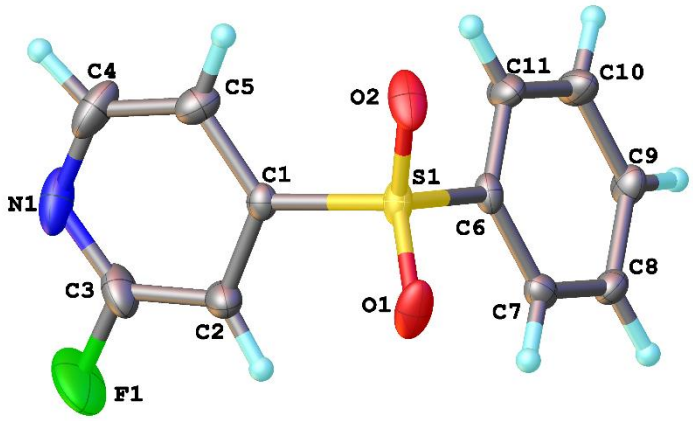

Figure A 1.6: Crystal structure of 4-(benzenesulfonyl)-2-fluoropyridine **244**. Crystal structure reported with a 50% thermal ellipsoid probability

Identification code	21srv347
Empirical formula	$C_{11}H_8FNO_2S$
Formula weight	237.24
Temperature/K	120.0
Crystal system	orthorhombic
Space group	Pbcn
a/Å	17.1116(5)
b/Å	8.2606(2)
c/Å	14.7668(4)
α/°	90
β/°	90
γ/°	90
Volume/Å^3	2087.32(10)
Z	8
ρ_{calc}g/cm^3	1.510
μ/mm^{-1}	0.306
F(000)	976.0
Crystal size/mm^3	0.28 × 0.25 × 0.14
Radiation	Mo Kα (λ = 0.71073)
2Θ range for data collection/°	4.76 to 60
Index ranges	-24 ≤ h ≤ 24, -11 ≤ k ≤ 11, -20 ≤ l ≤ 20
Reflections collected	46884

Independent reflections	3031 [R_{int} = 0.0404, R_{sigma} = 0.0162]
Data/restraints/parameters	3031/2/189
Goodness-of-fit on F^2	1.062
Final R indexes [I>=2σ (I)]	R_1 = 0.0415, wR_2 = 0.1011
Final R indexes [all data]	R_1 = 0.0448, wR_2 = 0.1033
Largest diff. peak/hole / e $Å^{-3}$	0.44/-0.33

Table A 1.6: Crystal data and refinement properties of compound **244**